ANALYSIS OF THE ROLE OF DEFECTS IN THE PERFORMANCE CHARACTERISTICS OF GaN-BASED EXCITON-POLARITON LASERS

by

A.K.M. Hasibul Hoque

Student ID: 1017062228 P

A thesis submitted in partial fulfillment of the requirements of the degree

of

Master of Science in Electrical and Electronic Engineering

Department of Electrical and Electronic Engineering
Bangladesh University of Engineering and Technology (BUET)
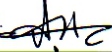Dhaka, Bangladesh

October, 2022
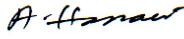
The thesis titled "ANALYSIS OF THE ROLE OF DEFECTS IN THE PERFORMANCE CHARACTERISTICS OF GaN-BASED EXCITON-POLARITON LASERS" submitted by A.K.M. Hasibul Hoque, Student ID: 1017062228 P, Session: October 2017 has been accepted as satisfactory in partial fulfillment of the requirements for the degree of Master of Science in Electrical and Electronic Engineering on October 31, 2022.

BOARD OF EXAMINERS

1.   Chairman

Dr. Md. Zunaid Baten   (Supervisor)

Dr. Md. Zunaid Baten
Associate Professor
Department of Electrical and Electronic Engineering
Bangladesh University of Engineering and Technology
Dhaka, Bangladesh.

2.   Member
                                                (Ex-Officio)

Dr. Md. Aynal Haque
Professor and Head
Department of Electrical and Electronic Engineering
Bangladesh University of Engineering and Technology
Dhaka, Bangladesh.

3.   Member

Dr. Sharif Mohammad Mominuzzaman
Professor
Department of Electrical and Electronic Engineering
Bangladesh University of Engineering and Technology
Dhaka, Bangladesh.

4.   Member
                                                (External)

Dr. A.K.M. Akther Hossain
Professor
Department of Physics
Bangladesh University of Engineering and Technology
Dhaka, Bangladesh.

Acknowledgement

Pursuing a Masters degree is not an easy task. I am thankful for the opportunity of pursuing the Masters degree in Electrical and Electronic Engineering department in BUET.

I would like to express my sincere gratitude to my adviser Dr. Md Zunaid Baten, Associate Professor of the Department of Electrical and Electronic Engineering, BUET, Dhaka for giving me the opportunity to do my research and providing invaluable guidance throughout my research work. I cannot thank enough for his vision, dynamism, sincerity and motivation. He has taught me the methodology to carry out my research work and present them as clearly as possible. Once he told me,"When do you understand that you have achieved the purpose of your thesis? When you know more than your supervisor on that topic"". My supervisor and other will judge me on that. But that comment has driven me till today to learn as much as I can. In this pursuit he always encouraged me to push my boundaries towards excellence and for which I am greatly indebted to him. I would also like to thank him for his patience he had during the discussion of my work. I would like to thank my parents and the members of my family for believing in me and constantly providing me support towards the completion of this work. Once my mother told me, "Clear understanding will make this complex and chaotic world simpler to you."". I believe this 'simple' quote guides me to realize the understanding of this work. I am not that talented to complete a research work solely on my own. I always seek help and inspiration from my surrounding environment and people. Finally, I would like to thank them for helping me in my endeavour. I believe my greatest inspiration is my surrounding natural and man-made events. I am grateful that I live in the midst of them.

A.K.M. Hasibul Hoque
October, 2022

Abstract

This study emphasizes on the theoretical analysis of defect on bosonic system, especially exciton-polariton bosonic system. Presence of defect may either stand as a barrier to realization of such phenomenon or pave the way for realization of something more exotic. This work is focused on the influence of defect on polariton lasing here. In polariton lasers using semiconductor microcavity with high quality factor, stimulated scattering facilitates dynamic condensation process. As a result, a macroscopic and coherent exciton-polariton state is formed. In this metastable coherent phase, condensate is not thermalized with the lattice rather thermalized among itself, according to micro-cannonical thermalization. Thus, effective polariton temperature of condensate near K=0, is generally larger than lattice temperature. Recently, for a defective MC, measured effective polariton temperature is sustainably smaller than 300K, for room temperature operation of GaN polariton diode lasers. Such finding is completely different from the generic case. With higher density of dislocation and other related defect in the active region of microcavity, this temperature lowering effect reinforce itself. To investigate the effect of defect on condensate formation and to explain phenomenon like this, open dissipative Gross-Pitaevskii (GP) equation coupled with external exciton reservoir has been solved numerically. Several situations have been considered regarding defect potential and pumping scheme. Open dissipative GP equation enables us to investigate the vortices kinetics during condensate formation with the presence of disorder potential and for different pumping scheme. To estimate the exciton polariton LASER performance with the presence of defect, semi-classical Boltzmann equations have been solve numerically. Along with all these, a thermodynamic approach with numerical solution of Bose-Hubbard model has been analyzed to understand the behavior of the system from different point of view. High frequency performance of such polariton laser diode is analyzed using simplified rate equation model. Finally, comparison between numerical and experimental result for polariton LASER diode has been provided.

Contents

List of Figures

List of Tables

Chapter 1

Introduction

1.1 Preface

Light-matter interaction is an emerging research field in the boundary of Condensed matter physics, Semiconductor science and Opto-electronics. This field has developed in both fundamental and applied directions. Recent advances in semiconductor fabrication technology [1–4] paves the way for realization of exotic theoretical concepts experimentally [5–11]. Although one might argue that, exact one-to-one mapping of experiment and theory is not possible. The real systems used for experiment are full of complications that prevent us form exactly diagnose and extricate the cause and effect relationship for our property of interest. Despite the argument of 'Chaos Theorist' [12] new experiments are designing to realize theoretical prediction with a hope to understand and tame this chaos [13]. Exciton-polariton was such a theoretical concept. Exciton-polariton is a part-light, part-matter quasiparticle boson has been experimentally realised by placing an emitter inside an well designed microcavity with strong light matter interaction [14, 15]. Due to hybrid nature, exciton-polariton can be exploited to study cavity quantum electrodynamics (QED) and many body physics such as Bose-Einstein condensation (BEC) [16], spontaneous symmetry breaking [17], superfluidity [18], Bardeen-Cooper-Schrieffer (BCS) states [19] and Berezinskii-Kosterlitz-Thouless (BKT) transition [20]. Anyway, in terms of practical applications in photonics and opto-electronics field, one of the most exotic prospect of exciton-polaritons is towards the realization of an 'inversionless coherent emitter'.

This sort of emitter was first proposed by Imamoglu et al. utilizing spontaneous radiative recombination from a coherent exciton-polariton condensate in a semiconductor microcavity [21]. Whereas the gain mechanism in a conventional photon laser is stimulated emission, for a polariton device the process is stimulated scattering. Unlike a conventional photon laser, the separation of stimulation and emission in a polariton device leads to coherent emission without the requirement of population inversion. As a result, it is expected that the threshold energy required for coherent emission from this sort of device would be much smaller than that of a photon laser [22, 23]. This new kind of a solid-state device, which is more commonly known as a polariton laser, holds great promise as a low-power coherent light source for medical and biomedical applications, short distance plastic fiber communications, high-speed optical interconnects and logic circuits, and quantum information processing [24–29]. Consequently, polariton lasing has continued to be an intense topic of research in recent years. In particular, advancements in areas of materials growth, device design and device fabrication technologies have led to numerous experimental realizations of this novel light source.

Most of the experimental realizations using exciton-polariton tried to imitate the ideal conditions or as close as possible to the ideal condition. Despite achieving tremendous progress in fabrication technology, defect in form of point defect, dislocation, impurity etc. [30] actually exist in material. This can severely hamper the performance of the device [31, 32]. The experimental study of the exciton-polariton system with defect revealed some fascinating exceptions [33–35]. As a result, a robust theoretical understanding based on existing exciton-polariton theoretical framework is essential to have a better prediction capability for various practical system.

1.2 Literature Review

Bose-Einstein statistics was hypothesised in 1924 by S.N. bose [36], even before the first appearance of Schrodinger equation in 1926 [37]. Although the original paper by Bose was rejected, Albert einstein considered the work to be interesting and recommended its publication in one of the most important scientific journals of that time: *Zeitschrift fur Physik*. He used the theory to describe the phenomenon of Bose-Einstein

condensation [38]. After that prediction, physics community was in a dilemma as whether this is just a mathematical construct or an actual that is waiting for discovery. In 1995, the discovery of such state of matter by Eric Cornell and Carl Wieman [5] put an end to such confusion. Bose-Einstein condensate (BEC) was observed for Rb-87 system confined by magnetic field at 170 nK with a lifetime of 15 seconds. After that researchers turn their interest to discover BEC state for different system [6, 39–41]. Most of these discoveries are with molecules at lower temperature, close to 0K. Observation of BEC for composite boson i.e. exciton-polariton was first reported by Kasprazak et. al. [42]. Due to very low mass of exciton-polariton, it was possible to observe BEC state in a temperature (19 K) much higher than originally observed with Rb-87 atom. This further increased interest in the research of composite bosons i.e. exciton polariton, phonon polariton etc.

The idea of exciton was first proposed by Yakov Frenkel in 1931 [43] as an excitation of atoms inside insulator lattice. He proposed that the resulting excitation can travel like particle. In certain ionic crystals (alkali halide crystals or organic molecular crystals composed of aromatic molecules, such as anthracene and tetracene) exciton can form with binding energy as high as 1 eV due to strong Coulomb interaction between electron and hole. These sort of exciton is known as 'Frenkel exciton'. Besides, in most semiconductor material (GaAs, GaN, ZnO etc.) Coulomb interaction is strongly screened by dielectric constant. As a result, exciton binding energy is low (around 10-40 meV) and binding radius is large. These sort of excitons are called 'Larger exciton' or 'Wannier-Mott excitons' [44]. Later theory of excitons and its properties has been investigated thoroughly [45–49]. Early experimental studies on excitons in semiconductors, showed significant influence of optical excitation on excitonic transition. In 1957, S. I. Pekar described these changes of the excitonic spectrum with respect to an additional wave appearing in the semiconductor crystal [50]. The observed phenomenon was later explained by J. J. Hopfield by considering new eigenstates of EM (Electromagnetic) field coupled exciton system, [51]. These eigenstates are polaritons states, or strictly speaking exciton-polaritons states, to distinguish them from other types of light-matter hybrid states i.e. phonon-polaritons or plasmon-polariton. Exciton-polariton was first experimentally observed by Frohlic in CuCl in 1971 using two-photon absorption

spectroscopy [52]. However, experimental observation of Wannier-Mott exciton was first observed in 1977 [53]. In this study, photoluminescence obtained from high purity GaAs epitaxial layers were explained within the polariton framework. Since then, there have been extensive reportings on the experimental finding of exciton-polaritons in different direct bandgap semiconductors, such as GaAs, CdS, ZnO, ZnTe, ZnSe and GaN [54]. All these experiments were performed using bulk semiconductors instead of having a quantum well (QW) active region, because light-matter coupling of two-dimensional QW exciton to the three-dimensional continuum of photons is precluded by enhanced radiative decay [55]. In 1992, Weisbuch et al. reported normal mode splitting in a GaAs quantum well based microcavity, which consisted of GaAs/AlGaAs quantum wells imbedded between two distributed Bragg reflectors (DBRs) [14], paving the way for observation of exciton-polariton states in QWs. This work was followed by numerous reports of normal mode splitting and light matter coupling in semiconductor microcavities, mostly in GaAs-based systems because of their relatively matured growth and fabrication technologies [56–59]. Imamoglu et.al. first explained the idea of generating coherent emission from a degenerate condensate of exciton-polaritons [21] as low dimensional semiconductor microcavity fabrication became feasible. This prospective idea lead to the first experimental observation of polariton lasing, reported by Le Si Dang et al. at liquid He temperature in a CdTe-based microcavity [60]. Since then, dynamic condensation of polaritons and polariton lasing in different material and nanostructure systems and with different dimensionality of the polaritons have been demonstrated in a series of experiments using optical excitation [16, 17, 42, 61–69]. Most of these measurements have been performed at cryogenic or low temperature because of appear of weak coupling at high temperature due to low exciton binding energy of the material system. Wide bandgap semiconductors like GaN and ZnO gained considerable interest because of their low exciton Bohr radii and high exciton binding energies. Polariton lasing at high temperatures, if not at room temperature, has been demonstrated using optical excitation in microcavities comprising of these material systems [62, 70]. The first observation of polariton lasing at room temperature was reported in 2007 in an optically pumped bulk-GaN based hybrid microcavity [67]. As far as the dimensionality and nanostructures are concerned, strong-coupling and polariton lasing have been reported using bulk [67, 71], QW(s) [64, 72, 73], micro- and NW(s) [69, 74] and QD(s) [75, 76].

It has been experimentally demonstrated that the polariton lasing threshold is 1-3 orders of magnitude smaller than the photon lasing threshold measured in the same device [64, 69, 77].

All these experimental work has given researcher essential perspective regarding exciton-polariton condensation and lasing. All these experiments mentioned above and others utilize a near ideal system with very few defects for experiments. But defect will always present in practical system due to presence of no-ideal condition during commercial fabrication process. Influence of defect on exciton polariton system has also been investigated experimentally [33, 35, 78–88]. In all these experiments, different effects of defect on exciton-polariton system have been observed such as change in excitonic photo-luminescence spectra, appearance of bound exciton, lowering of effective polariton temperature, change in resonant frequency for polariton LASER diode etc. Several theoretical explanations [89–93] for these experimental findings have given us some insight into the impact of defect. Most of these theoretical works have focused on the scattering of bound exciton by defect (impurity, dislocation etc. type) and their overall impact on photo-luminescence and Raman spectrum of the excitonic transition. Some theoretical explanations revolve around the idea of elasticity and non-elasticity of scattering mechanism and its eventual impact on the overall exciton-exciton scattering rate. Theories regarding exciton capture via defect have been presented. But none of the theories can explain the lowering effective polariton temperature satisfactorily. A new theory is needed to explain this phenomenon.

The effect of temperature can be explained by semi-classical Boltzmann theory or by quantum thermodynamics. Semi-classical Boltzmann equation has been successfully employed to explain polariton population dynamics in k-space [94–97]. A drawback of this approach is that it only permits the calculation of the populations of polaritonic quantum states. All other quantities of interest, like 'order parameter', various correlation functions are beyond scope. On the other hand, quantum thermodynamics, especially Eigenstate Thermalization Hypothesis (ETH) [98–103] has been successful to explain the thermalization dynamics for isolated quantum system under different quench. To explain the effect of lower effective polariton temperature it is essential to tackle the problem from

both direction.

1.3 Motivation of the Work

Experiment can give us different types of result. It is the job of theory to link between the results. Without a proper theory, experimental results do not coincide with understanding. It is the purpose of theory to explain the experiment. But sometimes exception happen. Researcher design experiment to prove a theory (Einstein gravitational wave theory [104]). But our purpose here is the first one, try to design a theory to explain experimental finding. Designing a new theory from ground up is extremely difficult. Thankfully, some theoretical work on bosonic system with defect has been done previously. We will focus on these existing theories and add necessary modifications to them to explain the phenomenon of 'Defect induced effective polariton temperature lowering' and 'Performance of defective polariton LASER diode with defect'. In an experimental work [33] it is reported that with the presence of dislocation type of defect effective polariton temperature is getting reduced. In polariton LASER, polariton creates a non-equilibrium state with the lattice. Most often, when there is very few defects this polariton gas is at higher temperature than the lattice temperature. With more and more defect this effective polariton temperature is lower than the one in pure case. With more and more defect this lowering effect increases. By incorporating only exciton-exciton scattering modification due to defect [91, 93] a proper explanation of this lowering effect is not possible. Furthermore, the effect of defect on parameters of polariton LASER diode such as lower resonant frequency, increased threshold etc. need proper explanation from one theory.

Additionally, one phenomenon should be tackled from multiple direction to understand the robustness of the experimental result whether it is a common phenomenon or it is just a rare event created by special condition in laboratory. To investigate this approach, this event was tried from three separate direction. First, using time and space dynamics (by Gross Pitaevskii equation) to understand the role of defect on exciton-polariton condensation process. Second, Coupled semi-classical Boltzmann rate equations incorporating defect modification have been solved to explain the phenomenon.

And lastly, a thermodynamic approach has been taken to investigate the temperature lowering effect by employing ETH and MBL (Many Body Localization) [105,106]. In case one theoretical investigation provides conflicting results, doubt has to be emphasized on theory has to be put or experimental finding. This theories will then be employed to investigate the performance of some practical system.

1.4 Objectives of the Work

The objectives of this work are the following:

1. To analyze and explain the role of defects on the dynamic condensation process of GaN-based optically and electrically pumped exciton polariton lasers.

2. To investigate the impact of defects on the steady-state performance of electrically and optically pumped exciton polariton lasers.

3. To explain the impact of defects on the high-frequency modulation response of exciton polariton lasers.

1.5 Outline of the Dissertation

Chapter 2 introduces the very basic of exciton polariton. Exciton polariton is a hybrid particle due to strong coupling between matter wave excitation (exciton) and optical excitation (photon). A brief discussion of exciton and cavity photon is provided there. Different concept of polariton LASING has been introduced in this chapter too. These concepts are, relaxation dynamics, stimulated scattering event, bottleneck phenomenon etc. There are some fundamental difference between polariton LASING and photon LASING. The main difference is photon LASER employs stimulated emission where polariton LASER employs stimulated scattering. These differences are also discussed in chapter 2.

Chapter 3 conceptualizes the idea of condensation of Quasi particle like exciton particle. Bose-Einstein condensation occurs only for pure bosons without any form of interaction. Exciton polariton are not exact bosons rather co-bosons and exhibit

particle-particle interaction. It is not possible for such quasi-particles to condensate exactly according to theory. Chapter 3 introduces the basic idea of Bose Einstein condensation process with explanation of necessary parameters. Despite unable to form ideal Bose Einstein condensate, quasi particle like exciton polariton form condensate state utilizing vortex pairing and undergoes Berezinskii-Kosterlitz-Thouless transition to form superfluid state of matter. Detailed of this superfluid state is discussed in this chapter. Finally discussion on Gross-Pitaevskii equation along with solution of such equation coupled with external exciton reservoir for zero potential is provided.

Chapter 4 discusses the details about quantum thermodynamics with some introductory discussion of discussion on classical thermalization and classical chaos. Characteristics of classical chaos and quantum chaos is fundamentally different which results in different nature of classical and quantum thermalization. nevertheless an analogue between classical thermalization and quantum thermalization exist. Such analogue has also been discussed in chapter 4. We put a special emphasis on Random Matrix Theory (RMT) and Eigenstate Thermalization Hypothesis (ETH) as these are most successful to describe quantum thermalization. But presence of defect cannot validate the use of these approach. For understanding why, concept of localization is discussed in detail starting from elementary level of Anderson localization. Finally in this chapter we provide some basic ideas about Bose-Hubbard model which will be solved numerically to analyze the influence of defect on bosonic system.

Chapter 5 provides the result of dynamics of polariton condensate in temporal, spatial and kinetic domain. Open dissipative Gross-Pitaevskii Equation coupled with external exciton reservoir provides spatial and temporal dynamics where coupled Semi-classical Boltzmann rate equation provides relaxation dynamics of polariton in kinetic domain. Both of these equation sets are essential to understand the influence of defect on polariton condensate dynamics. We use different types defect potential pattern and pumping scheme to analyze the polariton condensate dynamics by solving GP equation. To understand the dynamics in kinetic domain, different defect densities has been employed along with calculated exciton-phonon scattering rate and exciton-exciton scattering rate.

Chapter 6 provides the result from perspective of thermodynamics. Conclusion on the effect of defect has been reached from two direction, one is heuristic approach and another numerical approach. Heuristic approach utilizes existing theory of ETH and MBL to provide some insight about the thermalization of bosonic system under the presence of disorder or defect. Numerical approach utilizes exact diagonalization and Quantum Monte Carlo approach to solve disorder Bose Hubbard model numerically to evaluate some thermodynamic equilibrium value and provide important conclusion regarding defect impact.

Chapter 7 provides the comparison between numerical and experimental result. Defect influences experimental characteristics of polariton LASER diode. Using a simplified rate equation approach effect of defect on polariton LASER diode frequency characteristics has been analyzed compared with experimental results. Some prediction regarding the impact of defect on quantum information processing is provided based on the achieved conclusion.

Chapter 8 summarizes the whole work of this dissertation in short and sheds some light on the impact of such work. Additionally focus is given on the future work that could be done with the obtained results and necessity for further investigation.

PART I

THEORETICAL BACKGROUND

Chapter 2

Exciton-Polariton : Fundamentals

Until present all constituent particles of the universe can be put into one of the two classes: Bosons or Fermions. Bosons follow Bose-Einstein statistics with integer spin where Fermions follow Fermi-Dirac statistics, Pauli's exclusion principle with half integer spin. As a consequence, Bosons tend to bunch together and can create a macroscopic state under proper condition. But one state can only be occupied by one fermion. Some examples of boson and fermion are: Fermion-Lepton (electron, neutrino etc.), Baryons (proton, neutron etc.), Boson-Photon, Gluons, W boson, Z boson (four force-carrying gauge bosons of the Standard Model), Higgs bosons etc.

Besides the traditional example of bosons, a different branch of bosons exist. These bosons, sometimes coined as co-bosons are formed by paired fermions. Cooper pair from BCS superconductor theory, exciton are these types of boson. Due to even number of fermion, these particles shows an interger spin and also follows the other properties of boson i.e. Bose-Einstein statistics, macrscopic condensation etc. Exciton is a co-boson which is formed due to formation of elcetron-hole pair under the influence of strong Coulomb attraction between them. Exciton-polariton is a hybridized state due to strong interaction between semiconductor exciton and microcavity photon. In this chapter, a rigorous theoretical background of exciton polariton is being presented. For a detailed theory of exciton-polariton readers are requested to follow text [107, 108].

2.1 Cavity Photon

A microcavity is an optical resonator to confine light in small volume by some sort of reflecting mechanism [109]. Depending on the method of light confinement, a semiconductor microcavity can be of different classes i.e. planar, spherical, pillar or photonic crystal microcavity. In semiconductor microcavity this reflecting mechanism is implemented using metallic mirror reflector or by Distributed Bragg Reflector (DBR) [110, 111].Due to high reflectivity and current progress in fabrication technique, DBR reflector is efficient in light trapping. A DBR mirror consists of alternate layers of materials having different refractive indices. DBR mirror employs the principle of interference to achieve high reflectivity. Depending on the contrast of refractive indices, it is possible to achieve very high reflectivity [112, 113]. Due to this high reflectivity, semiconductor microcavity can achieve a very quality factor; Q $\left(Q = \frac{\pi (R_1 R_2)^{\frac{1}{4}}}{1-(R_1 R_2)^{\frac{1}{2}}}, \right.$ with R_1 and R_2 are the reflectivity of two mirrors $\left.\right)$ which enable the microcavity to stimulate strong light matter interaction. Strong light matter interaction is essential for exciton-polariton coupled eigenstate formation. For weak light-matter interaction, exciton and photon act as independent states, decoupled from each other.

Due to multiple reflection from both mirror, a photon is effectively is trapped inside cavity. This photon is known as cavity photon. This sort of photon has gained some mass compared to the one that is free.

For semiconductor microcavity (Fig. 2.1) energy momentum relationship can be written as,

$$E_c = \frac{\hbar c k}{n_c} = \frac{\hbar c k}{n_c}\sqrt{k_z^2 + k_x^2 + k_y^2} = \frac{\hbar c k}{n_c}\sqrt{k_z^2 + k_\parallel^2} \tag{2.1}$$

Here, c is the speed of light in vacuum, n_c is the effective refractive index of the cavity region and in-plane wave-vector $k_\parallel^2 = k_x^2 + k_y^2$. For $k_z >> k_\parallel$, equation 2.1 can be written as,

$$E_c \approx \frac{\hbar c k_z}{n_c} + k_\parallel^2 \frac{\hbar c}{n_c k_z} = E_{k_\parallel=0} + \frac{\hbar^2 k_\parallel^2}{2m_c} \tag{2.2}$$

which gives us the cavity photon mass m_c as,
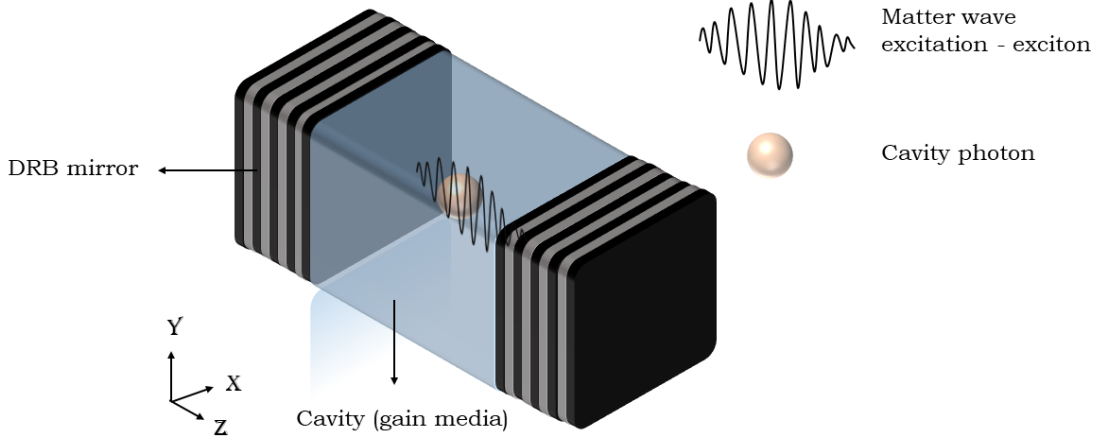
Figure 2.1: Schematic representation of a planar microcavity having DBR mirrors with cavity photon and exciton excitation.

$$m_c = \frac{\hbar n_c k_z}{2c} = \frac{\hbar p \pi n_c}{c L_c} \qquad (2.3)$$

here p is cavity mode no and L_c is cavity length. In case of free photon $L_c \to \infty$ mass goes to zero (2.3).

2.2   Matter Wave Excitation : Exciton

An exciton is a neutral quasi-particle results from the Coulombic interaction between an electron and a hole. Excitons are in fact the elementary excitations in a semiconductor (Wannier-Mott exciton) as the first excited state resulting from external excitation is a bound electron-hole pair. Exciton binding energy (E_{BX}) is the energy that binds this pair (or alternately this amount of energy will be released) and spatial distance between electron-hole pair is Bohr radius, a_{BX} (Fig. 2.2).

For Frenkel type of exciton E_{BX} is high (small a_{BX}) and for Wannier-Mott exciton has low E_{BX} (large a_{BX}).E_{BX} and a_{BX} are strongly dependent on the dimensionality and quantum confinement of the system [114–116]. For a 3D system, exciton hamiltonian can be described as,

$$H_X = -\frac{\hbar^2 \nabla_e^2}{2m_e^*} - \frac{\hbar^2 \nabla_h^2}{2m_h^*} - \frac{e^2}{4\pi\epsilon\epsilon_0 |r|} \qquad (2.4)$$

13
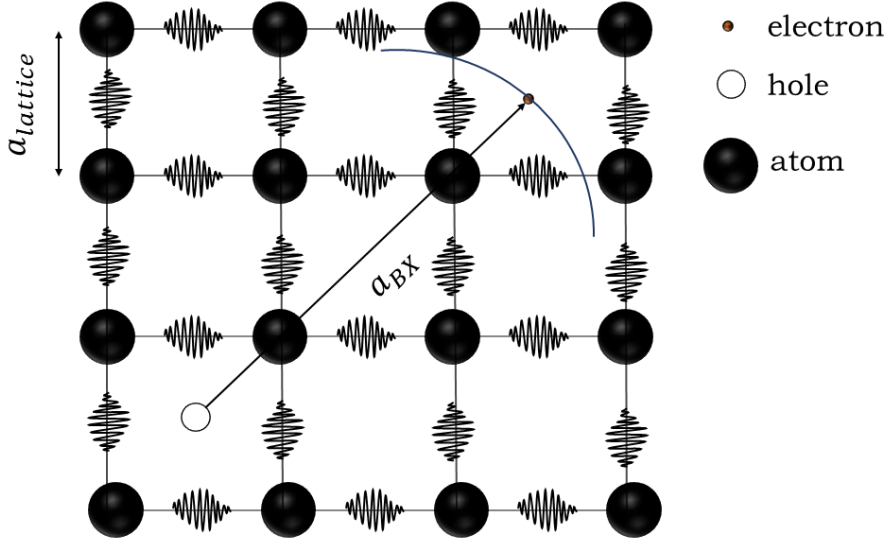
Figure 2.2: Schematic representation of an exciton inside a 2D lattice with lattice constant $a_lattice$. a_{BX} is exciton binding radius (average distance between electron and hole).

here, m_e^* and m_h^* are effective mass of electron and hole respectively inside the material, ϵ is dielectric constant of material, $|r| = |r_e - r_h|$ is the relative coordinate of the exciton. In the hamiltonian, first and second term correspond to electron and hole respectively while the third represents the interaction between them.

Considering the solution for hydrogen atom for 1s state only, we get exciton wavefunction $\psi_X(r)$, Bohr radius a_{BX} and binding energy E_{BX} as,

$$\psi_X(r) = \frac{1}{\sqrt{\pi a_{BX}^3}} exp[-\frac{r}{a_{BX}}] \tag{2.5}$$

$$a_{BX} = \frac{4\pi\hbar^2\epsilon\epsilon_0}{\mu e^2} \tag{2.6}$$

$$E_{BX} = \frac{\hbar^2}{2\mu a_{BX}^2} \tag{2.7}$$

here, $\mu = \frac{m_e^* m_h^*}{m_e^* + m_h^*}$ is the reduced mas off exciton. Considering the difference between the reduced mass μ and the free-electron mass the dielectric constant in the denominator, one can estimate that the E_{BX} is about three orders of magnitude less than the Rydberg

constant, R_y. E_{BX} and a_{BX} for some semiconductor material is shown in table 2.1. Data are taken from [107].

Table 2.1: Binding energies and Bohr radii for Wannier–Mott excitons in different semiconductor materials.

Semiconductor material	E_g (eV)	E_{BX} (eV)	$a_{BX}(A^0)$
InSb	0.237	0.5	860
Ge	0.89	1.4	360
GaAs	1.519	4.1	150
CdTe	1.6	10.6	80
GaN	3.5	22.7	40

For $M_x = m_e^* + m_h^*$ and higher state ($n = 1, 2, 3, ...$, considering beyond 1s state) exciton dispersion relation for 3D system,

$$E_{X,K,n} = E_g + \frac{\hbar^2 K_X^2}{2M_X} - \frac{E_{BX}}{n^2} \tag{2.8}$$

E_g is the band-gap energy of the material.

2.2.1 Exciton : Co-boson vs Boson

Boson are the particles following Bose-Einstein statistics. Additionally, bosons follow the symmetric wave-function rule, which allows it for macroscopic occupation of one single state. Second quantization of this wave-function gives the idea of boson creation and annihilation operator, b_0 and $b_0^\dagger$ respectively defined as,

$$b_i|n_i\rangle = \sqrt{n_i}|n_i - 1\rangle \tag{2.9}$$

$$b_i^\dagger|n_i\rangle = \sqrt{n_i + 1}|n_i + 1\rangle \tag{2.10}$$

These two operators follow commutation relationship as,

$$[b_i, b_j] = [b_i^\dagger, b_j^\dagger] = [b_i^\dagger, b_j] = [b_i, b_j^\dagger] = 0 \tag{2.11}$$

$$[b_i, b_i^\dagger] = 1 \tag{2.12}$$

15

Co-bosons or composite bosons are the bosonic particles by two fermions. From this definition, exciton is a composite bosons formed by electron and hole- two fermions. There are some differences between co-boson and elementary boson. Commutation relation for co-bosons (equation 2.11) has been modified as,

$$[B_i, B_i^\dagger] = 1 - d \tag{2.13}$$

here, $B_i(B_i^\dagger)$ is annihilation (creation) operator for co-bosons and d is deviation factor defined as,

$$d = \sum_{k_e, k_h, q_e, q_h} \langle \psi_i | k_e, k_h \rangle \langle q_e, q_h | \psi_i \rangle (\delta_{k_h, q_h} c_{k_e}^\dagger c_{q_e} + \delta_{k_e, q_e} d_{k_h}^\dagger d_{q_h}) \tag{2.14}$$

where, $\langle k_e, k_h | \psi_i \rangle$ is i^{th} state exciton wave-function in momentum space (k_e and k_h being the momentum of electron and hole respectively), $c_p(d_p)$ is annihilation operator at state p for electron (hole).

Due to presence of d, exciton is not exactly a boson, rather a composite boson [117]. Due to by such composite nature of the exciton is the uncertainty to identify an exact interaction potential between two excitons, even for the Coulomb contribution. It might be easier to identify e-e and h-h interaction but exact interaction picture between electron and hole for two excitons is ambiguous. Despite the existence of such ambiguity, most of work regarding exciton consider it as an elementary bosons.

2.3   Light Matter Interaction : Exciton Polariton

Light matter interaction can be explained from both classical and quantum perspective. Depending on interaction strength light-matter interaction can be classified into weak, strong coupling regime. Exciton polariton is a hybrid state arising due to coupling between light (cavity photon) and matter (exciton) in strong coupling regime. Before delving into detail of polariton, a brief discussion on the generic coupled state, dressed state from bare state has been discussed.

2.3.1 Dressed States

Consider two different mode (for ex. light and matter) with energy E_X and E_Y are interacting with each other by interaction energy G. Hamiltonian of such system is,

$$H = E_X x^\dagger x + E_Y y^\dagger y + G(xy^\dagger + x^\dagger y) \qquad (2.15)$$

The analysis of equation 2.15 can be made in $|x, y\rangle$ (x no of excitation in X field and y no of excitation in Y field) which is bare states (states if no interaction exists between X and Y). Due to presence of G, we can replace x and y as,

$$a = \alpha_1 x + \alpha_2 y \qquad (2.16)$$

$$b = \beta_1 x + \beta_2 y \qquad (2.17)$$

with $\alpha_1, \alpha_2, \beta_1, \beta_2 \in C$. Bosonic commutation relationship between a and b, hamiltonian (equation 2.15) implies

$$\alpha_1 \beta_1^* + \alpha_2 \beta_2^* = 0 \qquad (2.18)$$

$$\alpha_1 \beta_2^* + \alpha_2 \beta_1^* = 0 \qquad (2.19)$$

$$\alpha_1^2 + \alpha_2^2 = \beta_1^2 + \beta_2^2 = 10 \qquad (2.20)$$

For canonical unitary transformation solution of these results,

$$\alpha_1 = cos(\theta), \alpha_1 = sin(\theta), \beta_1 = -sin(\theta), \beta_1 = cos(\theta)$$

where $cos(\theta)$ is defined as,

$$cos(\theta) = \frac{\Delta + \sqrt{4G^2 + \Delta^2}}{\sqrt{2\Delta^2 + 8G^2 + 2\sqrt{4G^2 + \Delta^2}}} \qquad (2.21)$$

$\delta = E_X - E_Y$ is coined as detuning. So the substitution turns hamiltonian as (equation 2.15),

$$H = E_A a^\dagger a + E_b b^\dagger b \tag{2.22}$$

where plot for E_A and E_B are,
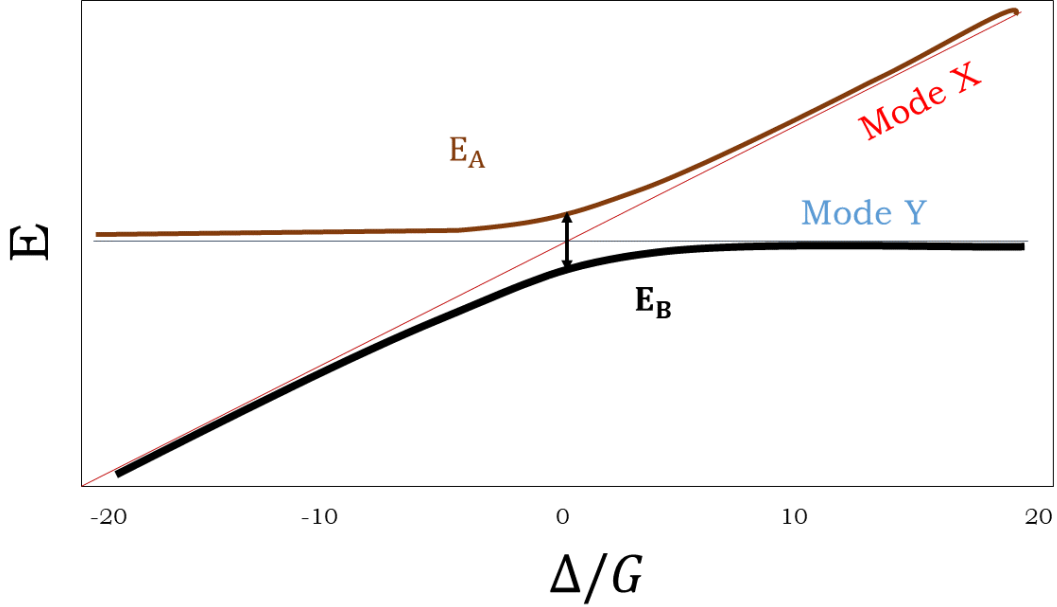
Figure 2.3: Eigen-energies for equation 2.15 as a function of detuning. Anti-crossing is observed at zero detuning. Dressed states can be suitably approximated as bare state for large detuning.

Let us consider a simple case with $\Delta = 0; E_A = E_B = E$ and coherent superposition of bare states as,

$$a = \frac{x + y}{\sqrt{2}} \tag{2.23}$$

$$a = \frac{x - y}{\sqrt{2}} \tag{2.24}$$

gives us the hamiltonian (equation 2.15),

$$H_{Dr} = (E - G)a^\dagger a + (E + G)b^\dagger b \tag{2.25}$$

For a dressed state $|n, m\rangle$ this hamiltonian ($H_D r|n, m\rangle = E(n, m)|n, m\rangle$) gives us the energy,

$$E(n, m) = E(n + m) - G(n - m) \tag{2.26}$$

If one excitation is taken away from the system, new state will be either $|n-1, m\rangle$ or $|n, m-1\rangle$ resulting in either $E(n+m-1) - G(n-m-1)$ or $E(n+m-1) - G(n-m+1)$. Existence of such two state upon transition is known as 'Rabi Doublet' although they remain in the same manifold in Fock space. Energy difference between two states is $2G$. This case is shown in Fig. 2.4 for H_2 manifold to H_1 manifold transition.
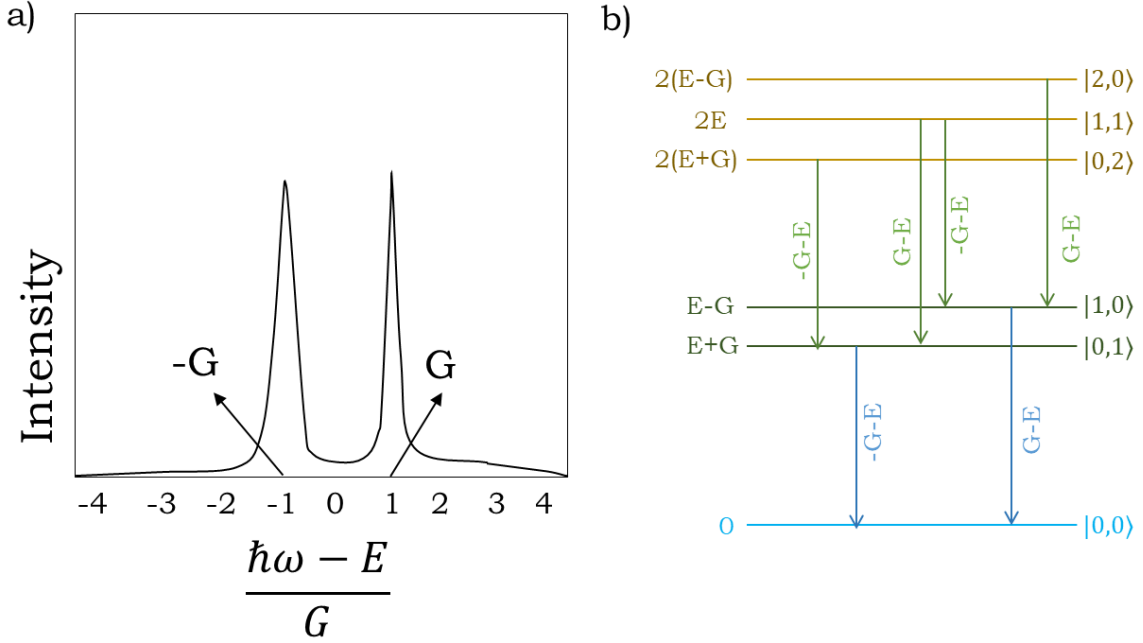
Figure 2.4: (a) Rabbi Doublet energy density diagram for dressed boson. (b) Transition from H_2 to H_1 to H_0 (vacuum state). H_2 manifold contains total 2 particles. There are 4 possible ways of this transition. Corresponding energy release for each possible configuration is shown.

2.3.2 Strong Coupling Regime

Exciton photon interaction strength ($\hbar g$) is governed by [118],

$$\hbar g = \sqrt{\frac{\pi e^2 f}{\epsilon \epsilon_0 m_e^* V}} \tau \tag{2.27}$$

Term τ contains overlap integral of the electron and hole wave-function, the angular momentum conservation term governed by the selection rule, and the projection of exciton dipole moment onto the photon field. Exciton oscillator strength f is defined as,

$$f = \frac{2m_e^*\omega}{\hbar}|\langle u_v|\vec{r}.\vec{E}|u_v\rangle|\frac{V}{\pi a_{BX}^3} \tag{2.28}$$

where, $u_c(u_v)$ is electron (hole) Bloch function, ω is incident photon frequency, $\vec{E}$ is photon field, V is interaction volume.

In a cavity with high Q factor, a periodic, reversible energy exchange between excitons and photons at a rate of $\hbar g$ which can be larger than exciton and cavity photon decay rate, γ_X and γ_c respectively. If $\hbar g >> (\gamma_X - \gamma_c)/2$ then, there is at least one coherent energy transfer between the exciton and the photon before they decay out of coherence. The interaction strength or energy transfer rate $\hbar g$ is often referred to as the 'vacuum Rabi splitting', whereas the periodic energy transfer phenomenon is commonly known as Rabi oscillation.

2.3.3   Exciton Polariton

Exciton polariton emerges as new eigenstate due in strong coupling regime. Hamiltonian for a strong coupling regime or alternatively hamiltonian for exciton polariton can be written as,

$$H_{pol} = E_{X,K}a_K^\dagger a_K + E_c c_K^\dagger c_K + \frac{\hbar g_K}{2}(c_K^\dagger a_K + a_K^\dagger c_K) \tag{2.29}$$

$E_{X,K}$ is defined in equation 2.8, E_c in equation 2.2, $a_K(c_K)$ is the annihilation operator for exciton (cavity photon). Employing a similar linear substitution of 2.16 and 2.17,

$$p_{LP,K} = X_K a_K + C_K c_K \tag{2.30}$$

$$p_{UP,K} = X_K a_K - C_K c_K \tag{2.31}$$

we can turn hamiltonian 2.29 into,

$$H_{pol} = E_{LP,K}p_{LP,K}^\dagger p_{LP,K} + E_{UP,K}p_{UP,K}^\dagger p_{UP,K} \tag{2.32}$$

X_K and C_K, the Hopfield coefficients are defined as,

$$|X_K|^2 = \frac{1}{2}\left[1 + \frac{\Delta_K}{\sqrt{\Delta_K^2 + (\hbar g)^2}}\right] \tag{2.33}$$

$$|C_K|^2 = \frac{1}{2}\left[1 - \frac{\Delta_K}{\sqrt{\Delta_K^2 + (\hbar g)^2}}\right] \tag{2.34}$$

This coefficients effectively determine the exciton fraction (X_K) and photon fraction (C_K) of the hybrid exciton polariton particles. From equation 2.32 dispersion relationship for $E_{LP,K}$ and $E_{UP,K}$ are,

$$E_{LP/UP,K} = \frac{1}{2}\left[E_{X,K} + E_c \pm \sqrt{(\hbar g)^2 + \Delta_K^2}\right] \tag{2.35}$$

where + indicates the dispersion relationship for $E_{UP,K}$, upper polariton branch and + indicates the dispersion relationship for $E_{LP,K}$, lower polariton branch.
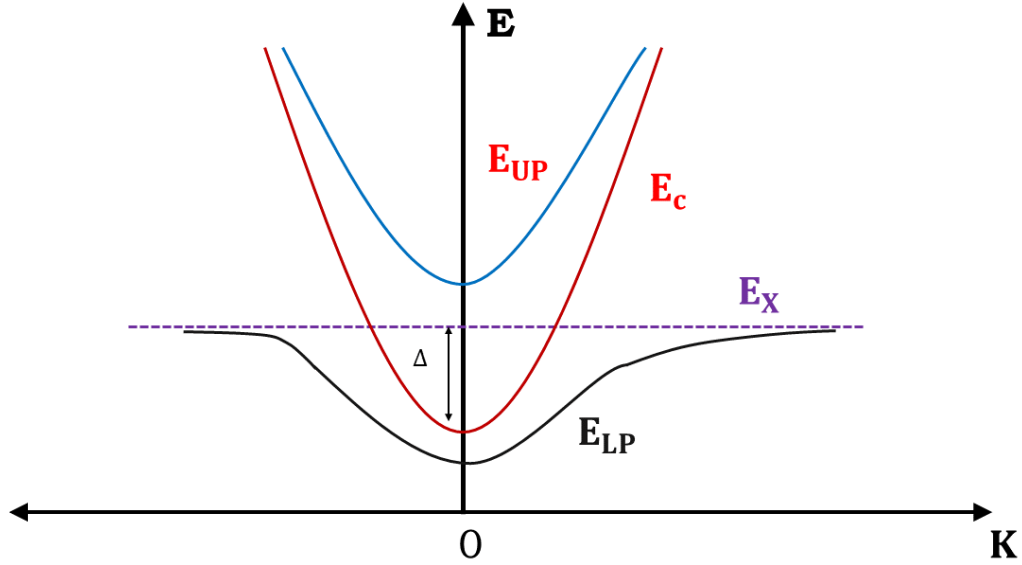
Figure 2.5: Exciton polariton dispersion relationship from equation 2.35, blue and black curve are for E_{LP} and E_{UP} dispersion respectively.

At high k LP branch becomes exciton like and UP branch is cavity photon like. From equation 2.33, 2.34 and 2.35 it is clear that detuning Δ_K plays an important role in determining the dispersion relation and hopfield coefficient. That is why at small k, LP branch is more photon like for negative detuning and exciton like for positive detuning.

Another aspect of exciton polariton is its mass is different from M_X and m_c. Effective polariton mass is two fold, one is lower polariton mass (m_{LP}) and another is upper polariton mass (m_{UP}), defined as,

$$\frac{1}{m_{LP}} = \frac{|X_K|^2}{M_X} + \frac{|C_K|^2}{m_c} \tag{2.36}$$

$$\frac{1}{m_{UP}} = \frac{|X_K|^2}{m_c} + \frac{|C_K|^2}{M_X} \tag{2.37}$$

Despite polariton mass being a mathematical function of exciton and photon mass, near $k \approx 0$ polariton mass is dominated by m_c as exciton mass is often many times larger than cavity photon mass.

This far, we do consider lifetime of interacting modes to be infinite ($\gamma_X = \gamma_c = 0$) which is not even close to ideal. Considering a finite γ_X and γ_c, polariton hamiltonian can be modified as,

$$H_{pol} = \begin{bmatrix} E_c + i\gamma_c & \frac{\hbar g}{2} \\ \frac{\hbar g}{2} & E_{X,K} + i\gamma_X \end{bmatrix} \tag{2.38}$$

which gives us LP and UP branch dispersion relationship as,

$$E_{LP/UP,K} = \frac{1}{2}\left[E_{X,K} + E_c + i(\gamma_X + \gamma_c) \pm \sqrt{(\hbar g)^2 + [\Delta_K + i(\gamma_c - \gamma_X)]^2} \right] \tag{2.39}$$

From equation 2.35 and 2.39, presence of homogeneous and non-homogeneous broadening modify effective Rabi splitting.

2.4 Polariton Lasing

Due to bosonic (composite bosonic) nature of exciton polariton macroscopic condensation of ground can facilitate lasing action of polariton particles. In this section, a somewhat detailed discussion of polariton scattering events, LP relaxation, stimulated scattering, fundamental contrast between polariton and photon lasing is provided.

2.4.1 Polariton Lifetime and Scattering Events

After a finite time (τ_p), polariton decays radiatively as a photon. Lifetime for LP and UP can be expressed as,

$$\frac{1}{\tau_{LP,K}} = \frac{|X_K|^2}{\tau_X} + \frac{|C_K|^2}{\tau_c} \tag{2.40}$$

$$\frac{1}{\tau_{UP,K}} = \frac{|X_K|^2}{\tau_c} + \frac{|C_K|^2}{\tau_X} \tag{2.41}$$

In many cases, the exciton lifetime ($\tau_X = 1/\gamma_X$) is in the order of much much greater than cavity photon lifetime ($\tau_c = 1/\gamma_c$). This indicates that the τ_p is governed by the τ_c which in turn depends on cavity property i.e. Q-factor. For GaN with detuning 20 meV, recombination rate (in meV) is shown is Fig. 2.6. Clearly at higher K, LP lifetime gets closer to exciton one wheres and UP lifetime gets closer to cavity photon lifetime. Detail of these radiative recombination rate calculation can be found [119]. For calculating radiative recombination rate, γ_c is taken as 1.6 meV and γ_X is taken as zero.

Due to constituent excitonic fraction, polaritons may undergo three different types of scatterings before decay. These are,

1. Polariton-photon scattering.

2. Polariton-polariton scattering.

3. Polariton-electron scattering.

1. Polariton-photon scattering [107]: Phonon are quantized lattice vibration which can effectively scatter polariton. Polariton can be effectively scattered by both optical and acoustic phonon but at low temperature probability for acoustic phonon scattering is low due to its high energy. Scattering rate between polariton state at K_i (initial wave vector) and K_f (final wave vector) can be written according to Fermi's golden rule,

$$W^{ph}(K_i \rightarrow K_f) = \frac{2\pi}{\hbar} \sum_q |M(q)|^2 (\theta_\pm + N_{ph}(q)) \delta(E(K_f) - E(K_i) \pm E^{ph}(q)) \tag{2.42}$$
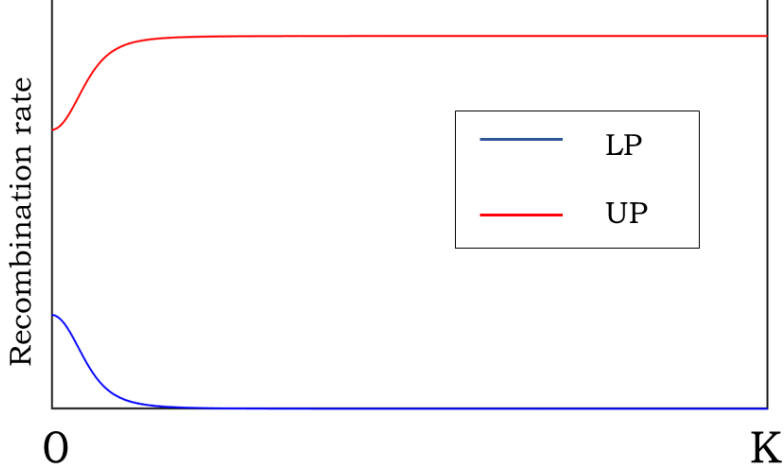
Figure 2.6: Radiative recombination rate for upper and lower polariton branch. Interaction strength is taken as 35 meV.

here, $+$ is for phonon emission and $-$ is for absorption and N_{ph} is Bose distribution of phonon with wave vector q and $|M(q)|$ is matrix element of interaction between polariton and phonon defined as,

$$|M(q)|^2 = |X_{K_i}|^2 |X_{K_f}|^2 |\langle \psi_X(K_i)|H_q^{pol-ph}|\psi_X(K_f)\rangle|^2 \tag{2.43}$$

H_q^{pol-ph} is polariton phonon interaction hamiltonian. For acoustic phonon, equation 2.43 reads,

$$M^{ac}(q) = \sqrt{\frac{e}{2\mu\rho uSL}} D_e D_h \left[1 + \left(\frac{m_e^* q a_{BX}}{2M_X}\right)\right]^2 \left[1 + \left(\frac{m_h^* q a_{BX}}{2M_X}\right)\right]^2 \tag{2.44}$$

here, ρ is material density, u is speed of sound inside the material, $D_e(D_h)$ is conduction (valance) band deformation potential and S, L are normalization area, microcavity length respectively. Matrix element for optical phonon with energy $E^{Oph}(q)$ reads,

$$M^{Oph}(q) = -\frac{e}{q}\sqrt{\frac{4\pi E^{Oph}(q)}{SL\epsilon_0}\left(\frac{1}{\epsilon_h} - \frac{1}{\epsilon_l}\right)} \tag{2.45}$$

ϵ_h and ϵ_l are the high frequency (optical) and low frequency (static) dielectric constant respectively.

2. Polariton-polariton scattering [107]: Due to dipole-dipole interaction between excitonic component of polariton, polariton-polariton scattering can effectively redistribute polariton population among the states. This is most effective scattering mechanism for stimulated scattering and macroscopic ground state occupation. Polariton-polariton scattering rate can be defined as,

$$W^{pol}(K_i \rightarrow K_f) = \frac{2\pi}{\hbar} \sum_q |M^{ex}|^2 |X_{K_i}|^2 |X_{K_f}|^2 |X_q|^2 |X_{q+K_f-K_i}|^2 N(q)(1+N(q+K_f-K_i))$$

$$\delta(E(K_f) - E(K_i) + E(q + K_f - K_i) - E(q)) \quad (2.46)$$

q is the momentum exchanged during scattering event and N is polariton Bose distribution. Polariton–polariton scattering has been shown to be extremely efficient for a resonantly excited microcavity. even for non-resonant excitation. This scattering events can solely self-thermalize the whole exciton depending on the excitation condition and on the nature of the semiconductor.

3. Polariton-electron scattering [107]: Polariton-electron scattering is more efficient than polariton-phonon scattering du to the small effective mass of electron and strong charge-dipole interaction. For optical pumping, electron polariton scattering can be imitated by exciting a secondary quantum well adjacent to the emitter of the microcavity [120]. Polariton-electron scattering rate can be written as,

$$W^{el}(K_i \rightarrow K_f) = \frac{2\pi}{\hbar} \sum_q |M^{el}(q, K_i, K_f) + M^{el}(q, K_i, K_f)|^2 |X_{K_i}|^2 |X_{K_f}|^2 N_e(q)$$

$$(1 + N_e(q + K_f - K_i))\delta(E(K_f) - E(K_i) + E_e(q + K_f - K_i) - E_e(q)) \quad (2.47)$$

where, N_e is Fermi distribution $E_e(q)$ is defined as $\frac{\hbar^2 q^2}{2m_e^*}$. The polariton–electron interaction is a dipole-charge interaction that takes place on a picosecond time scale. An equilibrium electron gas can thermalize a polariton gas quite efficiently. A more complex effect may, however, take place such as trion formation or exciton dephasing.

2.4.2 LP Relaxation and Bottleneck Effect

Relaxation of energy (with momentum) along LP branch dispersion and eventual accumulation close to the ground state is related to polariton lasing phenomenon. In this context, the LP dispersion can be divided into three regions: polariton-trap region (I), bottleneck region (II) and thermalization region (III) as shown in Fig. 2.11. With external pumping, the electron-hole plasma form excitons which inside a microcavity with high Q strongly couple with photons to form polaritons.
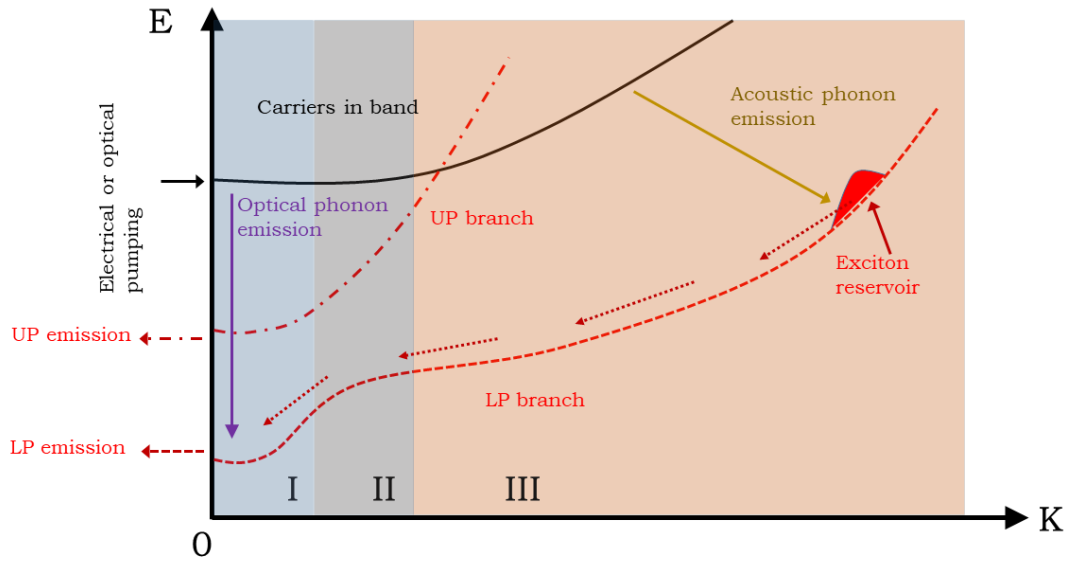
Figure 2.7: LP relaxation along LP dispersion indicating different region of interest.

Initial formation of excitons is incoherent. These excitons, having high energy and momentum (K) effectively form 'exciton reservoir' (red area in LP dispersion branch). At high in-plane momenta of the polariton dispersion, polaritons are essentially exciton-like and therefore they have relatively long lifetimes, heavy effective masses and large density of states (DOS). As a result, over region III of dispersion, phonon mediated LP relaxation processes are very efficient over the thermalization region (Fig. 2.7). The energy difference between the bottleneck region (region II) and $K = 0$ state of the LP dispersion is known as 'polariton-trap depth'. As can be observed from Fig. 2.7, in the polariton dispersion, LP relaxation from the bottleneck (region II) down to the polariton-trap (region I) requires a significant change of energy (*polariton-trap depth*), and a simultaneous small change of momentum [121] and alternatively this in order to get out of region I, LP need to hurdle

this amount of energy. Close to region I, the polariton lifetime decreases by about two orders of magnitude and becomes significantly smaller than the timescales of acoustic phonon scattering, the dominant scattering mechanism at low temperatures. Also, the polariton effective mass decreases by about 4 orders of magnitude in this region, thereby significantly reducing the LP DOS. As a result, at low pump densities, there is also a lack of polariton-polariton scattering in this transitional region. In the presence of these effects, which are altogether known as the bottleneck effect. it is very likely that polaritons will decay as photons before they can relax down to the bottom of the polariton trap. There are several ways of overcoming the bottleneck effect in semiconductor microcavities. These are the following.

- *increased the pumping density:* This increases polariton-polariton scattering rate. But the system may cease to be in the strong-coupling regime if the pumping density becomes comparable to the Mott density. The scattering rate can be enhanced by increasing the exciton fraction near the bottleneck region. This can be attained by increasing positive detuning. However if the positive detuning is too large, the polaritons essentially become excitons.

- *Increased temperature:* This will increase phonon scattering rate. But this also results homogenous broadening of the exciton linewidth. Moreover excitons tend to dissociate if the $K_B T$ value is higher than the corresponding exciton binding energy, where K_B is the Boltzmann constant.

- *Excess carrier:*By introducing excess carriers in the form of modulation doping, the polariton electron scattering rate can be enhanced.

2.4.3   Polariton Lasing Dynamics and Stimulated Scattering

The polariton lasing dynamics can be described using the semiclassical Maxwell-Boltzmann rate equations. In this context, if N_K is defined as the LP occupation at at state with momentum K, then its rate of change is given by,

$$\frac{dN_K}{dt} = P_K - \frac{N_K}{\tau_{LP,K}} - \sum_{K_f} W(K \to K_f) N_K (1 + N_{K_f}) + \sum_{K_f} W(K_f \to K) N_{K_f} (1 + N_K)$$

(2.48)

where, P_K is pumping rate, $W(K \to K_f) = W^{ph}(K \to K_f) + W^{pol}(K \to K_f) + W^{el}(K \to K_f)$ is the net scattering rate. These scattering events are explained in 2.4.1. When $N_K \ll 1$, phonon scattering dominates LP relaxation process. With the increase of external pumping density , $W^{pol}(K_i \to K_f)$ becomes prominent. Because energy and momentum is conserved during this scattering process, polariton-polariton scattering process plays a substantial role in overcoming the relaxation bottleneck. During a single polariton-polariton scattering event, a LP from the bottleneck region may relax down to the polariton trap and at the same time a LP is scattered from the bottleneck region to a higher energy, exciton-like state. This process, which is also known as pair-scattering, is an incoherent two-body scattering process [122]. As the LP occupation increases (especially N_0), pair-scattering increases quadratically in the system and at a sufficiently high pumping density, LP relaxation to the final state i.e. to the ground state is dominated by the term $(1 + N_0)$ where N_0 is the ground state population in equation 2.48. Under this condition, the overall scattering rate increases non-linearly by what is known as the Bosonic final state stimulation. The enhanced scattering initiated by this Bose-Einstein statistical process is known as 'stimulated scattering'. This is a phase coherent process where both polariton-polariton and polariton-phonon scattering rates are enhanced significantly. Because $N_0 \gg 1$ for stimulated scattering to take place, it can be said that the system achieves quantum degeneracy during this process. This means a macroscopic population of polaritons having same energy, momentum and phase builds up at the ground state. Because of the short lifetime, these polaritons though may nor attain thermal equilibrium with the lattice, they can remain at a metastable condensed state where they are in thermal equilibrium among themselves. Hence it can be said that the stimulated scattering process leads to the formation of a non-equilibrium polariton condensate. This process is often referred to as the 'dynamic condensation' of polaritons. The formation of such a quasi- or non-equilibrium degenerate condensate means that upon decay by means of spontaneous

radiative recombination, the exciton-polaritons will generate coherent light output and the system will act as a coherent emitter i.e. a laser. Though there is no stimulated emission of radiation, but only stimulated scattering in the process, the misnomer of 'polariton laser' is commonly used to indicate its operation as a coherent light source.
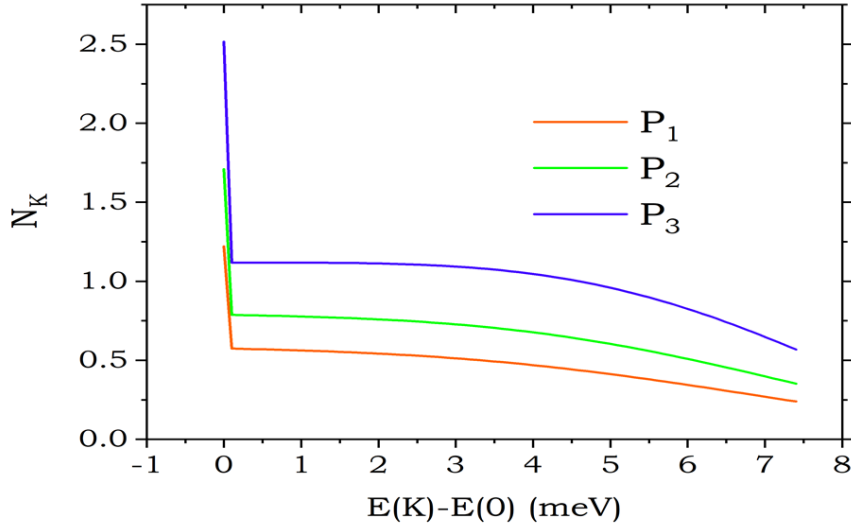
Figure 2.8: Numerical solution of equation 2.48 for three different pumping rate with $P_3 > P_2 > P_1$.

In Fig. 2.8 numerical solution of coupled rate equation 2.48 is shown. Detail of this solution and other technique will be discussed later. A close observation of solution reveals the appearance of macroscopic ground state with $N_0 >> 1$ which enables 'stimulated scattering' process.

2.4.4 Polariton Lasing vs Photon Lasing

We will finish this chapter by showing the distinctions between polariton and photon lasing. In conventional photon lasers, 'stimulated emission' is source of lasing. Population inversion (electronic inversion of the system $N_1 > N_2$ with $E_1 > E_2$) initiates this sort of stimulated emission. This 'stimulated emission' is also reason behind the light amplification (photon generated by stimulated emission > photon lost due to decay or absorption). On the other hand, the underlying dynamics of polariton lasing is the

'stimulated scattering' process, which is the result of stimulation of Bosonic final state in the ground state of the polariton dispersion. The coherent emission in this case is generated by spontaneous radiative recombination of the degenerate polariton condensate (degenerate state in the ground state, N_0). Therefore, whereas photon loss has to be balanced by stimulated emission in a photon laser, in a polariton laser stimulation and emission processes are independent, thereby eliminating the requirement of 'population inversion'. For this reason a polariton laser is often referred to as an 'inversion-less laser'.

Besides the physics, several distinct differences are observed between the output characteristics of polariton and photon lasers. These are the following.

- Low effective mass and DOS of polaritons forces the lasing threshold can be 2-3 orders of magnitude lower than an equivalent photon laser. The photon lasing threshold has to be larger than the transparency density (pumping density at which losses are equal to the gain). This density is always several orders of magnitude higher than the critical density.

- Collapse of the emission line-width at the edge of lasing is observed for both polariton and photon lasers. For both the cases, there is an associated coherence time, $\tau_{coh} = \frac{\lambda^2}{c\Delta\lambda}$ with λ is the emission wavelength, c is the speed of light and $\Delta\lambda$ is the emission line-width. In a photon laser, the coherence time increases in proportion to the photon occupation number and the line-width decreases accordingly to reach the Schawlow-Townes line-width limit. However in a polariton laser, polariton-polariton scattering in the non-equilibrium degenerate condensate leads to the loss of coherence time and corresponding increase of the emission line-width.

- Unless there is screening of the built-in electric field, as in GaN-based quantum well lasers, a red-shift of the emission peak in photon lasers may be observed because of device heating. However, in polariton lasers the emission peak blue-shifts because of energy re-normalization caused by polariton-polariton scattering in the non-equilibrium polariton condensate.

- The spontaneous coupling factor β, which is a measure of the fraction of spontaneous emission coupled to the lasing mode, is usually greater than 0.01 in microcavity

photon lasers because of Purcell effect. However in the polariton lasing regime, spontaneous emission emerges in the polariton mode which undergoes stimulated scattering and hence β is usually significantly smaller [67].

- Polariton lasers exhibit a characteristic magnetic field dependent Zeeman splitting because of the exciton-fraction of polaritons. As photon lasing is mediated by stimulated emission of uncoupled cavity photons in the weak coupling regime, such a magnetic field dependence is not observed [123].

2.5 Bound Exciton

This research work will mainly focus on the effect of defect on exciton-polariton system. A short description of bound exciton is given for convenience. For a defective system (system with any type of defect e.g. point defect, dislocation, impurity (intentional or doped), vacancy) free exciton localized at potential trap formed by defect, lose all its kinetic energy and formed 'bound exciton'. These excitons are not mobile as they are fixed in space-time. They do not thermalize like the free exciton. Bound exciton formation is dependent on the nature of defect (ionized defect, neutral dopant, dislocation). Nature of such excitons will be described in short in this section.

2.5.1 Exciton bound to ionized defect (donor/acceptor)

The capturing event of a free exciton can be stated as,

$$FE + T^{+/-} = T^{+/-}X + E_1 \tag{2.49}$$

Here, FE = free exciton, $T^{+/-}$ = ionized defect (donor (+)/ acceptor (-)), $T^{+/-}X$ = Bound exciton, E_1 = energy released by exciton during localization (or alternatively energy required to convert a bound exciton into a free one).

Radiative recombination of these bound exciton gives D^+X or A^-X line in photo luminescence spectra. Simultaneous existence of both D^+X and A^-X is not possible. A stable ionized defect bound exciton is only possible under certain condition [124]. For D^+X this condition implies, $\sigma = m_e/m_h < 0.43$ for A^-X, $\sigma > 0.43$. E_1 becomes negative beyond this region and it is energetically favorable for exciton to remain free rather than

bound to an ionized defect.

2.5.2 Exciton Bound to Neutral Defect (Donor/Acceptor)

At any value of σ, a stable neutral defect bound exciton is stable. Formation of neutral defect bound exciton can be represented as,

$$FE + T^0 = T^0X + D_1 \tag{2.50}$$

D_1 = Disassociation energy of exciton.

For any arbitrary value of σ, D_1 stays positive (although can vary depending on defect type). So, exciton bound to neutral donor is energetically favorable.

Due to presence of another particle (electron in neutral donor and hole neutral acceptor), exchange interaction between bound exciton and the existing particle causes energy level to split. The calculation for exciton bound to neutral donor has been shown below. The approach followed has been discussed detail by Ungier and Suffczyriski [91]. The wavefunction of these three particles (electron and hole from exciton and another electron/hole from defect) can be written as,

$$\psi_m = \sum_{k_1,k_2,k_3} A(k_1, k_2, k_3)|\psi\rangle \tag{2.51}$$

where the slater determinant $|\psi\rangle$ is,

$$|\psi\rangle = \frac{1}{\sqrt{2}}[\psi_{k_1}(r_1)\psi_{k_2}(r_2) - \psi_{k_2}(r_1)\psi_{k_1}(r_2)]K\psi_{k_3}^*(r_3) \tag{2.52}$$

In equation 2.52, r_1 and r_2 corresponding to two electrons coordinate and r_3 corresponding to hole coordinate. K is time reversal operator. k_1, k_2, k_3 are corresponding to electron 1, electron 2 and hole wave-vector respectively. Equation (10) is the result of anti-symmetric condition followed by fermion (Same goes for co-efficient A, $A(k_1, k_2, k_3) = -A(k_2, k_1, k_3)$). So equation 2.51 becomes,

$$\psi_m = \frac{1}{\sqrt{2}} \Big[\sum_{k_1,k_2,k_3} c_1 A(k_1, k_2, k_3)[\psi_{k_1}(r_1)\psi_{k_2}(r_2) - \psi_{k_2}(r_1)\psi_{k_1}(r_2)]$$
$$- \sum_{k_1,k_2,k_3} c_2 A(k_2, k_1, k_3)[\psi_{k_1}(r_1)\psi_{k_2}(r_2) - \psi_{k_2}(r_1)\psi_{k_1}(r_2)]]\psi_{k_3}^*(r_3) \quad (2.53)$$

Due to exchange interaction between $\psi_{k_1}(r_1)$ and $\psi_{k_2}(r_2)$ energy of bound exciton is not exactly the same as that of free exciton. Hamiltonian for can be written as,

$$\begin{bmatrix} H + W^+ & W^- \\ W^- & H + W^+ \end{bmatrix} \begin{bmatrix} c_1 X_1 \\ c_2 X_2 \end{bmatrix} = E \begin{bmatrix} c_1 X_1 \\ c_2 X_2 \end{bmatrix} \quad (2.54)$$

In equation 2.54, X is the Fourier transform of A, H is Hamiltonian of defective system without exchange interaction and exchange part of Hamiltonian is determined as,

$$W^+ = \langle\psi(r_1)|\frac{e^2}{|r_1 - r_3|}|\psi(r_3)\rangle + \langle\psi(r_2)|\frac{e^2}{|r_2 - r_3|}|\psi(r_3)\rangle$$
$$W^+ = \langle\psi(r_1)|\frac{e^2}{|r_1 - r_3|}|\psi(r_3)\rangle - \langle\psi(r_2)|\frac{e^2}{|r_2 - r_3|}|\psi(r_3)\rangle$$

This exchange interaction results in a split of bound exciton energy. Here we show the case for neutral donor. Same energy splitting occurs for neutral acceptor.

2.5.3 Multiple Bound Exciton Complexes (MBEC)

It has been proven experimentally that a single defect center can trap several excitons [125]. This multi exciton complexes formation is harder as exciton number increases as the localization energy for bound exciton decreases. After a certain number of excitons, free exciton is energetically favorable than adding another one to the complex. Formation of multi exciton complex around a neutral defect can be expressed as,

$$FE + T^0 = T^0X + D_1^1$$

$$2FE + T^0 = T^0XX + D_1^1 + D_2^1$$

$$3FE + T^0 = T^0XXX + D_1^1 + D_2^1 + D_3^1$$

here D_i^m stands for disassociation energy for m^{th} exciton.

During further calculation, we consider the bound exciton in lower energy level. Any bound state has been modeled as ,

$$\psi_b(r) = Cexp(-\alpha r) \tag{2.55}$$

where, α is a phenomenological parameter. For bound exciton, defect size is considered to be big enough to quantize the exciton as a whole. In case of bound electron/hole, same wavefunction has been considered with different normalization constant C.

Chapter 3

Condensation of Exciton-Polariton Quasi-particle

Is our universe strange or we think in a strange way? Or all the strange result the universe is presenting us is due to way of thinking? Study of quantum mechanics give me such revelation. Quantum mechanics bring about some strange result beyond our strangest imagination. One of its fascinating strange result is the concept 'Bose-Einstein Condensation' or BEC. For a long time most physicists considered this concept merely as a mathematical construct developed by Alber Einstein in 1925 [38]. Only after the discovery of such event in 1995 [5] convinced science community about the actual existence of such exotic state of matter. In this chapter, a detail discussion of BEC following by condensation of quasi-particle like exciton-polariton will be presented.

3.1 Overture

Bosons are fundamental particles follows many particle wave-function symmetry with Bose-Einstein statistics,

$$n[E(i), T, \mu] = \frac{1}{exp\left(\frac{E(i)-\mu}{k_B T}\right) - 1} \tag{3.1}$$

here, μ is the chemical potential (energy required to add one particle to the system). Consider total $N(= \sum_{E(i)} n_i)$ no. of particles with parabolic dispersion relation and mass m are placed inside a square potential of volume V in 3-D space. From equation 3.1, N can be divided into two parts, particles occupying ground state (N_0) and particles not

occupying the ground state or particles in the excited states (N_E) with definition as,

$$N = N_0 + N_E = \frac{1}{exp\left(\frac{-\mu}{k_B T}\right) - 1} + \sum_{E(i) \neq 0} + \frac{1}{exp\left(\frac{E(i)-\mu}{k_B T}\right) - 1} \tag{3.2}$$

Considering bosonic wave-function $\psi(x, y, z)$ follows periodic boundary condition, in the thermodynamic limit excited state total population becomes,

$$N_E = \frac{V}{\lambda_T^3} g_{3/2}\left(exp\left[\frac{-\mu}{k_B T}\right]\right) \tag{3.3}$$

where, De broglie wavelength λ_T is defined as,

$$\lambda_T = \sqrt{\frac{2\pi\hbar^2}{m k_B T}} \tag{3.4}$$

and function $\zeta_n(p)$,

$$g_n(p) = \frac{1}{\Gamma(n)} \int_0^\infty \frac{x^{n-1}}{z^{-1}e^x - 1} \tag{3.5}$$

Integral 3.4 converges for $z \leq 1$ and $\zeta_{3/2}(1) = 2.16 = \zeta(3/2)$, the Riemann zeta function. So a hard and fast condition on the value of N_E is,

$$N_E \lambda_T^3 \leq \zeta(3/2) \tag{3.6}$$

If particles number are increased beyond this limit, extra particles will start to accumulate in the ground state and create a macoscopically occupied state. This phenomenon is defined as 'Bose Einstein Condensation' or BEC.

BEC can occur for a fixed no of particles by reducing temperature as reduced cause the distribution function to change and cause the value of N_E to decrease. This temperature, at which the macroscopic ground state occupation starts is known as critical temperature, T_c and is defined as [126] for fixed density $n = N/V$,

$$T_{BEC} = \frac{2\pi\hbar^2}{k_B m} \left[\frac{n}{\zeta(3/2)}\right]^{\frac{2}{3}} \tag{3.7}$$

Most often this critical temperature is in nK range which is one of the factor for 70 years delay in discovering of BEC.
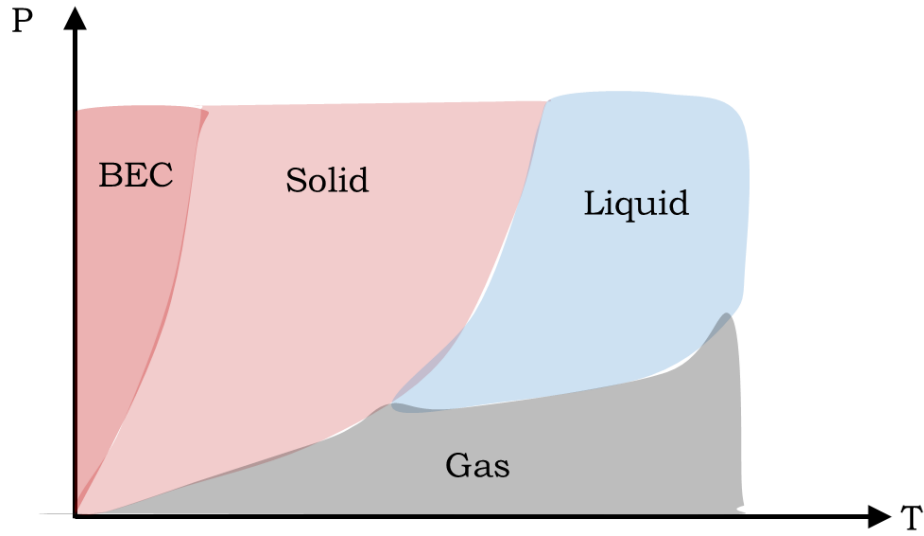
Figure 3.1: Phase diagram indicating different zone Solid, Liquid, Gas and BEC region. BEC region lies as a subset of solid region.

BEC is considered a metastable phase of matter. A close look at phase diagram of Fig. 3.1 gives us the insight that Bose-Einstein condensed gas can only exist as metastable condition as stable state of matter is solid at this temperature and pressure. Conditions for such metastability are,

- *Low density of gas:* Low density of gas prevents collision among the particle, especially three body collision to form the solid state.

- *Internal thermalization:* Gas phase thermalized internally quickly to prevent it come in canonical ensemble with the external system.

- *Longer lifetime for Bose gas particles:* Longer lifetime ensures that it will take longer time for gas particle to enter solid phase than to reach BEC phase.

3.2 Fundamentals of BEC

Some important concepts to understand BEC will be discussed in this section. These topic are order parameter, spontaneous symmetry breaking, Goldstone boson, off-diagonal long rang range order.

3.2.1 Order Parameter

Order parameter is a physical observable that identifies a phase transition for example liquid to solid, superfluid to normal fluid etc. Based on how order parameter changes during a phase transition, phase transition can be first order and second order. BEC is also a state of matter (Fig. 3.1). So transition from normal gas condensed gas is associated with a change in order parameter.

As we have already established that, BEC state of matter is a macroscopic occupation of ground state. A normal state of bosons in Fock space can be expressed as,

$$|N_0, N_1, ..., N_k, ...\rangle = \frac{(b_0^\dagger)^{N_0}}{\sqrt{N_0!}}|0\rangle \otimes \frac{(b_1^\dagger)^{N_1}}{\sqrt{N_1!}}|0\rangle \otimes ... \frac{(b_k^\dagger)^{N_k}}{\sqrt{N_k!}}|0\rangle... = \otimes \prod_k \frac{(b_k^\dagger)^{N_k}}{\sqrt{N_k!}}|0\rangle \qquad (3.8)$$

If ground state occupation N_0 is much greater than other states, $N_0 = N >> N_1, N_2, ...N_k$, we can consider effectively all the particles accumulated in ground state for simplicity. Later we consider a more general state with particles in all state. In case of all particle N is ground state and other states being empty, we can rewrite the effective representation of BEC state in Fock space as,

$$|N, 0, 0, ...\rangle = \frac{(b_0^\dagger)^N}{\sqrt{N!}}|0\rangle \qquad (3.9)$$

Before moving further we need to discuss in brief about field operator, Bosonic field annihilation operator $\hat{\psi}_b(r)$, which annihilates a boson at position r can be expressed using bosonic annihilation operator (b_i) as,

$$\hat{\psi}_b(r) = \sum_i \psi_i(r)b_i \qquad (3.10)$$

here, $\psi_i(r)$ is single particle wavefunction for state i and can be as simple as $\frac{1}{\sqrt{\kappa}}exp(i\vec{p}.\vec{x})$ for free boson to more complicated case. This single particle wavefunction follows orthogonality condition in both space and time domain as,

$$\int \psi_i(r)\psi_j^*(r)dr = \delta_{ij} \qquad (3.11)$$

$$\sum_i \psi_i(r)\psi_i(r') = \delta(r - r') \tag{3.12}$$

As a result, bosonic field operator follows bosonic commutation rule. This enables us to write bosonic operator in momentum space in terms of bosonic field operator utilizing Fourier transform as,

$$b_i = \int dr \psi_I(r)\hat{\psi}_b \tag{3.13}$$

Replacing bosonic creation operator with bosonic field creation operator (equation 3.13) in equation 3.9, we got the following form of BEC state in Fock space.

$$|N, 0, 0, ...\rangle = \frac{1}{\sqrt{N!}} \left[\int dr \psi_0(r)\hat{\psi}_b^\dagger \right]^N |0\rangle \tag{3.14}$$

From equation 3.14, the macroscopic wavefunction of ground state, $\psi_{BEC}(r)$ is formed by N bosons each with same wavefunction $\psi_0(r)$ and can be expressed as,

$$\psi_{BEC}(r) = \sqrt{N}\psi_0(r) \tag{3.15}$$

The expectation value of $\psi_{BEC}(r)$ gives us N, total particle number of the system. This is the idea of 'order parameter'. In normal gaseous state above critical BEC temperature T_{BEC}, wavefunction with N different in different states would be much different than the one in equation 3.15 and also gives a very different expectation value than N.

To remove the no-ideal case of all particles in ground state, we now consider a N particle system with most of then in ground state but other states also have some bosons. In that case, bosonic field operator can be expressed as,

$$\hat{\psi}_b(r) = \psi_0(r)b_0 + \sum_{i \neq 0} \psi_i(r)b_i \tag{3.16}$$

For macroscopic occupation of ground state $N_0 >> 1$, using Bogoliubov approximation [127] of replacing bosonic operator by complex numbers, $b_0 = \sqrt{N_0}$ with $N_0(= \langle b_0^\dagger b_0 \rangle)$ being the ground state occupation, equation 3.16 becomes,

$$\hat{\psi}_b(r) = \sqrt{N_0}\psi_0(r) + \delta\hat{\psi}(r) = \psi_{BEC}(r) + \delta\hat{\psi}(r) \tag{3.17}$$

Clearly, the ground state wavefunction expression is same as equation 3.15, for a more ideal case, only now containing the actual ground state occupation instead of all the particles of system. Expression 3.17 is particularly useful to describe the averaged nonlinear dynamics of the condensate via the closed form equation for the classical field $\psi_{BEC}(r)$ and the small fluctuations around the average value. This classical field, $\psi_{BEC}(r)$ acts as order parameter for BEC and can be dissolved into real and imaginary part (due to Bogoliubov approximation),

$$\psi_{BEC}(r) = \sqrt{|n(r)|}e^{iP(r)} \tag{3.18}$$

here, $n(r)$ is the particle density and and $P(r)$ is the phase term, characterize the coherence.

3.2.2 Spontaneous Symmetry Breaking

Robert Browning once said,"On the earth the broken arcs; in the heaven, a perfect round". A system or event cannot can only maintain its perfect symmetry in ideal condition, it will eventually break for slight perturbation. It is hard to overestimate the topic of broken symmetry on condensed matter physics, particle physics or QFT (quantum field theory). Here, a introductory discussion of this beautiful topic is given.

Before delving into broken, a brief discussion of symmetry should be provided. Intuitively, if an object possess some form of symmetry if it looks same from different viewpoint. For example, a sphere looks same from any angle, and we can say that it is rotationally symmetric. Within quantum mechanics the definition is symmetry is somewhat same. A state $|\psi\rangle$ is said to be symmetric under transformation U if it follows,

$$U|\psi\rangle = e^{i\delta}|\psi\rangle \tag{3.19}$$

Appearance of phase term in equation 3.19 is due to QM axiom, 'total phase of state cannot be measured'. Like state laws of motion (hamiltonian or Lagrangian) can also be symmetric for some operator U if if follows,

$$[U, H] = 0 \tag{3.20}$$

This sort of symmetry has profound importance on physical system. According Noether's theorem 'Symmetries in natural laws implies some conserved quantities and vice versa'. For example, translation invariance in laws of motion implies momentum conservation. That's why identifying proper symmetry in physical problem is important.

Despite most of the natural laws follow some form of symmetry, asymmetric state is found. Eigenstate for a symmetric system is symmetric. If a system hamiltonian H which is symmetric under operator U, has a state $|\psi\rangle$ which is not invariant under the same transformation operator U that it can be said state has broken the symmetry of the system. Let us explain that case more. Consider the following Lagrangian which has $\phi \to -\phi$ symmetry,

$$\mathcal{L} = \frac{1}{2}(d_d(\phi))^2 - V(\phi) \tag{3.21}$$

where the potential term $U(\phi)$ reads,

$$V(\phi) = \frac{a^2}{2}\phi^2 + \frac{b}{4!}\phi^4 \tag{3.22}$$

Plot of $U(\phi)$ is shown in Fig. 3.2 for $a^2 > 0$ and $a^2 < 0$. For $a^2 > 0$, a non-degenerate minimum occurs at $\phi = 0$. But for negative a^2, we got a degenerate vacuum state at $\phi = \pm\sqrt{\frac{6a^2}{b}}$. System will spontaneously choose one and the symmetry of $\phi \to -\phi$ for vacuum state (or ground state) is broken.
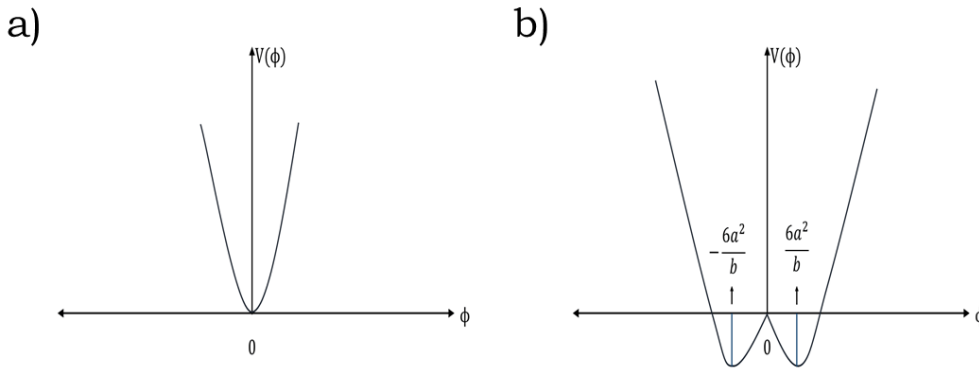
Figure 3.2: Plot of $U(\phi)$ for (a) $a^2 > 0$ with a minimum at $\phi = 0$ and (b) $a^2 < 0$ with minimum at $\phi = \pm\sqrt{\frac{6a^2}{b}}$.

For Lagrangian in equation 3.21 have a discrete global symmetry. For such a system we got only two discrete degenerate ground state. But for continuous global symmetry we can get an infinite number of degenerate vacuum state. For example, following Lagrangian has global $SO(2)$ symmetry,

$$\mathcal{L} = \frac{1}{2}\big[(d_d(\phi_1))^2 + (d_d(\phi_2))^2\big] + \frac{a^2}{2}(\phi_1^2 + \phi_2^2) - \frac{b}{4!}(\phi_1^2 + \phi_2^2)^2 \tag{3.23}$$

The broken ground state of such system follows,

$$\phi_1^2 + \phi_2^2 = \frac{6a^2}{b} \tag{3.24}$$

an infinite number of combination for ϕ_1 and ϕ_2 is possible for such ground state. System will spontaneously choose one of these infinite possibility.

As we have seen in equation 3.18, order parameter for BEC system has a phase term. However, one can always add additional phase e^{iQ} to it without changing the physical property of such system. This implies 'Gauge Symmetry' of the problem. A random phase will be chosen for condensate due to lack of a phase fixing force . However, in the BEC phase transition, a condensate system spontaneously chooses a particular phase, $P(r)$. A spontaneous selection for the phase $P(r)$ is referred to as a spontaneous breaking of gauge symmetry. According QFT, SSB (Spontaneous Symmetry Breaking) of condensate state means it is close to or in a coherent state defined by linear superposition of particle number eigenstate as [128],

$$|\alpha\rangle = \sum_N \frac{e^{-\frac{N_0}{2}}|N\rangle}{\sqrt{N!}} \tag{3.25}$$

Considering time evolution of number eigenstate as $e^{-i\frac{E_N t}{\hbar}}|N\rangle$ gives us time evolution of coherent state as $e^{-i\mu t}|\alpha\rangle$ with $\hbar\mu = E(N) - E(N-1)$ chemical potential of the condensate.

From Fig. 3.3 coherent state's phase is localized to a specific value through the destructive and constructive interferences between particle number eigenstates. Above the T_{BEC}, the ground state is occupied by the statistical mixture of other particle number eigenstates but for $T < T_{BEC}$ ground state approaches a pure coherent state.
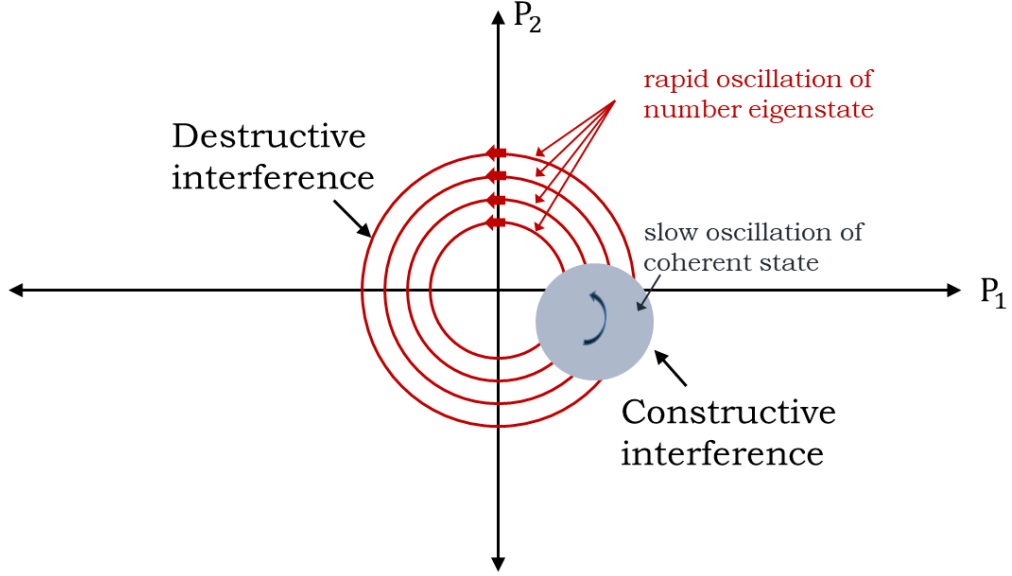
Figure 3.3: Time evolution of particle number eigenstate $|N\rangle$ and a coherent state $|\alpha\rangle$. The phase of coherent state is localized by the destructive and constructive interference among the existing particle number eigenstates in a phase space (P_1, P_2).

3.2.3 Goldstone Mode

SSB is inevitably accompanied by gap-less (meaning that these modes do not cost any energy to excite) Nambu–Goldstone modes with slow long-wavelength fluctuations of the order parameter. For example, vibrational modes in a crystal, known as phonons, are associated with slow density fluctuations of the crystal's atoms. The associated Goldstone mode for magnets are oscillating waves of spin known as spin-waves.

To get a more quantitative idea about, lets focus on the system represented by Lagrangian equation 3.23. Ground state can spontaneously take any one of the infinite value from equation 3.24. Consider, ground state takes a particular point $(\phi_1, \phi_2) = (\phi_1^0, \phi_2^0) = (\sqrt{\frac{6a^2}{b}}, 0)$. We can expand the potential function $U(\phi_1, \phi_2) = -\frac{a^2}{2}(\phi_1^2 + \phi_2^2) + \frac{b}{4!}(\phi_1^2 + \phi_2^2)^2$ around this (ϕ_1^0, ϕ_2^0) point in $\phi_1 - \phi_2$ plane using Taylor expansion,

$$U(\phi_1 - \phi_1^0, \phi_2 - \phi_2^0) = U(\phi_1^0, \phi_2^0) + \left(\frac{dU}{d\phi_1}\right)_{\phi_1^0} (\phi_1 - \phi_1^0) + \left(\frac{dU}{d\phi_2}\right)_{\phi_2^0} (\phi_2 - \phi_2^0)$$

$$+ \frac{1}{2}\left(\frac{d^2U}{d\phi_1^2}\right)_{\phi_1^0} (\phi_1 - \phi_1^0)^2 + \left(\frac{d^2U}{d\phi_2^2}\right)_{\phi_2^0} (\phi_2 - \phi_2^0)^2 + \frac{1}{2}\left(\frac{d^2U}{d\phi_1 d\phi_2}\right)_{\phi_1^0, \phi_2^0} (\phi_1 - \phi_1^0)(\phi_2 - \phi_2^0)$$

$$(3.26)$$

Clearly due to minima $\left(\frac{dU}{d\phi_1}\right)_{\phi_1^0} = \left(\frac{dU}{d\phi_2}\right)_{\phi_2^0} = 0$, and from the definition of $U(\phi_1, \phi_2)$ we get $\left(\frac{d^2U}{d\phi_1^2}\right)_{\phi_1^0} = 2a^2$ and $\left(\frac{d^2U}{d\phi_2^2}\right)_{\phi_2^0} = \left(\frac{d^2U}{d\phi_1 d\phi_2}\right)_{\phi_1^0, \phi_2^0} = 0$. So finally equation 3.26 becomes

$$U(\phi_1 - \phi_1^0, \phi_2 - \phi_2^0) = a^2(\phi_1 - \phi_1^0)^2 \tag{3.27}$$

which gives us the Lagrangian of equation 3.23 in terms of $(\phi_1', \phi_2') = \phi_1 - \phi_1^0, \phi_2 - \phi_2^0$,

$$\mathcal{L} = \frac{1}{2}\left[(d_d(\phi_1'))^2 + (d_d(\phi_2'))^2\right] - a^2\phi_1'^2 \tag{3.28}$$

From Lagrangian (equation 3.28), ϕ_1' field particle has a mass is $\sqrt{2}a$ but ϕ_2' field particle are mass-less (no quadratic term for ϕ_2'). We can understand presence of this mass-less particles from Fig. 3.4.
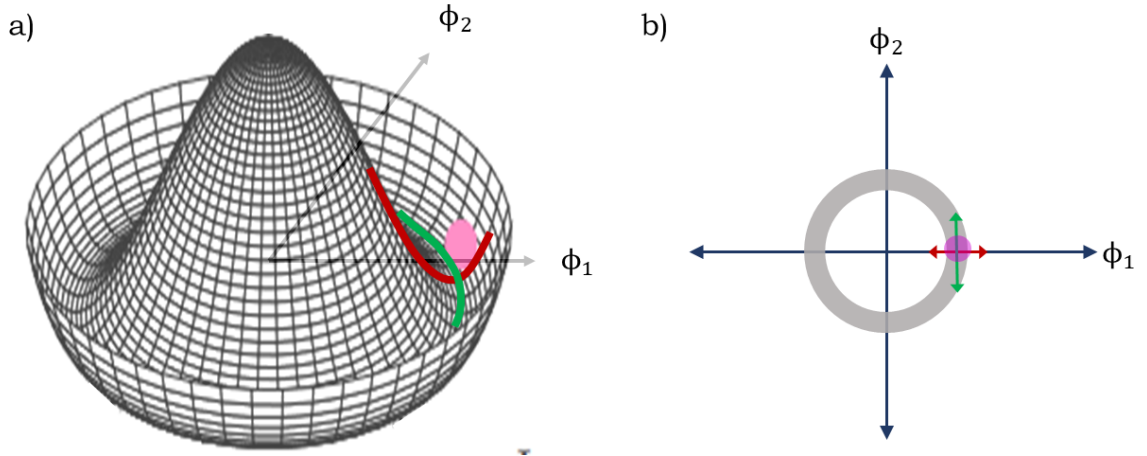
Figure 3.4: a) Mexican hat look alike potential profile for SO(2) symmetry corresponding to equation 3.23 (b) Prospect of particles with and without mass. For detail discussion see text.

For particle to move along ϕ_1 direction (along red curve) particle will need energy to

climb up the wall. So particles gain mass. But to move along ϕ_2 direction (along green curve), particle just will roll around the gutter, no energy is needed, as a result no mass. This mass-less particles are known 'Nambu-Goldstone Boson'.

In the condensate, bosons have repulsive interaction among them. This interaction causes long-wavelength fluctuations in the condensate. To see this, we can start with the simplified Gross-Pitaevskii (detail in section 3.3) equation for the order parameter,

$$i\frac{d}{dt}\psi_{BEC}(r,t) = \left[-\frac{\hbar\nabla^2}{2m} + g|\psi_{BEC}(r,t)|^2 \right]\psi_{BEC}(r,t) \tag{3.29}$$

g characterizes the interaction and $g > 0$ indicates repulsive interaction. Eigenvalues of condensate will be,

$$E_{eig}(K) = \pm\sqrt{\frac{\hbar^2 K^2}{2m}\left[\frac{\hbar^2 K^2}{2m} + \frac{\hbar g|\psi_{BEC}(r)|^2}{2}\right]} \tag{3.30}$$

For small K, the eigen-frequencies ($\omega_{eig}(K) = \frac{E_{eig}}{\hbar}$) of propagating excitonic wave,

$$\omega_{eig} = \pm uK \tag{3.31}$$

with $u = \sqrt{\frac{\hbar g|\psi_{BEC}|^2}{2m}}$ is effective sound velocity. This is exactly the mass-less boson that we just discussed. Due to interaction long-wavelength fluctuation globally appears in SSB process in particle and condensed matter systems, and nothing but 'Nambu-Goldstone modes' (Fig. 3.5).

3.2.4   Off Diagonal Long Range Order (ODLRO)

Intuitively, ODLRO is defined as a measure of phase coherence between particles at long distance. To understand this concept, we need to define reduced one body density matrix which is defined by field operator,

$$\rho(r,r') = \langle\hat{\psi}_b^\dagger(r)\hat{\psi}_b(r')\rangle \tag{3.32}$$

Using equation 3.10, 3.11, 3.12 and setting $\sum_i b_i^\dagger b_i = N$, total no. of particle in the system, one body reduced density matrix turns to,
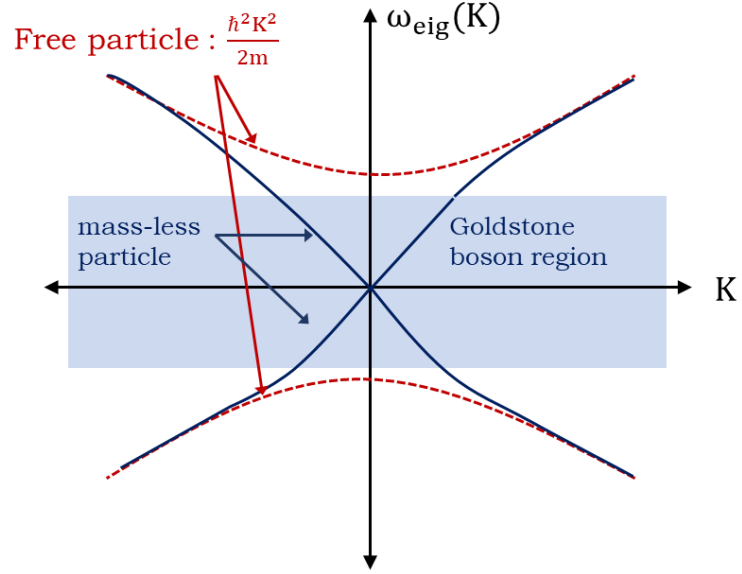
Figure 3.5: $\omega_{eig}(K)$ vs K plot. Mass-less particle region is highlighted in blue close to $K = 0$ line. As we move further away from $K = 0$ line relation 3.31 doesn't hold and particles achieve some and for higher K it particles behave like free particle.

$$\rho(r, r') = N \int dr_2 dr_3 ... dr_N \psi^*(r, r_2, r_3, ..., r_N) \psi(r', r_2, r_3, ..., r_N) \qquad (3.33)$$

Here integration is done along co-ordinates of $N - 1$ particles. This reduced density matrix gives us the probability amplitude to annihilate a particle at r' and create simultaneously create one at r. If we take $r = r'$, then one body density matrix represents local particle number density,

$$n(r) = \langle \hat{\psi}_b^\dagger(r) \hat{\psi}_b(r) \rangle \qquad (3.34)$$

For N dimensional system dot product between position and momentum eigenstate $(|p\rangle, |r\rangle)$ can be written as [129],

$$\langle p|r \rangle = \frac{1}{\sqrt{(2\pi\hbar^N)}} e^{-i\frac{\vec{p}.\vec{r}}{\hbar}} \qquad (3.35)$$

From equation 3.35 using completeness relation $\int dr |r\rangle\langle r| = 1$ and $\int dp |p\rangle\langle p| = 1$ we find the following relationship between $\hat{\psi}_b(r)$ (in spatial domain) and $\hat{\psi}_b(p)$ (in momentum space),

$$\hat{\psi}_b(r) = \frac{1}{\sqrt{(2\pi\hbar)^N}} \int dp \hat{\psi}_b(p) e^{-i\frac{\vec{p}.\vec{r}}{\hbar}} \tag{3.36}$$

$$\hat{\psi}_b(p) = \frac{1}{\sqrt{(2\pi\hbar)^N}} \int dr \hat{\psi}_b(r) e^{i\frac{\vec{p}.\vec{r}}{\hbar}} \tag{3.37}$$

From equation 3.36 and 3.37, we can say that $\hat{\psi}_b(r)$ and $\hat{\psi}_b(p)$ are Fourier transform of each other. So we can write momentum distribution of particle $n(p)$ (Fourier transform of $n(r_1)$) from equation 3.34 as,

$$n(p) = \langle \hat{\psi}_b^\dagger(p) \hat{\psi}_b(p) \rangle \tag{3.38}$$

So we can write using equation 3.32

$$\rho(r, r') = \frac{1}{V} \int dp n(p) e^{i\frac{\vec{p}.(\vec{r}-\vec{r'})}{\hbar}} \tag{3.39}$$

V is volume. Now lets consider a homogeneous system with N particles and V volume. In thermodynamic limit $N, V \to \infty$ but keeping $n = \frac{N}{V} = constant$, $\rho(r, r)$ depends soly on the distance between r and r', $x = \vec{r} - \vec{r'}$, so equation 3.39 becomes,

$$\rho(x) = \frac{1}{V} \int dp n(p) e^{i\frac{\vec{p}.\vec{x}}{\hbar}} \tag{3.40}$$

For $T > T_{BEC}$, $n(p)$ is a smooth function of p which results in $\lim_{x \to \infty} \rho(x) = 0$, one-body density matrix will decay to zero for a distance larger than de-broglie wavelength (3.4). But if BEC occurs with macroscopic occupation of ground state, then $n(p)$ is not a smooth function of p but has a singularity at $p = 0$ which we can write,

$$n(p) = N_0 \delta(p) + N_{p \neq 0} \tag{3.41}$$

which gives us one body reduced density matrix for longer distance some finite value other than zero,

$$\lim_{x \to \infty} \rho(x) = \frac{N_0}{V} \tag{3.42}$$

This asymptotic behavior of was discussed by Landau and Lifshitz [130], Penrose [131] and Penrose and Onsager [132], and is often referred to ODLRO as it coherence is

described for off-diagonal element of the density matrix.

Limiting case for one particle density matrix is shown in Fig. 3.6. For a normal state with smooth momentum distribution of particle, reduced density matrix reduced to zero for high x (for $x > \lambda_T$). But in case of formation of coherent condensate, a finite value of $\frac{N_0}{V}$ sustain for a long value of x.
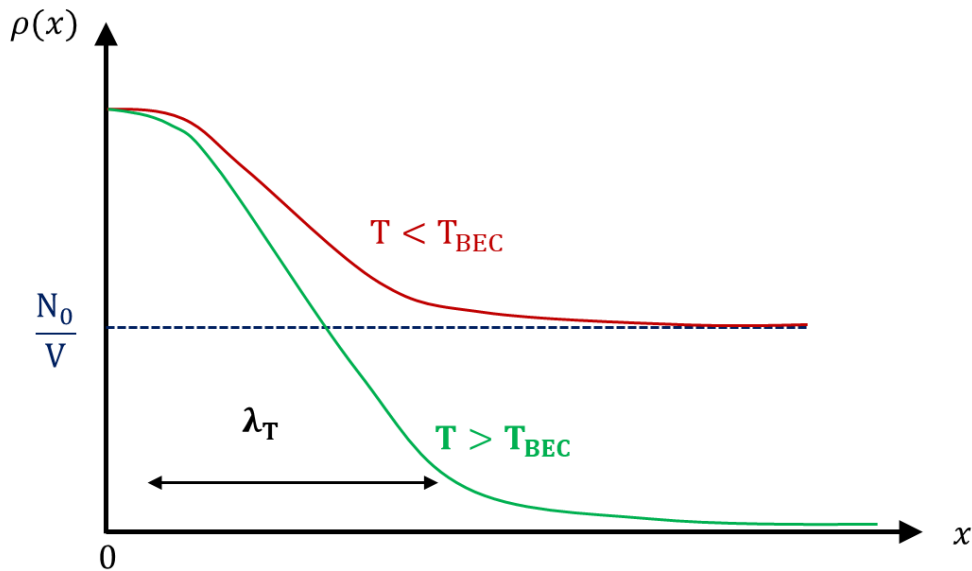
Figure 3.6: One particle density matrix vs relative distance.For normal state $(T > T_{BEC})$ $\rho(x)$ vanishes for large x but sustain a fixed value for BEC state $(T > T_{BEC})$.

One particle density matrix measurement does not provide any information regarding quantum statistical properties of the condensate. In order to distinguish various possible quantum states i.e. particle number eigenstate, coherent state or thermal state higher order reduced density matrix measurement is required.

3.3   Interacting Bosons and Gross-Pitaevskii Equation

When we formulate the condition for BEC, no interaction among bosons is considered. There is severe implication for that. We will discuss that in short here. Total energy of an ideal non-interacting Bose gas is,

$$E = \sum_i E(i)n[E(i), T, \mu] = \frac{2}{\sqrt{\pi}}k_B T \frac{V}{\lambda_T^3} \int_0^\infty dx x^{3/2} \frac{1}{Z^{-1}e^x - 1} \qquad (3.43)$$

Here, Z is fugacity and for $T < T_{BEC}$, $Z = 1$. Pressure of such ideal bose gas will be below BEC critical temperature will be,

$$P = \frac{2}{3}\frac{E}{V} = \frac{4}{3}k_B T \frac{V}{\lambda_T^3} \int_0^\infty dx\, x^{3/2} \frac{1}{e^x - 1} = 1.789 k_B T \frac{V}{\lambda_T^3} \tag{3.44}$$

So pressure of gas does not depend on volume of gas, ideal bose gas has infinite compressibility in BEC state. For not considering interaction among boson is the reason of such abnormal answer. To remove such pathological feature, interaction among boson needs to be considered. In this section we will discuss nature of interacting dilute bose gas. Additional to this, we will discuss about Gross-Pitaevskii equation. Gross-Pitaevskii equation describe the dynamics of ground state of a quantum system with identical bosons taking Hartree-Fock approximation and pseudopotential interaction.

3.3.1 Interacting Dilute Bose Gas

We are familiar two particle interaction potential profile (Fig. 3.7) which indicates interaction range r_0. For a dilute gas inter-particle distance a is much higher than interaction range $a >> r_0$.
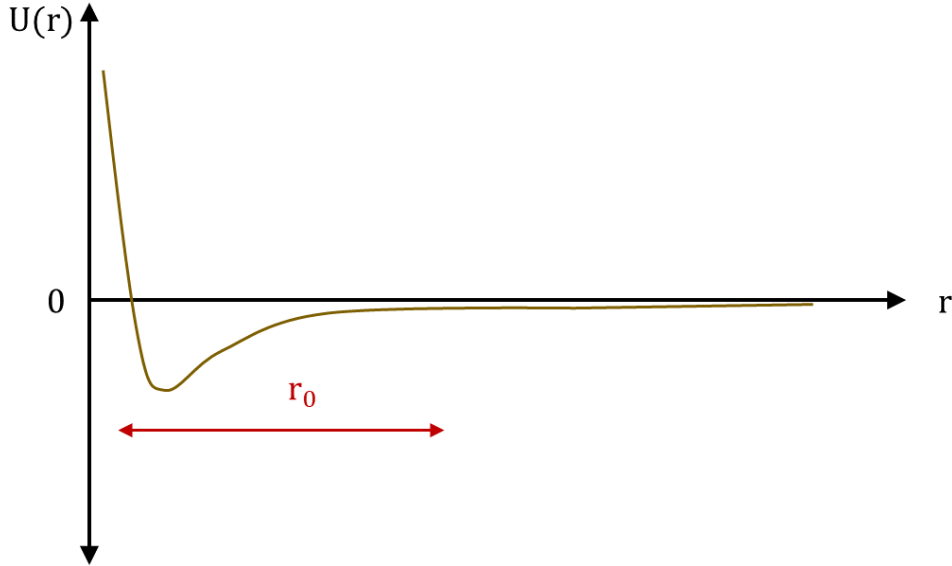
Figure 3.7: Two body scattering potential. For $r > r_0$ interaction potential effectively vanishes defining the range of interaction.

This condition effectively allows us to ignore three or more body interaction inside

dilute bose gas. Two particle interaction hamiltonian can be expressed within second quantization scheme,

$$H = \sum_i \frac{p_i^2}{2m} b_i^\dagger b_i + \frac{1}{2V} \sum_{p_i,p_j,q} U(q) b_{p_i+q}^\dagger b_{p_j-q}^\dagger b_{p_i} b_{p_j} \tag{3.45}$$

where, m is the mass of boson, $U(q) = \int dr U(r) exp(-i\frac{\vec{q}.\vec{r}}{\hbar})$. We can replace $U(q)$ with an effective potential U_0 as we are interested only in macroscopic property. Under Born approximation, we can write U_0 as,

$$U_0 = \frac{4\pi\hbar^2}{m} s_0 \tag{3.46}$$

s_0 is scattering length. Using Bogoliubov approximation, we will separate operator as b_0 (ground state annihilation operator) and b_i (operator for state other than ground state) and hamiltonian in equation 3.45 can be decomposed as,

$$H = \frac{U_0}{2V} b_0^\dagger b_0^\dagger b_0 b_0 + \sum_i \frac{p_i^2}{2m} b_i^\dagger b_i + \frac{U_0}{2V} \sum_{i\neq 0} (4b_0^\dagger b_i b_0 b_i + b_i^\dagger b_{-i}^\dagger b_0 b_0 + b_0^\dagger b_0^\dagger b_0 b_{-i}) \tag{3.47}$$

During discussion of order parameter, we see that Bogoliubov approximation allow us to replace b_0 with a complex number. We will same thing here but with better accuracy as,

$$b_0^\dagger b_0 + \sum_{i\neq 0} a_i^\dagger a_i = N \tag{3.48}$$

which transforms the hamiltonian of equation 3.47 into,

$$H = \frac{U_0 N^2}{2V} + \sum_i \frac{p_i^2}{2m} b_i^\dagger b_i + \frac{U_0 N}{2V} \sum_{i\neq 0} (2b_i^\dagger b_0 + b_i^\dagger b_{-i}^\dagger + b_i b_{-i}) \tag{3.49}$$

Third term represents self energy of excited state, simultaneous creation and annihilation of boson at i and $-i$ state. Invoking Bogoliubov transformation,

$$b_i = \alpha_i a_i + \alpha_{-i} a_{-i}^\dagger \tag{3.50}$$

$$b_i^\dagger = \alpha_i a_i^\dagger + \alpha_{-i} a_{-i} \tag{3.51}$$

These transformation is similar to the one we consider during dressed boson (equation 2.16 and 2.17). Here we consider boson to be a linear superposition of forward propagating quasi-particle (a_i) and backward propagating quasi-particle (a_{-i}). We can uniquely determine the coefficient α_i, α_{-i} as,

$$\alpha_i, \alpha_{-i} = \pm \left(\frac{\frac{p_i^2}{2m} + \frac{U_0 N}{V}}{2E(p_i)} \right)^{\frac{1}{2}} \tag{3.52}$$

where $E(p_i)$ follows,

$$E(p_i) = \sqrt{\frac{p_i^2}{2m} \left(\frac{p_i^2}{2m} + \frac{2U_0 N}{V} \right)} \tag{3.53}$$

which is the exact relationship that we have obtained for Goldstone boson in equation 3.30. Putting Bogoliubov transformation into hamiltonian (equation 3.49) gives us,

$$H = E_0 + \sum_{i \neq 0} E(p_i) a_i^\dagger a_i \tag{3.54}$$

$$E_0 = \frac{U_0 N^2}{2V} + \frac{1}{2} \sum_{i \neq 0} \left[E(p_i) - \frac{U_0 N}{V} - \frac{p_i^2}{2m} + m \left(\frac{U_0 N}{V p_i} \right)^2 \right] \tag{3.55}$$

As we have seen for dressed boson, here transformation transform hamiltonian in interaction picture (equation 3.45) into hamiltonian of non-interacting particles following dispersion relation of $E(p_i)$ with ground state energy being E_0.

As we consider dilute gas, other excited state has very small occupation as most of particles are in ground state. So we can neglect energy associated with those particles and take total energy of the interacting bose gas as,

$$E_0 \approx \frac{U_0 N^2}{2V} \tag{3.56}$$

So now the pressure of condensed becomes,

$$P = -\frac{dE_0}{dV} = \frac{U_0}{2} \left(\frac{N^2}{V} \right)^2 \tag{3.57}$$

Pressure is a function of volume, so no infinite compressibility here. Inclusion of two body interaction removes the paradoxical conclusion of infinite compressibility.

To understand the dynamics of BEC under interaction potential we need the help of Gross-Pitaevskii Equation.

3.3.2 Gross-Pitaevskii Equation: Derivation

We will start by deriving time independent Gross-Pitaevskii (GP) equation first. We will start with the same hamiltonian in equation 3.45 but without second quantization.

$$H = \sum_n \left(\frac{p^2(n)}{2m} + U_{ext}(\vec{r_n}) \right) + \sum_{n,m,n \neq m} U(|\vec{r_n} - \vec{r_m}|) \tag{3.58}$$

To avoid confusion in equation 3.45 p_i is defined as momentum of ith state and here in equation 3.58 $p(n)$ is defined as momentum of nth particle. Due to the complexity associated with many-bodied system, a mean-field approach is used, all bosons exist in the same single-particle state $\kappa(r)$. So many body wavefunction for N particle can be written as,

$$\psi(r_1, r_2, ..., r_N) = \prod_{n=1}^{N} \kappa(r_n) \tag{3.59}$$

Both many body and single particle wavefunction are normalized. With equation 3.60 we can determine energy for hamiltonian (equation 3.58),

$$E = N \int dr \left[\frac{\hbar^2}{2m} |\nabla \kappa(r)|^2 + V_{ext} |\kappa(r)|^2 + \frac{N-1}{2} U_0 |\kappa(r)|^4 \right] \tag{3.60}$$

U_0 is defined in equation 3.46. For macroscopically occupied ground state, we can approximate condensate wavefunction as,

$$\psi_{BEC}(r) = \sqrt{N} \kappa(r) \tag{3.61}$$

So energy E of equation 3.60 can be written considering $N - 1 \approx N$,

$$E = \int dr \left[\frac{\hbar^2}{2m} |\nabla \psi_{BEC}(r)|^2 + V_{ext} |\psi_{BEC}(r)|^2 + \frac{U_0}{2} |\psi_{BEC}(r)|^4 \right] \tag{3.62}$$

From thermodynamics we know that free energy F is defined as $F = E - \mu N$ with μ being chemical potential. To minimize F we need $\delta E - \mu \delta N = 0$, which ends up with time independent GP equation,

$$-\frac{\hbar^2}{2m}\nabla^2\psi_{BEC}(r) + V_{ext}(r)\psi_{BEC}(r) + U_0|\psi_{BEC}(r)|^2\psi_{BEC}(r) = \mu\psi_{BEC}(r) \tag{3.63}$$

If we consider time evolution of condensate wavefunction as $\psi_{BEC}(r,t) = \psi_{BEC}(r)e^{-i\mu t}$ then we get time dependent GP equation from equation 3.63 as,

$$-\frac{\hbar^2}{2m}\nabla^2\psi_{BEC}(r,t) + V_{ext}(r)\psi_{BEC}(r,t) + U_0|\psi_{BEC}(r,t)|^2\psi_{BEC}(r,t) = i\frac{d}{dt}\psi_{BEC}(r,t) \tag{3.64}$$

This is the same equation that we mentioned in equation 3.29 with $V_{ext} = 0$. GP equation is very useful for understanding dynamics of BEC state. Next we will discuss about some analytical solution of GP equation.

3.3.3 Gross-Pitaevskii Equation: Analytical Solution

Equation 3.64 is in fact a nonlinear Schrodinger equation considering mean field approach. Analytical solution for such types of equation is quite complicated due to presence of non-linear term $U_0|\psi_{BEC}(r)|^2$. Here, we will present analytical solution of time-dependent 1D GP equation,

$$-\frac{\hbar^2}{2m}\frac{d^2\psi_{BEC}(r,t)}{dx^2} + V_{ext}(x)\psi_{BEC}(x,t) + U_0|\psi_{BEC}(x,t)|^2\psi_{BEC}(x,t) = i\frac{d}{dt}\psi_{BEC}(x,t) \tag{3.65}$$

under weak and strong repulsive interaction potential for external potential,

$$V_{ext}(x) = \begin{cases} 0 & \text{if } x \leq L \\ 0 & \text{if } x > L \end{cases} \tag{3.66}$$

Replacing $t, x, \psi_{BEC}(x)$ from 3.65 as follows,

$$t \rightarrow \frac{\hbar t_n}{mL^2}, \quad x \rightarrow Lx_n, \quad \psi_{BEC}(x) \rightarrow \sqrt{L^3}\psi_{BEC}(x_n)$$

and multiplying it by $\frac{(mL^2/\hbar)^2}{m\sqrt{L}}$ gives us dimensional GP equation ,

$$\left[-\frac{1}{2}\frac{d^2}{dx_n^2} + V_{ext}(x_n) + U_n|\psi_{BEC}(x_n, t_n)|^2 \right] \psi_{BEC}(x_n, t_n) = i\frac{d}{dt}\psi_{BEC}(x_n, t_n) \qquad (3.67)$$

where, $U_n = \frac{U_0 N}{mL^5}$. This transformation also causes energy (equation 3.62) to be dimensionless as $E = \frac{E}{E_0} = \frac{E}{\frac{\hbar^2}{mL^2}}$. In new co-ordinate we can take $\psi_{BEC}(x_n, t_n) = e^{-i\mu t_n}\psi_{BEC}(x_n)$ with $\int dx_n|\psi_{BEC}(x_n)|^2 = 1$ we got,

$$\left[-\frac{1}{2}\frac{d^2}{dx_n^2} + V_{ext}(x_n) + U_n|\psi_{BEC}(x_n, t_n)|^2 \right] \psi_{BEC}(x_n) = \mu\psi_{BEC}(x_n) \qquad (3.68)$$

We need to find the solution of equation 3.68 for external trapping potential.

Weak interaction potential ($U_n \approx 0$): In this case we can consider interaction term equation ($U_n|\psi_{BEC}(x_n, t_n)|^2$) negligible compared to kinetic term ($-\frac{1}{2}\nabla^2$). We can rewrite equation 3.68 for $0 \leq x_n \leq 1$ as,

$$-\frac{1}{2}\frac{d^2}{dx_n^2}\psi_{BEC}(x_n) = \mu\psi_{BEC}(x_n) \qquad (3.69)$$

Solution of this is straight forward. Considering $\psi_{BEC}(x_n = 0) = \psi_{BEC}(x_n = 1) = 0$, ground state wavefunction $\psi_{BEC}(x_n)$ and energy E_{BEC} is,

$$\psi_{BEC}(x_n) = [\sqrt{2}sin(\pi x_n)]^N \qquad (3.70)$$

$$E_{BEC} = \frac{N\pi^2}{2} \qquad (3.71)$$

Strong repulsive interaction potential ($U_n >> 1$): We will another approximation here, Thomas-Fermi (TF) approximation. This approximation ignores kinetic term with respect to interaction term. Under such approximation, from equation 3.68 we can write,

$$U_n|\psi_{BEC}^{TF}(x_n)|^2\psi_{BEC}^{TF}(x_n) = \mu^{TF}\psi_{BEC}^{TF}(x_n) \qquad (3.72)$$

which gives us wavefunction as,

$$\psi_{BEC}^{TF}(x_n) = \sqrt{\frac{\mu^{TF}}{U_n}} \qquad (3.73)$$

54

Clearly TF approximation does not suit zero boundary condition rather suggest the appearance of boundary layer. Normalization of equation 3.73 gives us chemical potential under Thomas-Fermi approximation,

$$\mu^{TF} = U_n \tag{3.74}$$

Using equation 3.60, 3.73, 3.74 we find Thomas-Fermi energy as,

$$E_{BEC}^{TF} = \frac{U_n}{2} \tag{3.75}$$

Using such approximation we can solve equation 3.68. As boundary layer now exist at both $x_n = 0$ and $x_n = 1$, we will solve the problem at region $0 \leq x_n \leq 1/2$. We need to further re-scale equation 3.68 by introducing $x_n \to \frac{y}{\sqrt{\mu^{TF}}}$ with conditions,

$$\psi_{BEC}(0) = 0, \quad \psi_{BEC}(\infty) = 1$$

we find solution as,

$$\psi_{BEC}(x_n) = tanh(\sqrt{\mu^{TF}} x_n) \tag{3.76}$$

Similarly for region $1/2 \leq x_n \leq 1$

$$\psi_{BEC}(x_n) = tanh(\sqrt{\mu^{TF}}(1 - x_n)) \tag{3.77}$$

So complete solution for strong interaction potential,

$$\psi_{BEC}(x_n) = tanh(\sqrt{\mu^{TF}}(1 - x_n)) + tanh(\sqrt{\mu^{TF}}(1 - x_n)) \tag{3.78}$$

with ground state energy,

$$E_{BEC} = \frac{\mu^{TF}}{2} + \frac{4}{3}\sqrt{[(\mu^{TF})^2 + 1]} + 2 \tag{3.79}$$

Solution is shown in Fig. 3.8

For the most simplest 1D potential, finding analytical solution for GP equation is quite cumbersome. With the introduction of defect, finding an exact solution will be impossible. So we need to resort to numerical technique for solving GP equation for any
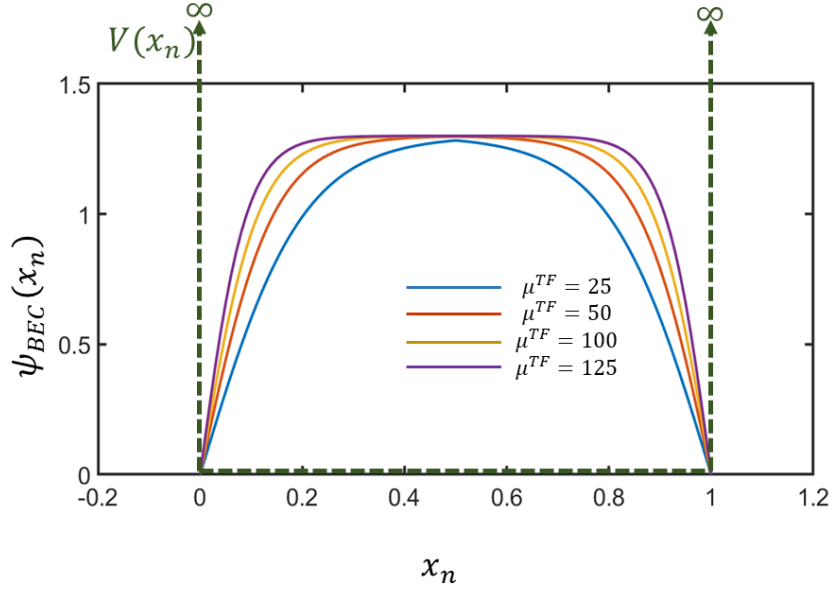
Figure 3.8: Analytical solution for ground state wavefunction of BEC state in strong with different μ^{TF}. Solution is shown for 1D infinite potential.

random potential. Detail of this numerical technique will be discussed in appendix and in Chapter 5.

3.4 Superfluidity

In Fig. 3.9 variation of specific heat with temperature for helium liquid is shown. Around 2.2K, singularity in specific heat indicates a phase transition of helium liquid. This transition is from normal helium liquid to superfluid helium. Due to similarity of the graph with Greek letter λ, often this transition is regraded in literature as 'Lambda transition' or 'λ-transition'. This sort of transition was first discovered by M. Wolfke and W.H. Keesom in 1927. Besides the capability of extreme heat transport superfluid shows persistence flow through narrow tube without dissipation, fountain effect etc.

In this section we will discuss superfluid phenomenon from phenomenological and field theoretic perspective with the concept of quantized vortices and Berezinskii-Kosterlitz-Thouless (BKT) phase transition.
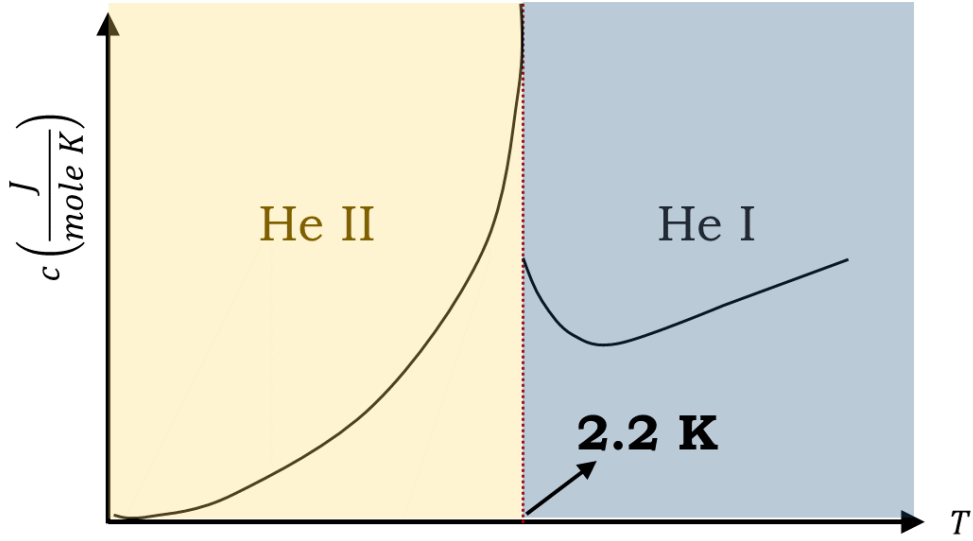
Figure 3.9: Lambda transition in helium. Change of heat capacity in helium shows at 2.2K temperature specific heat shows singularity. This temperature, 2.2K indicates the boundary between normal helium (He I) and superfluid helium (He II).

3.4.1 Phenomenological Explanation of Superfluidity

Lev Landau first tackle the problem of superfluidity from phenomenological point of view [133]. This theory revolves around the idea of Galilean transformation. One phenomenon of superfluid is persistence flow through capillary tube without any dissipation. Consider two reference frame F and F' with relative velocity $\vec{v}$ (velocity at which fluid moves through capillary tube). Reference frame F is at rest with respect to fluid and F' is at rest with respect to capillary tube. If E and $\vec{K}$ are energy and momentum in F frame, then movement of viscous fluid through tube creates elementary particle with dispersion $E(K)$ to cause dissipation. Considering Galilean transformation energy (E') and momentum $\vec{K'}$ in frame F' can be written as,

$$\vec{K'} = \vec{K} + m\vec{v} \tag{3.80}$$

$$E' = E_0 + E(K) + \vec{K}.\vec{v} + \frac{1}{2}m|\vec{v}|^2 \tag{3.81}$$

E_0 being the ground state energy. For such generation of elementary excitation to be spontaneous, total energy associated with excitation $E(P) + \vec{K}.\vec{v}$ should be negative

which implies,

$$|\vec{v}| < \frac{E(P)}{\vec{K}} \quad \text{and} \quad \vec{K}.\vec{v} \tag{3.82}$$

means velocity $\vec{v}$ should have a minimum value of $\frac{E(K)}{\vec{K}}$ and elementary excitation should have the momentum $\vec{K}$ opposite to the fluid velocity $\vec{v}$. Elementary excitation will disappear if velocity goes down than this minimum value. This is known as 'Landau's critical velocity', v_c

$$v_c = min_{\vec{K}} \frac{E(K)}{|\vec{K}|} \tag{3.83}$$

Minimum is calculated over all possible $\vec{K}$. Dispersion of elementary excitation can be different for weak interaction and strong interaction among the excitation. This is shown in Fig. 3.10.
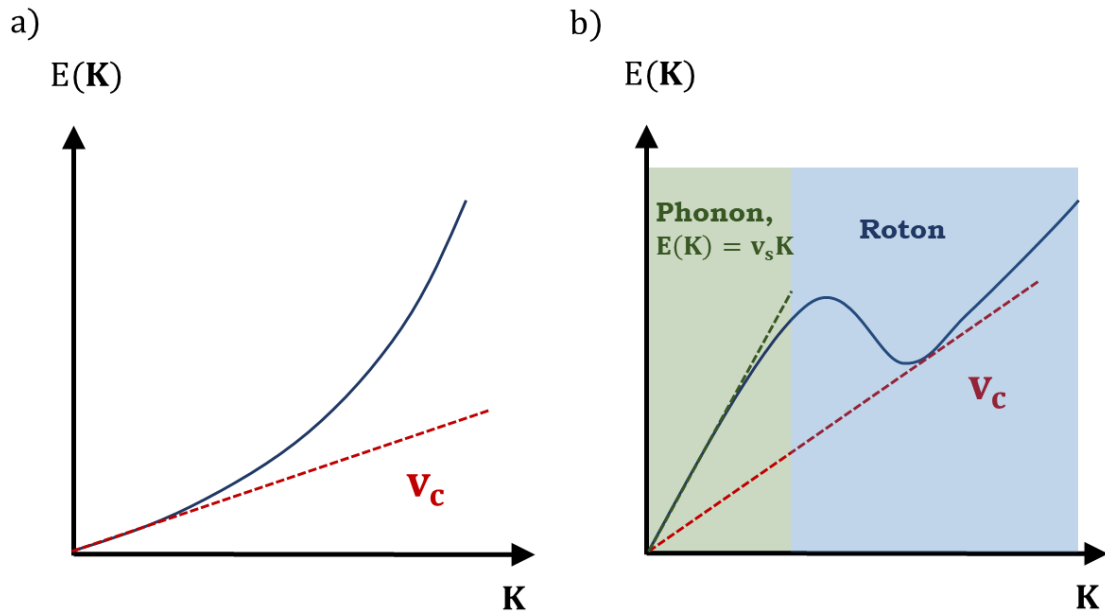
Figure 3.10: (a) Dispersion for a weakly interacting particle excitation. In this case critical velocity v_c = sound velocity. (b) Dispersion for a weakly interacting particle excitation.Here critical velocity is lower than sound velocity v_s (from phonon dispersion relation).

For weak interaction we get a situation similar to Goldstone boson (Fig. 3.5) with linear dispersion relation close to $\vec{K} = 0$. Here, sound velocity is defined and critical velocity is equal to that. But for strong interaction, we got two types of excitation:

phonon and roton. Although here sound velocity, v_s is defined by phonon dispersion but critical velocity is quite different than v_s.

Now question can be risen regarding normal fluid to superfluid transition process. For this to answer, we need to look at 'Two Fluid Model' proposed by Tisza [134] and Landau [133]. According to this model, According to this model, system consists of two fluids, superfluid and normal fluid. The superfluid fraction is formed by condensate, while the normal component consists of the excitations like phonon and roton excitations. At absolute zero temperature, only superfluid part of system sustains, a perfect condensate. With rising temperature, more and more elementary excitations appear and form the normal fluid. As temperature rises, normal fluid gradually becomes dominant until the superfluid completely vanishes beyond critical temperature. According to this model, total density of fluid, ρ_t is summation of normal fluid and superfluid fraction as,

$$\rho_t = \rho_{sup} + \rho_{norm} \tag{3.84}$$

where, ρ_{sup} and ρ_{norm} are density of superfluid and normal fluid respectively. These two types of fluid also has different velocities v_{sup} for superfluid and v_{norm} for normal liquid. As a result of this model, a new type sound velocity has appeared, known as 'second sound' which is due fluctuation of temperature and entropy rather than density, as is the case for 'first sound'.

3.4.2   QFT perspective

Phenomenological modeling gives us a clear overview of nature of superfluidity. We will now try understand superfluidity using Quantum Field Theory (QFT). Some of the important concepts of QFT to understand superfluidity has already been discussed in section 3.2. We can start directly from GP equation but instead of finding BEC state we can find the evolution of ground state (BEC always form in ground state of Bose-Einstein distribution), $\psi_G(r,t)$.

$$-\frac{\hbar^2}{2m}\nabla^2\psi_G(r,t) + V_{ext}(r)\psi_G(r,t) + U_0|\psi_G(r,t)|^2\psi_G(r,t) = i\frac{d}{dt}\psi_G(x,t) \tag{3.85}$$

As we have seen in section 3.4.2 superfluid is actually a component in 'Two Fluid Model'. In this model, superfluid is stable ground state and normal is fluctuations induced by elementary excitation. So we can consider ground state below critical temperature as,

$$\psi_G(r,t) = \psi_{sup}(r,t) + \delta\psi_{norm}(r,t) \approx \psi_{sup}(r,t) \tag{3.86}$$

Same case like equation 3.41 but below critical temperature superfluid fraction is dominant part, $\delta\psi_{norm}(r,t) = 0$. So under Bogoliubov approximation, we can write down $\psi_{sup}(r,t)$ as,

$$\psi_{sup}(r,t) = \sqrt{n_{sup}(r,t)}exp(i\theta_{sup}(r,t)) \tag{3.87}$$

Equation 3.87 is same as 3.61 with $\kappa(r,t) = exp(i\theta(r,t))$ and as usual $n_{sup}(r,t) = |\psi_{sup}(r,t)|^2$ is particle density. $\psi_{sup}(r,t)$ is order parameter for normal fluid to superfluid transition. From equation 3.87 and continuity equation we can determine superfluid velocity. From elementary quantum mechanics [135], we can write for particle number dynamics and particle current density $J(r,t)$,

$$\frac{dn_{sup}(r,t)}{dt} + \vec{\nabla}.J(\vec{r},t) = 0 \tag{3.88}$$

where particle current density is defined as,

$$J(r,t) = \frac{i\hbar}{2m}[\psi_{sup}^*(r,t)\vec{\nabla}\psi_{sup}(r,t) - \psi_{sup}(r,t)\vec{\nabla}\psi_{sup}^*(r,t)] \tag{3.89}$$

Using $\psi_{sup}(r,t)$ from equation 3.87 in the definition of particle current density $J(r,t)$

$$J(r,t) = n_{sup}(r,t)\frac{\hbar}{m}\vec{\nabla}\theta_{sup}(r,t) \tag{3.90}$$

So superfluid velocity v_{sup} can be written as,

$$\vec{v_{sup}} = \frac{\hbar}{m}\vec{\nabla}\theta_{sup}(r,t) \tag{3.91}$$

From normal to superfluid transition, ODLRO forces a coherence (same phase) over large distance. What exact value of such phase will be chosen will be determined by SSB (exactly what point in the degenerate ground state (fig. 3.4) be chosen). This phase then determine superfluid velocity.

3.4.3 Quantized Vortices
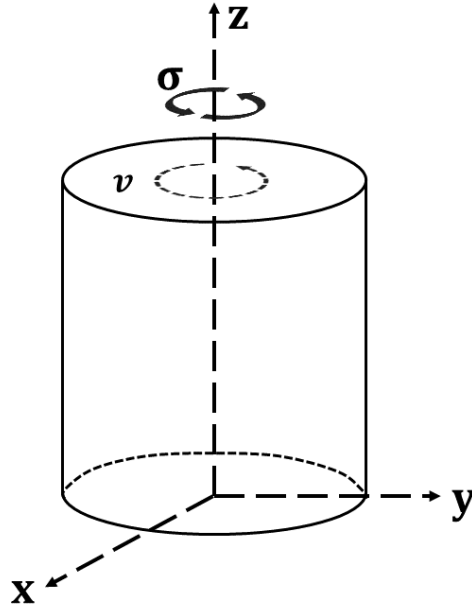
Figure 3.11: Essential co-ordinate system for solving rotational quantization in superfluid.

Consider the cylinder in Fig. 3.11 is filled with normal fluid. For a rotational velocity σ, fluid will have a linear velocity along tangent of rotation $v_{norm} = \vec{\sigma} \times \vec{r}$, $\vec{r}$ being radial component of cylindrical co-ordinate system or position vector of the point of interest (point where we want to determine linear velocity v_{norm}).

Now what will happen if we replace normal fluid with superfluid? If we take curl of equation 3.91 using first null identity of vector calculus,

$$\vec{\nabla} \times \vec{v_{sup}} = \frac{\hbar}{m}\vec{\nabla} \times \vec{\nabla}\theta_{sup}(r,t) = 0 \tag{3.92}$$

So superfluid cannot rotate. How does superfluid act under external rotational force? In that case, we need to look closer to at order parameter, $\psi_{sup}(r,\phi) = \sqrt{n(r,\phi)}e^{i\theta(r,\phi)}$ for cylindrical co-ordinate. Due to symmetry for such condition, $\sqrt{n(r,\phi)}$ will only depend on r and $\theta(r,\phi)$ will be a function of ϕ (angular component of cylindrical co-ordinate). If we take $\theta(\phi) = l_s\phi$ then superfluid velocity is found,

$$v_{sup} = \frac{\hbar}{m}\frac{l_s}{r} \tag{3.93}$$

where $l_s = \pm 1, \ \pm 2, \ \pm 2, \ .... = \pm m_s$. Circulation of v_{sup} around closed surface centered around z-axis is found as,

$$\oint v_{sup} r d\phi = 2\pi l_s \frac{\hbar}{m} \tag{3.94}$$

which is integral of $\frac{\hbar}{m}$. This is called 'Onsager-Feynman quantization condition'. So rotation over the whole closed path will be divided into several closed path as shown in Fig. 3.12 (b). These are known as 'Quantized Vortices'
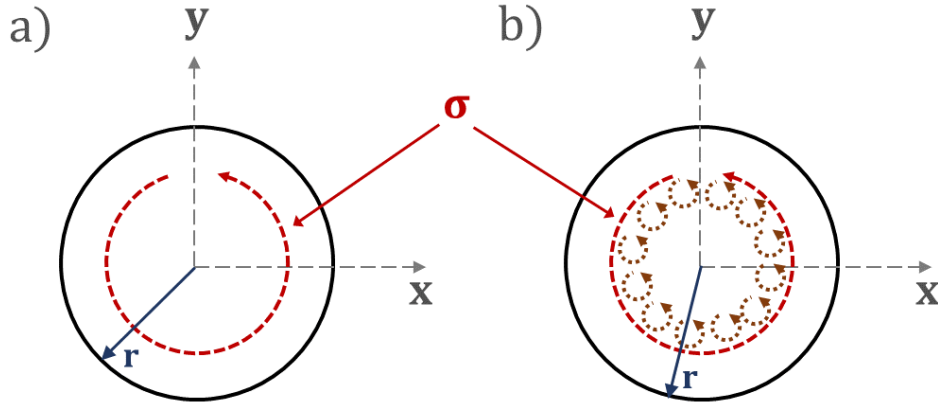
Figure 3.12: Difference between rotational mechanics between normal fluid (a) and superfluid (b). Normal fluid rotates with well defined tangential velocity but in case of superfluid rotation is quantized.

Close loop integral can result in either $2\pi m_s \frac{\hbar}{m}$ or $-2\pi m_s \frac{\hbar}{m}$ based on the charge of quantized vortex. For charge $+1$, we consider it as simply 'vortex' and for charge -1 'anti-vortex'. This sort of pair vortex will be important in the discussion of BKT phase transition.

Typically size of a single vortex is [136],

$$d_v = \sqrt{\frac{\hbar^2 V}{2mU_0 N}} \tag{3.95}$$

and energy of such vortex,

$$e_v = \frac{\pi N}{V} \frac{\hbar^2}{m} ln\left(\frac{r_v}{d_v}\right) \tag{3.96}$$

Energy of vortex is function of position vector, r_v, measured from the center of the

vortex. At the center of vortex, we get $e_v = \infty$. Due to this infinite energy, no condensate particle can stay at the center of vortex.

We will numerically evaluate presence of vortex by solving GP equation under a rotational force being applied. GP equation which has been solved numerically for the purpose of this section is,

$$\left[-\frac{\hbar^2}{2m}\frac{d^2}{dx^2} + -\frac{\hbar^2}{2m}\frac{d^2}{dy^2} + c_1(|x|^2 + |y|^2) + c_2(|x|^2 + |y|^2)^2 + U_0|\psi_G(x,y,t)|^2 \right.$$
$$\left. + \sigma L_z \right]\psi_G(x,y,t) = i\frac{d}{dt}\psi_G(x,t) \quad (3.97)$$
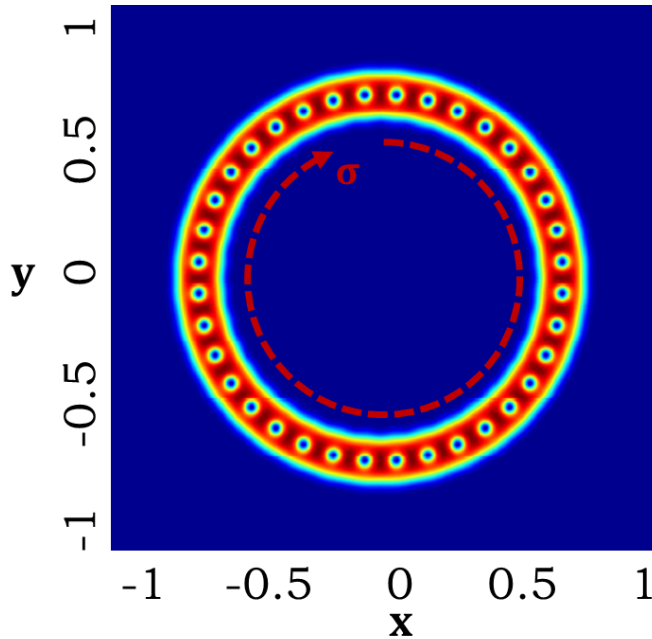
Figure 3.13: $|\psi_G(x,y)|^2$ after steady state in numerical solution has been achieved. The vortices are clear from condensate density plot.

Here, we consider an additional term σL_z to introduce rotational energy in non-linear SC (Schrodinger) equation or GP equation. We are prompt to use quadratic and quartic potential to confine the ground state inside the narrow loop as shown in Fig. 3.13.

Clearly we can see the quantized vortices throughout the condensate. Existence of vortex is extremely important for understanding of condensate dynamics under the presence of defect potential. We will come to the implication of vortex presence in detail

in Chapter 5.

3.4.4 Berezinskii-Kosterlitz-Thouless (BKT) Transition

According to Mermin-Wagner Theorem [137], long range order, in a strict sense, cannot be formed in 1D or 2D dimension. Using xy model we can easily prove one body density matrix $\rho(r, r')$ for different dimension becomes (taking nearest neighbour spin interaction potential $J = 1$),

$$
\rho(r, r') \approx \begin{cases} e^{-(const)T} & \text{if } d > 2 \\ \left(\frac{|r'-r|}{a_{lattice}} \right) & \text{if } d = 2 \\ exp\left(-\frac{Tr}{2a_{lattice}} \right) & \text{if } x > L \end{cases} \tag{3.98}
$$

Here, T is temperature. Any 2D system, like xy model with a continuous symmetry will have a massless field by the Goldstone theorem (Goldstone boson section 3.2.3). The fluctuations created by these Goldstone modes destroy this long range order. Now questions arises "How does condensation occur for 2D or 1D system?"

A 2D system can achieve quasi-condensation and superfluidity below a critical temperature, T_{BKT}. For $T > T_{BKT}$, thermal energy is enough to excite vortex (with energy e_v) and sustain it for long time. But as temperature is decreasing, $T < T_{BKT}$, single vortex and anti-vortex is not stable anymore due to lack of thermal energy. They start to pair up, as shown in Fig. 3.14.

Due to removal of such topological defect, a topological order has been established and long range fluctuation of phase $\theta(r)$ has been removed. This sort of transition is more prominent in quasi-particle Boson like exciton-polariton as they are inherently a 2D particle (cavity photon is restricted in one direction) [138].

3.5 Dynamic Condensation of Exciton-Polariton

In this section we will present dynamic condensation of exciton-polariton quasi-particle for zero potential. As we have already discussed, time independent GP equation provides the time dynamic solution for ground state condensate wavefunction for both condensate
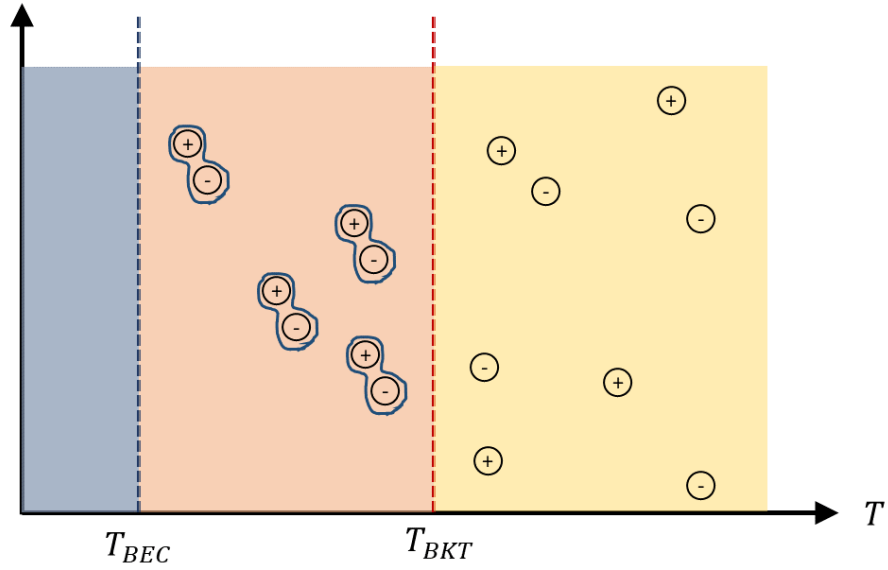
Figure 3.14: Different state of condensation for 2D weakly interacting Bose gas.

density and condensate phase. As we have discussed already, BKT transition below T_{BKT} forms a quasi condensate for 2D system like exciton polariton. In Fig. 3.15 we show numerical result for ground state condensate phase term $\theta(x, y)$. for three different time.
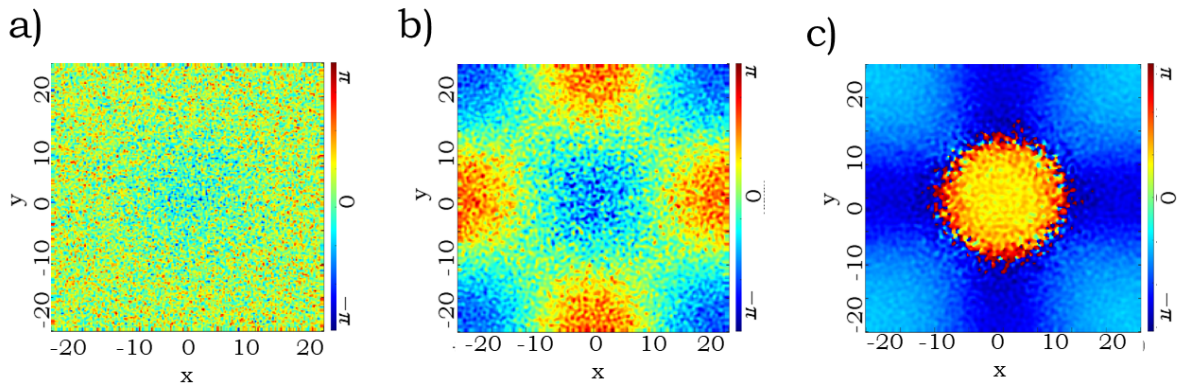
Figure 3.15: Phase of ground state condensate for time (a) 0.66 ps (b) 9.9 ps (d) 33.2 ps.

Initially system has no phase coherence (3.15 (a)). But as time passes SSB breaks some local symmetry and forces creation of topological defect like vortex (or anti-vortex). As time passes, these vortex (and anti-vortex) moves and pair up with anti-vortex (vortex) and annihilate each other. As a result with time, phase fluctuation eventually goes away and long range topological order is starting to appear. For example in Fig. 3.15 we see a phase coherence of over a distance 20 (unit-less).

Chapter 4

Thermalization of Condensate

One of characteristics of a mature theory is that to understand it one does not need to know its history. One may start leaning about classical mechanics without the need for knowing Parisian scholastic. But in case of 'Statistical Mechanics', a study to explain thermal behavior in macroscopic level lacks a common set of assumptions is not found due to its development from several school with each having different goal in mind. From early work of Maxwell, Boltzmann, Gibbs [139] to extended work by Von Neumann, Schrodinger [140] statistical physics gets a solid footing to give us more or less a clear idea of thermalization of generic system. One of the foundational problems of statistical physics is probabilistic assumption which makes detail understanding of statistical physics very difficult. We will not even try that here. Some basic concept regarding classical and quantum thermalization and localization especially many body localization will be discussed here. Many body localization (MBL) can significantly influence thermalization process. At the end of this chapter we will discuss in short about Bose-Hubbard model and thermalization process for such model.

4.1   Fundamentals on Classical Thermalization

There is no universal definition of chaos. Mathematician Edward Norton Lorenz after after discovering 'Butterfly effect' commented"When a butterfly flutters its wings in one part of the world, it can eventually cause a hurricane in another." This can be taken as an overall definition of chaos. In this sense, chaos is defined as exponential divergence in phase-space trajectory due to slight perturbation in initial condition. Consider two initial

condition for a hamiltonian H are $X_1(0)$ and $X_2(0)$. After time t, their values becomes. Due to presence of chaos,

$$|X_1(t) - X_2(t)| = e^{\lambda t}|X_1(0) - X_2(0)| \qquad (4.1)$$

λ is Lyapunov's exponent. Despite H being deterministic in nature, presence of chaos ($\lambda \neq 0$) can give very different result for slight change in initial condition. Such a system is known as 'Chaotic System' or 'Non-integrable System'. An integrable system, $H(p, r)$ with $p = (p_1, p_2, ..., p_N) =$ momentum and $q = (r_1, r_2, ..., r_N) =$ position has N different no. of conserved quantities $C = (C_1, C_2, ..., C_N)$, Number of conserved quantities is equal to degrees of freedom. So, a chaotic system can be defined alternatively as the system which have lower number of independent conserved quantities than degrees of freedom. Besides being sensitive to initial condition, a chaotic system possess important properties like ergodicity and mixing property. A brief discussion of these two properties along with KAM theorem is provided.

We will start the discussion with ergodicity. Consider hamiltonian of N identical classical particles of mass m with potential $V(r_1, ..., r_N)$ as,

$$H(p, r) = \frac{1}{2m} \sum_i p_i^2 + V(r_1, ..., r_N) \qquad (4.2)$$

(p, r) ,a point in phase-space, evolve in time following a trajectory constrained by energy hyper-surface, $H(p, r) = E$. One of many possible such trajectories is shown in Fig. 4.1.

Probability to find trajectory point at current time t, $(p(t), r(t))$ in a region of phase-space with $dv = (dp_1, dp_2, ..., dp_N, dr_1, dr_2, ..., dr_N)$ volume considering that general trajectory has visited every corner of phase-space is,

$$P(p, r)dv = \frac{1}{\int \delta H(p, r)}\delta(H(p, r) - E)dv \qquad (4.3)$$

This sort of stationary probability distribution, micro-canonical distribution, $\rho_{mc}(p, r) = \frac{1}{\int \delta H(p, r)}\delta(H(p, r) - E)$ was first approximated by Boltzmann and implies that probability of finding a state in a region of phase-space depends on volume of region. This constant probability gives us the idea of thermal equilibrium value of the system; it is phase-space average of the value interest as trajectory remains a equal time at equal
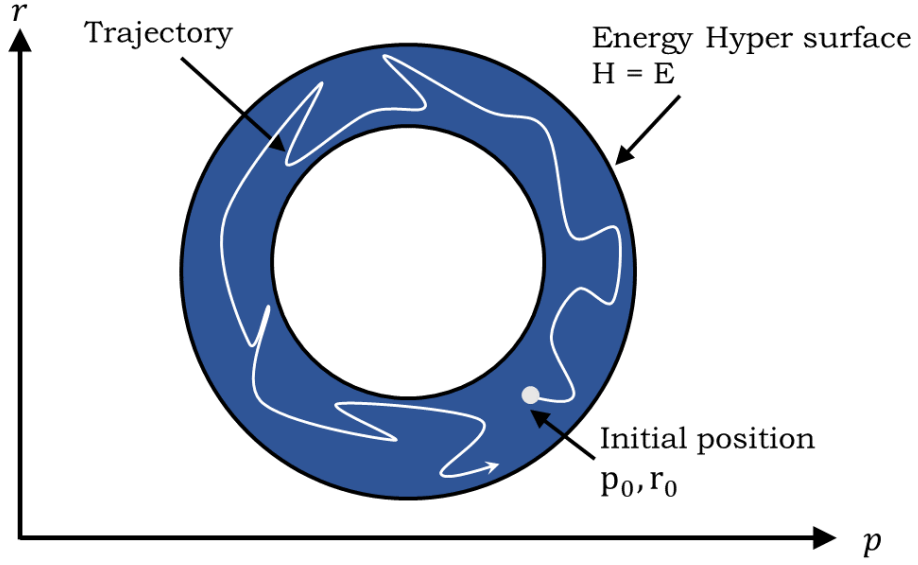
Figure 4.1: Phase space with one possible trajectory within energy hyper-surface $H = E$.

volume.

We can determine conditional probability of finding a particle within momentum $[p_1, p_1 + dp_1]$ with position given as $(dr_1, dr_2, ..., dr_N)$ as follows,

$$P(p_1|r_1, r_2, ..., r_N)dp = \frac{\int P_{mc}(p, r)dp_2 dp_3...dp_N}{\int P_{mc}(p, r)dp_1 dp_2...dp_N}dp_1 \tag{4.4}$$

where, marginal probability of finding a particle with momentum p_1 is,

$$P(p_1, r_1, r_2, ..., r_N) = \int P_{mc}(p, r)dp_2 dp_3...dp_N$$

$$= \frac{\sqrt{\pi^{3N}}}{\mathcal{T}(\frac{3N}{2})\int \delta H(p, r)}\sqrt{\left(E - V - \frac{p_1^2}{2m}\right)^{3N-3}} \tag{4.5}$$

Using such expression of marginal probability and joint probability distribution, we can find a closed form expression of conditional probability for equation 4.4 as

$$P(p_1|r_1, r_2, ..., r_N) = \frac{1}{\sqrt{2m\pi}}\frac{\mathcal{T}(\frac{3N}{2})}{\mathcal{T}(\frac{3N-1}{2})}\frac{\sqrt{(E - V - \frac{p_1^2}{2m})^{\frac{3N-2}{2}}}}{\sqrt{(E - V)^{\frac{3N-3}{2}}}} \tag{4.6}$$

For large N ($N \rightarrow \infty$) and for constant kinetic energy for each degree of freedom ($\frac{1}{2}k_B T$), expression for conditional probability becomes,

$$P(p_1|r_1, r_2, ..., r_N) = \frac{1}{\sqrt{2\pi m k_B T}} exp\left[- \frac{p_1^2}{2m k_B T} \right] \tag{4.7}$$

which is same as Maxwell distribution. Ergodicity gives us equilibrium momentum distribution for large number of particle system.

Mixing hypothesis is also essential to understand classical thermalization. Statistically speaking a system contain mixing property if statistical dependence of some property $X(t_1)$ and $X(t_2)$ of the system decreases as $|t_1 - t_2|$ increases. More precisely a dynamical system F is mixing if property of the system X in two different sub-spaces of phase-space A and B follows,

$$X(A \cap T^{-t}B) = X(B \cap T^{-t}A) \tag{4.8}$$

Intuitively, mixing property means that the dynamical evolution will evolve the phase points in such a way that points initially contained in subspace A eventually become homogeneously distributed over all measurable subspace B.

Using mixing property, we can divide the whole phase-space into several different block, c_i and replace original probability distribution $\rho(p, r)$ by average over such blocks as,

$$P(p, r) \longleftrightarrow \sum_i \frac{\int_{c_i} dr dp P(p, r)}{\int_{c_i} dr dp} U_{c_i}(p, r) \tag{4.9}$$

where,

$$U_{c_i}(p, r) = \begin{cases} 1 & \text{if } (p, r) \in c_i \\ 0 & \text{otherwise} \end{cases} \tag{4.10}$$

Dynamic evolution of such coarse grained probability distribution will eventually resort to micro-canonical distribution.

4.1.1 Kolmogorov-Arnold-Moser (KAM) Theorem

Clearly introduction of chaos causes appearance of chaotic trajectory (or ergodic trajectory). But an integrable system doesn't possess such trajectory, with periodic trajectory preventing it from being thermalized. A general classical dynamical system can be said to be a composition of non-integrable (chaotic) and integrable regions with limit relying on some parameters such as energy or the interaction strength. KAM theorem tells us under what condition a system can be considered as 'Chaotic' or 'Integrable' or an integrable system can achieve chaotic nature. KAM theorem tells us,

If the bounded motion of an integrable Hamiltonian H_0, described along a set of N invariant tori with frequencies ω_i, is disturbed by a small perturbation, ΔH, that makes the total Hamiltonian, $H = H_0 + \Delta H$ non integrable and if two conditions are satisfied:

- *the perturbation ΔH is small.*

- *the frequencies ω_i of H_0 are incommensurate,*

then the motion remains confined to an invariant N-torus, except for a negligible set of initial conditions that results in a meandering trajectory on the energy surface.

For a sufficiently small perturbation, some periodic trajectory lost its periodic nature and turn quasi periodic. The case of "except for a negligible set of initial conditions" suggests in-applicability of KAM theorem for a set of particular initial conditions. Moreover the applicability of the KAM theorem is only for an sufficiently small perturbation and chaotic behavior appears typically when unperturbed hamiltonian and perturbation are on the same order.

4.2 Quantum Thermalization

Consider a system with hamiltonian H has eigenstate $|\psi\rangle$ which describe the behavior of the system in Hilbert space completely. But in quantum statistical, $|\psi\rangle$ is not enough, we need density operator $\rho(t)$ which evolve as,

$$i\hbar \frac{d\rho(t)}{dt} = [H, \rho(t)] \tag{4.11}$$

Clearly system is well defined, no chaos is here. According to discussion of section 4.1 we cannot expect such a quantum system to be thermalized as it holds information of initial state of system throughout the whole evolution. How can one expect thermalization in quantum system? We will discuss some topic of quantum thermalization in this section.

4.2.1 Quantum Chaos

We cannot precisely define a phase-space for quantum system like we did for classical system as according to uncertainty principle, simultaneous determination of momentum and space is not possible. That's why quantum chaos has some difference from its classical counterpart, focus is mainly given on statistical study of eigenfuction and energy rather than time evolution. Quantum chaos appears due to presence of large number frequencies and random phase in a wave packet [141] presenting chaos as chaotic eigenstates. As we have seen from ergodicity property, for a non-chaotic system, motion is confined to invariant tori in phase-space but for chaotic system the whole phase-space is filled in a uniform way. Now how can we say that a quantum is whether chaotic or not? According to Berry-Tabor conjecture [142], a quantum system, in classical limit which is integrable, has energy eigenvalues generically behave like a sequence of independent random variables, follows a Poisson distribution. On the other hand, a quantum system with a non-integrable classical counterpart, energy eigenvalues follows a Wigner-Dyson distribution [143].

But there are some exceptions to such simple conjecture. For example, eigenfunction in chaotic billiard shows complicated spatial profile [144]. This prompts a new conjecture, eigenfunction of chaotic system is a sum of plane waves with random amplitude and phase [145]. We will discuss structure of such chaotic eigenstate in RMT (Random Matrix Theory) discussion in 4.2.2. This concept of defining quantum chaos in terms of eigenstate structure rather than level statistics was first discussed in [146] as vanishing correlation between eigenstates in appropriate basis.

4.2.2 Berry's Conjecture

As we have already discussed regarding the structure of chaotic wavefunction that it is random superposition of plane waves. We can write a chaotic eigenfunction $\psi(r)$ of N

particle state in a 3-dimensional system with r position coordinate and p momentum coordinate as,

$$\psi(r) = N \int dp_1 dp_2...dp_N A(p)\delta(E - \frac{p^2}{2m})e^{\frac{i\vec{p}.\vec{r}}{\hbar}} \qquad (4.12)$$

N is normalization constant, $A(p)$ is Gaussian random variable with $A^*(p) = A(-p)$ and E is eigen energy corresponding to state $\psi(r)$. Two point correlation function of such function at distance s is defined as,

$$\langle \psi^*\left(r + \frac{\Delta r}{2}\right)\psi\left(r - \frac{\Delta r}{2}\right)\rangle = \frac{1}{V}\int dp_1 dp_2...dp_N \delta(E - 2mp^2)exp\left(-\frac{i\vec{p}.\vec{\Delta r}}{\hbar}\right) \qquad (4.13)$$

here, $V = \frac{1}{N^2} = \int\int dr_1...dr_N dp_1...dp_N \delta(E - 2mp^2)$. Wigner function for such eigenfunction $\psi(r)$ is,

$$W(r,p) = \frac{1}{(2\pi\hbar)^{3N}}\int d(\Delta r)_1 d(\Delta r)_2...d(\Delta r)_N \psi^*\left(r + \frac{\Delta r}{2}\right)\psi\left(r - \frac{\Delta r}{2}\right)exp\left(\frac{i\vec{p}.\vec{\Delta r}}{\hbar}\right) \qquad (4.14)$$

Fourier transform of $\psi(r) \Longleftrightarrow \psi_F(p)$, gives us the expression of Wigner function as,

$$W(r,p) = \frac{1}{(2\pi\hbar)^{3N}}\int d(\Delta p)_1 d(\Delta p)_2...d(\Delta p)_N \psi_F^*\left(p + \frac{\Delta p}{2}\right)\psi_F\left(p - \frac{\Delta p}{2}\right)exp\left(\frac{i\vec{r}.\vec{\Delta p}}{\hbar}\right) \qquad (4.15)$$

So Wigner function acts as quasi-probability distribution in phase-space. We can take average of such distribution as,

$$W(\bar{r},p) = \int_{\Delta V_1}\frac{dr_1 dp_1}{2\pi\hbar}\int_{\Delta V_2}\frac{dr_2 dp_2}{2\pi\hbar}....\int_{\Delta V_N}\frac{dr_N dp_N}{2\pi\hbar}W(r,p) \qquad (4.16)$$

with $V = \cup\Delta V_1 \cup \Delta V_2.... \cup \Delta V_N$ with ΔV_i is centered around (r_i, p_i) and $\Delta V_i \to 0$. In thermodynamic limit, average of quasi probability distribution (Wigner function) is,

$$W(\bar{r},p) = \frac{\delta(E - 2mp^2)}{\int\int dr_1...dr_N dp_1...dp_N \delta(E - 2mp^2)} \qquad (4.17)$$

which is nothing but 'Micro-canonical Distribution'. So a quantum system with chaotic classical limit , the Wigner function of energy eigenstates reduces to the micro-canonical

distribution. This understanding will help us to further move down the road to realization of RMT (Random Matrix Theory) and ETH (Eigenstate Thermalization Hypothesis).

4.2.3 Random Matrix Theory

Consider a hamiltonian H as,

$$H = H_0 + V \tag{4.18}$$

where, system H_0 in integrable and has component $(H_0)_{i,j} = \delta_{i,j}C$ and V is perturbation to system H_0 with component $V_{i,j} = V_{j,i}^*$ drawn from a Gaussian distribution with mean 0 and variance σ^2. So hamiltonian H becomes a random matrix. For simple analytical calculation lets consider a 2×2 hamiltonian as,

$$H = \begin{bmatrix} C & V \\ V^* & C \end{bmatrix} \tag{4.19}$$

Eigen-energies of such hamiltonian is,

$$E_{1,2} = C \pm \sqrt{|V|^2} \tag{4.20}$$

Considering $V = V^*$ (for only real value of V), energy level statistics $P(\Delta E = E_2 - E_1)$ gives us,

$$P(\Delta E) = \frac{\Delta E}{\sigma^2} exp\left(-\frac{(\Delta E)^2}{2\sigma^2} \right) \tag{4.21}$$

Considering complex value of V (no time reversal symmetry), energy level statistics $P(\Delta E = E_2 - E_1)$ gives us,

$$P(\Delta E) = \frac{(\Delta E)^2}{\sqrt{\pi}\sigma^3} exp\left(-\frac{(\Delta E)^2}{2\sigma^2} \right) \tag{4.22}$$

It is as we have discussed earlier, chaotic eigenstate level statistics follow Wigner-Dyson statistics. Exact level spacing distributions do not have a closed analytic form. However, they are qualitatively (and quantitatively) close to the Wigner distribution.

If perturbation V is sufficiently strong, the eigenstates of the total H can be considered

as chaotic super-positions of many-body eigenstate of H_0. If eigenstate for system H is $|\psi_i^H\rangle$ with eigen-energy E_i^H and eigenstate for system H_0 is $|\psi_j^{H_0}\rangle$ with eigen-energy $E_i^{H_0}$,

$$|\psi_i^H\rangle = \sum_i a_i^j |\psi_j^{H_0}\rangle \tag{4.23}$$

where co-efficient a_i^H follows,

$$\langle a_i^j a_{i'}^{j'} \rangle = \delta_{i,i'}\delta_{j,j'} P(i,j) \tag{4.24}$$

where, $P(i,j)$ is chaotic wavefunction probability distribution, a function of $E_i^{H_0} - E_i^{H_0}$. Probability distribution of eigenfunction is found by Deutsch as,

$$P(i,j) = \frac{\frac{\delta E \Delta E}{\pi}}{(E_i^H - E_j^{H_0})^2 + (\delta E)^2} \tag{4.25}$$

where, δE is energy width of the system. Such Lorentzian probability distribution will later help us approximate thermal equilibrium value to micro-canonical average. We will discuss in 4.2.4 about the matrix elements of the operator under RMT.

In the above discussion, Mean field H_0 acts as a "natural" basis, where the most regular part of the dynamics is absorbed, thus defining the single particle states. In contrast, the residual component V may include interaction among particles and fluctuations. As a result, the whole system H acquires both collective motion on the background of the mean field, and chaotic dynamical features.

4.2.4 Matrix Structure of Operator under RMT

As we have seen, presence of interaction (or perturbation) causes even quantum system become chaotic. Interaction becomes effectively stronger with the growth of the excitation energy. Therefore, in an isolated system, thermalization can emerge for sufficiently high energy when the interaction effectively mixes the simple states (equation 4.23). It is to be noted that the randomness in V does not ensure chaotic nature of eigenfunction. Generic interactions without randomness can produce chaotic features in a region of a sufficiently high level density.

Consider a hermitian operator O defined in H basis as,

$$O = \sum_j O_{jj} |\psi_j^H\rangle\langle\psi_j^H| \tag{4.26}$$

where,

$$O|\psi_j^H\rangle = O_{jj}|\psi_j^H\rangle \tag{4.27}$$

Now for eigenfunction $|\psi_m^H\rangle$ and $|\psi_n^H\rangle$ matrix element of operator O is,

$$\langle\psi_m^H|O|\psi_n^H\rangle = O_{mn} = \sum_j O_j \langle\psi_m^H|\psi_j^H\rangle\langle\psi_j^H|\psi_n^H\rangle \tag{4.28}$$

Eigenfunction of a random matrix is itself a random unit vector and follow orthogonality property. Considering such orthogonality ψ_i^H we can write from equation 4.28

$$O_{mn} = \frac{1}{D}\sum_j \delta_{mj}\delta_{jn}O_{jj} \tag{4.29}$$

D is dimension of Hilbert space. So we have very different value for diagonal and off-diagonal component. Diagonal component of operator O is,

$$O_{mm} = \frac{1}{D}\sum_j O_{jj} = \bar{O} \tag{4.30}$$

and off-diagonal elements are,

$$O_{mn} = 0 \text{ for } m \neq n \tag{4.31}$$

Similarly we can determine fluctuation between diagonal and off-diagonal element (variance in matrix O_{mn}) as,

$$|O_{mn}^-|^2 - |O_{mm}^-|^2 = \frac{1}{D}\bar{O}^2 \tag{4.32}$$

4.2.5 Eigenstate Thermalization Hypothesis

Consider same hamiltonian H of equation 4.18. System is prepared at $|\psi^H(0)\rangle$ and allowed to evolve in time. At time t system wave function is $|\psi^H(t)\rangle$. We have already defined

eigenfunction of hamiltonian H, so we can express initial wavefunction as,

$$|\psi^H(0)\rangle = \sum_i c_i^H |\psi_i^H\rangle \tag{4.33}$$

So evolved wavefunction can be written as,

$$|\psi^H(t)\rangle = \sum_m e^{-iE_m^H t} c_m^H |\psi_m^H\rangle \tag{4.34}$$

Using expression 3.34, we can determine time-dependent expectation value of operator O (definition of such operator is given in equation 4.26) as,

$$\langle O(t)\rangle = \langle \psi^H(t)|O|\psi^H(t)\rangle = \sum_{m,n} (c_m^H)^* c_n^H e^{i(E_m^H - E_n^H)t} O_{mn} \tag{4.35}$$

with O_{mn} defined as,

$$O_{mn} = \langle \psi_m^H |O|\psi_n^H\rangle \tag{4.36}$$

Taking long time average of equation 4.35,

$$\langle \bar{O(t)}\rangle = \lim_{t\to\infty} \frac{1}{t} \int_0^t dt \left[\langle \psi^H(t)|O|\psi^H(t)\rangle\right] = \sum_{m,n} (c_m^H)^* c_n^H e^{i(E_m^H - E_n^H)t} O_{mn} \tag{4.37}$$

For exponential part of the function we can write,

$$\int_0^\infty dt e^{i(E_m^H - E_n^H)t} = \delta(E_m^H - E_n^H) = \delta_{mn} \tag{4.38}$$

which turn equation 4.37 as,

$$\langle \bar{O(t)}\rangle = \sum_m |c_m^H|^2 O_{mm} \tag{4.39}$$

As other term $\lim_{t\to\infty} \frac{\int_0^\infty \sum_{m,n,m\neq n}(c_m^H)^* c_n^H e^{i(E_m^H - E_n^H)t} O_{mn}}{t}$ goes to zero due to very small value of $O_{mn,m\neq n}$ (equation 4.31).

There are two conditions for thermalization of operator O. These are

- after some relaxation time, the average expectation value of this observable agrees

with the micro-canonical expectation value.

- temporal fluctuations of the expectation value about the micro-canonical prediction are small at most later times.

Close observation of equation 4.30 and 4.31 and considering small energy fluctuation in diagonal ensemble lets us assume that that diagonal element of observable O_{mm} does not depend on m so

$$\sum_m |c_m^H|^2 O_{mm} = \bar{O} \sum_m |c_m^H|^2 = Tr(\rho_{MC} O) = O_{MC} \tag{4.40}$$

where, ρ_{MC} is micro-canonical ensemble density matrix. So first condition of thermalization is satisfied.

We can determine temporal fluctuation of time averaged observable in long time limit as,

$$(\delta \bar{O})^2 = \lim_{t \to \infty} \frac{1}{t} \int_0^t dt[(O(t))^2 - O_{MC}^2] = \sum_{m,n,m \neq n} |c_m^H|^2 |c_n^H|^2 |O_{mn}|^2 \tag{4.41}$$

Temporal fluctuation of observable expectation is significantly small. So condition two of thermalization is satisfied. Equation 4.41 and 4.40 tells us that at any time t, expectation value of an observable O is the equal to its micro-canonical ensemble average value, implying ergodicity in quantum system.

Based on the above discussion ETH ansatz for matrix element of observable O can be written as [147],

$$O_{mn} = O(\bar{E})\delta_{mn} + e^{-\frac{S(\bar{E})}{2}} f_0(\bar{E}, \Delta E) R_{mn} \tag{4.42}$$

where, $\bar{E} = \frac{E_m^H + E_n^H}{2}$, $S(E)$ is thermodynamic entropy, and R_{mn} is a matrix with random element drawn from a normal distribution with zero mean and unit variance.

4.2.6 Other Approach to Thermalization

There are some other approach to thermalization. We will not discuss them in detail rather give an overview of those ideas. 'Typicality' takes the approach of majority state, observable behavior. Any chosen random state is likely in connection with canonical

ensemble. A detail overview of typicality can be found in [148]. 'Equilibration' takes the idea of thermalization condition for non-thermal atypical initial state. If inverse participation ratio of initial state (a measure of the number of eigenstates that contribute a non-trivial weight to the initial state) is small for such initial state then equilibration can be realised. A more detail discussion for equilibration condition is discussed in [149].

4.3   Localization

Theoretical analysis requires *'simple'* systems to analyze efficiently rather than a *'complex'* system. Simpler the law governing the system, it is easier to understand. Our notion of worldview is simple: Nature follows some fundamental laws and these laws can be expressed by some partial or ordinary differential equation. Everything is simple and neat except, of course, nature itself. Despite the complexity of nature, standard reductionism [150] split such complex system into small, simple constituent parts which can be described by *'simple'* laws. In his paper [150], P.W.Anderson write the success of reduction hypothesis as ***"The reductionist hypothesis may still be a topic for controversy among philosophers, but among the great majority of active scientists I think it is accepted without question. The workings of our minds and bodies, and of all the animate or inanimate matter of which we have any detailed knowledge, are assumed to be controlled by the same set of fundamental laws, which except under certain extreme conditions we feel we know pretty well."***

Despite the success of reductionism, one question remains, *'can one always reconstruct the properties of composed systems from the workings of their parts?'* The ability to reduce everything to simple fundamental laws does not necessarily mean the ability to start from those laws and reconstruct the universe. In fact, the more the elementary particle physicists tell us about the nature of the fundamental laws, the less relevance they seem to have to the very real problems of the rest of science, much less to those of society. The behavior of large and complex composition of simple systems cannot be understood by simple extrapolation of the constituent system's properties. Instead, at each level of complexity, entirely new properties appear, and the understanding of the new behaviors requires research.

A system with defect is one such complex system. Without defect, analysis of system

can be done utilizing 'reductionism' ideas. But presence of defect makes system complex to be explained beyond such 'simplistic' ideas. Until now, discussion of thermalization considers only pure system without any form of disorder. But as we intend to analyze influence of defect in this thesis, it is essential for some discussion on the influence of defect on thermalization process. That can be translated to understanding a 'complex system'. Disorder in a system can induce localization which can effectively hamper thermalization process. Localization is a fascinating phenomenon that can give rise to some remarkable result. In this section we will discuss about theoretical framework of such localization process.

4.3.1 Anderson Localization (AL) : Transfer Matrix

A periodic crystal with periodic potential has Bloch eigenstate, a propagating state. But when such a periodicity is broken by randomness in a non-interacting system, quantum back-scattering of single-particle eigenstates can eventually localize particles in a finite region of space, leading to the absence of diffusion. This is the summary of Anderson localization. Experiments at Bell Labs [151] found that the relaxation times of electron spins in phosphorous-doped Si semiconductors was abnormally large. The theoretical framework at the time was based on band theory, Bloch states and Drude's theory of conductivity, predicting thus a diffusive motion of electrons. It was considered electrons in metal to be acting as quantum random walkers, losing memory after each collision with an impurity center. Larger the concentration of impurities, larger the number of collision, larger the resistance. Anderson's analysis suggested that beyond a critical disorder strength resistance will just get abnormally high (mean free path being lower than Fermi wavelength, conductance = 0) which prevents the diffusive motion of electrons. Eigenstates are localized by the valleys of the disordered potential.

First we will try to develop some intuition on such localization in disordered systems using solvable models. It turns out that in a one-dimensional system with the barriers at random positions provides such a solvable model. Such disordered potential is shown in Fig. 4.2.

For a perfect periodic crystal distance between two adjacent barrier is fixed, Δx. But for for disordered potential, such distance is not fixed rather a random variable. We can
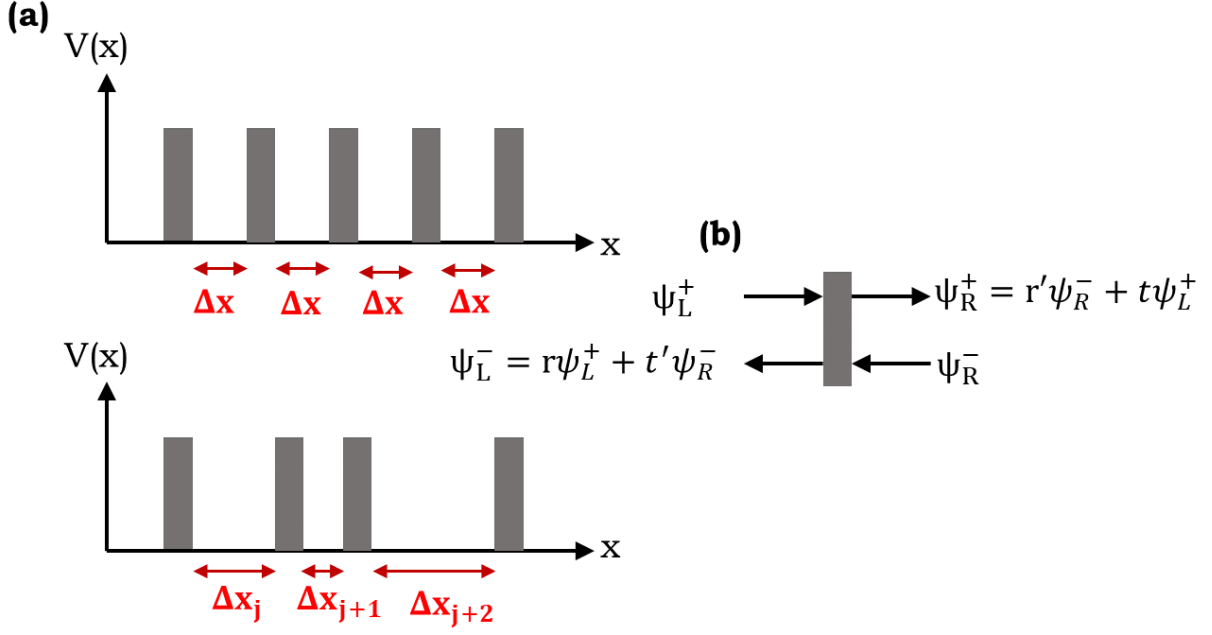
Figure 4.2: (a) 1D periodic potential with period Δx and random potential with Δx being random. (b) Transfer matrix map for one potential barrier.

model such barrier as, $V_i(x) = V_0 \delta(x - x_i)$ with variable x_i being random. For one barrier (Fig. 4.2 (b)), transfer matrix M can map wave-function from left to right as,

$$\begin{bmatrix} \psi_R^+ \\ \psi_R^- \end{bmatrix} = M \begin{bmatrix} \psi_L^+ \\ \psi_L^- \end{bmatrix} \tag{4.43}$$

where m is defined as,

$$M = \begin{bmatrix} \frac{1}{t} & \frac{r*}{t*} \\ -\frac{r}{t} & \frac{1}{t*} \end{bmatrix} \tag{4.44}$$

Here we eliminate r', t' with unitarity relations in favor of r, t and their complex conjugates to get this simple form of M. For two barrier, indexed as 1 and 2, we find combined transfer matrix $M_{12} = M_2 M_1$ and resulting transmission coefficient,

$$\frac{1}{t_{12}} = \frac{1}{t_1 t_2} + \frac{r_1 * r_2}{t_1 * t_2} \tag{4.45}$$

This transmission amplitude contains the entire series of repeated internal reflection between the two barriers as $t_{12} = t_1 t_2 + t_2 r_1 r_2 t_1 + t_2 (r_1 r_2)^2 t_1 + \dots$. The transmission probability $(T = |t|^2)$ reads,

$$T_{12} = \frac{T_1 T_2}{|1 - \sqrt{R_1 R_2} e^{i\theta}|^2} \tag{4.46}$$

where, θ is total phase accumulated during one complete internal reflection. Due to random placement of barrier this θ is a random variable with $[0, 2\pi]$. Taking ensemble average of equation 4.46 we get,

$$\langle T_{12} \rangle = \frac{T_1 T_2}{1 - R_1 R_2} \tag{4.47}$$

The so-called element resistance of barrier, $\frac{R}{T}$, calculated with the classical transmission, is additive for two barriers.

$$\frac{R_{12}}{T_{12}} = \frac{1 - T_{12}}{T_{12}} = \frac{1 - T_1}{T_1} + \frac{1 - T_2}{T_2} \tag{4.48}$$

Classical resistance across N identical barriers along 1D wire of length L with density $n = N/L$ is $\frac{R_1}{T_1} N$

$$R_{tot} = \frac{R_1}{T_1} N = \frac{L}{L_1} \tag{4.49}$$

where $L_1 = \frac{T_1}{nR_1}$ is length characterizing the back-scattering strength of a single impurity. Within the constrain of electronic conduction, equation 4.49 is the famous Ohm's Law, A wire's resistance grows with length. Ensemble averaging has cleared any phase-coherence and made the system a purely classical transport process. But equation 4.48 cannot be easily generalized to more than two barriers due to complication to average of the product of transmission matrices even over random phases. So rather than averaging over T_{12}, we intend to average over $ln(T_{12})$ which results in,

$$\langle ln(T_{12}) \rangle = \langle ln(T_1) \rangle + \langle ln(T_2) \rangle \tag{4.50}$$

Due to the analyticity of the complex logarithm for all $0 < R_1 R_2 < 1$,

$$\int_0^{2\pi} \frac{d\theta}{2\pi} ln(|1 - \sqrt{R_1 R_2} e^{i\theta}|) = 0 \tag{4.51}$$

The generalization for many barriers is now easy because $\langle ln(T) \rangle$ is additive. Such value for a channel of length L grows on average like $\langle ln(T) \rangle = nL \langle ln(T_1) \rangle$. With this scaling behavior, one obtains that the log-averaged transmission

$$exp(\langle ln(T) \rangle) = e^{-\frac{L}{L_{loc}}} \tag{4.52}$$

which drops exponentially fast with increasing sample length L and L_{loc} is defined as $1/n|ln(T_1)|$. This is a hallmark of strong localization by disorder.

4.3.2 Anderson Localization (AL) : Tight Binding Hamiltonian

A simple calculation only in one dimension is given in previous section. In this section we will provide more generic case for arbitrary dimension case. Considering the lattice in d-dimensional space with sites labeled by i, tight binding Anderson Hamiltonian can be written as,

$$H = -h \sum_{i,j}(a_i^\dagger a_j + a_j^\dagger a_i) + \sum_i V_i a_i^\dagger a_i \tag{4.53}$$

where $a_i(a_i^\dagger)$ is annihilation (creation) operator for particles at site i (particles can be Fermion or boson with corresponding commutation relationship), h is hopping amplitude (or tunneling coefficient from site i to site j) and V_i the on-site energies, independent, identically distributed (iid) random variables (RVs) that are uniformly distributed in $[-W/2, W/2]$ with W is the strength of the 'disorder'. We will consider solution of equation 4.53 for three different cases; (i) Disorder free case. (ii) Infinite disorder case. (iii) Diffusion case.

Disorder Free Case (W = 0) : Consider the hamiltonian in equation 4.53 with $W = 0$ and a periodic potential with period L. In this case eigenstate is defined as,

$$\psi(t, r_i) = \frac{1}{L^d} \sum_k e^{i\vec{k}.\vec{r_i} + 2i \sum_{i=1}^d cos(k_i)ht} \tag{4.54}$$

where k is momentum vector with $\frac{2\pi n}{L}$ and k_i is momentum along i^{th} dimension $(k_x, k_y, k_z$ for 3d xyz coordinate). In thermodynamic limit $(L \to \infty)$ wavefunction $\psi(t, r_i)$ reads,

$$\psi(t, r_i) = i^d \prod_{i=1}^d J_{r_i}(2th) \tag{4.55}$$

where, J_{r_i} is Bessel function of first order. We can determine probability of $\psi(t, r_i)$ to

return to initial state after some time t,

$$p(t) = |\psi(t,0)|^2 \sim \frac{1}{t^d} \tag{4.56}$$

and mean square displacement of the centre of wave-packet is,

$$\langle r(t) \rangle^2 = \sum_{r_i} r_i |\psi(t,r_i)|^2 = 2dh^2 t^2 \tag{4.57}$$

From equation 4.55 we can see that, with time wave-packet return probability goes to zero and wave-packet diverges rapidly with time. This is the condition for 'Ballistic transport'.

Infinite Disorder Case ($W = \infty$) : Now we consider hamiltonian in equation 4.53 with $W = \infty$ or more accurately $h/W \sim 0$. In this case eigenstate is defined as (with initial excitation is at $r_i = 0$),

$$\psi(t,r_i) = e^{-iV_0 t}\delta_{r_i,0} \tag{4.58}$$

We can determine return probability and mean square displacement for such wave-packet. It can be easily determined that for

$$p(t) = 1 \text{ and } \langle r(t) \rangle^2 = 0 \text{ for } t \to \infty \tag{4.59}$$

State is completely localized at $r_i = 0$.

Diffusion Case ($0 \le W \le \infty$) : Complication arises when g/W is neither zero nor infinity but rather a finite value, a finite competition between the hopping and the 'localizing' disordered term of the Hamiltonian. Classical understanding predicts the motion of the particle consists in a succession of ballistic propagation (in region without disorder) and elastic scattering against impurities. Such a picture leads to a diffusive propagation as,

$$\langle r(t) \rangle^2 = Dt \text{ for } t \gg \tau \tag{4.60}$$

where $D = v^2\tau$ is diffusion coefficient, τ and v is mean free time and velocity between successive collision. The scattering rate $(\frac{1}{\tau})$ can be found using perturbation theory by adding disorder with the plane wave case (case (i)). In semiclassical sense, we can assume

the particle has a definite momentum k and compute the scattering probability per unit time using the Fermi golden rule,

$$\frac{1}{\tau} = \frac{2\pi}{\hbar} \sum_{k'} |\sum_i \langle k|i\rangle\langle i|k'\rangle|^2 \delta(E_k - E_k') \tag{4.61}$$

Average over disorder i gives us the result,

$$\frac{1}{\tau} = \frac{\pi W^2}{12}\rho(E_k) \tag{4.62}$$

$\rho(E_k)$ is density of states at energy $E = E_k$. For such case expression for diffusion coefficient, D becomes,

$$D = \frac{12v^2(E)}{\pi W^2 \rho(E)} \propto \frac{1}{W^2} \tag{4.63}$$

Here, diffusion velocity is considered as a function of energy, E ($v = \frac{\delta E_k}{dk}$). Diffusion coefficient is inversely proportional to disorder strength (W) but never zero (equation 4.63). Anderson predicted that the diffusion coefficient might in fact vanish for a sufficiently strong (but finite) disorder, $W > W_c$ [152].This is 'Anderson localization'. In such case, $\langle r(t)\rangle^2$ and $p(t)$ remains finite for all t.

All eigenstates are localized above a critical value of the disorder strength. Now question can be asked whether extended (disorder free) and localized states (infinite disorder) can simultaneously exist at different energy densities. If the answer is yes, one can have mobility edges, defined as the energy which separates localized states from extended (delocalized) states. Typically, extended and localized states cannot coexist at the same energy density. As such, mobility edges must separate localized and extended bands. Such mobility edge is shown in Fig. 4.3.

4.3.3 Localization: Scaling Theory

A scaling theory explains a property of a physical system by considering their behavior under changes of size. Utilizing scaling theory, one can expect to capture those microscopic insensitive features on macroscopic scales. One cannot expect to get some precise location of critical point in parameter or system specific data from such semi-quantitative approximation of scaling theory. Scaling theory can provide surprisingly accurate
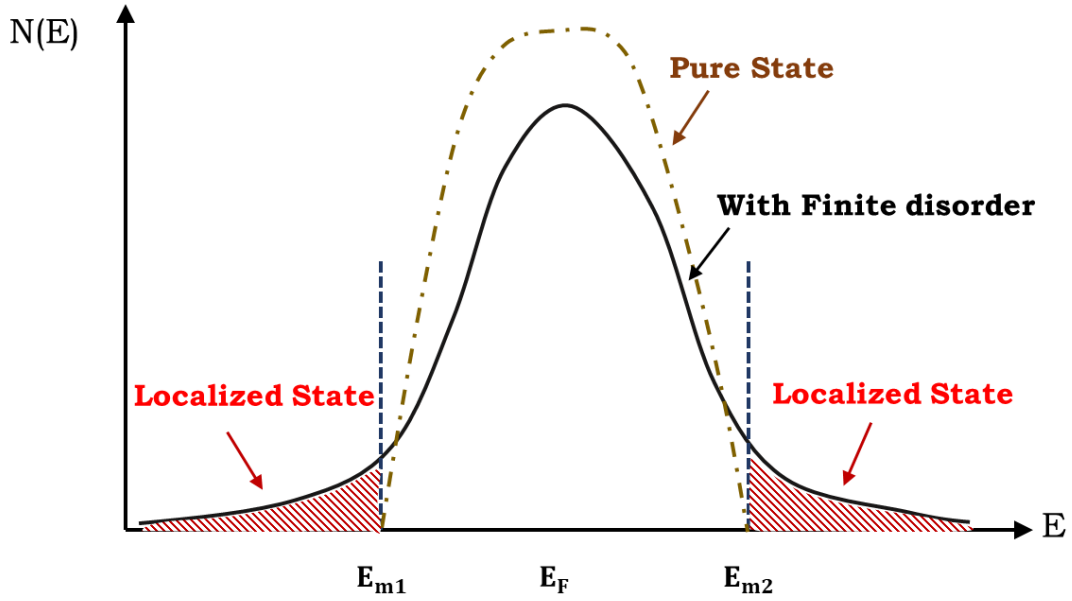
Figure 4.3: Energies E_{m1} and E_{m2} which separate the regions of localized and delocalized (pure) states are mobility edges. For strong disorder $E_{m1} \approx E_{m2}$ and all the states are localized. When the Fermi energy, E_F crosses the mobility edge we have the Metal Insulator transition.

prediction based on microscopic behavior.

Traditionally, the scaling theory of localization is formulated in terms of a channel's proper conductance, a dimensionless parameter defined as $g = \frac{T}{R}$. A perfectly transmitting channel $T = 1$ has a proper conductance of $g = \infty$, and a perfectly resisting channel with $T = 0$ has $g = 0$, which seems a reasonable definition. We have already used such definition in equation 4.48 which gives us resistivity behavior of equation 4.52. We can write down equation 4.52 as a function of sample length L,

$$g(L) = \begin{cases} \frac{L_{loc}}{L} & \text{if } L << L_{loc} \\ \frac{1}{e^{L/L_{loc}-1}} & \text{if } L >> L_{loc} \end{cases} \tag{4.64}$$

Length of the channel changes the behavior of channel as seen from Fig. 4.4. Short channel follows Ohm's law where long channel (channel length is long compared to localization length) do not. But in order to understand behavior of g with length L, we need β function which is defined as,

$$\beta(L) = L \frac{\delta ln(g)}{\delta L} \tag{4.65}$$
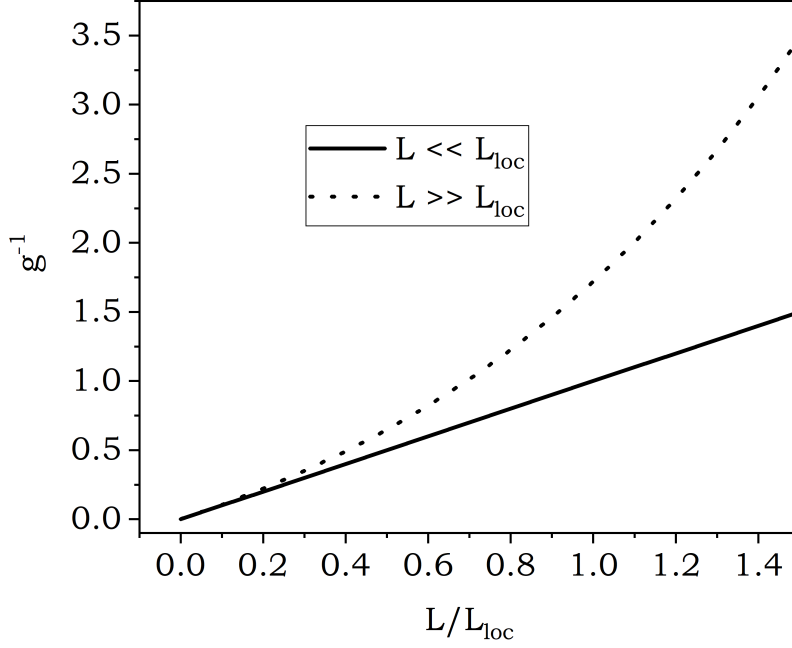
Figure 4.4: Resistance of a 1D channel as function of L . Short channel's resistance grows linearly (according to Ohm's law, solid line), whereas long channel's resistance shows exponential behavior (dash line).

$\beta = 0$ means value of g does not change with L. For 1D long channel using g from equation 4.64 one can determine β as,

$$\beta(L) = \frac{L}{L_{loc}} \frac{1}{e^{L/L_{loc}} - 1} \tag{4.66}$$

which can be utilized to express β as function of g, $\beta(g)$

$$\beta(g) = -(1+g)ln(1+g^{-1}) \tag{4.67}$$

For a generalized d dimensional system, we can generalize expression from equation 4.67 as,

$$\beta(g) = (d-1) - (1+g)ln(1+g^{-1}) \tag{4.68}$$

A plot of $\beta(g)$ vs $ln(g)$ for three different dimension $(d = 1, 2, 3)$ is shown in Fig. 4.5.

In 1D, for short samples the conductance g is large, and $lim_{g\to\infty}\beta(g) = -1$ and for long samples asymptotically $\beta(g) = ln(g)$. $\beta(g)$ can thus explain the change in system behavior with system size. Although for $d = 1$, $\beta(g) < 0$ for all g implying system
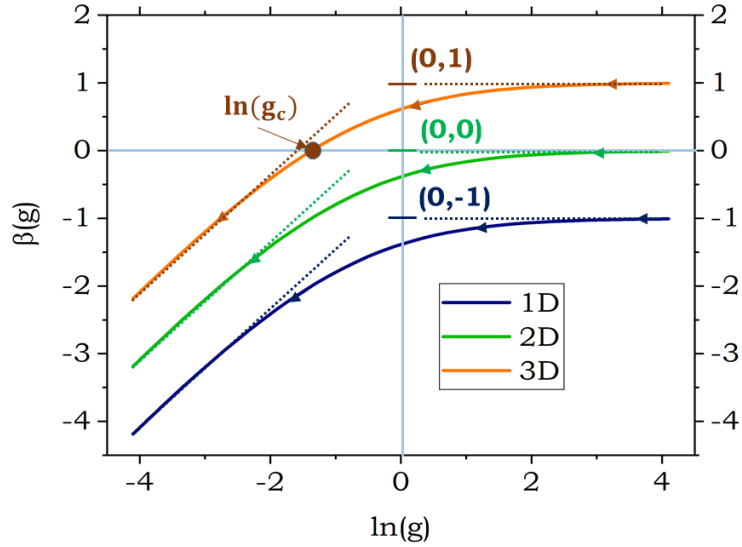
Figure 4.5: $\beta(g)$ vs $ln(g)$ plot for 1D, 2D and 3D system. Arrow sign in each plot shows the direction of increasing channel length (transition from Ohmic region to localization region). Critical point g_c indicates metal insulator transition.

resistance increases with increase in system size. But for $d = 2$, $lim_{g\to\infty}\beta(g) = 0$ implies length independent conductance. Both one and two dimensional case shows that $\beta(g) < 0$ for all g, indicating insulator at any length. But for 3D system, for $g > g_c$ a metal insulator transition occurs .Although scaling theory can only give a semi-quantitative idea of such critical point rather than its precise location.

4.3.4   Localization: Disorder with Interaction

So far only disorder can induce localization. But in reality interaction among particles can also cause localization. This might led someone to think that presence of both components would strengthen insulating behavior. This naive assumption underestimates the considerable richness of the disordered many-body problem. Interactions can destroy disorder-induced localization, and disorder can transform localized state to something quite different (Mott insulator to exotic glassy states). Discussion in this section will not contain too much mathematical expression like previous section.

Consider a system shows sharp phase transition due to some parameter (for example temperature) change when it contains no disorder. With introduction of disorder, how does the behavior of such phase transition will modify? In 1974, Harris formulated a general criterion that can guide our answer for such question [153]. Consider the pure

system shows phase transition with temperature, correlation length L_c diverges with temperature as, $|T - T_c|^-x$. But for a disordered system, instead of a single critical temperature T_c, there are *'local critical temperature'*, $T_{c,loc}$ with spatial variation due to local variations in the couplings. The central limit theorem suggests that fluctuations of the mean of $T_{c,loc}$ in a localization volume decay as $L_c^{-d/2}$. So,

$$L_c^{d/2} = |T - T_c|^{-xd/2} \tag{4.69}$$

Critical point in disorder must follow,

$$xd > 2 \tag{4.70}$$
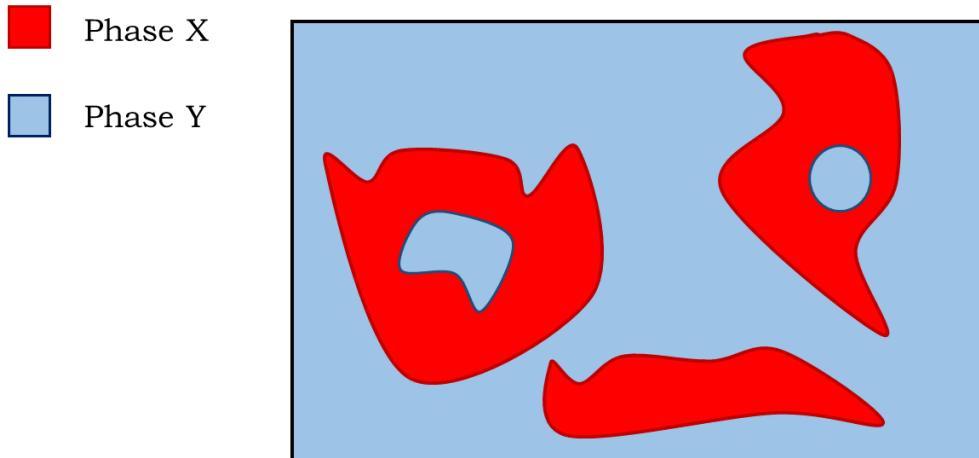
Figure 4.6: Schematic depiction of a Griffiths phase in a disordered system.

Equation 4.70 is known as 'Harris Criterion'. If a clean critical point follows such criterion, weak disorder cannot change universal properties of clean system. Otherwise, weak disorder will impact transition characteristics of the system. Consider in clean system shows phase X for $T < T_c$ and phase Y for $T > T_c$. Disorder as we have discussed induces spatial variation in the couplings which results in local phase transition. When the bulk of the system is in phase X, there can still be regions that are locally in phase Y, as shown in Fig. 4.6. These regions are known as Griffiths regions, and the phase in which they appear is known as a Griffiths phase. If the disorder is spatially uncorrelated, the Griffiths regions get exponentially rare as their size increases. But Griffiths region

can arbitrarily appear [154, 155].

4.3.5   Many Body Localization (MBL): Lack of Thermalization

Up until now, we only consider only single particle hamiltonian (equation 4.53) except some phenomenological study at section 4.3.4. Adding interaction $U(i-j)$ to equation 4.53 we get,

$$H = -h \sum_{i,j} (a_i^\dagger a_j + a_j^\dagger a_i) + \sum_i V_i a_i^\dagger a_i + \sum_{i,j} a_i^\dagger a_j^\dagger U(i-j) a_j a_i \qquad (4.71)$$

If all single particle wavefunction, $\psi_\alpha(r_i)$ is localized for some disorder strength W with eigen energy E_α then we can write hamiltonian H from equation 4.71 as,

$$H = \sum_\alpha E_\alpha n_\alpha \sum_{\alpha,\beta,\gamma,\delta} u_{\alpha,\beta,\gamma,\delta} a_\alpha^\dagger a_\beta^\dagger a_\gamma a_\delta \qquad (4.72)$$

Here a_α is annihilation operator defined as, $a_\alpha = \sum_i \psi_\alpha(r_i) a_i$. So presence of disorder and interaction can indeed localize many body wavefunction with $\sum_\alpha E_\alpha$ energy.

It is easy to understand that presence of localization can change ETH picture. Presence of strongly localized state with site dependent energy (equation 4.58) prevent any sort of energy exchange between sites, prevents thermalization. Even for many body case, many body eigenfunction is simply product state $(|\psi(r)\rangle = |\psi(r_1)\rangle \otimes |\psi(r_2)\rangle \otimes ... \otimes |\psi(r_i)\rangle...)$. But question can be asked regarding will thermalization prevail with the introduction of interaction as has been done in equation 4.71? Answer is based on relative strength of disorder compared to strength of interaction. As done in [156, 157], non-thermalization situation can survive even with weak interaction. We can expect a transition from insulating state to metal for relative strength of interaction to disorder. For $W/u >> 1$ we find the system in complete localization, a Mott insulator state without any thermalization. In the limit of $u/W \rightarrow \infty$, superfluid (metal in case of Fermionic particles) state appears following ETH ansatz. But in the middle, as we have already discussed in section 4.3.4 presence of Griffiths phase and local temperature is dominant, a 'Glassy State' appears with local region having different phase that the whole system. Such state can present thermalization in small local region rather across the whole system. As in thermalization of quantum system, we expect whole system acts as thermal bath of its

own (whole system is thermal to one of its component), presence of disorder can change the size of such bath and subsystem. As a result, we find ourselves with a system with only local thermalization occurs.

4.4 Bose Hubbard Model

Analysis of disordered system is often too complex to perform analytically. As a consequence, we need to resort to numerical analysis of the problem based on some standard model. One of such example is numerical analysis of XXZ Heisenberg model for analysis of ferromagnetism. For a better understanding the thermodynamic behavior of disordered bosonic system, numerical calculation of Bose-Hubbard Model has been done in this dissertation. In this section, a brief introduction of this Bose-Hubbard model is given.

Bose-Hubbard (BH) model is defined for spinless bosonic particle with repulsive interaction

$$H = -t \sum_{\langle ij \rangle} (b_i^\dagger b_j + b_j^\dagger b_i) - \mu \sum_i \hat{n}_i + \frac{U}{2} \sum_i \hat{n}_i(\hat{n}_i - 1) + \sum_i V(r_i)\hat{n}_i \tag{4.73}$$

Here, t is tunneling parameter, U is on-site interaction and μ is chemical potential, $b_i^\dagger(b_i)$ is boson creation (annihilation) operator and $\hat{n}_i = b_i^\dagger b_i$ is number operator for site i with position r_i. Summation over $\langle ij \rangle$ indicates nearest neighbour hopping only and $V(r_i)$ is confining potential. Discussion for ideal case $V(r_i) = 0$ and disordered case $V(r_i) \neq 0$ is essential for understanding the influence of defect on overall phase transition characteristics.

4.4.1 Ideal Case

For ideal situation, $V(r_i) = 0$. In this case, BH model can describe two different states of bosonic system; superfluid state (In the lime of $U/t \to 0$) and Mott Insulator (In the lime of $t/U \to 0$) state accurately. Before delving into the detail into each state and phase transition, initial analysis is needed to be done on BH model. Interaction term in Hamiltonian of equation 4.73 plays an important role. First, lets consider $t = 0$, no hopping is present and only interaction is present. In that case,

$$H_{int} = -\mu \sum_i \hat{n}_i + \frac{U}{2} \sum_i \hat{n}_i(\hat{n}_i - 1) \tag{4.74}$$

In this case, different sites are completely decoupled. So wavefunction of such function in Fock space is,

$$|n_{int}\rangle = |n_1\rangle \otimes |n_2\rangle...|n_N\rangle \tag{4.75}$$

here N is total number of site and $n = n_1 + n_2 + ... + n_N$, total number of boson in that state $|n_{int}\rangle$. Wavefunction is a simple combination of total number of particles of each site. This case is almost identical to the case of Many-Body Localization (MBL) effect. Ground state energy of interaction hamiltonian, H_{int} depends on n, number of boson in ground state,

$$\text{For } n = 0, \ E_{int} = 0$$

$$\text{For } n = 1, \ E_{int} = -\mu$$

$$\text{For } n = 2, \ E_{int} = -2\mu + U$$

$$\text{For } n = 3, \ E_{int} = -3\mu + 3U$$

So ground state energy is,

$$E_{int} = -n\mu + \frac{U}{2}n(n-1) \tag{4.76}$$

and ground state boson number follows the following criterion,

$$(n-1)U < \mu < nU \tag{4.77}$$

There are level crossing between states with different integer fillings. Adjacent states have sufficient gap away from level crossing. Evolution of ground state energy and ground state boson number with chemical potential, μ is shown in Fig. 4.7.

Absence of hopping amplitude causes the system to go into Mott-insulator phase. In
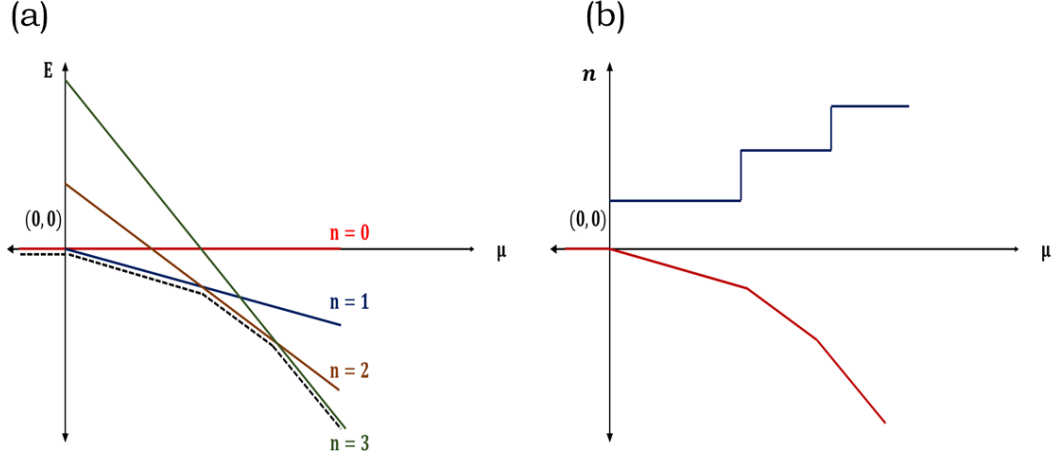
Figure 4.7: (a) Energy of ground state vs chemical potential plot for different ground state boson number. (b) Evolution of ground state energy along with particle number with chemical potential. Red dashed line shows the evolution of ground state energy while blue line shows evolution of ground state occupation. (equation 4.46 and 4.77).

the opposite extreme limit $(U/t \to 0)$, superfluid phase sustains. In that limit we can write wavefunction simply as,

$$|\psi\rangle = \frac{1}{\sqrt{N!}}(b_{k=0}^{\dagger})^N|0\rangle \tag{4.78}$$

To understand the transition from superfluid to Mott-insulator state we need to resort to Site Decoupled Mean Field Theory (SDMFT) and use the following decoupling ,

$$b_i^{\dagger}b_j = \langle b_i^{\dagger}\rangle b_j + b_i^{\dagger}\langle b_j\rangle - \langle b_i^{\dagger}\rangle\langle b_j\rangle \tag{4.79}$$

As a result, Hamiltonian from equation 4.73 is decoupled as,

$$H = -t\sum_{\langle ij\rangle}(\langle b_i^{\dagger}\rangle b_j + b_i^{\dagger}\langle b_j\rangle - \langle b_i^{\dagger}\rangle\langle b_j\rangle + \langle b_j^{\dagger}\rangle b_i + b_j^{\dagger}\langle b_i\rangle - \langle b_j^{\dagger}\rangle\langle b_i\rangle) + H_{int} \tag{4.80}$$

H_{int} is defined in equation 4.74. By considering $\langle b_i^{\dagger}\rangle = x$, we get,

$$H = -2dt\sum_i(xb_j + x^*b_i^{\dagger} - |x|^2 + h.c.) + H_{int} \tag{4.81}$$

Ground state energy for such hamiltonian is

$$E = E_{int} + E^{(2)} \tag{4.82}$$

where only second order perturbation theory has been considered and E_{int} is defined in equation 4.76. Second order correction can be determined as,

$$E^{(}2) = 2dt|x|^2 + \sum_{|n\rangle \neq |n_{int}\rangle} \frac{|\langle n_{int}|(-2dt[xb^\dagger + x^*b])|n\rangle|}{E_{int} - E_n} \tag{4.83}$$

where, E_n is eigenstate of H corresponding to wavefunction $|n\rangle$. Using the following relationship we can determine a close form for E^2.

$$\langle n_{int}|(-2dt[xb^\dagger + x^*b])|n_{int} + 1\rangle = -2dtx^*\sqrt{n+1}$$

$$\langle n_{int} - 1|(-2dt[xb^\dagger + x^*b])|n_{int}\rangle = -2dtx\sqrt{n} \tag{4.84}$$

Close form of second order correction to ground state energy is (taking $z = -2dt$),

$$E^{(2)} = z|x|^2 + z^2|x|^2\left[\frac{n+1}{\mu - Un} - \frac{n}{\mu - U(n-1)}\right] \tag{4.85}$$

If $E^{(2)}/|x|^2 > 0$, we find a stable Mott-insulator state. Transition line in plane $(t/U, \mu/U)$ is defined as,

$$\frac{1}{z} = \frac{n}{\mu - U(n-1)} - \frac{n+1}{\mu - Un} \tag{4.86}$$

Such transition line for Mott-insulator to superfluid transition or BH model phase diagram is shown in Fig. 4.8 for different n along with Mott lobes. To determine Mott lobes, we need to find solution of μ from equation 4.86. We get solution for μ as,

$$\mu_{\pm,z} = -\frac{z}{2} \pm \frac{1}{2}\sqrt{z^2 - 4z\left(n + \frac{1}{2}\right) + U^2} \tag{4.87}$$

We can easily determine the critical value of $z = 2dt$ for Mott-insulator to superfluid transition by setting both solution of $\mu_{\pm,z}$ equal to one another. Critical value of z (hopping amplitude) becomes,

$$z_c = U(2n + 1 - 2\sqrt{n^2 + n}) \tag{4.88}$$
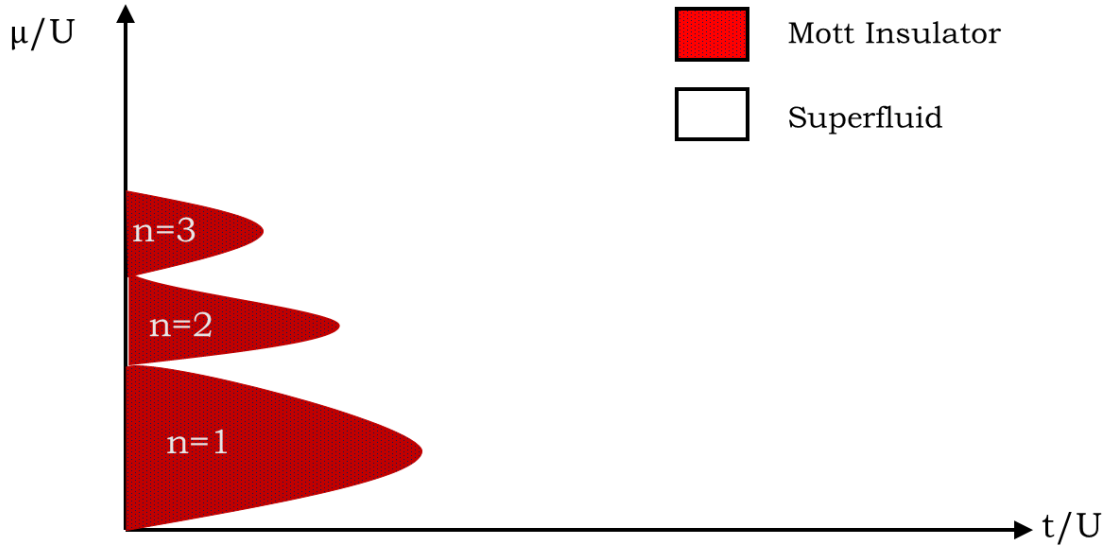
Figure 4.8: SDMFT phase diagram of the Bose-Hubbard model with first three Mott lobes.

We thus obtain a series of Mott lobes labeled by the integer n with peaks defined by equation 4.88. Some key parameters to determine such transition are number density and compressibility. Number density is defined as,

$$\langle n \rangle = \sum_i \langle b_i^\dagger b_i \rangle \tag{4.89}$$

And compressibility is defined as,

$$\kappa = \frac{d\langle n \rangle}{d\mu} \tag{4.90}$$

In MI phase of matter compressibility is zero as number density during this state is fixed and is equal to an integer value according to Mott lobes it is in. As the system goes to superfluid phase, non-integer number density and non zero compressibility is found.

4.4.2 Disorder BH Model: Bose Glass Phase of Dirty Bosons

Presence of disordered confining potential can change transition of MI-SF significantly. As we have discussed in previous section of localization, disorder induces localization. Even slight presence of disorder can result in complete localization for 1D system. But in that

discussion we do not consider any sort of interaction. A simplistic discussion with both disorder and interaction is provided in section 4.3.4. Based on that discussion, we can say that MI-SF transition can be significantly influenced by disorder strength compared to interaction strength. Disorder induced change in BH phase diagram is shown in Fig. 4.9. Presence of disorder potential causes the appearance of new phase, Bose glass phase [158].
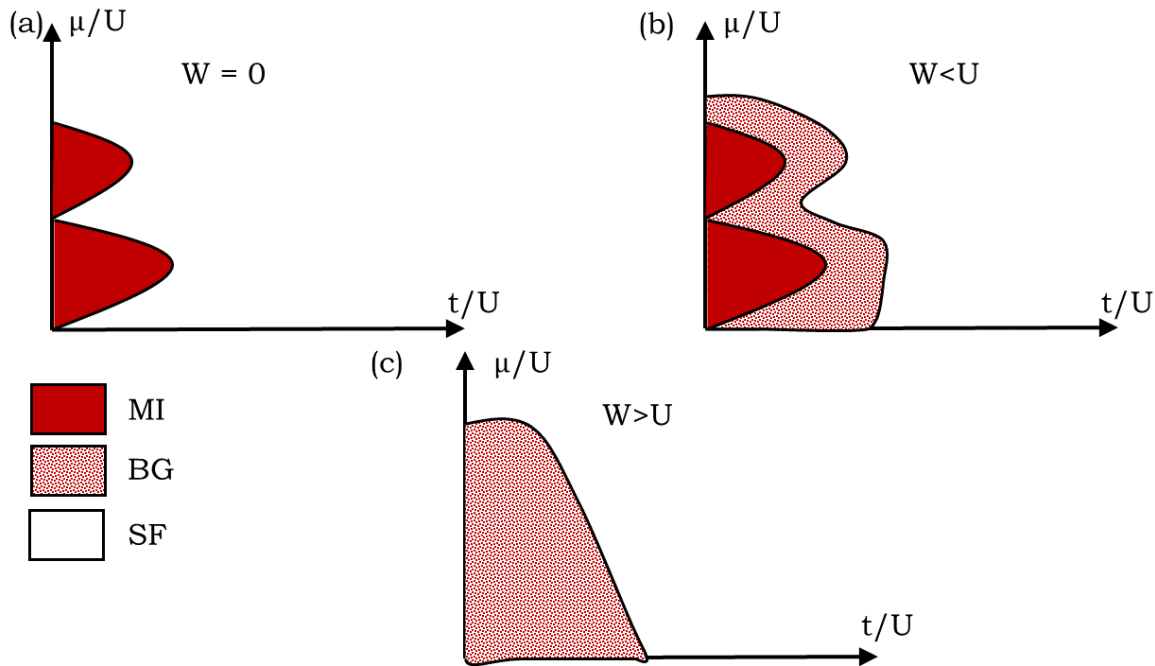
Figure 4.9: Phase diagram for dirty bosons for different disorder strength. (a) Without any disorder (same as Fig. 4.8). (b) Disorder strength is less than interaction strength (c) Disorder strength is higher than interaction strength. Presence of disorder creates a new phase, Bose glass phase.

Disorder can be modeled by various method, Box disorder, Speckle disorder, exponential disorder etc. to be considered in disordered BH (DBH) model. For a Box disorder disorder potential is drawn randomly from set $[-W/2, W/2]$ with W being disorder strength. If W is large enough, it is energetically favourable for the system to be localized in energy minima, a Mott-Insulator phase. In this case, jumping from one site to other would require W order energy. Density distribution, $\langle n(k) \rangle$ give us an ideal on the level of localization. Width of such plot in inversely proportional to spatial extent of condensate [159, 160]. While disorder (W) solely tends to localize non-interacting particles in the absolute lowest energy state (AL), repulsion (U) can screen effect of the disorder and bring the system back to a degree of coherent, extended SF phase, passing through an intermediate glassy phase.

This standard idea of the MI-BG-SF transition is generally accepted is in the form of percolation clusters [11, 161, 162]. At $W = 0$, in superfluid phase, coherence is present over long distance, forming ODLRO and macroscopic condensate. With introduction of disorder ($W \neq 0$), long range coherence becomes energetically unfavourable. But depending on the strength of disorder, some form of ODLRO can still be present. As disorder strength is increased, the superfluid global coherence reduced to zero. This picture follows the concept of percolation. The system now exhibits spatially separated superfluid puddles that not correlated with one another. So the expectation is that the BG consists of puddles embedded in an incoherent background.

PART II

RESULTS AND DISCUSSION

Chapter 5

Numerical Study of Condensation Dynamics with and without Defect

Understanding the dynamics of condensate is essential to further analyze the effect of defect on condensation process. We will analyze this process in temporal-spatial and kinetic domain. This will enable us to get a better understanding on condensation process. We will analyze for both pure and defective case. For spatial and temporal analysis, open dissipative GP equation coupled with external exciton reservoir will be solved. And for analysis in kinetic domain coupled semiclassical Boltzmann equation will be solved numerically.

5.1 Condensation Dynamics in Spatial-Temporal Domain

Polariton condensate formed under non-resonant pumping is a non-equilibrium system. While the condensate state can be described by a mean-field approximation, it is necessary for a full theoretical treatment to consider incoherent excitations generated by non-resonant pumping that couple to the condensate. Furthermore, for system with the presence of defect (point defect, dislocation, impurity or vacancy), free exciton localizes near trap potential, loses all its kinetic energy and forms 'Bound Exciton'. Single trap center can localize several exciton but with high energy cost. To understand the influence of defect on exciton polariton condensate formation, Gross-Pitaevskii equation coupled with active and inactive exciton reservoirs [163] has been solved numerically.

$$\frac{dn_i(r,t)}{dt} = -\frac{n_i(r,t)}{\tau_i} - \frac{n_i(r,t)}{\tau_r} + P(r,t) \tag{5.1}$$

$$\frac{dn_x(r,t)}{dt} = -\frac{n_x(r,t)}{\tau_x} + \frac{n_i(r,t)}{\tau_r} + R|\psi(r,t)|^2 n_x(r,t) \tag{5.2}$$

$$i\hbar\frac{d\psi(r,t)}{dt} = \left[-\frac{\hbar^2}{2m}\nabla^2 + \hbar g|\psi(r,t)|^2 + V(r) + \hbar g_R(n_X(r,t) + n_i(r,t)) + \frac{i\hbar}{2}(Rn_x(r,t) - \gamma)\right]\psi(r,t) \tag{5.3}$$

Here,

$n_i(r,t)$ = inactive exciton reservoir density.

$n_x(r,t)$ = active exciton reservoir density.

$\psi(r,t)$ = ground state condensate wavefunction.

$\frac{1}{\tau_i}$ = non-radiative recombination rate of inactive exciton.

$\frac{1}{\tau_r}$ = Inactive to active exciton conversion rate.

$P(r)$ = Pumping rate.

$\frac{1}{\tau_x}$ = radiative recombination rate of active exciton.

R = scattering rate of active exciton into ground state condensate.

m = polariton mass.

g = Inter condensate interaction strength.

g_R = Interaction between condensate and exciton reservoir.

γ = Condensate decay rate.

Defect is introduced into the system using potential profile V(r). For ideal condition without any defect, V(r) = 0, has been analyzed first. Condensation process is significantly influenced by pumping mechanism. For the whole work we consider incoherent pumping with four different pumping scheme. These four pumping schemes are:

1. **Pumping Scheme 01 : Uniform pumping across the whole sample**

$$P(r,t) = P_0 u(t) \tag{5.4}$$

Pumping is uniform across the whole sample with strength P_0 and is active for the whole simulation time.

2. **Pumping Scheme 02 : Continuous Gaussian pumping**

$$P(r,t) = P_0 exp\left[-\frac{(r-r_0)^2}{\sigma^2}\right]u(t) \tag{5.5}$$

Similar to uniform pumping, pumping is active for the whole simulation time, σ is spot size and P_0 is strength of Gaussian pulse at $r = r_0$.

3. **Pumping Scheme 03 : Gaussian pumping single pulse**

$$P(r,t) = P_0 exp\left[-\frac{(r-r_0)^2}{\sigma^2}\right][u(t) - u(t-t_0)] \tag{5.6}$$

Here pumping only sustained for t_0 time from the start of simulation.

4. **Pumping Scheme 04 : Gaussian oscillatory pulse pumping**

$$P(r,t) = P_0 exp\left[-\frac{(r-r_0)^2}{\sigma^2}\right]\sum_i rect(\frac{t-t_d}{T}) \tag{5.7}$$

Time interval between two pulses is T and duration of each pulse is, t_d.

Detail of numerical calculation and value used for numerical calculation is given in appendix A.

Numerical solution for different potential profile and pumping scheme has been discussed below. We are only presenting selective pumping scheme for different potential profiles to get a good idea of the physical aspects of defect in condensation process.

5.1.1   For Zero Potential, V(r) = 0

We start our discussion for ideal case with no disorder of any type, potential $V(r) = 0$. We will analyze the result for such potential under two different pumping scheme; pumping scheme 02 and pumping scheme 03. Pumping scheme 01 and 04 produces similar sort of result.
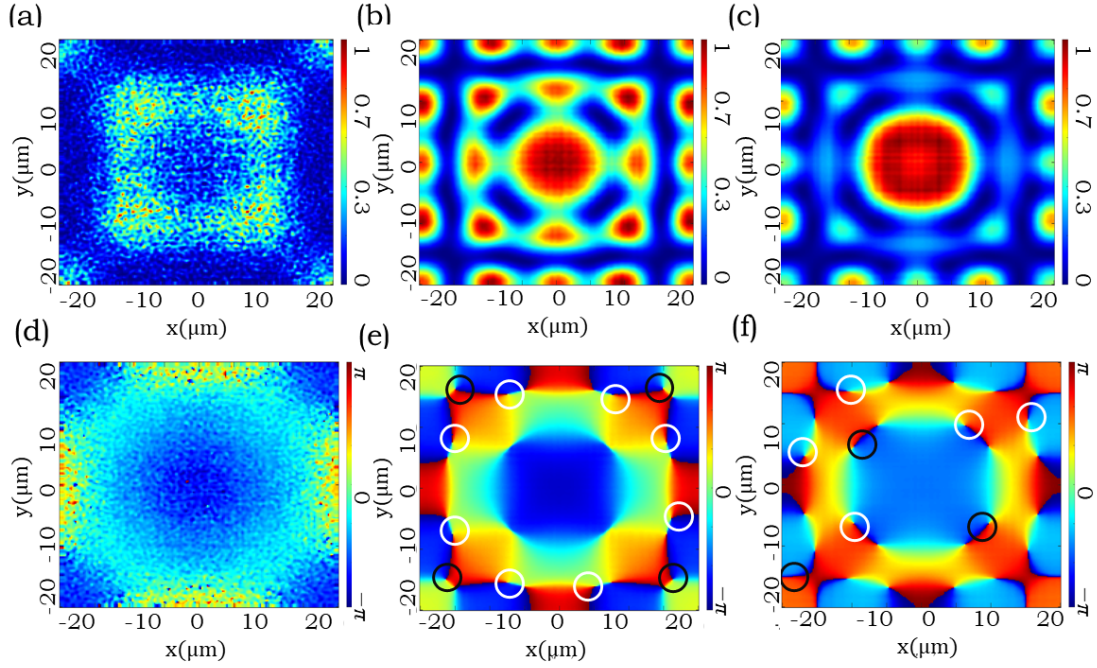
Figure 5.1: $|\psi(r)|^2$ and $\theta(r)$ for V(r) = 0 and pumping scheme 02 for three different time (a) $|\psi(r)|^2$ and (d) $\theta(r)$ at t = 8.57 ps, (b) $|\psi(r)|^2$ and (e) $\theta(r)$ at t = 19.11 ps, (c) $|\psi(r)|^2$ and (f) $\theta(r)$ at t = 30.98 ps. Location of vortex (anti-vortex) is marked by white (black) circle.

5.1.1.1 Pumping Scheme 02

Fig. 5.1 shows the solution of $|\psi(r,t)|^2$ along with $\theta(r,t)$ at three different times for open dissipative GP equation coupled with external reservoir under ideal no defect potential ($V(r) = 0$) and Continuous Gaussian pumping (pumping scheme 02 with $r_0 = 0$). Initially, (fig. 5.1 (a)+ (d)) some local condensate without any long range correlation has been formed. Going through fig 5.1 (b) + (e), and (c) + (f), local condensates percolate and form condensate of considerable size (a macro condensate) and long range order has been established. As in this pumping scheme is active whole time, spontaneous vortex generation process continues for the whole time. Besides such long range ordered macroscopic condensate, presence of small regional condensate is also present (fig. 5.1(b), 5.1(c)) due to presence of vortex at the edge of central macroscopic condensate (fig. 5.1(e) and fig. 5.1(f)). Outward propagation of vortex is also observed in this case. Characteristics of such vortex has been discussed in theoretical section. We have shown the position of vortex (anti-vortex) in white (black) circle. Determination of vortex position will be discussed for periodic potential with pumping scheme 02 in next section.

5.1.1.2 Pumping Scheme 03
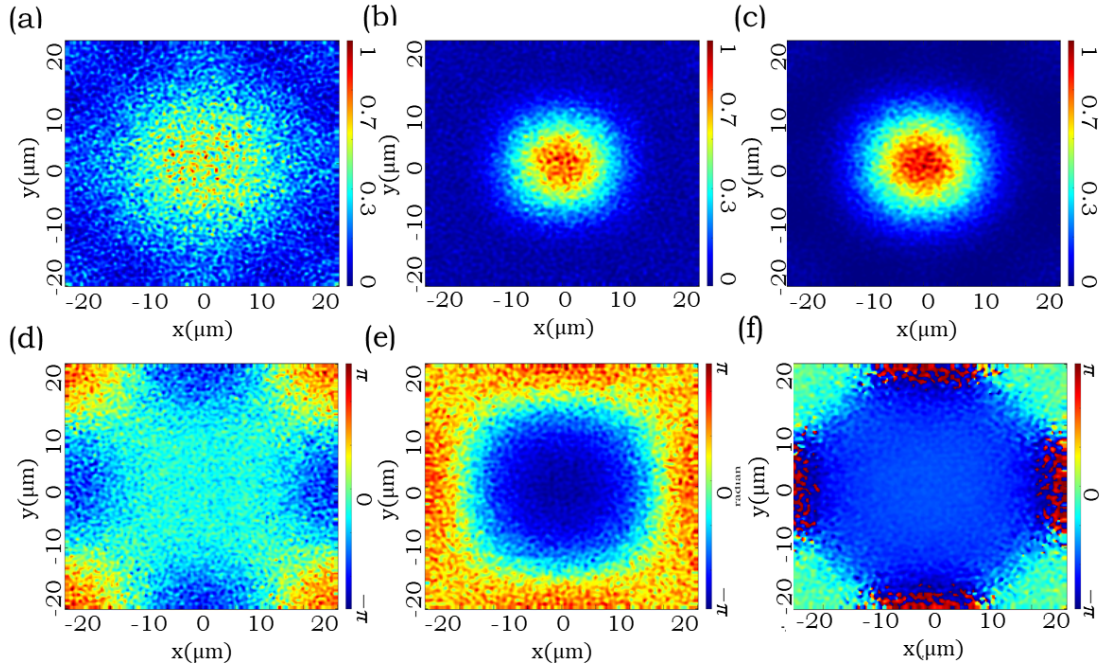
Figure 5.2: $|\psi(r)|^2$ and $\theta(r)$ for V(r) = 0 and pumping scheme 03 for three different time (a) $|\psi(r)|^2$ and (d) $\theta(r)$ at t = 9.9 ps, (b) $|\psi(r)|^2$ and (e) $\theta(r)$ at t = 23.1 ps, (c) $|\psi(r)|^2$ and (f) $\theta(r)$ at t = 32.96 ps. Location of vortex (anti-vortex) is marked by white (black) circle.

Fig. 5.2 shows the solution of $\psi(r,t)$ (both magnitude and phase of condensate) at three different times for open dissipative GP equation coupled with external reservoir under ideal no defect potential (V(r) = 0) and Gaussian pumping single pulse (pumping scheme 03 with $r_0 = 0$ and $t_0 = 3.03ps$). Almost as same result for pumping scheme 02 can be observed but with much less number of vortices. Sufficient energy is needed for vortex to be stable. This energy can come from different source, chemical energy induced by defect, thermal energy or excitation energy. In scheme 03, we see a much lower number of vortices are generated due to limited time of pumping as here an effective low amount of energy. As the pumping is turned off and calculation has been done below BKT temperature, very few new vortices have been generated and existing vortices (anti-vortices) have annihilated by combining with anti-vortices (vortices). Nevertheless, we see as the case for pumping scheme 02, a macroscopic condensate formed close to $r_0 = 0$ with phase coherence $20\mu m$.

5.1.2 Potential Profiles

To understand condensation process under different potential profile and different pumping scheme, different potential profiles have been considered. These are shown in Fig. 5.3.
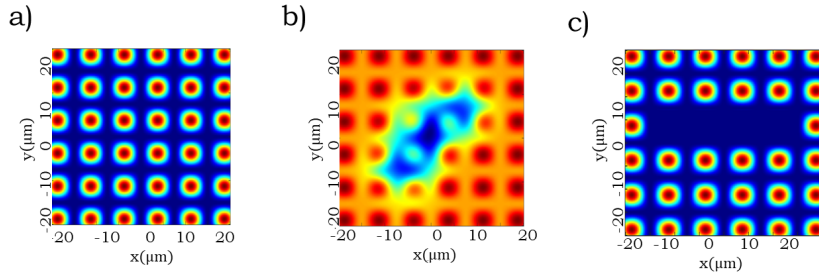
Figure 5.3: $V(r)$ for solving coupled open-dissipative Gross-Pitaevskii equation. Here $V(r)$ is (a) sinusoidal potential in both x and y direction, (b) sinusoidal potential in both x and y direction with superimposed random disorder, (c) sinusoidal potential in both x and y direction with some potential maxima missing, mimicking a dislocation.

5.1.3 For Periodic Potential

From complete absence of disorder, we now introduce a periodic disorder (effectively) as shown in fig. 5.3 (a) . We will analyze the result for such potential under two different pumping scheme; pumping scheme 02 and pumping scheme 04. Pumping scheme 01 and 03 gives us similar sort of results.

5.1.3.1 Pumping Scheme 02

Fig. 5.4 shows the solution of $\psi(r,t)$ (both magnitude and phase) at three different times for open dissipative GP equation coupled with external reservoir for periodic potential shown in fig. 5.3 with Continuous Gaussian pumping (pumping scheme 02). Here we point out the position of vortex (anti-vortex) by white (black) circle. Determination of such vortex position is discussed thoroughly here.

We can determine velocity of superfluid, $v(r,t)$ from phase distribution $\theta(r,t)$ according to equation 3.91. In fig. 5.5 velocity for that correspondent phase (7.9 ps, 13.4 ps, 23.72 ps) are shown.

Position of vortex is determined from such velocity plot. We are showing one vortex and one anti-vortex in fig at position (-8, 13.5) μm and (-3, 15.5) μm respectively for time

Figure 5.4: $|\psi(r)|^2$ and $\theta(r)$ for periodic potential and pumping scheme 02 for three different time (a) $|\psi(r)|^2$ and (d) $\theta(r)$ at t = 7.9 ps, (b) $|\psi(r)|^2$ and (e) $\theta(r)$ at t = 13.4 ps, (c) $|\psi(r)|^2$ and (f) $\theta(r)$ at t = 23.72 ps. Location of vortex (anti-vortex) is marked by white (black) circle.
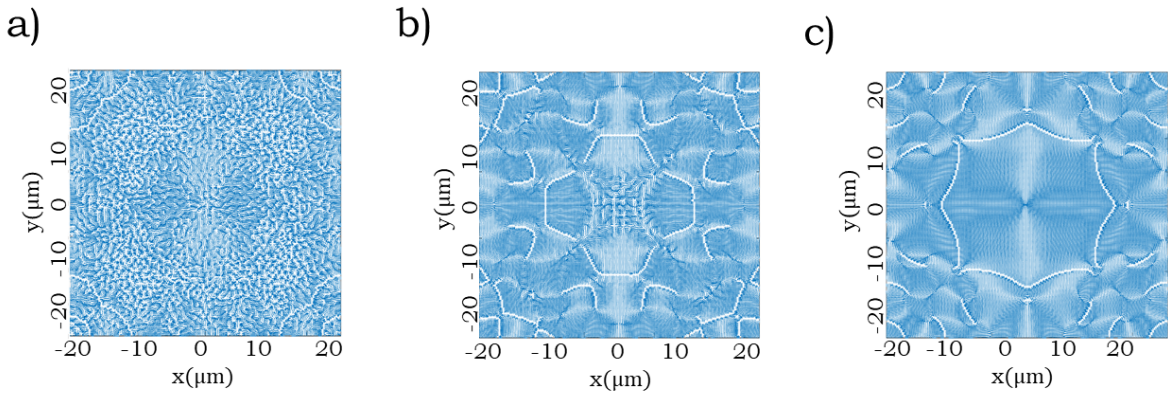
Figure 5.5: Velocity of condensate for time (a) t = 7.9 ps, (b) t = 13.4 ps, (c) t = 23.72 ps. Determination of superfluid velocity is done according equation 3.91.

.

13.4 ps in fig 5.6. In vortex position, superfluid has a quantized clockwise rotation while in anti-vortex position we see a counter clockwise rotation.
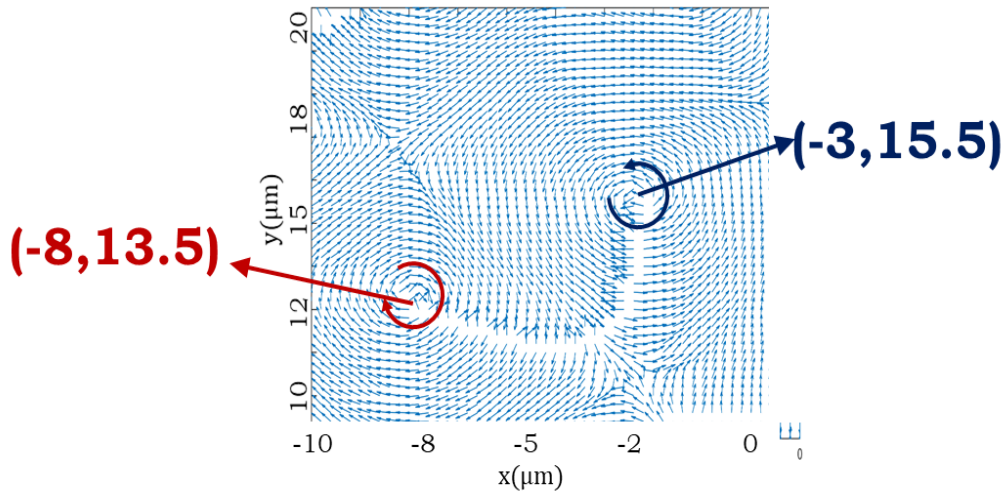
Figure 5.6: Position of vortex (clockwise rotation) and anti-vortex (counter clockwise rotation).

Position of some other vortex and anti vortex for same time ($t = 13.4ps$) is shown in fig. 5.7. Numerically we determine the position of such vortex (anti-vortex) by taking localized curl of velocity field. The position at which curl produces an integer result of $\frac{\hbar}{m}$ gives us the position of vortex.
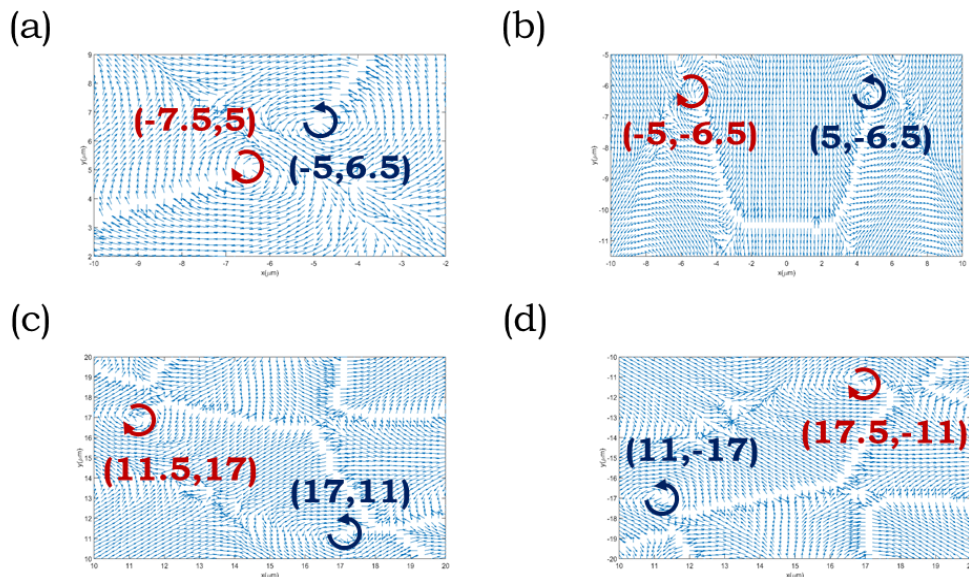
Figure 5.7: Position of vortex (clockwise rotation) and anti-vortex (counter clockwise rotation) for time $t = 13.4ps$.

Such quantized rotation (clockwise or counter-clockwise) prevents local condensate to form a macro condensate with long range order. Due to presence of potential fluctuation in sinusoidal potential, some vortices get pinned close to potential dip or maxima. Position of some more vortices for same time are shown in fig. These vortices if no potential fluctuation exist, normally travel some distance before getting annihilated via combining with another anti vortex. But potential fluctuation can cause a vortex to get pinned and can enhance its lifetime several times

5.1.3.2 Pumping Scheme 04

Fig. 5.8 shows the solution of $\psi(r, t)$ for three different time of open dissipative GP equation coupled with external reservoir for periodic potential under pumping scheme 04 with $t_d = 3.03 ps$ and $T = 12.13 ps$. As pumping is now continuously turned on and off, we see local condensate more clearly. And due to pseudo continuous pumping, vortex generation rate is less than the case of continuous Gaussian pumping. Pumping scheme can change vortex generation as we have already seen for zero potential.
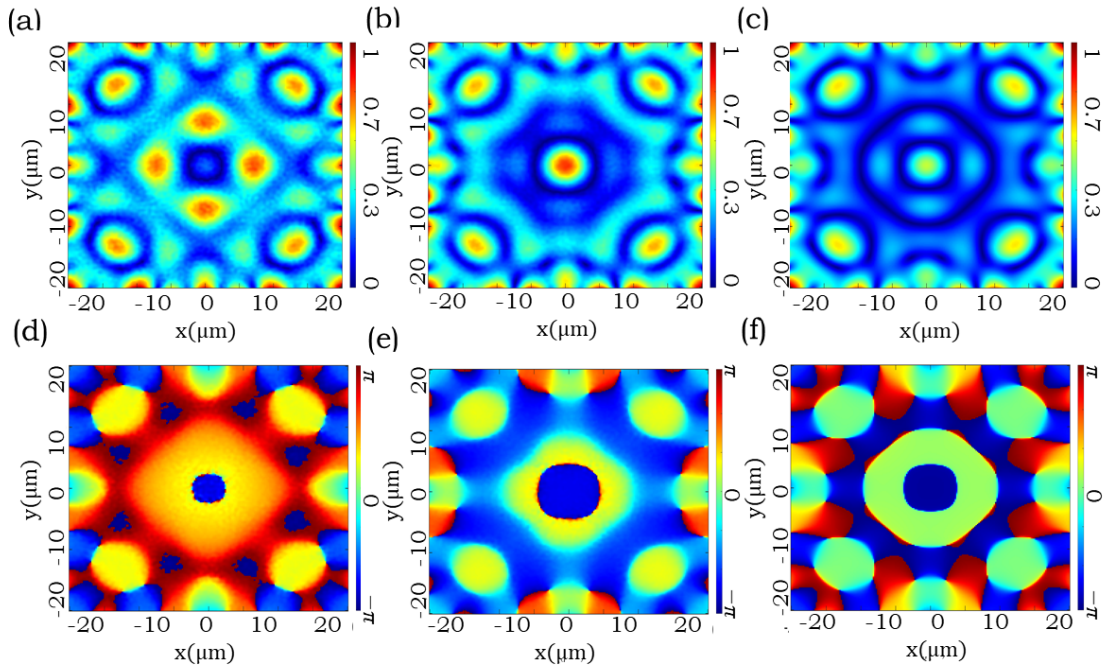

Figure 5.8: $|\psi(r)|$ and $\theta(r)$ for periodic potential and pumping scheme 04 for three different time (a) $|\psi(r)|$ and (d) $\theta(r)$ at t = 9.48 ps, (b) $|\psi(r)|$ and (e) $\theta(r)$ at t = 14.23 ps, (c) $|\psi(r)|$ and (f) $\theta(r)$ at t = 36.37 ps. Location of vortex (anti-vortex) is marked by white (black) circle.

Another important thing to be observed here, spontaneous generation pattern is

also influenced by pumping mechanism even for same potential profile. For sinusoidal potential, this has been shown in fig. 5.9. This can significantly influence percolation scheme to produce macroscopic coherent condensate. With change in pumping scheme, it is thus possible to observe local condensate of different size as we will see later.
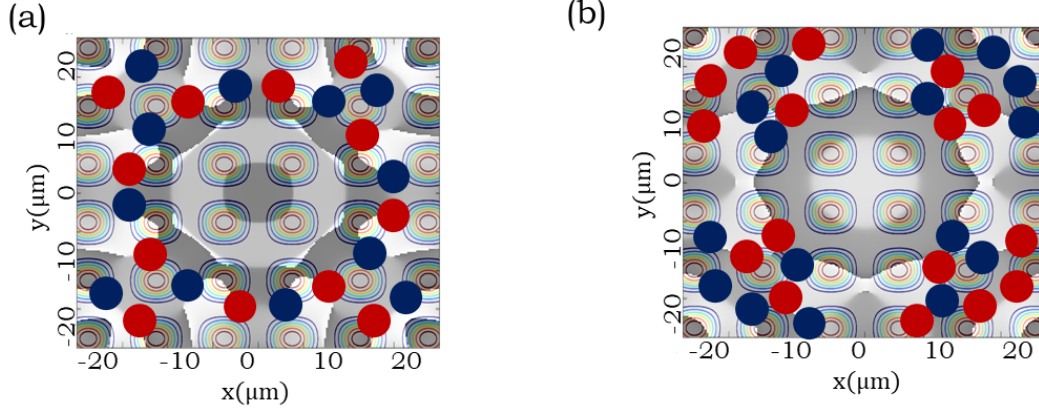
Figure 5.9: Vortex pattern for sinusoidal potential for periodic potential under two different pumping scheme (a) Continuous Gaussian pumping (b) Gaussian oscillatory pulse pumping.

.

5.1.4 For Defective Potential 01

Here we introduce a some random disorder superimposed on a periodic potential as shown in fig. 5.3 (b). Random disorder exist between $x = -15\mu m$ to $x = 15\mu m$ and $y = -15\mu m$ to $y = 15\mu m$ and follows Gaussian distribution.We will analyze the result for such potential under three different pumping scheme; pumping scheme 01, pumping scheme 02 and pumping scheme 04.

5.1.4.1 Pumping Scheme 01

For defective potential shown in Fig.5.10, we are studying the effect of defective potential under pumping scheme 01. From fig, we show $\psi(r,t)$ at time 5.27, 9.89 and 30.97 ps. As time have passes, more and more vortices are centered around the potential minima. This is due to pinning of vortices near disordered potential. Local condensate forms around such minima. But due to presence of such vortex, no macroscopic condensate is not formed, as seen from fig. 5.10 (c). Pumping scheme and additional disorder potential causes vortex

Figure 5.10: $|\psi(r)|$ and $\theta(r)$ for defective potential 01 and pumping scheme 01 for three different time (a) $|\psi(r)|$ and (d) $\theta(r)$ at t = 5.27 ps, (b) $|\psi(r)|$ and (e) $\theta(r)$ at t = 9.89 ps, (c) $|\psi(r)|$ and (f) $\theta(r)$ at t = 30.97 ps. Location of some vortex (anti-vortex) is marked by white (black) circle.

generation rate and spontaneous vortex pattern to change as we will in section 5.1.3.2 and 5.1.3.3 . Pinned vortex cannot travel [138] as is the case of no disorder. As a result such vortex can survive longer than ideal case, increasing its life time.

A detailed vortex mapping is shown in fig. 5.11. As we see, with passing of time, more and more vortices (and anti-vortices) are accumulated around defect. In this accumulation vortex pair can be annihilated by combination with each other. But presence of one vortex anti-vortex pair can effectively act as domain wall, prevents the local condensate to percolate.

As a result of increased accumulation of vortices with longer lifetime around defect potential, local condensate cannot form a macro condensate for long time and cause local condensate to exist. Absence of macroscopic condensate due to presence of excessive no. of vortex can be seen from fig. 5.12. One pair of vortex and anti-vortex stand between two local condensate. Influence of defect over creation of macroscopic condensate can cause some serious implication i.e. increase of lasing threshold, lowering of effective temperature, decrease of resonant frequency for laser diode. We will discuss this in later chapters.
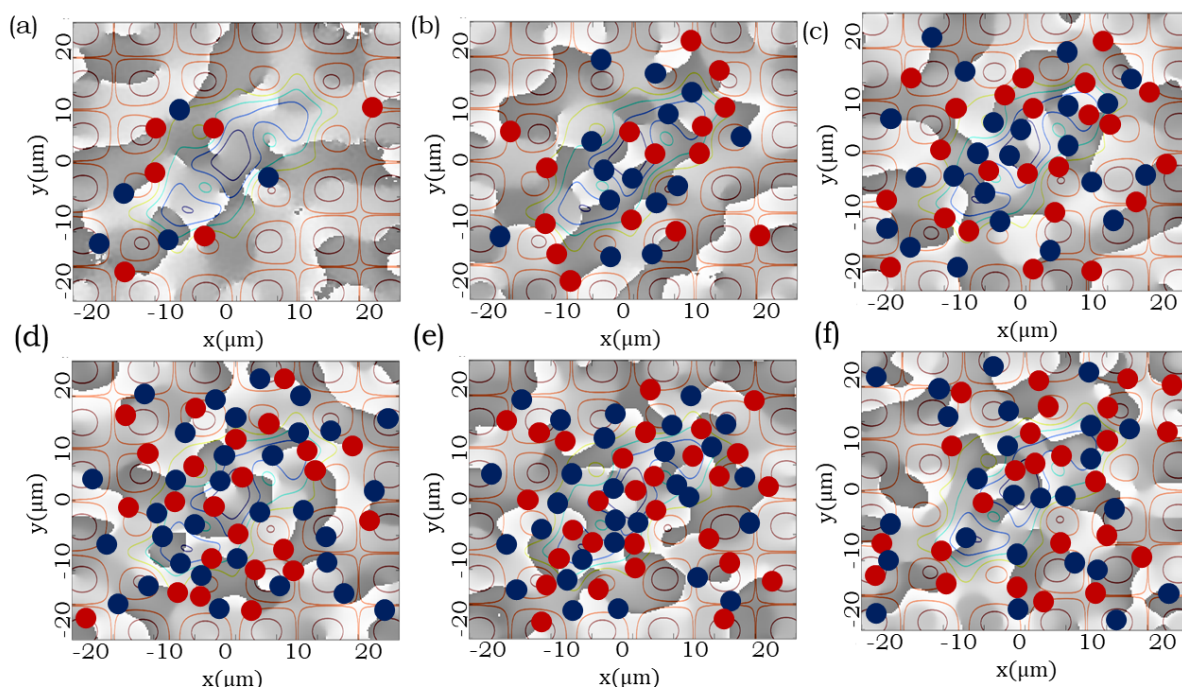
Figure 5.11: Vortex mapping along with potential and phase distribution for defective potential 01 under pumping scheme 01 for time (a) 9.88 ps (b) 13.18 ps (c) 16.47 ps (d) 19.77 ps (e) 23.06 ps (f) 30.97 ps. Vortex (anti-vortex) is represented by red circle (blue circle).
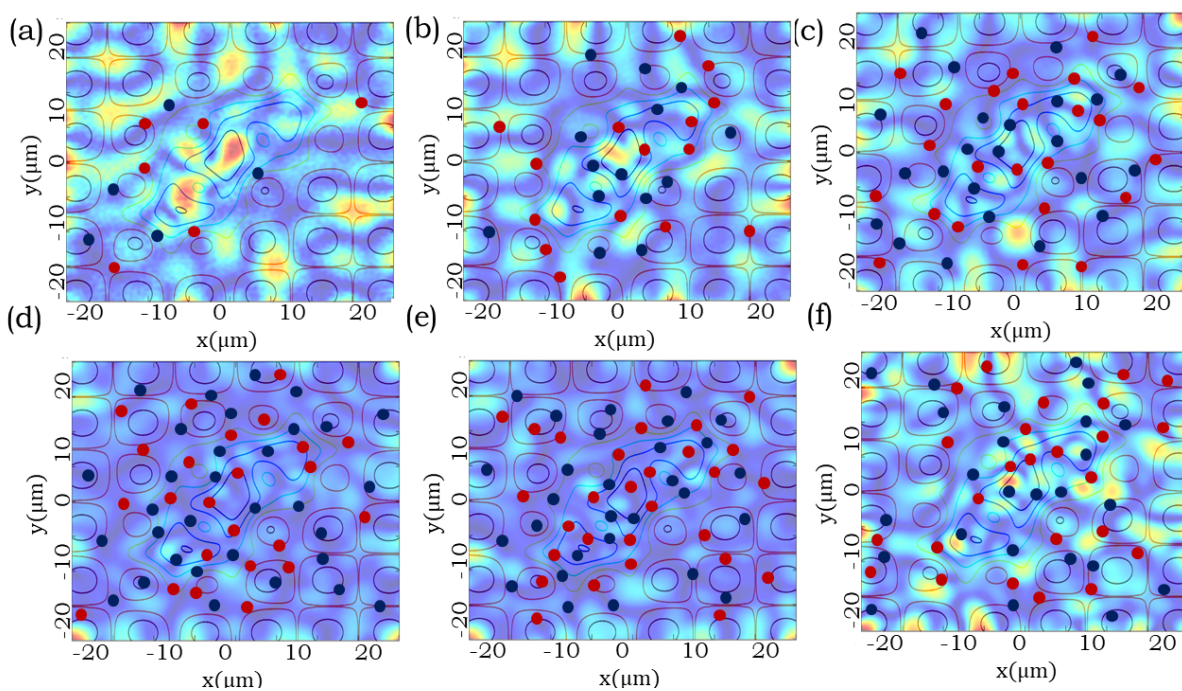
Figure 5.12: Vortex mapping along with potential and $|\psi(r)|$ for defective potential 01 under pumping scheme 01 for time (a) 9.88 ps (b) 13.18 ps (c) 16.47 ps (d) 19.77 ps (e) 23.06 ps (f) 30.97 ps. Vortex (anti-vortex) is represented by red circle (blue circle).
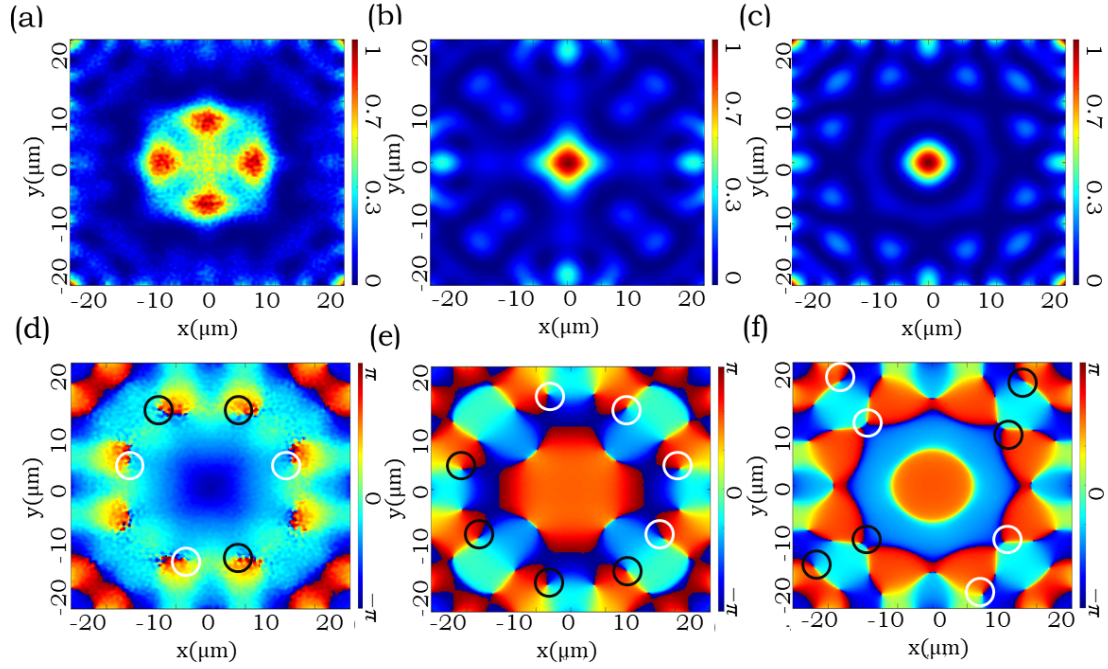
5.1.4.2 Pumping Scheme 02

Figure 5.13: $|\psi(r)|^2$ and $\theta(r)$ for defective potential 01 and pumping scheme 02 for three different time (a) $|\psi(r)|^2$ and (d) $\theta(r)$ at t = 6.59 ps, (b) $|\psi(r)|^2$ and (e) $\theta(r)$ at t = 16.48 ps, (c) $|\psi(r)|^2$ and (f) $\theta(r)$ at t = 32.3 ps. Location of some vortex (anti-vortex) is marked by white (black) circle.

With same potential as in 5.1.3.1 a change in the pumping scheme from 01 to 02, a continuous pulse with $r_0 = 0$ and $\sigma = 16$ has been made. We have already seen for the case of sinusoidal potential the effect of pumping is two-fold, a change in vortex pattern and a change in vortex generation rate. This sort of change has also been observed here. But despite dramatic change in vortex formation pattern, we find the same end result, *'Vortex prevents to form a macroscopic condensate from local condensate'*. Most of the survived vortices are accumulated close to disordered potential. Even from fig. 5.13(c) and (f) we see that, at t= 32.3 ps, most two prominent local condensate exist at (x,y)=(0,0) μm and (x,y)=(-7,-5) μm, close to potential minima with a coherence length around 1 μm. A detailed vortex map for such case is also shown in fig. 5.14. Clearly most vortices are centered around disordered potential. This in turn prohibits local condensate formed inside defect potential to come in contact with other local condensate. As a result, no phase coherence between local condensate inside defect potential and other defect free zone has been established.

111
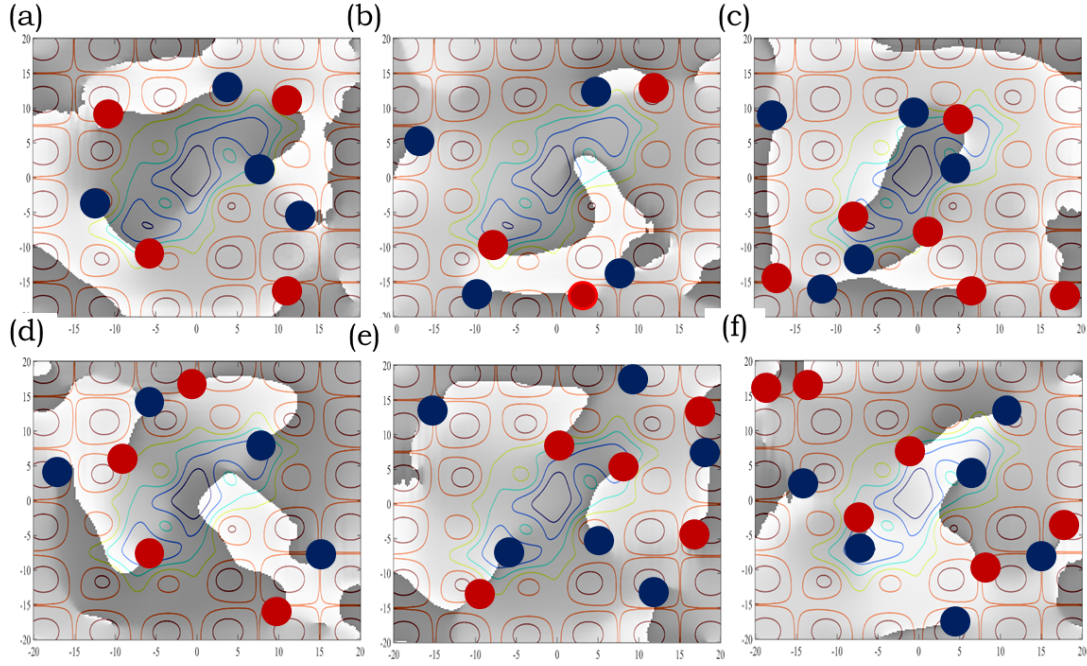
Figure 5.14: Vortex mapping along with potential and phase distribution for defective potential 01 under pumping scheme 02 for time (a) 15.82 ps (b) 19.11 ps (c) 24.38 ps (d) 28.33 ps (e) 30.97 ps (f) 32.95 ps. Vortex (anti-vortex) is represented by red circle (blue circle).

5.1.4.3 Pumping Scheme 04

At a first glance at fig 5.15, one might think that for pumping scheme 04, the different result other than 5.1.3.1 and 5.1.3.2 comes forward. But if we look $\theta(r)$ for different time actually same result also happened here. We can see phase distribution, $\theta(r)$ for six different time in fig. 5.16. As vortex pattern has changed for different pumping scheme, all the vortices are shaped as a ring around the disorder potential. This ring sustains for longer time, preventing local condensate inside the disorder minima to percolate with other local condensate and form a macro-condensate. This is the same case as we seen before (5.1.3.1, 5.1.3.2). The appearance of vortices is solely due to change in vortex generation patter under different pumping scheme.

With proper pumping scheme and suitable defect engineering one can achieve a considerable size of condensate. One such case has been reported in [62]. One big potential trap has been created. As polariton diffused inside the trap, it has very low probability to leave from there. Having a such long lifetime, polariton slowly create a condensate state.

112

Figure 5.15: $|\psi(r)|$ and $\theta(r)$ for defective potential 01 and pumping scheme 01 for three different time (a) $|\psi(r)|$ and (d) $\theta(r)$ at t = 3.95 ps, (b) $|\psi(r)|$ and (e) $\theta(r)$ at t = 10.54 ps, (c) $|\psi(r)|$ and (f) $\theta(r)$ at t = 25.7 ps. Location of some vortex (anti-vortex) is marked by white (black) circle.
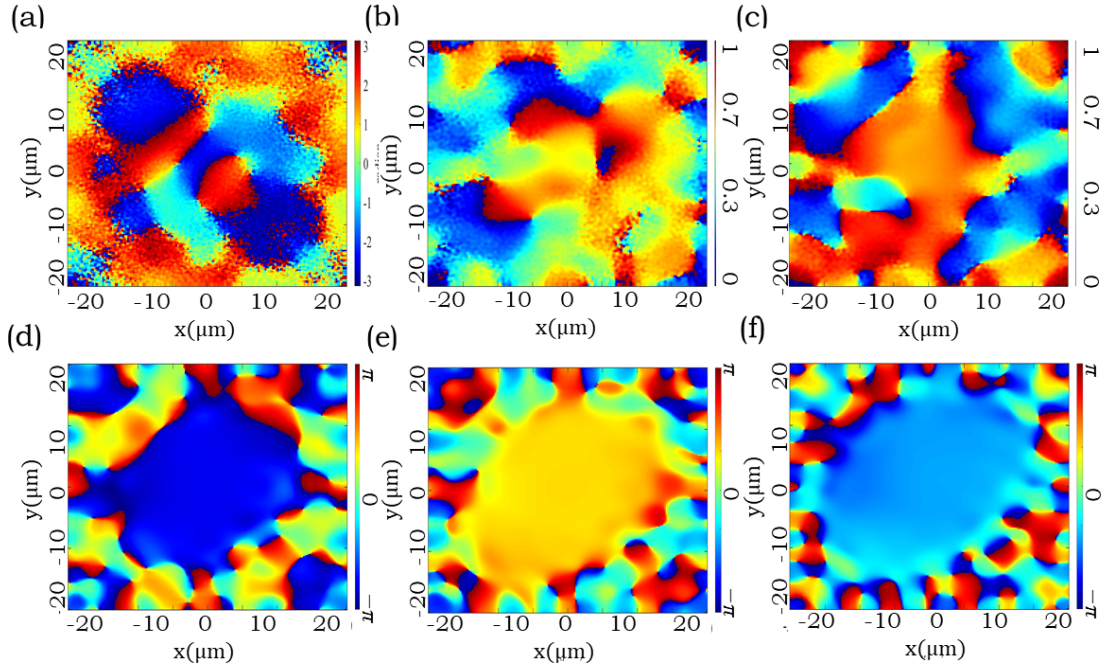
Figure 5.16: Phase distribution, $\theta(r)$ for defective potential 01 under pumping scheme 04 for time (a) 3.95 ps (b) 7.24 ps (c) 10.54 ps (d) 19.77 ps (e) 26.36 ps (f) 33.29 ps.

5.1.5 For Defective Potential 02

Instead some random disorder, we take away one row of periodic potential maxima from periodic potential profile as shown in fig. 5.3(c). We will analyze the result for such potential under two different pumping scheme; pumping scheme 02 and pumping scheme 03.
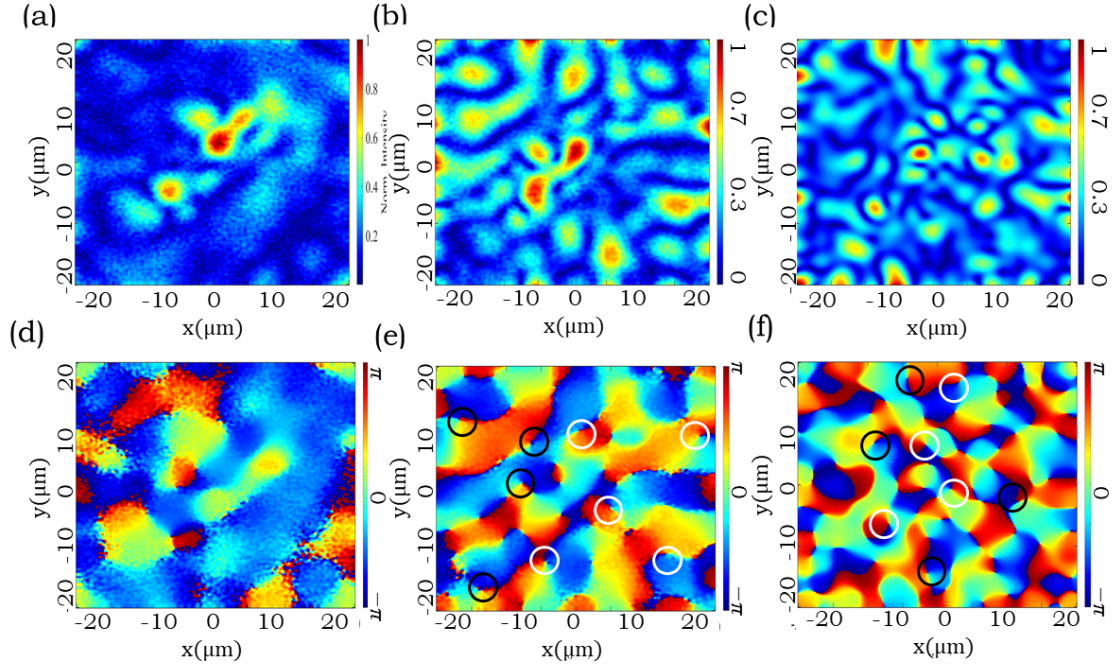
5.1.5.1 Pumping Scheme 02
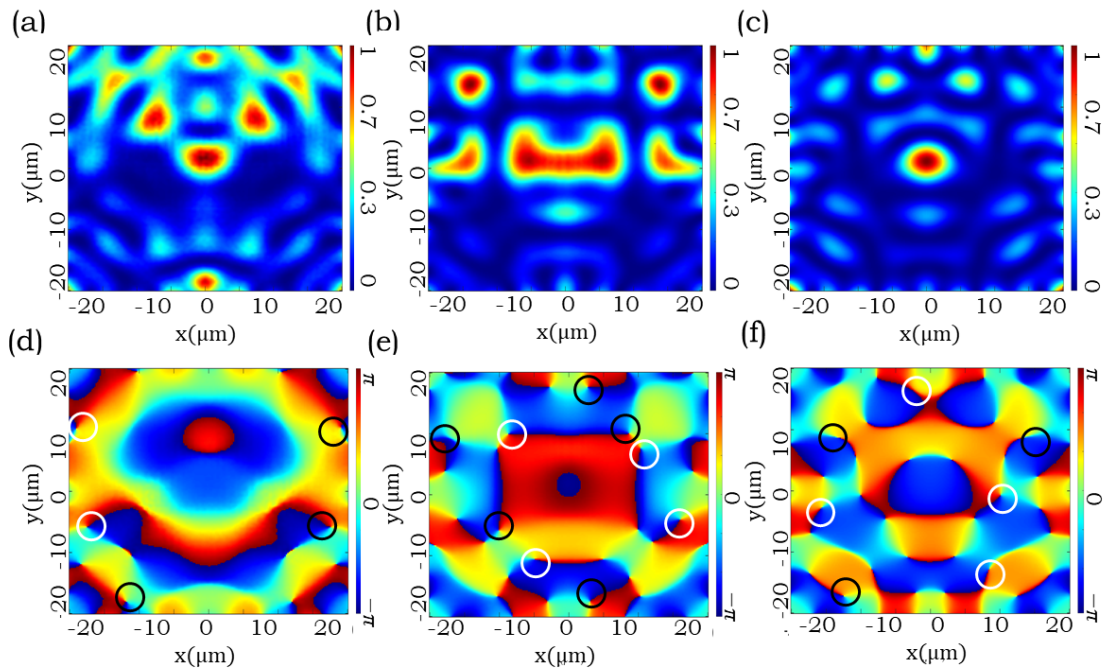
Figure 5.17: $|\psi(r)|^2$ and $\theta(r)$ for defective potential 02 and pumping scheme 02 for three different time (a) $|\psi(r)|^2$ and (d) $\theta(r)$ at t = 13.84 ps, (b) $|\psi(r)|^2$ and (e) $\theta(r)$ at t = 17.13 ps, (c) $|\psi(r)|^2$ and (f) $\theta(r)$ at t = 21.74 ps. Location of some vortex (anti-vortex) is marked by white (black) circle.

For defective potential shown in fig. 5.3(c), we are showing the effect of defective potential under pumping scheme 02, with $r_0 = 0$ and $\sigma = 16$ in fig. 5.17. For such potential pattern and pumping scheme, a detailed mapping of vortices for different time has also been shown in fig. 5.18. Here just like the case of 5.1.3.1 and 5.1.3.2, vortices pattern themselves around the dislocation (missing potential maxima). And as a result of that, we see local condensate formed near dislocation (around (x,y) = (0,0) μm) cannot percolate with other local condensate (around (x,y) = (15,15) μm or around (x,y) = (-15,15) μm), same as previous case.

We are also showing condensate amplitude with mapped vortex to get a better

114
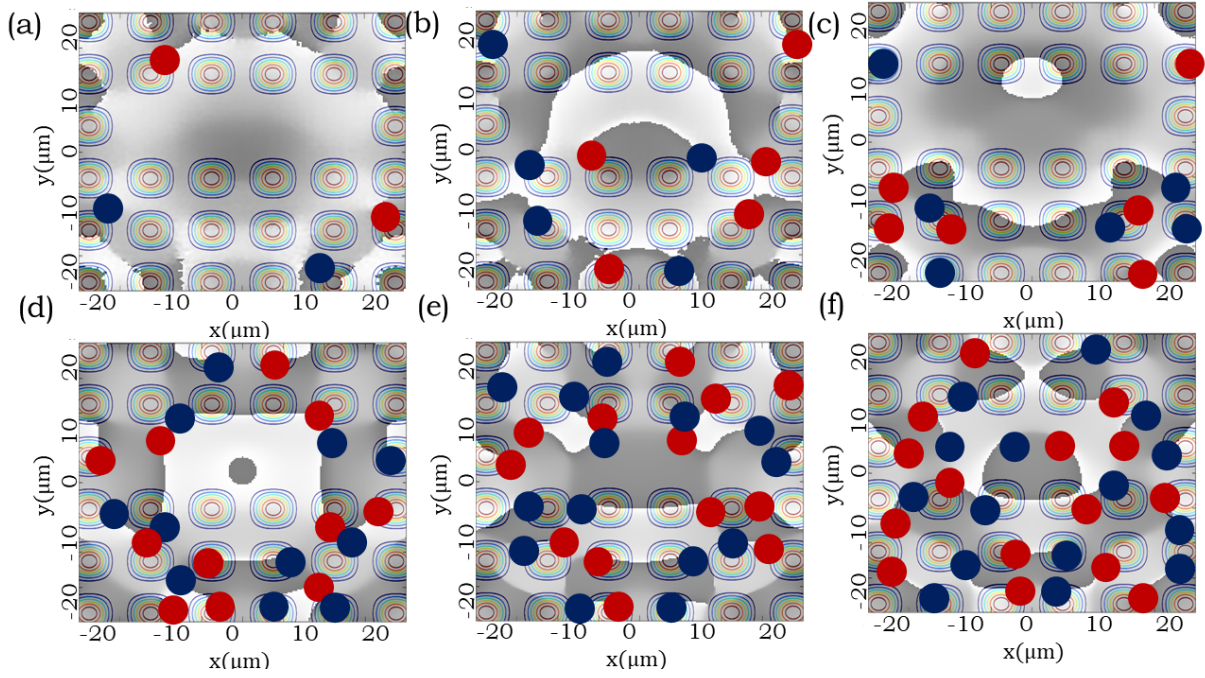
Figure 5.18: Phase distribution, $\theta(r)$ for defective potential 02 under pumping scheme 02 for time (a) 9.23 ps (b) 11.2 ps (c) 13.84 ps (d) 17.13 ps (e) 19.77 ps (f) 21.74 ps.
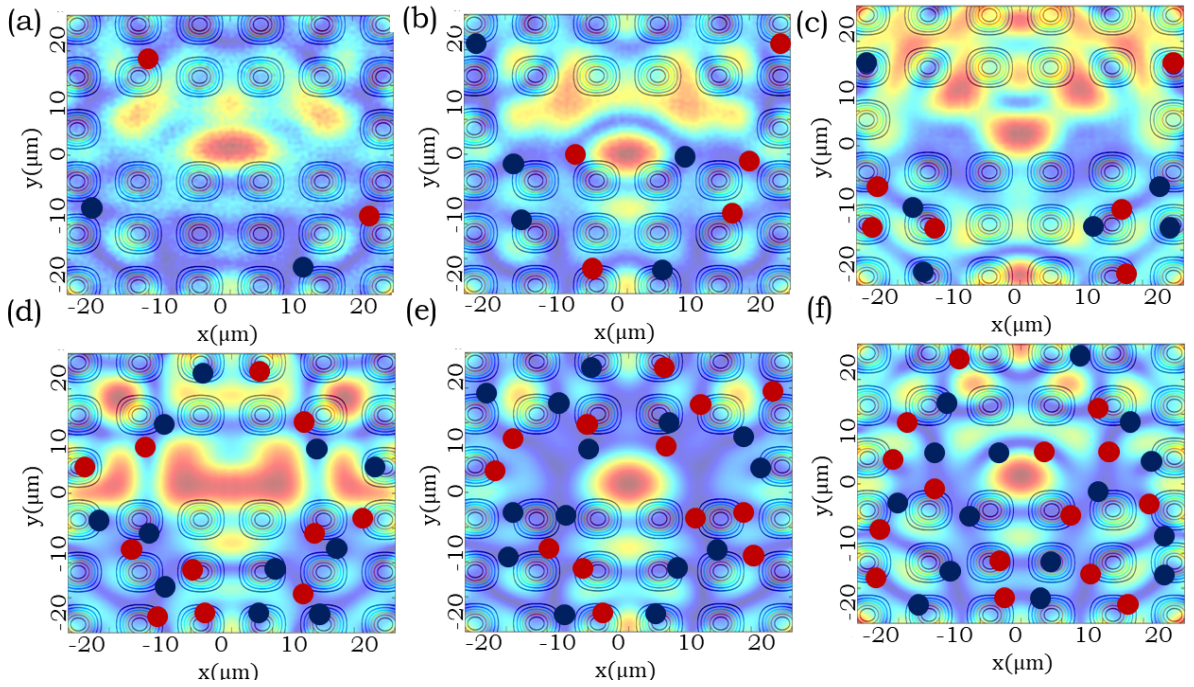
Figure 5.19: Phase distribution, $|\psi(r)|$ for defective potential 02 under pumping scheme 02 for time (a) 9.23 ps (b) 11.2 ps (c) 13.84 ps (d) 17.13 ps (e) 19.77 ps (f) 21.74 ps.

understanding on how vortices prevent the percolation of local condensate. Here also, we see that due to position, size of defect and pumping scheme, we achieve a local condensate of considerable size close to (x,y) = (0,0) μm.

5.1.5.2 Pumping Scheme 03
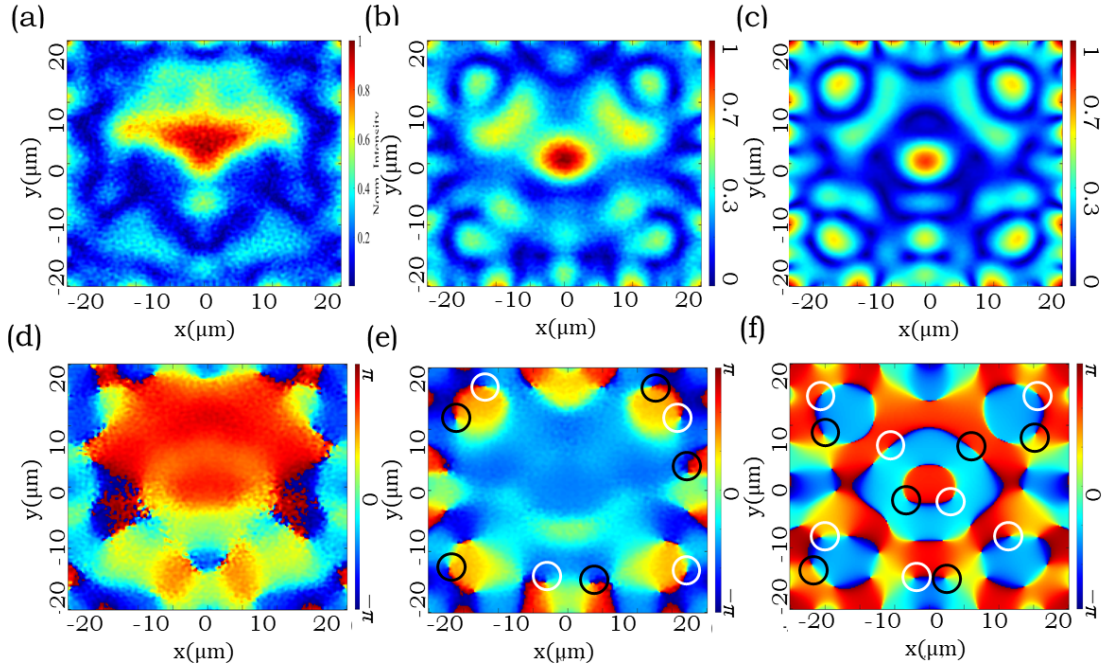
Figure 5.20: $|\psi(r)|$ and $\theta(r)$ for defective potential 02 and pumping scheme 03 for three different time (a) $|\psi(r)|$ and (d) $\theta(r)$ at t = 7.91 ps, (b) $|\psi(r)|$ and (e) $\theta(r)$ at t = 10.54 ps, (c) $|\psi(r)|$ and (f) $\theta(r)$ at t = 15.16 ps. Location of some vortex (anti-vortex) is marked by white (black) circle.

Same potential profile as fig. 5.3(c), with pumping scheme 03, Gaussian pumping with only a single pulse for time duration of 3.03 ps. Here pumping scheme changes the vortex pattern as we have seen earlier, with a reduced rate of vortex generation.

Whatever pumping scheme is, one thing that we have observed for all case so far, pinned vortex close to dislocation or defect. Any sort of disorder in potential cause such pinning to occur. If we look at phase distribution especially fig. 5.20 (f), we see that vortices pattern themselves around dislocation and pinned to that location for some time, longer than a vortex normally does. This phenomenon results in our usual conclusion, *'Pinned Vortex prevents local condensate to percolate with each other to generate macroscopic condensate'*. Local condensate around (x,y) = (0,0) μm, (x,y) = (-15,-15) μm, (x,y) = (15,-15) μm, (x,y) = (15,15) μm, (x,y) = (-15,15) μm and others (fig. 5.20 (c)) stays

separated from each other without forming any sort of long range coherence.

5.1.6   For Other Defective Potential

Here we introduce a some random disorder superimposed on $V(r) = 0$ as shown in .
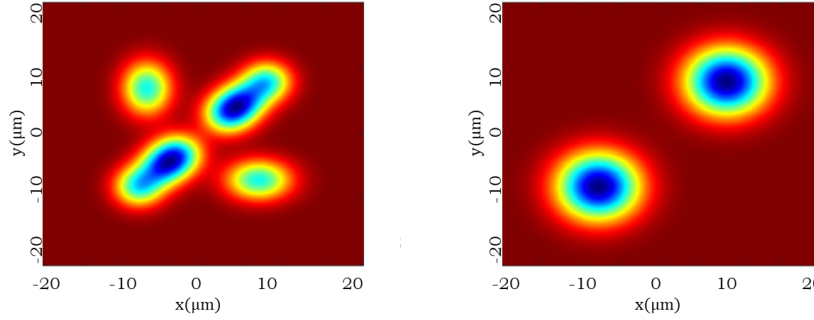
Figure 5.21: $V(r)$ for solving coupled open-dissipative Gross-Pitaevskii equation. Here $V(r) = 0$ with superimposed random disorder of Gaussian distribution.

We will analyze the result for such potential under only one type of pumping scheme; pumping scheme 02.

5.1.6.1   Pumping Scheme 02

For two different disordered potential shown in fig. 5.21, Gaussian continuous pumping produce same result. It is same as we have discussed earlier. Even in this case we can observe local condensate palette more clearly from fig. 5.22 (a), (b), (c) and from fig. 5.23 (a), (b), (c). From fig. 5.23 (c), we see a local condensate between defect bound local condensates around (x,y) = (-10,-10) μm and (x,y) = (10,10) μm. This local condensate is not at all coherence with other local condensates. This will be clear if we take a closer look of phase distribution at that time (t = 32.95 ps fig. 5.23 (f)). Presence of such well defined defect can be utilized to create local zone of high co-relation for extraordinary computing advantage. Defect does not always come as disadvantage rather can be engineered to get some really exotic result.
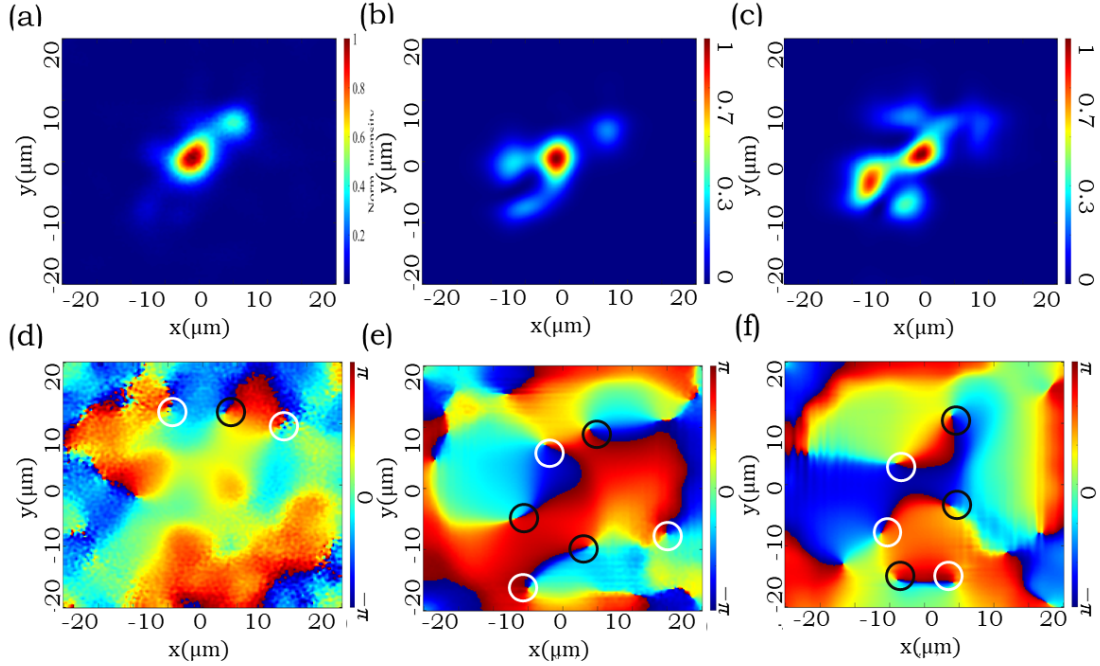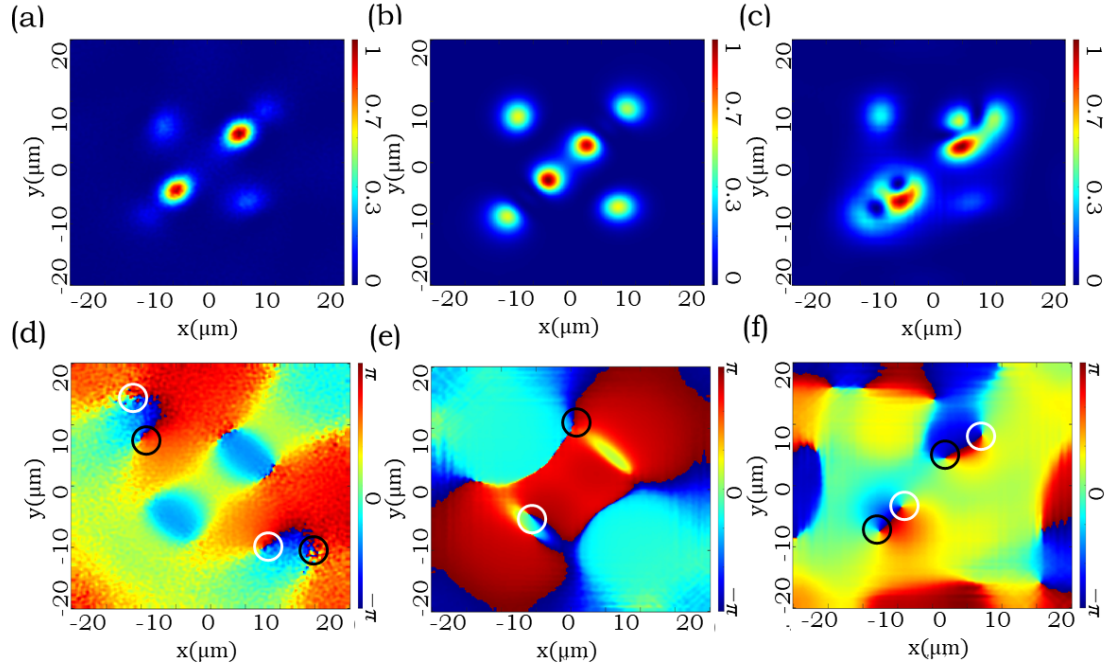
Figure 5.22: $|\psi(r)|^2$ and $\theta(r)$ for defective potential 03 and pumping scheme 02 for three different time (a) $|\psi(r)|^2$ and (d) $\theta(r)$ at t = 6.6 ps, (b) $|\psi(r)|^2$ and (e) $\theta(r)$ at t = 19.77 ps, (c) $|\psi(r)|^2$ and (f) $\theta(r)$ at t = 32.95 ps. Location of some vortex (anti-vortex) is marked by white (black) circle.
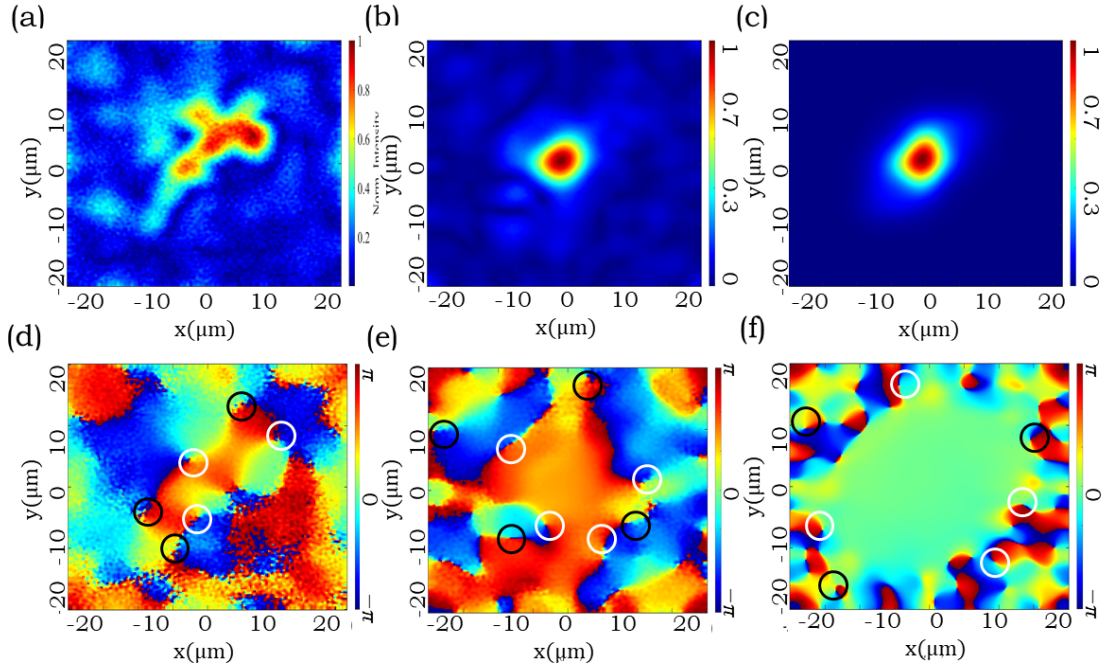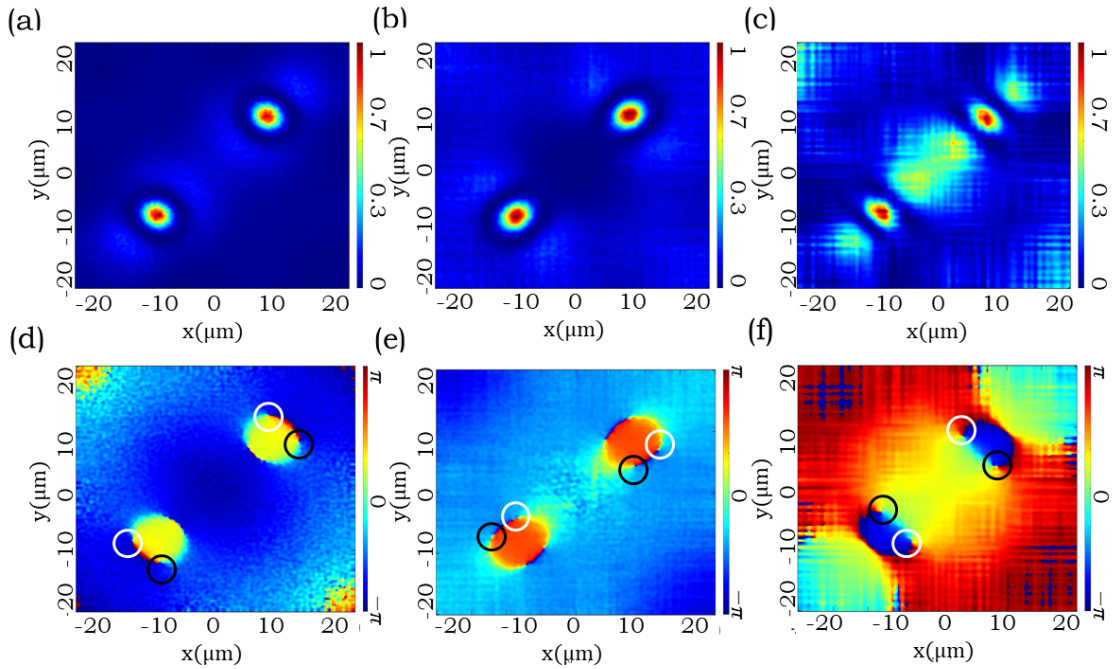

Figure 5.23: $|\psi(r)|^2$ and $\theta(r)$ for defective potential 04 and pumping scheme 02 for three different time (a) $|\psi(r)|^2$ and (d) $\theta(r)$ at t = 6.6 ps, (b) $|\psi(r)|^2$ and (e) $\theta(r)$ at t = 19.77 ps, (c) $|\psi(r)|^2$ and (f) $\theta(r)$ at t = 32.95 ps. Location of some vortex (anti-vortex) is marked by white (black) circle.

5.1.7 Final Remark On Condensation in Spatial-Temporal Domain

So far we have argued that presence of defect causes vortex to get pinned which in turn prevents percolation of local condensate to create a macroscopic condensate. Here we present same result but with 30 different initial condition for Gaussian Continuous pumping and defect potential pattern 01. Red dots represent position of a vortex.
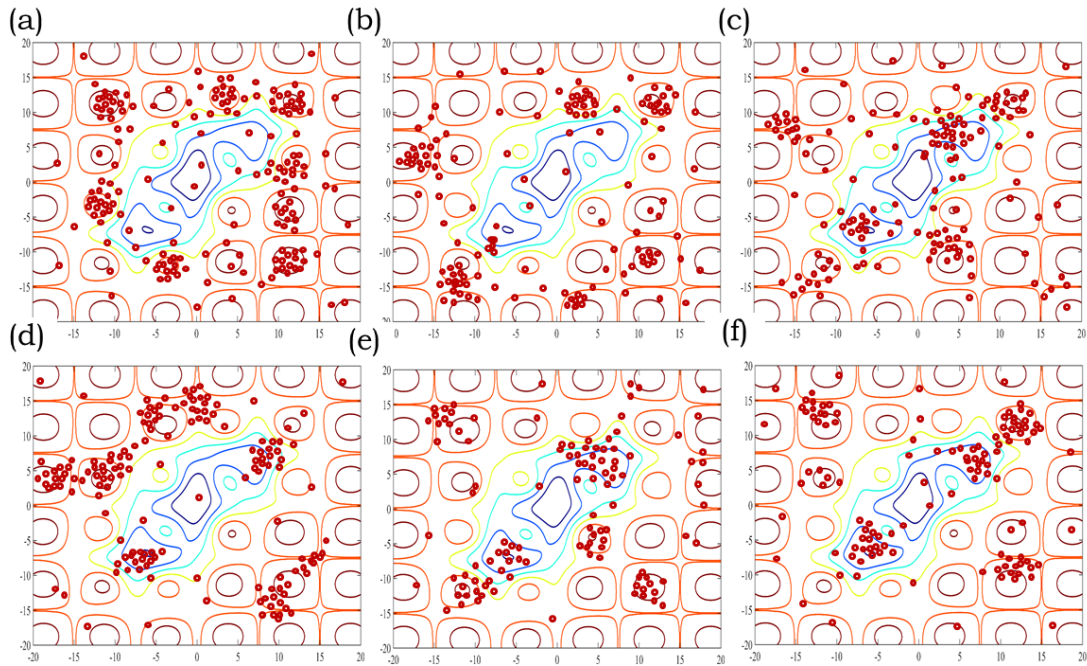
Figure 5.24: Vortex mapping for 30 different initial condition for defective potential 01 under pumping scheme 02 for time (a) 15.81 ps (b) 19.1 ps (c) 24.38 ps (d) 28.33 ps (e) 30.97 ps (f) 32.95 ps.

Whatever the initial condition is, vortices keep their pattern. Some additional vortices are created at different positions but they eventually gets annihilated by recombining with other anti-vortices. And time forces vortices to get accumulated close to defect potential (accumulation of red dots near disordered potential).

What is the significance of such case on overall performance of the system? When no defect is present, we find a overall macroscopic condensate with long range order. But as such long range order hasn't established, local condensation takes place and local condensate with short range order has been formed. This can significantly influence thermalization process of condensate. Due to strong localization of condensate, each local zone can have its own local energy, define its local temperature. We will see in Chapter

06, how this same result can be achieved by introducing localization in thermalization process. Furthermore, as local condensate dominates condensation process, more and more energy will be required to achieve a lasing action for exciton polariton LASER. Analysing the influence of defect is a very complex calculation from both numerical and numerical perspective. Existence of randomness in defective system cause it sometime very hard to predict. But with the advancement of theoretical treatment of randomness like the one we are going to use in Chapter 06, 'Random Matrix Theory', we now have at least some solid foothold facing such complex defect ridden system. And analysis of such complex system, it is at least my understanding that defect is actually a new frontier for engineer and physicist. Most often, we consider defect as undesirable condition, damaging our system. In some case they really are. But careful engineering of defect can bring some extra-ordinary result.

In this section, results regarding condensation process in spatial domain at different times have been presented. Such result does not show a clear picture of single state coherence which is fundamental for lasing action. As we have discussed in theoretical section, stimulated scattering process accumulates huge number of exciton-polariton particles close to $K = 0$ state which gives us coherent emission. We mainly focuses in this section about the result of condensation in spatial domain, how coherence has been achieved over distance? Now we will turn our focus on to coherence in K domain. A macroscopic coherence indicates effectively a very confined state in K space. We will focus on such results in the next section.

5.2 Condensation Dynamics in Kinetic Domain

Relaxation kinetics of classical particles is described by semiclassical Boltzmann equations. These sets of equation, modified to take into account of quantum nature of particle, are essential to understand the dynamics of condensate with respect to energy over time [164]. Kinetics of condensate without defect has been studied previously [94, 165, 166]. In this section we will analyze condensation dynamics using same approach of [121] but considering defect.

5.2.1 Preliminaries: Coupled Boltzmann Rate Equation

We have already talked about coupled semiclassical Boltzmann equation in section 2.4.3 and how does these coupled equations describe condensation dynamics of polariton lasing or ground state condensation process. Here we will present essential procedure for solving such coupled equations.

For solving such equations numerically, we consider non-resonant excitation. Usually, free electron—hole pairs are created by such excitation process, as the exciton binding energy amounts to some tens of meV only. These electron-hole pairs cool down, and form hot excitons (bound electron-hole pairs), by emitting phonons. A simple rate equation analysis indicates a strong non-equilibrium situation biased towards free carriers at low temperatures in typical III-V materials, owing to long formation times of excitons compared with their short radiative lifetime.

5.2.1.1 Discrete Polariton Dispersion Relation

Discretized Boltzmann equation results in a finite set of rate equations. A natural discretization of the modes of the system results when the system is enclosed in a large box. The quasiparticle momenta are then quantized into a uniform mesh. But this mode of discretization has certain drawbacks. Exciton-like polaritons and strongly coupled polaritons have very different masses. A dense grid in k space for the light-mass polariton would result in a grid for the heavy-mass exciton-like polaritons having a extremely large number of mesh. Alternatively, energy can be discretized into uniform mesh. The uniform energy grid allows us to impose exactly the energy conservation condition for elastic exciton—exciton scattering, avoiding drifts in the energy conservation in the numerical

integration of the rate equations. The energy grid is defined as ,

$$E(j) = E(0) + (j + \frac{1}{2})\Delta E \tag{5.8}$$

The choice of ΔE is determined by many factors. These are

- Population distributions, population should vary by only a small amount over ΔE. This implies $\Delta E < k_B T$.

- A good description of the scattering matrix elements with phonons. This implies $\Delta E <$ energy exchange during a phonon scattering.

- A good description of exciton-exciton scattering matrix elements.

We have already shown polariton dispersion relationship in fig. 2.5. A discretized version of that dispersion relation is shown in fig. 5.25
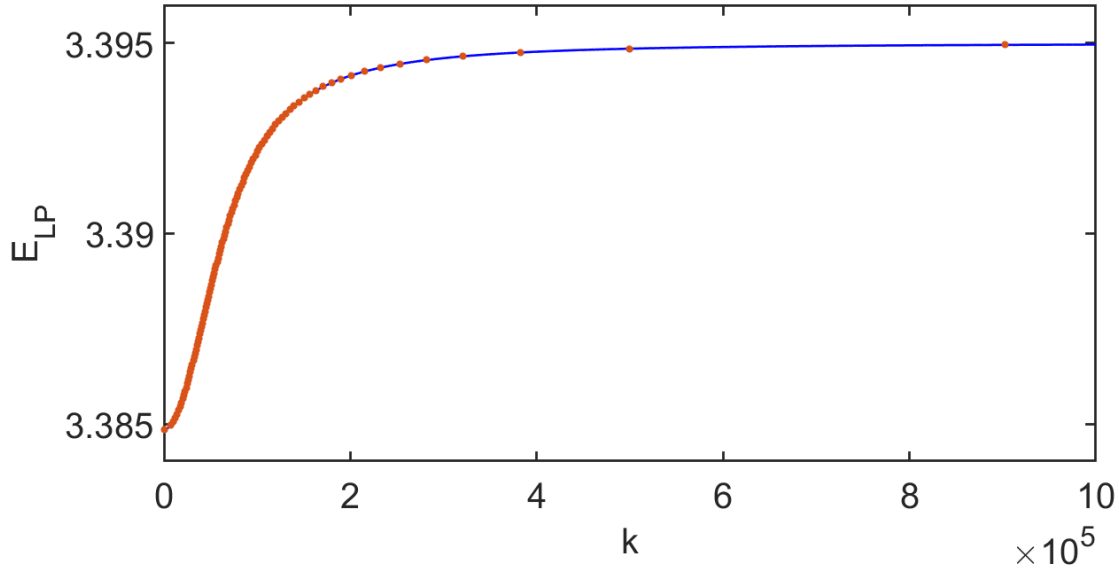
Figure 5.25: Discretized lower polariton dispersion relation. Blue line shows the continuous version and red dots are the energy grids for numerical solution purpose.

And radiative recombination rate has been discretized accordingly.

5.2.1.2 Discretized Rate Equations

Due to such discretization, semiclassical rate equation now reads,

$$\frac{dN(i)}{dt} = P(i) - \frac{N(i)}{\tau_i} - \sum_j W_{ph}(i,j)N(i)(1+N(j)) + \sum_j W_{ph}(j,i)N(j)(1+N(i))$$

$$- \sum_{j,i1,j1} W_{ex}(i,j,i1,j1)N(i)N(j)(1+N(i1))(1+N(j1))$$

$$+ \sum_{j,i1,j1} W_{ex}(i1,j1,i,j)N(i1)N(j1)(1+N(i))(1+N(j)) \quad (5.9)$$

$W_{ph}(i,j)$ is the scattering rates of polaritons with phonons from energy bin i to j, $W_{ex}(i,i1,j,j1)$ is the exciton—exciton scattering rates where two exciton from energy bin i and j are scattered to energy bin $i1$ and $j1$, $N(i)$ is the population of energy bin i, and $P(i)$ is the pumping rate.

5.2.1.3 Exciton-Phonon Scattering rate

We have already discussed exciton phonon scattering rate in section 2.4.1 (rate can be determined from equation 2.42). For discretized picture, exciton-phonon scattering rate is [94] for phonon absorption,

$$W_{ph}(i,j) = \frac{\Delta E (\Delta k)^2}{4\hbar \rho u} \frac{X(i)X(j)}{\pi^2 [DOS(j)]^{-1}} [1 + N_{ph}(|E(j)| - E(i))]Int(i,j) \quad (5.10)$$

and for phonon emission,

$$W_{ph}(i,j) = \frac{\Delta E (\Delta k)^2}{4\hbar \rho u} \frac{X(i)X(j)}{\pi^2 [DOS(j)]^{-1}} N_{ph}(|E(j)| - E(i))Int(i,j) \quad (5.11)$$

where, integrand $Int(i,j)$ is defined as,

$$Int(i,j) = \int_0^{\theta_{max}} d\theta \frac{I_\perp(q_z(\theta))}{q_z(\theta)} [a_e I_\parallel \left(\frac{m_e}{m_e + m_h} \Delta k_\parallel a_{BX} \right) - a_h I_\parallel \left(\frac{m_h}{m_e + m_h} \Delta k_\parallel a_{BX} \right)]$$
$$(5.12)$$

And θ_{max} is defined here as,

$$
cos(\theta_{max}) = \begin{cases} 1 & \text{if } c > 1 \\ c & \text{if } c \in [-1, 1] \\ -1 & \text{if } c < -1 \end{cases} \tag{5.13}
$$

Some definitions of the terms is in order. First we define term c in equation 5.12. If momentum corresponding to energy bin i is $k(j)$ and energy bin j is $K(j)$, then c is defined as,

$$
c = \frac{K(i)^2 + k(j)^2 - (\Delta k)^2}{2K(i)K(j)} \tag{5.14}
$$

here, Δk is defined as phonon energy for scattering between two subsequent energy bin,

$$
\Delta k = \frac{\Delta E}{\hbar u} \tag{5.15}
$$

Another important in the integrand is, $q_z(\theta)$ which is defined as,

$$
q_z(\theta) = \sqrt{(\Delta k)^2 - k(i)^2 - K(j)^2 + 2k(i)k(j)cos(\theta)} \tag{5.16}
$$

and here we consider $I_\perp(q_z(\theta)) \approx 1$. $a_e(a_h)$ is deformation potential for conduction (valance) band. Other terms are, ρ is density of material, u is sound velocity, $DOS(j)$ is density of state (inverse of effective mass) corresponding to momentum $k(j)$, X is Hopfield coefficient. Values used for numerical calculation is given table 5.1. For such values exciton-phonon scattering for some state is shown fig. 5.26.

Figure shows exciton phonon scattering rate from a state (state mentioned in legend is initial state) to final state (momentum of final state is along x axis). Clearly, scattering rate for transition with phonon absorption is higher than the transition with phonon emission.

5.2.1.4 Exciton-Exciton Scattering Rate

We have already discussed basic of exciton-exciton scattering in section 2.4.1. For numerical evaluation of discretized coupled rate equation, exciton-exciton scattering rate is,
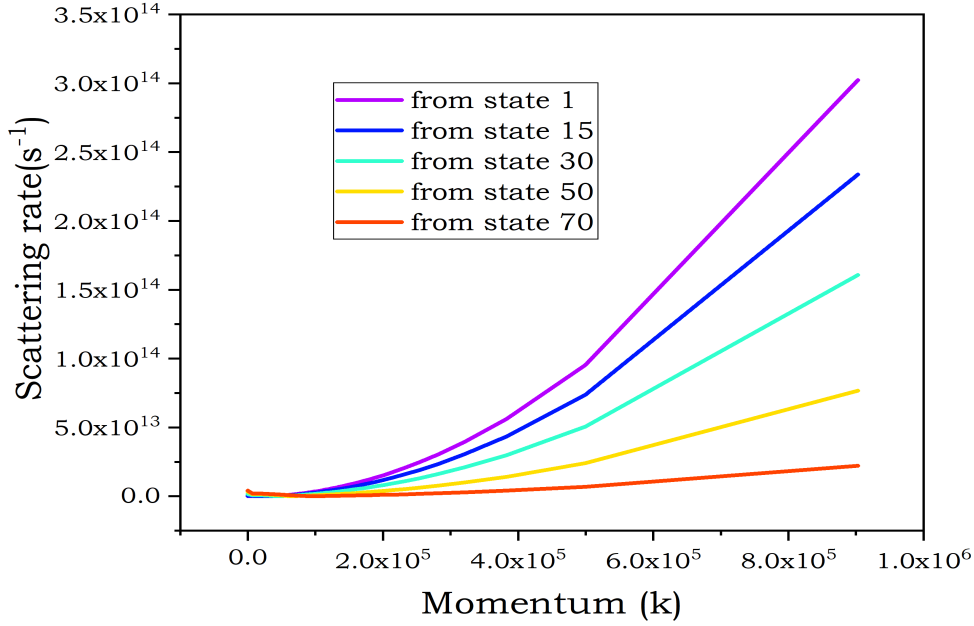
Figure 5.26: Exciton phonon scattering from different state. x axis shows the momentum value of final state exciton in after scattering rate. Legend shows exciton initial energy bin no. Unit of scattering rate is s^{-1}.

$$W_{ex}(i,j,i1,j1) = \frac{(\Delta ES)^2}{16\pi^3 h}|M|^2 \frac{|X(i)|^2|X(i1)|^2|X(j)|^2|X(j1)|^2}{[DOS(i1)]^{-1}[DOS(j)]^{-1}[DOS(j1)]^{-1}}Int(i,i1,j,j1)$$

(5.17)

where, $M = 6E_{BX}\frac{a_{BX}^2}{S}$ and integrand $Int(i,i1,j,j1)$ is defined as,

$$Int(i,i1,j,j1) = \int dx \frac{1}{\sqrt{[(k(i)+K(i1))^2 - x][x - (k(i)-K(i1))^2]}}$$
$$\frac{1}{\sqrt{[(k(j)+K(j1))^2 - x][x - (k(j)-K(j1))^2]}}$$

(5.18)

where Integration limit is,

$$I = [(k(i)-K(i1))^2, (k(i)+K(i1))^2] \cap [(k(j)-K(j1))^2, (k(j)+K(j1))^2]$$

This integration needs to be adaptive to handle singularity at the edge of the integration region. This integration is kind of different from the other scattering rate

125

defined i.e. exciton-phonon scattering rate. Here, scattering rate is due to interaction between two exciton at energy bin i and j and after scattered they are in energy bin $i1$ and $i2$. And $K(i), k(j), k(i1), k(j1)$ is momentum associated with energy bin (or state no) $i, j, i1, j1$ respectively. This sort of scattering mechanism is dominant in polariton relaxation dynamics.

5.2.2 Modification to Coupled SB Equations due to Defect

Due to introduction of defect, we are suggesting the following modification of discretized rate equation 5.9 as,

$$
\begin{aligned}
\frac{dN(i)}{dt} = P(i) - \frac{N(i)}{\tau_i} &- \sum_j W_{ph}(i,j)N(i)(1+N(j)) + \sum_j W_{ph}(j,i)N(j)(1+N(i)) \\
&- \sum_{j,i1,j1} W_{ex}(i,j,i1,j1)N(i)N(j)(1+N(i1))(1+N(j1)) \\
&+ \sum_{j,i1,j1} W_{ex}(i1,j1,i,j)N(i1)N(j1)(1+N(i))(1+N(j)) \\
&- \frac{N(i)}{\tau_d} \quad (5.19)
\end{aligned}
$$

Another term corresponding to exciton capture to defect is introduced via term $\frac{N(i)}{\tau_d}$ to each energy bin. Calculation of exciton capture rate due to defect has been done according to [92] with additional effect of effective capture cross section of exciton. Here we are providing a somewhat detailed calculation to determine $R_d(= \frac{1}{\tau_d})$.

Hamiltonian of a system with conduction band, valance band and defect level in bandgap region can be written as,

$$
H_0 = \sum_k E_c(k)c^\dagger(k)c(k) + \sum_k E_v(k)v^\dagger(k)v(k) + \sum_d E_d d^\dagger d \quad (5.20)
$$

One careful thing to consider here is k (lowercase) is actually single particle momentum vector wheres K (uppercase) is in-plane exciton momentum vector. For convenience we replace K (uppercase) by Q. $c(v)$ is annihilation operator for conduction (valance) band electron where d is annihilation operator for defect level with energy E_d. And q will be exchanged momentum during any sort of interaction as we have discussed in scattering

event. Exciton is is eigen-function of hamiltonian H which is $H = H_0 + H_{int}$, where interaction hamiltonian is defined as,

$$H_{int} = \sum_{k_1, k_2, q} V(q) c^\dagger(k_1 + q) v^\dagger(k_2 - q) c(k_1) v(k_2) \tag{5.21}$$

$V(q)$ is Coulomb interaction potential in momentum domain. Exciton wavefunction with momentum K is an eigenstate of $H(= H_0 + H_{eh})$ and is defined as,

$$|\psi_X(Q)\rangle = \sum_k \psi_{X,Q}(k) c^\dagger\left(k + \frac{m_e}{m_e + m_h} Q\right) v\left(k - \frac{m_e}{m_e + m_h} Q\right) |\psi_X(0)\rangle \tag{5.22}$$

where $\psi_{X,Q}$ is Fourier transform of envelop wavefunction of equation 2.5 with $|\psi_X(0)\rangle$ is state corresponding to filled valance band and empty conduction band. This wavefunction $\psi_X(Q)$ follows same dispersion relationship as equation 2.8 (with Q replacing K). Here one difference is presentation of wavefunction in terms of creation and annihilation operator. An exciton is actually a linear superposition of all electron and hole wavefunction which can exchange momentum $\frac{m_e}{m_e + m_h} Q$. Equation 5.22 is an indication of that.

Defining wavefunction close to defect is one of the approximation of this research work. In [92], defect is taken as periodic potential which causes the appearance of extra phase term with periodicity to appear in defect state wavefunction. But as in the experiment [33, 87], disorder is due to dislocation which is random in nature. This prompts us to approximate defect state wavefunction as,

$$\psi_d(r) = C exp(-\zeta r^2) \tag{5.23}$$

here r is location of defect and ζ is confinement factor which is a phenomenological parameter. ζ needs to be tuned along with some other parameters to fit numerical results close to experimental results.

Main exciton capture process is considered due to capture of hole and electron through the defect. Hole capture process as defined in [92] is used with modification here as,

$$H_{hc} = \sum_{k_1, k_2, q} V(q) X_d(k_2 - q) c^\dagger(k_1 + q) v^\dagger(k_2 - q) c(k_1) v(k_2) d + H.c. \tag{5.24}$$

$X_d(k_2 - q)$ is Fourier transform of equation 5.23. Using equation 5.22 as basis, we can

127

use time dependent perturbation theory to determine hole capture rate. Electron capture hamiltonian can be defined in the same way with now an electron is created at defect level. Keeping only first order term, we get hole capture rate,

$$R_{hc}(Q) = \frac{2\pi}{\hbar} n_d f_d |X(Q)|^2 N(Q) \sum_k N_c(k)|V(k)|^2 |\psi_d(k)|^2 \qquad (5.25)$$

here, k is momentum of scattered electron with $E_c(k) - E_c(0) = E_{BX} - E_d$. n_d is density of defect with occupation f_d. N_c is conduction band density of states, $|X|$ is Hopfield coefficient squared and occupation $N(Q)$ is defined as

$$N(Q) = \langle b^\dagger(Q)b(Q)\rangle \qquad (5.26)$$

with $b^\dagger(Q)(b(Q))$ being exciton creation (annihilation) operator at momentum Q. Same procedure for electron capture results in electron capture rate as,

$$R_{ec}(Q) = \frac{2\pi}{\hbar} n_d (1 - f_d)|X(Q)|^2 N(Q) \sum_k N_v(k)|V(k)|^2 |\psi_d(k)|^2 \qquad (5.27)$$

with N_v is now valance band density of state. This two capture rate is same as capture rate from Shockley-Read-Hall theory of recombination [167, 168] with excitonic transition of momentum between hole and electron is taken into account and additional effect of localization near defect region.

Another important factor to be considered here for the calculation of τ_d is the effect of exciton capture cross-section and exciton momentum. Clearly, defect capture rate is directly proportional to capture cross-section of exciton ($\approx \pi a_{BX}^2$) and velocity of exciton center of mass . Considering all the effect we can write exciton capture rate as,

$$R_d(Q) = A(Q)n_d(1 - f_d)|X(Q)|^2 N(Q)|Q| \sum_k N_v(k)|V(k)|^2 |\psi_d(k)|^2 \qquad (5.28)$$

where, term $A(Q)$ contains universal constant like $\hbar, \pi$ with exciton center of mass m and exciton capture cross section which can be a function of $|Q|$.

5.2.2.1 Data Table for Coupled Rate Equation

Various data that is needed for numerical calculation of condensation dynamics from semiclassical Boltzmann equation is given in the following table. Data are taken from

[33, 87, 169], NSM archive etc.

Table 5.1: Data for Numerical Solution of Coupled Boltzmann Rate Equation.

Property	Symbol	Value
Effective mass of electron	m_e	$0.2\ m_0$
Effective mass of heavy hole	m_{hh}	$1.1\ m_0$
Effective mass of light hole	m_{lh}	$0.259\ m_0$
Exciton Bohr radius	a_{BX}	$40\ nm$
Refractive index	n	2.6
Photon energy at $k = 0$	E_{ph0}	$3.415\ eV$
Exciton binding energy	E_{BX}	$20\ nm$
Micro-cavity quality factor	Q	2090
Lower refractive index of DBR mirror	n_l	1.59
Higher refractive index of DBR mirror	n_l	2.87
Coupling factor	$\hbar g$	$-0.035\ eV$
Normalization area	S	$138\ \mu m^2$
Density	ρ	$6.15\ gcm^{-3}$
Sound velocity	u	$7960\ ms^{-1}$
CB deformation potential	a_e	$11\ eV$
VB deformation potential	a_h	$11\ eV$
Temperature	T	$300\ K$
Exciton formation rate	W	$1e10\ s^{-1}$
Energy mesh size	ΔE	$0.1\ meV$
Electron-hole plasma lifetime	τ_{eh}	$5\ ns$

5.2.2.2 Non-resonant Pumping

As we have already mentioned, we considered non-resonant pumping condition. So $P(i)$ from equation 5.9 is defined as,

$$P(i) = \begin{cases} \frac{W n_{eh}}{\tilde{N}} & \text{if } E(i) - E_X(i) > \Delta \\ 0 & \text{otherwise} \end{cases} \tag{5.29}$$

where, Δ exciton binding energy and E_X is exciton energy as a function of in-plane momentum. Value of n_{eh} (electron hole plasma concentration) has been deduced from the

129

following rate equation at each time t.

$$\frac{dn_{eh}}{dt} = \frac{JS}{q} - \frac{n_{eh}}{\tau_{eh}} - W n_{eh} \tag{5.30}$$

here W is exciton formation rate, q is electron charge τ_{eh} is electron-hole plasma lifetime.

5.2.3 Numerical Result of Coupled SB Equations

In this section we will present numerical results of coupled SB rate equations. We take time mesh of size $\Delta t = 0.01\ ps$ for calculation purpose.

5.2.3.1 Checking Steady State

Clearly, we first check how many calculation step is needed to achieve stable state.
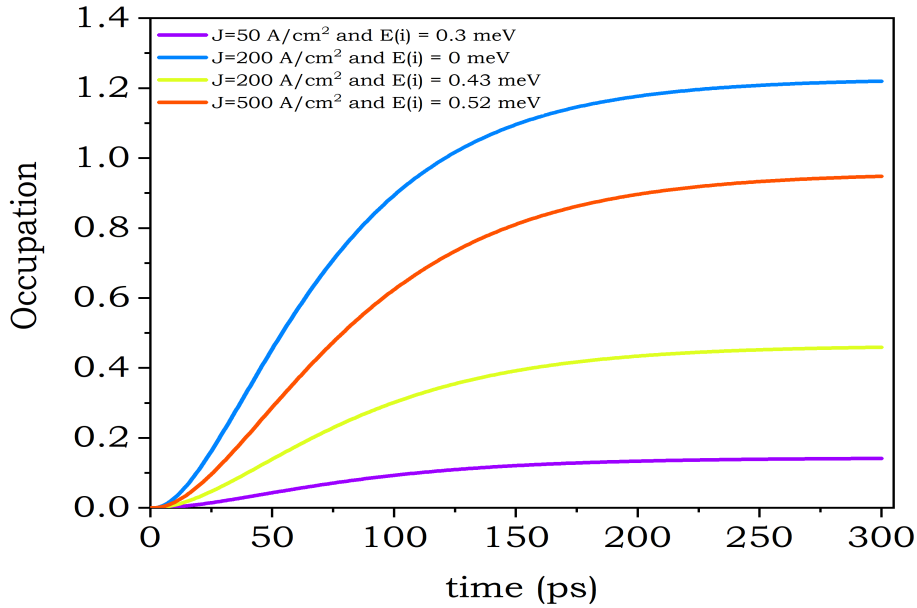
Figure 5.27: Occupation as a function of time. Steady state condition has been achieved after approximately 200 ps. Several different states are shown for better testing purpose of numerical calculation.

In fig. 5.27 variation of occupation with respect to time is shown. Steady state has been achieved around 200 ps. To avoid any unwanted numerical error, calculation has been done up-to 300 ps. This ensure a better stability condition than the one achieved at 200 ps. For the rest of this section we present result that has been achieved at $t = 300ps$. Fig.

5.27 shows four different state with each having different energy and for three different current density. Such analysis has to be performed for each state to ensure existence of steady state of the system.

If one state cannot achieve steady state, calculation has to be continued for further time until that state has not reached stable steady state. In our calculation, we see that for different current density whole system reaches steady state well before 300 *ps*.

5.2.3.2 System with No Defect
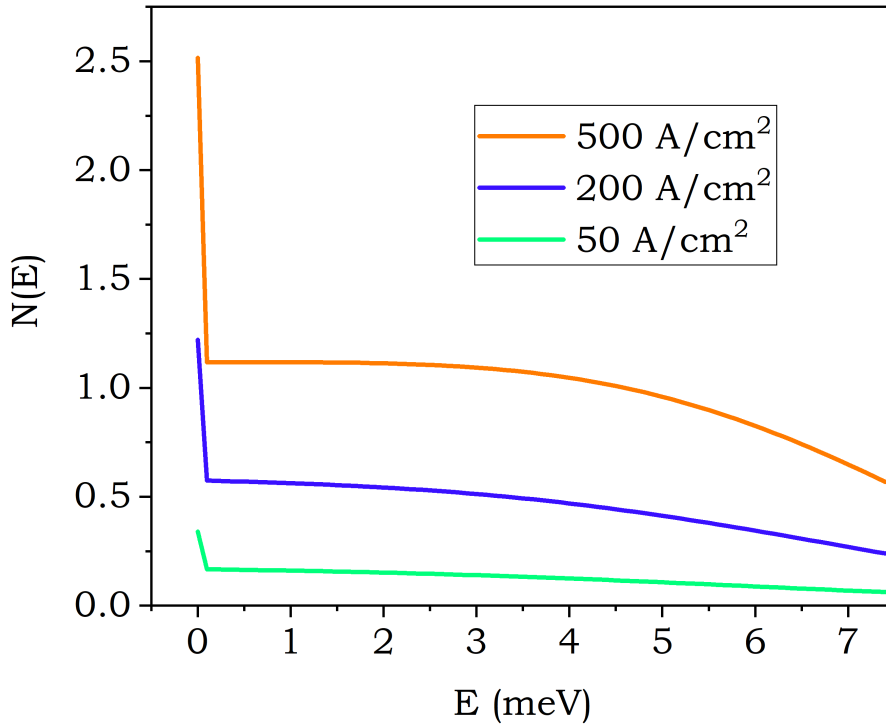
Figure 5.28: Occupation as a function of energy for three different current densities $50A/cm^2$, $200A/cm^2$ and $500A/cm^2$.

We will start with equation set 5.9 where we take no defect into account. Fig. 5.28 shows the plot of occupation, N as a function of energy, E.

For experimental data used for such calculation (table 5.1), threshold current was found to be $200A/cm^2$. So for current density of $50A/cm^2$, we see a very low occupation value and for current density much larger than threshold current density, $500A/cm^2$, occupation value gets quite big. This is an indication of LASING phenomenon.

Another important thing to be noticed here is ground state occupation $N(E = 0)$ is

abnormally larger than other state especially for $J \geq J_{th} \approx 200A/cm^2$. The reason behind this is explained in section 2.4.1 as 'Stimulated Scattering'. Such scattering mechanism forces a macroscopic amount of polariton to be accumulated at state $E = 0$ which causes emitted light to be coherent. This is the fundamental difference between a 'photon LASER' and 'polariton LASER'.
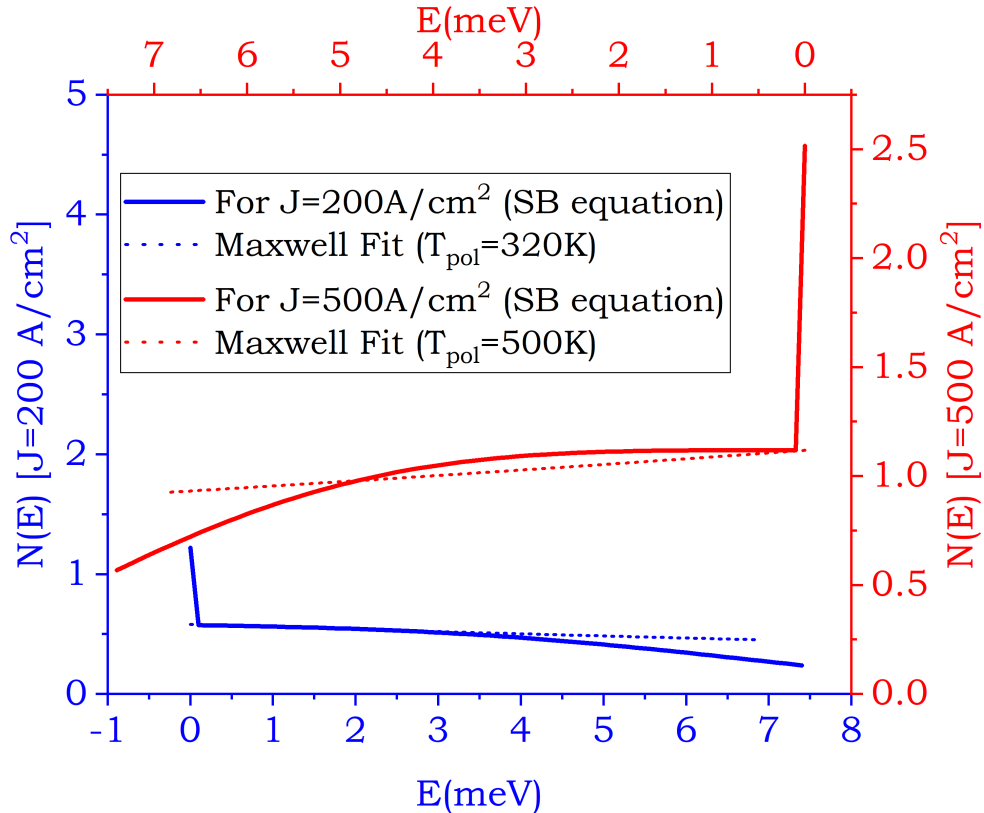
Figure 5.29: Occupation plot, $N(E)$ along with Maxwell distribution fit for two different current densities $200A/cm^2$ and $500A/cm^2$.

One of our main objective of this research work is to analyze the effective temperature of polariton LASER under different condition. We can fit $N(E)$ plot with Maxwell Distribution $\left(= N_0 exp\left(-\frac{E}{k_B T_{pol}}\right)\right)$. We consider polariton does not thermalize with lattice but rather thermalize among themselves. That's why we use T_{pol} rather than lattice temperature, $T_{lattice}$ which is room temperature here, 300 K.

Fig. 5.29 shows such a fit for two different current densities. For both cases, $T_{pol} > T_{lattice}$ i.e. for $J = 200A/cm^2$, effective polariton temperature is found as $320K$ and for $J = 500A/cm^2$ such temperature is $500K$ whereas for both cases is $300K$. A higher effective polariton temperature ensures pseudo-thermalization of polariton particle rather than a conventional thermalization with lattice and environment. This result is consistent

with several experimental findings.

5.2.3.3 System with Defect
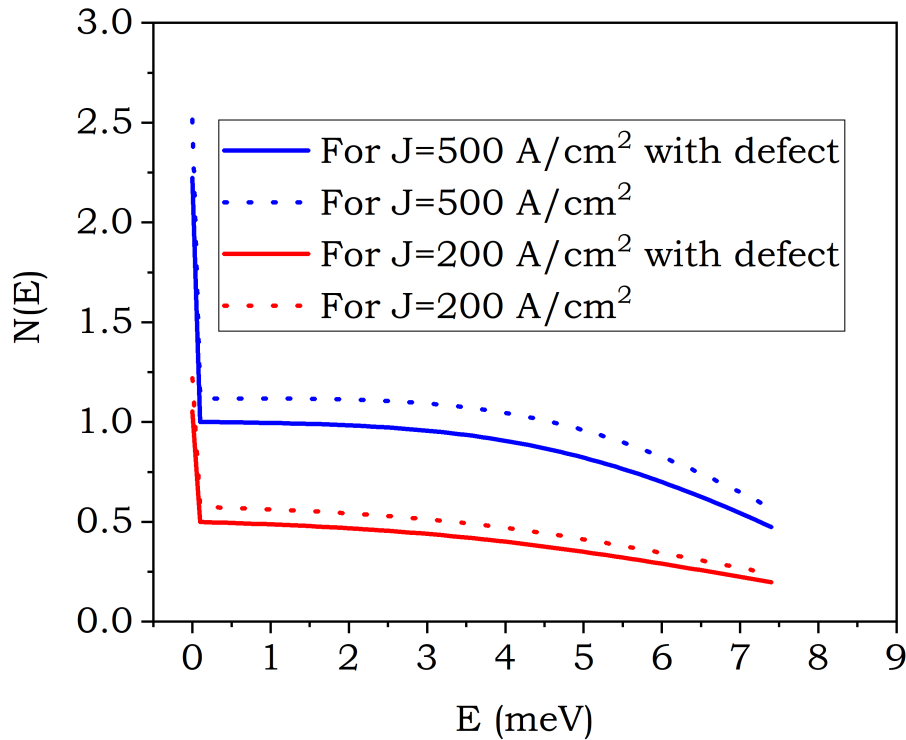
Figure 5.30: Occupation plot, $N(E)$ for two different current densities $200A/cm^2$ and $500A/cm^2$ with defect density $n_d = 1 \times 10^7 cm^{-2}$.

In fig. 5.30, numerical results for defect density $n_d = 1 \times 10^7 cm^{-2}$ has been shown for two different current densities $200A/cm^2$ and $500A/cm^2$ along with the results with no defect. Result is intuitively obvious as we solve here equation set 5.19 instead of equation set 5.9.

Addition of $-\frac{N(i)}{\tau_d}$ is clear from calculation result, Occupation at each energy bin is reduced. Amount of reduction depends on exact value of $R_d(Q)$ at the corresponding energy bin. This effect is clear from fig. 5.30. Another important understanding from our analysis of defect capture rate (equation 5.27) that this reduction in occupation number should depend on defect density. This is also clear from numerical results shown in fig. 5.31 and 5.32. As we increase defect density from $1 \times 10^7 cm^{-2}$ to $1 \times 10^8 cm^{-2}$ (an increase in one order) causes occupation each corresponding energy bin to decrease further. This decrease with defect densities is consistent with experimental results [33]. Our calculated
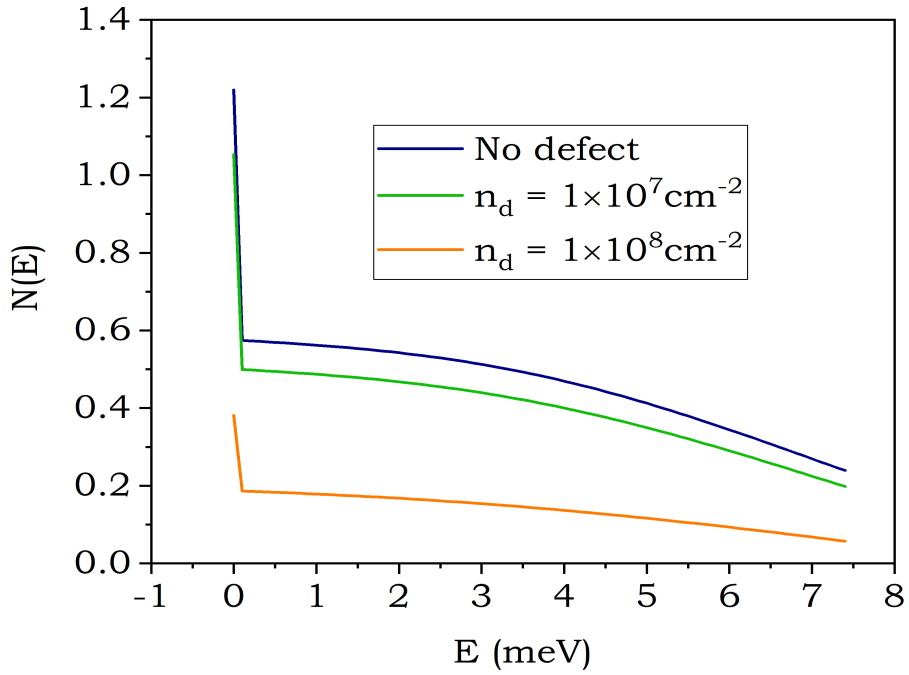
Figure 5.31: Occupation plot, $N(E)$ for two different defect densities, $n_d = 1 \times 10^7 cm^{-2}$ and $n_d = 1 \times 10^8 cm^{-2}$ for current density of $200A/cm^2$.
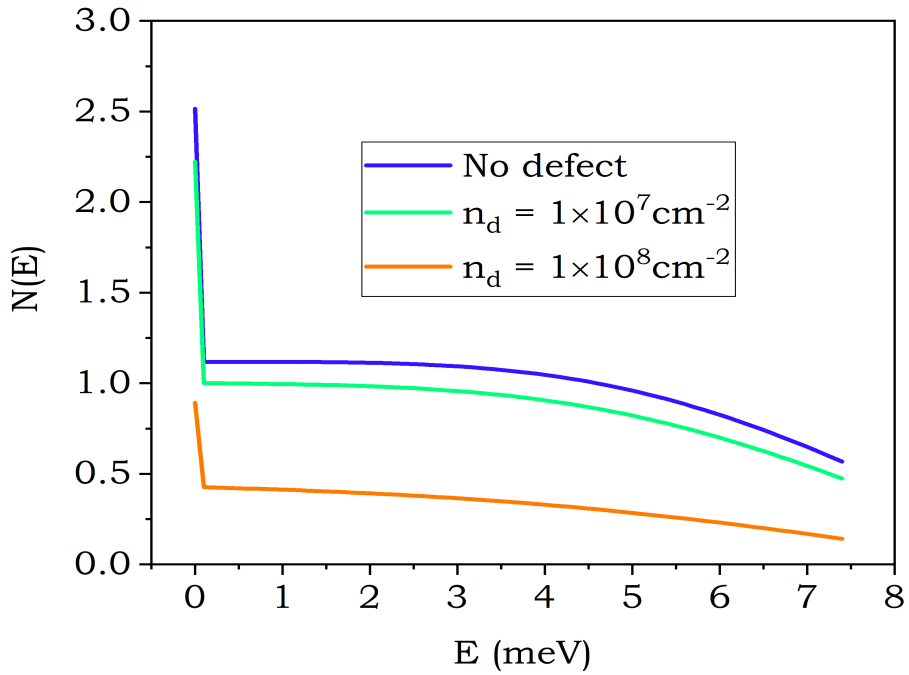
Figure 5.32: Occupation plot, $N(E)$ for two different defect densities, $n_d = 1 \times 10^7 cm^{-2}$ and $n_d = 1 \times 10^8 cm^{-2}$ for current density of $500A/cm^2$.

result even match well with experimental results. Such a fit shown in fig. 5.33.
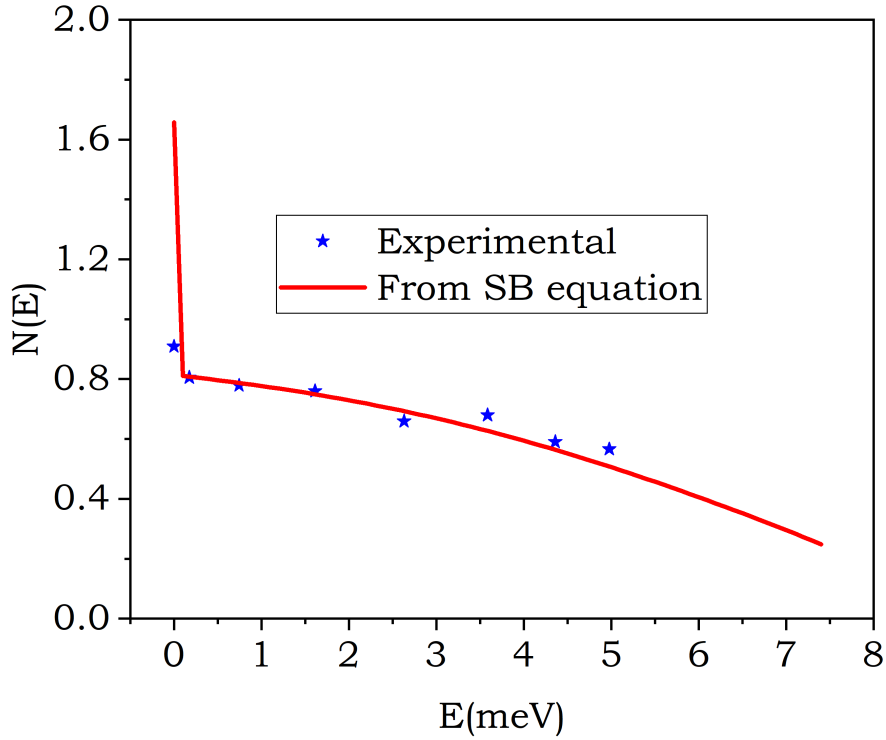
Figure 5.33: Calculated occupation plot $N(E)$ along with experimental data found for GaN device 2 (see text for detail). For numerical calculation, defect density $n_d = 1 \times 10^7 cm^{-2}$ and current density of $200 A/cm^2$ was used.

Although we can claim from fig. 5.33 calculated result shows a good fit with experimental data, there are some discrepancies. In experiment, GaN device 2 had a dislocation density of $7.22 \pm 0.34 \times 10^8 cm^{-2}$ where in our calculation we find the same result for defect density of $1 \times 10^8 cm^{-2}$. This sort of mismatch can be attributed to our approximation of equation set 5.19 where we take consider influence of defect as an independent term, not effecting other scattering mechanism like exciton-phonon or exciton-exciton interaction mechanism. Additionally, there might be some error regarding E_d estimation along with defect bound wavefunction. For our calculation of defect, we consider E_d to be mid gap region (equation 5.28), taking defect as deep level trap center. This sort of idealization might lead to such mismatch between experimental results and numerical results.

As we have already mentioned in previous section, polariton condensate is quasi-thermalized state rather than actually thermalize with lattice, having a different

temperature T_{pol} other than lattice temperature $T_{lattice}$. Such polariton effective temperature is found by fitting polariton occupation plot with a Maxwell distribution with temperature T_{pol} as we have done in fig. 5.29.

Same procedure has been followed for defect case. Occupation plot along with Maxwell distribution fit is shown in fig. 5.34 for current densities $200 A/cm^2$ and fig. 5.35 for current densities $200 A/cm^2$ In both cases, defect density has been varied from $1 \times 10^7 cm^{-2}$ to $1 \times 10^8 cm^{-2}$.

An interesting can be seen from these figures. When no defect is present (equation set 5.9), effective polariton temperature is always greater than lattice temperature ($T_{pol} > T_{lattice}$). This is general convention in terms of polariton effective temperature and has been experimentally verified by many experiment [61,67,69]. Although polariton effective temperature can vary with applied current density but nevertheless $T_{pol} > T_{lattice}$ will always maintain for current density above threshold current density (For $J = 200 A/cm^2$, $T_{pol} = 320K$ and for $J = 500 A/cm^2$, $T_{pol} = 420K$ where lattice temperature $T_{lattice} = 300K$).
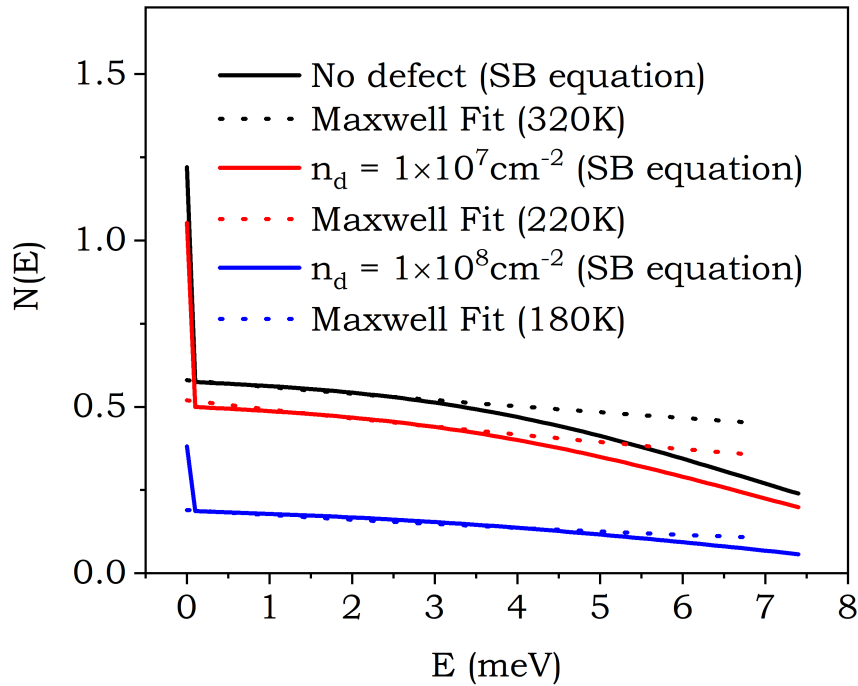
Figure 5.34: Occupation plot, $N(E)$ along with Maxwell distribution fit for two different defect, $n_d = 1 \times 10^7 cm^{-2}$ and $n_d = 1 \times 10^8 cm^{-2}$.Here current density is $200 A/cm^2$.

But with the introduction of defect such case of $T_{pol} > T_{lattice}$ is not always followed
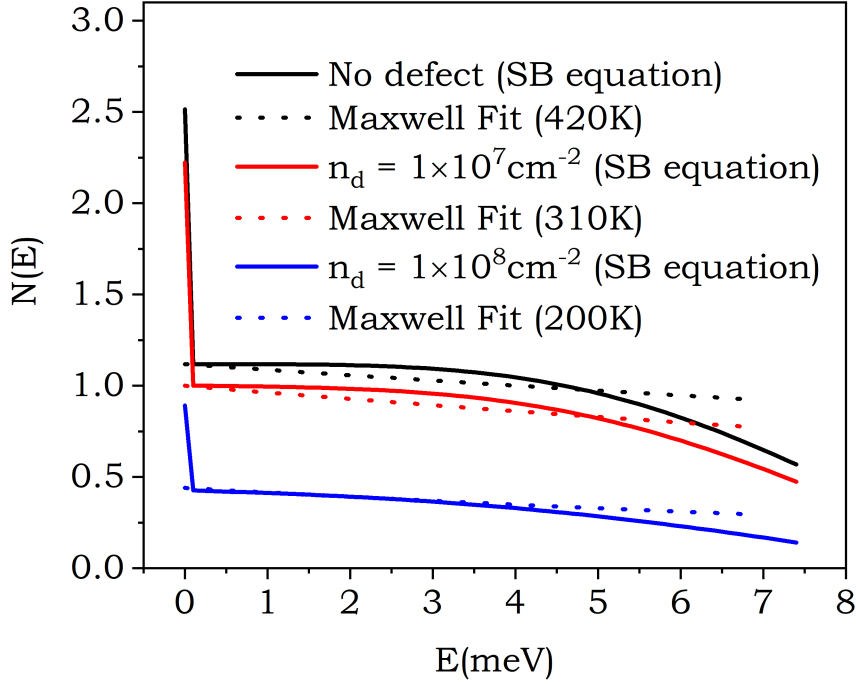
Figure 5.35: Occupation plot, $N(E)$ along with Maxwell distribution fit for two different defect, $n_d = 1 \times 10^7 cm^{-2}$ and $n_d = 1 \times 10^8 cm^{-2}$. Here current density is $500A/cm^2$.

as we can see from fig. 5.34 and 5.35. For $J = 200A/cm^2$ and defect density of $n_d = 1 \times 10^7 cm^{-2}$ we find an effective polariton temperature of $T_{pol} = 220K$ and for defect density of $n_d = 1 \times 10^8 cm^{-2}$ we find an effective polariton temperature of $T_{pol} = 180K$. Both of these polariton temperature is much lower than lattice temperature, $T_{lattice} = 300K$. Again for $J = 200A/cm^2$ we find same type of result. Here, defect density of $n_d = 1 \times 10^7 cm^{-2}$ we find an effective polariton temperature of $T_{pol} = 310K$ and for defect density of $n_d = 1 \times 10^8 cm^{-2}$ we find an effective polariton temperature of $T_{pol} = 200K$. Here, for defect density, $n_d = 1 \times 10^7 cm^{-2}$ polariton effective temperature is almost equal to lattice temperature ($T_{pol} \approx T_{lattice}$). But for higher defect density polariton effective temperature can get lower than lattice temperature ($210K$). This same sort of result was found in one experiment [33] where introduction of defect causes polariton effective temperature to get decreased (dislocation density of $6.44 \pm 0.34 \times 10^8 cm^{-2}$ resulted in T_{pol} of $270 \pm 8.9K$ and density $7.22 \pm 0.34 \times 10^8 cm^{-2}$ resulted in T_{pol} of $230 \pm 9.7K$). Same effect due to defect has been found by solving equation set 5.19 numerically taking defect capture rate by considering defect capture rate by equation 5.28.

5.3   Summary

In chapter 05, we present result for analysis on the impact of defect from two different point of view, one is in condensation in spatial and temporal domain and other in condensation in kinetic domain. Both of these perspective give us a better insight of the effect of defect in polariton like bosonic system. Spatial analysis shows us that defects prevent local condensate forming spontaneously from creating a long range coherence, a macro-condensate. And kinetic analysis shows us that defect reduces occupation number of each state and effectively reduces effective polariton temperature. Such two different dramatic result might not seem no connection in them, why absence of a macro-condensate results in a lower effective polariton temperature? Answer of such question will need a detail analysis of quantum thermodynamics which will be presented in chapter 06.But this seemingly two different results give us a better understanding of how defect can 'possibly' influence a system. We her emphasize on the word 'possibly' as we have to resort some sort of approximation to analyze the influence of defect. Limit of such approximation is needed to be tested to better understand the complex nature of defect in a system.

Chapter 6

Thermodynamics of Defective System

Thermodynamic study of a system is normally done in the limit of large number of system constituents. In this regard, probability plays a key role to understand thermodynamic behavior. But in quantum mechanics, unlike classical mechanics system is very well defined by hamiltonian. So a state evolves exactly as equation suggests. So thermalization in quantum system is thought to occur for each individual eigenstate and for their phase coherence. Addition of defect will change this picture. In this chapter, we will take a heuristic approach to tackle the problem of defect induced thermalization phenomenon. Additionally, we will solve disordered Bose Hubbard model numerically to understand the influence of defect on clean system especially on thermodynamic property of the system. It is our aim to reach a meaningful conclusion of the question raised in previous chapter, *why absence of a macro-condensate results in a lower effective polariton temperature?*. In heuristic approach, Theoretical background of this results are provided in Chapter 04.

6.1 Heuristic Approach

In this section, understanding the lower effective temperature is tackled from two viewpoint, percolation cluster and complete localization of low energy eigenstate. Discussion of both approach with slight mathematical aid is provided.

6.1.1 Approach 01: Percolation Cluster

As we have already discussed in section 4.4.2, presence of defect prevents long range correlation, results in disconnected superfluid puddle. We got somewhat similar result

in Chapter 05 when we evaluated ground state dynamics under the presence of defect. Local condensate cannot combine and create a macro condensate due to pinned vortices. We define local hamiltonian of the system containing such superfluid puddle or local condensate as $H_{V(i)}$ and total hamiltonian is defined as,

$$H = \prod_{i=1}^{N} \bigotimes H_{V(i)} = H_{V(1)} \otimes H_{V(2)} \otimes ... \otimes H_{V(N)} \tag{6.1}$$

where, $V(i)$ is the volume of ith region and there are N different regions with local condensate (total volume $V = \sum_{i=1}^{N} V(i)$). No coupling between two region is considered. Eigenstate of such a region or eigenstate for $H_{V(i)}$ is defined as,

$$\psi_l^i(r_i) = N_l^i \int d^d p C_l^i(p_i) \delta(p_i^2 - 2mU_l^i) e^{\frac{i}{\hbar} \vec{p_i} \cdot \vec{r_i}} \tag{6.2}$$

where, d is dimension of the system, U_l^i is eigen-energy of state l in such a local region (i^{th} region), m is mass of the particles and N_l^i is defined as,

$$\int_{V(i)} d^d r |\psi_l^i(r_i)|^2 = 1 \tag{6.3}$$

We here consider eigenfunction in each region is just a random summation of plane wave function with the coefficients following Gaussian distribution. Coefficients $C_l^i(p_i)$ follows,

$$\langle C_l^i(p_i) C_k^i(p_i) \rangle_{EE}|_{V(i)} = \delta_{lk} \tag{6.4}$$

$$\langle C_l^i(p_i) C_l^j(p_j) \rangle_V = \delta_{ij} \tag{6.5}$$

$$\langle C_l^i(p_i) C_k^j(p_j) \rangle_V = 0 \tag{6.6}$$

$$\langle C_l^i(p_i) C_l^i(q_i) \rangle_{EE} = \delta(p_i - q_i) \tag{6.7}$$

Purpose of equation 6.4 - 6.7 is to isolate one region of local condensate from other, even eigenstates. Equation 6.5 defines that eigen state from two region i and j are completely uncorrelated. We can use equation 6.2 to define eigenfunction for system

defined by hamiltonian in equation 6.1 as,

$$\psi_\alpha(r) = \prod_i \bigotimes \psi_l^i(r_i) \tag{6.8}$$

As a result of equation 6.8, eigen-energy of hamiltonian H (from equation 6.1) can be written as,

$$U_\alpha \approx \sum_{i=1}^{N} U_l^i \tag{6.9}$$

Fourier transform of eigenstate of H can be defined as,

$$\psi_\alpha(P) = \frac{1}{\sqrt{\hbar^d}} \int d^d r \psi_\alpha(r) e^{-\frac{i}{\hbar}\vec{P}.\vec{r}} \tag{6.10}$$

We can consider eigenstate of each region separately because of equation 6.5 and 6.6. We can write,

$$\langle \psi_\alpha(p)\psi_\beta(q)\rangle_{EE} = \sum_{i=1}^{N}\langle\psi_l^i(p_i)\psi_k^i(q_i)\rangle_{EE} = \sum_{i=1}^{N}(N_l^i)^2\delta_{lk}\delta(p_i - q_i)\delta(p_i^2 - 2mU_l^i) \tag{6.11}$$

For an initial state $\psi(P, 0)$,

$$\psi(P, 0) = \sum_\alpha a_\alpha \psi_\alpha(P) \tag{6.12}$$

For such a system, microcanonical average of any observable is defined according to equation 4.39. We can determine diagonal component of such observable as,

$$O_{\alpha\alpha} = \langle\psi_\alpha(P)|O|\psi_\alpha(P)\rangle \tag{6.13}$$

which can be expressed in terms of $\psi_l^i(p_i)$ as,

$$O_{\alpha\alpha} = \sum_{i=1}^{N}\langle\psi_l^i(p_i)|O^i|\psi_l^i(p_i)\rangle = \sum_{i=1}^{N} O_{ll}^i \tag{6.14}$$

Here, O^i is observable in i^{th} region. So a thermodynamic average is summation of its value in different region where local superfluid phase exist. This result in quite intuitive according to percolation picture.

Based on above discussion, we will determine probability of finding a particle from a system of n particle around momentum P_1 which is defined in equation 4.4. For non defective case, similar calculation is given in [99, 100, 147]. For 3D quantum mechanical system with initial condition of equation 6.12, such probability is defined as,

$$\rho_{QM}(P_1, t) = \int \int ... \int d^3P_2 d^3P_3 ... d^3P_n |\psi(P,t)|^2 = \sum_{\alpha\beta} a_\alpha^* a_\beta e^{i(U_\alpha - U_\beta)t/\hbar} O_{\alpha\beta}(P_1) \quad (6.15)$$

Using equation 6.14, 4.5, 4.38 and 4.39, we can write $\rho_{QM}(P_1, t)$ as,

$$\rho_{QM}(P_1, t) = \sum_\alpha |a_\alpha|^2 \sum_{i=1}^N \frac{I_{3n(i)-3}(2mU_l^i - P_1^2)}{I_{3n(i)}(2mU_l^i - P_1^2)} \quad (6.16)$$

where $I_n(x)$ is defined as,

$$I_n(x) = \frac{(\pi x)^{\frac{D}{2}}}{\mathcal{T}(\frac{D}{2})x} \quad (6.17)$$

In the above we consider a uniform density across the whole sample. As a result of such assumption, $n(i) = \frac{n}{V}V(i)$, is local density of particles. If we calculate each region individually, each system will show Maxwell Boltzmann distribution for large $n(i)$ limit ($n(i) \to \infty$). Now each region will show a different equilibrium distribution with different temperature, T_i due to difference in U_l^i among different regions. For each individual region we can express $\frac{I_{3n(i)-3}(2mU_l^i - P_1^2)}{I_{3n(i)}(2mU_l^i - P_1^2)}$ using $U_l^i = \frac{3}{2}n(i)k_B T_l^i$ as

$$\frac{I_{3n(i)-3}(2mU_l^i - P_1^2)}{I_{3n(i)}(2mU_l^i - P_1^2)} = \frac{1}{(2\pi m k_B T_l^i)^{3/2}} e^{-\frac{P_1^2}{2m k_B T_l^i}} = \rho_{MB}^i(T_l^i) \quad (6.18)$$

which in turn gives us the probability distribution as,

$$\rho_{QM}(P_1, t) = \sum_\alpha |a_\alpha|^2 \sum_{i=1}^N \rho_{MB}^i(T_l^i) \quad (6.19)$$

If initial energy of the system is U and for close quantum system there is no exchange of energy between the system and outside environment, energy U will remain constant throughout the whole dynamics. Such total energy now can be expressed as,

$$U = \sum_\alpha |a_\alpha|^2 U_\alpha = \sum_\alpha |a_\alpha|^2 \sum_{i=1}^N U_l^i \quad (6.20)$$

142

From equation 6.19, we see that for exchange inside individual region i, energy is thermalized with temperature, T_l^i. This local temperature 4.3.5 depends on the local energy quantity. Net distribution of such disordered system is micro-canonical average of eigenstates which is again a weighted average of local distribution. Without defect, such local distribution do not occur which causes overall temperature to be higher.

6.1.2 Approach 02: Eigenstate Localization

This approach is quite simpler than the previous case. Instead of dividing whole region into small region containing local condensate, we instead consider localization of eigenstates. Eigenstate is considered here is same as before (equation 6.2) for whole sample space instead of only for a local region. For clarity, eigenstate is considered here,

$$\psi_a(r) = N \int dp C_a(p) \delta(p^2 - 2mU_a) e^{\frac{i}{\hbar}\vec{p}.\vec{r}} \tag{6.21}$$

with $C_a(p)$ is Gaussian random variable follows equation 6.4 and 6.7 over the whole sample rather than only a local region. Fourier transform of such random wavefunction is,

$$\psi_a(p) = N \int dK C_a(K) \delta(p^2 - 2mU_a) \int dr e^{\frac{i}{\hbar}\vec{p}.\vec{r}} \tag{6.22}$$

where U_a is eigen energy corresponding to state $\psi_a(p)$. If dynamics start from initial condition,

$$\psi(P, 0) = \sum_a c_a \psi_a(p) \tag{6.23}$$

with energy U as,

$$U = \sum_a |c_a|^2 U_a \tag{6.24}$$

Now our assumption is here that some eigenstates thermalize themselves wheres others localize themselves thus avoid thermalization. We can divide initial state of the system into two components as,

$$\psi(P,0) = \sum_l c_l \psi_l(p) + \sum_t c_t \psi_t(p) \tag{6.25}$$

where $\psi_l(p)$ and $\psi_t(p)$ are the localized and thermalized states respectively. Similarly energy can also be divided into two parts,

$$U = \sum_l |c_l|^2 U_l + \sum_l |c_t|^2 U_t = U(l) + U(t) \tag{6.26}$$

And further we also approximate,

$$\langle \psi_l(p) | \psi_t(p) \rangle = 0 \tag{6.27}$$

Such approximation makes this approach quite simpler than approach 01. Validity of such approximation can be questioned. Our logic behind such assumption is that with defect some state is found to be localized especially the low lying state as they do not posses sufficient energy to surpass the defect barrier. Additionally, we have already seen in section 4.3.5 how localization can prevent thermalization with is the basis of our approximation of equation 6.27. Nevertheless, such assumption should be put through experiment and scrutiny for better understanding. We will not do such scrutinising activity here but rather keep it for future work.

Following the assumption of equation 6.25, 6.26 and 6.27 from discussion of approach 01 it can be easy said that thermalized energy will attain an equilibrium temperature, T_t but localized energy corresponding to localized eigenstate do not thermalize. If we consider a simple model that each particle attain an average energy, then $U_t = \frac{3}{2} N k_B T_t$ and system total energy can be written as as,

$$U = U_l + \frac{3}{2} N k_B T_t \tag{6.28}$$

where, N is total no. of particles (Considering only a small fraction of particle has been thermalized). If no defect present then whole energy will be thermalized which will result in temperature $T > T_t$ as $U_l > 0$. This can be thought of another alternative answer to the question effective lowering of polariton temperature due to defect.

6.2 Numerical Approach

Heuristic approach has several drawbacks, most significant of which is that it is based on some through assumptions. Although validity and detail of such assumption can be tested experimentally, such assumption prevents to bring a complete and tentative analytical conclusion on the question, *why absence of a macro-condensate results in a lower effective polariton temperature?* So we resort to numerical approach. Here, we solve DBHM numerically. DBHM is defined as,

$$H = -t \sum_{\langle ij \rangle} (b_i^\dagger b_j + b_j^\dagger b_i) - \mu \sum_i \hat{n}_i + \frac{U}{2} \sum_i \hat{n}_i(\hat{n}_i - 1) + \sum_i V(r_i)\hat{n}_i \qquad (6.29)$$

with V_i being drawn randomly from $[-W/2, W/2]$ with disorder strength W. Detail of such model is described in section 4.4.

Numerical solution of such model requires heavy computational resources and time. To optimize both, we resort to Quantum Monte Carlo (QMC) simulation method for system which has hamiltonian of large dimension. Hamiltonian with smaller dimension is solved by complete diagonalization method. Introductory discussion regarding QMC simulation methods is provided in appendix.

In Fig. 6.1, we show the lattice to solve Bose Hubbard Model with and without any disorder. Initially, 4 bosons are located lower right corner (blue lattice points). At $t = 0$, red bond has been established and bosons are allowed to roam within 13 lattice points according to equation 6.29 with disorder strength $W = 0$. Same procedure has been followed to report thermalization of isolated quantum state in [170]. We consider singly occupied site which makes dimension of Hamiltonian to be 715. Momentum distribution along x axis is obtained as,

$$n(k_x) = \sum_{k_y} n(k_x, k_y) \qquad (6.30)$$

where $n(k_x, k_y)$ is defined as,

$$n(k_x, k_y) = \frac{1}{L^2} \sum_{i,j} e^{-i2\pi \vec{k} \cdot (\vec{r_i} - \vec{r_j})/L} \langle b_i^\dagger b_j \rangle \qquad (6.31)$$

The position vector $r_i = (i_x d, i_y d)$ with lattice constant d and $L = 4$. In Fig. 6.2, thermalization of $n(k_x = 0)$ is shown, with time value approaches close to 1.
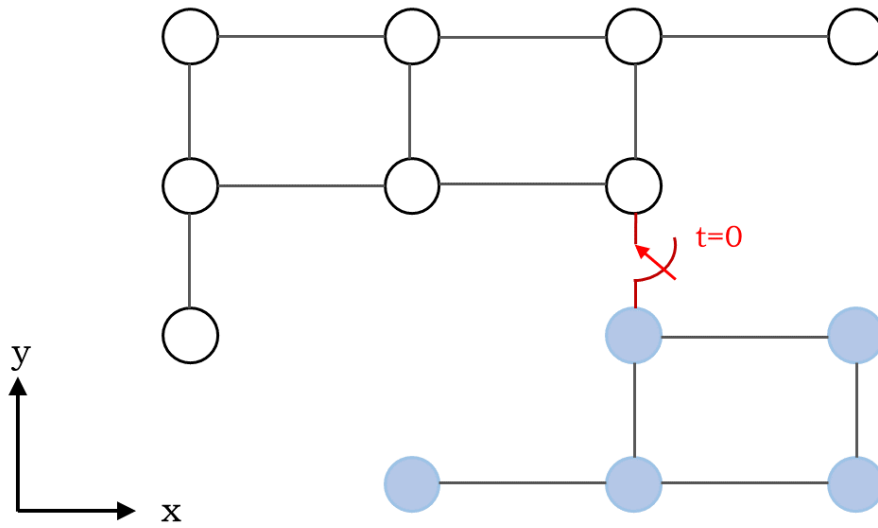
Figure 6.1: Lattice diagram for evaluating $n(k)$. A 4×4 lattice (4 sites missing) with 4 atoms. Initially, atoms were located in blue zone with no connection with rest of the lattice. At $t = 0$ connection has been established (red bond) and system is allowed to thermalize.
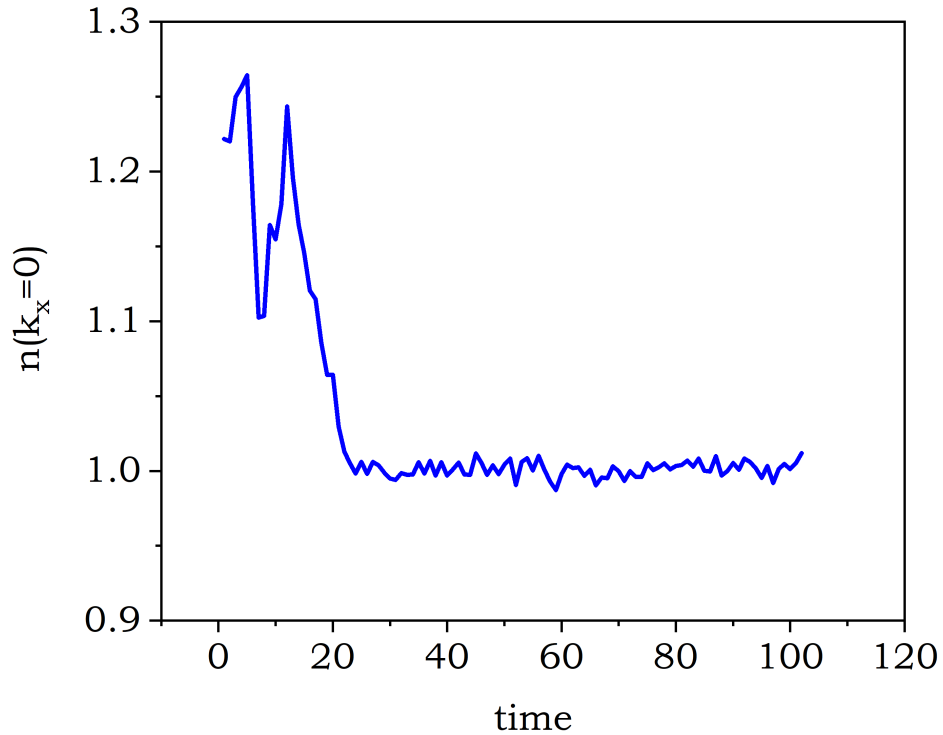
Figure 6.2: Evolution of $n(k_x = 0)$ with time. Here, hopping amplitude is considered as t=2.2U to ensure the system is in superfluid phase. x axis time ordinate is normalized by t.

146
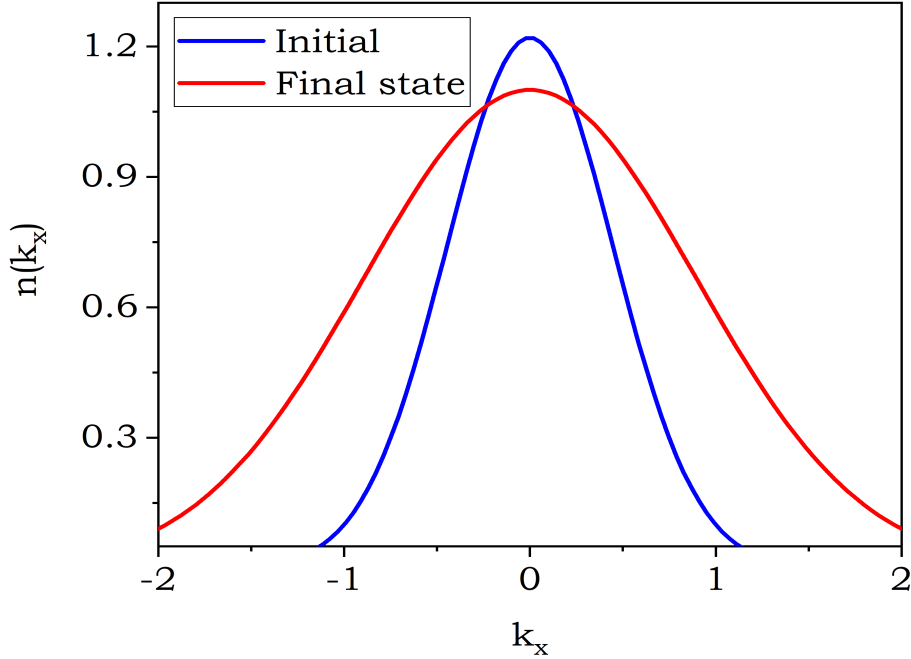
Figure 6.3: Momentum distribution along x axis for initial and thermalized state (after 60 unit of normalized time).

In Fig. 6.3, complete momentum distribution for initial and final state without any disorder is shown. Initially, whole system is comprised of 4 bosons in 5 lattice points. As the these bosons are allowed to roam in 13 lattice points. Final momentum distribution is take at 50 unit of normalized time (time normalized by hopping amplitude.) As explained in [170], such thermalized value can be very well approximated by ETH, a micro-canonical average with mean of ground state energy of hamiltonian and very small deviation.

So far, these results have already been found in [170]. Our addition to that results is study the influence of defect. In Fig. 6.4, momentum distribution with and without disorder. We consider disorder potential $V(i)$ to be drawn from set $[-W/2, W/2]$ with uniform distribution. Presence of disorder can prevent thermalization of the system as discussed in section 4.3.5 by localizing particles in spatial domain. This effect is clear from momentum distribution. Disorder spread momentum distribution further, a delocalization is momentum space is an indication of localization of phase space. Such delocalization, as expected, cannot be approximated by micro-canonical average predicted by ETH (equation 4.40). Presence of disorder makes application ETH invalid here.

So far, we use exact diagonalization method to study BH model. This was possible
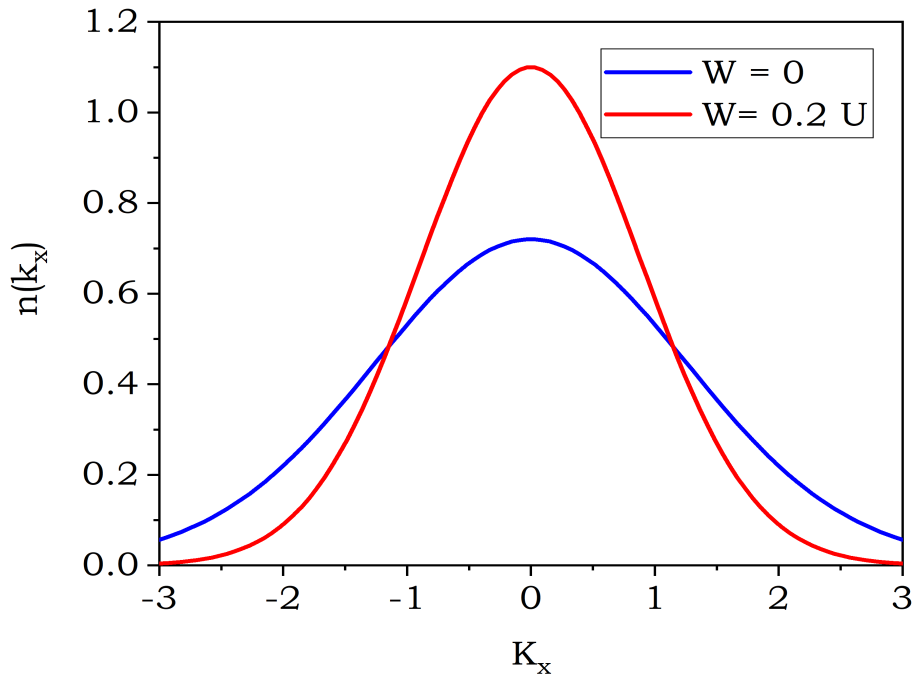
Figure 6.4: Comparison of momentum distribution $n(k_x)$ for system without ($W = 0$) and with ($W = 0.2U$) disorder potential. Delocalized state for a system without disorder gets partially localized due to disorder as can be seen from momentum distribution function.
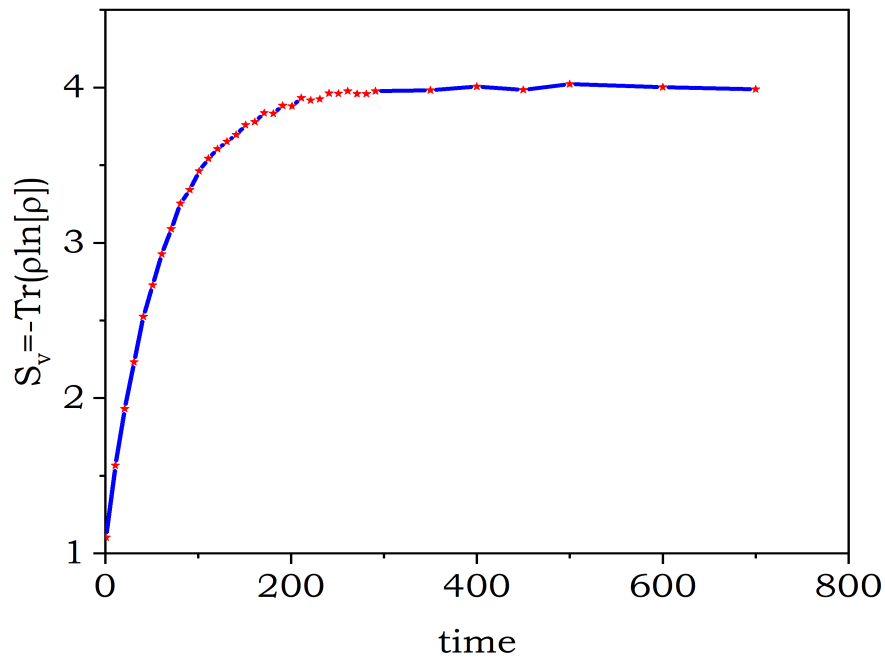
Figure 6.5: Evolution of Von Neumann entanglement entropy for a system for $L = 12$ with time. Entropy starts from an initial condition and eventually saturates to a maximum value.
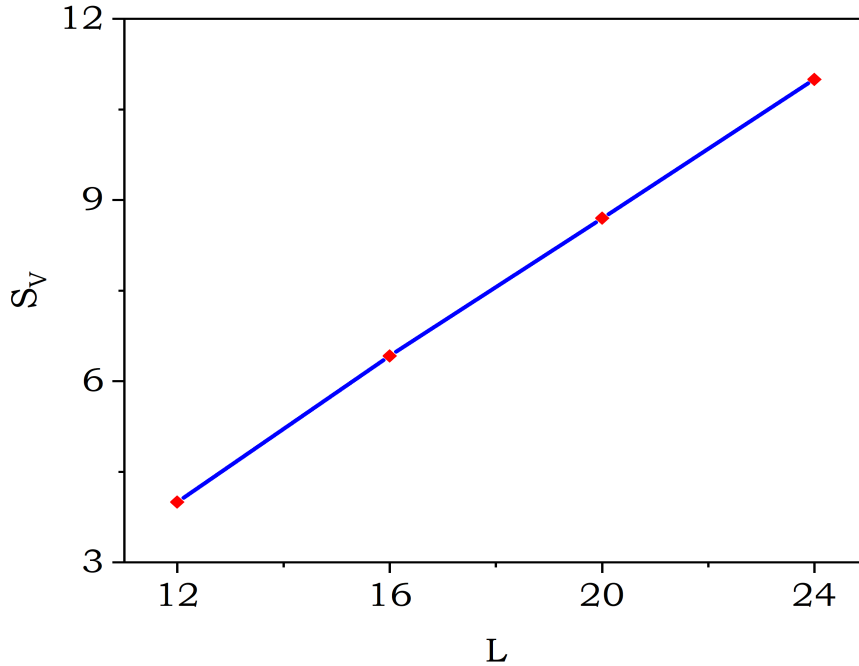
Figure 6.6: Evolution of Von Neumann entanglement entropy for a system with varying lattice size.

due to low dimension of the hamiltonian which is a consequence of low number of lattice sites and low number of bosons. But as explained in [98], to accurately describe thermalization property, larger system should be evaluated. As system size grows, hamiltonian dimension grows exponentially. For example, for 1D lattice with size 24 and 12 bosons, hamiltonian dimension is 2704156. For larger system, it will be impossible to utilize exact diagonalization (Creating a matrix of 2704156×2704156 will require a lot of memory and solving such a system will also require further memory with time). Instead of exact diagonalization, Stochastic Series Expansion (SSE) method has been used to get the follwoing results with $1D$ BH model containing L lattice points to reduce computational resources. In Fig. 6.5 von neumann entropy is shown as a function of time and in Fig. 6.6 as a function of lattice point, L. As time passes, system eventually thermalizes, reaching maximum entropy state. The saturation value of this entropy is a function of lattice points. Although we do not find any saturation characteristics in entropy as a function of L, in [98], such saturation characteristics appear for larger L. For following results, we will use 1D BH model with $L = 24$ along with incommensurate filling of $\langle n \rangle = 0.5$.
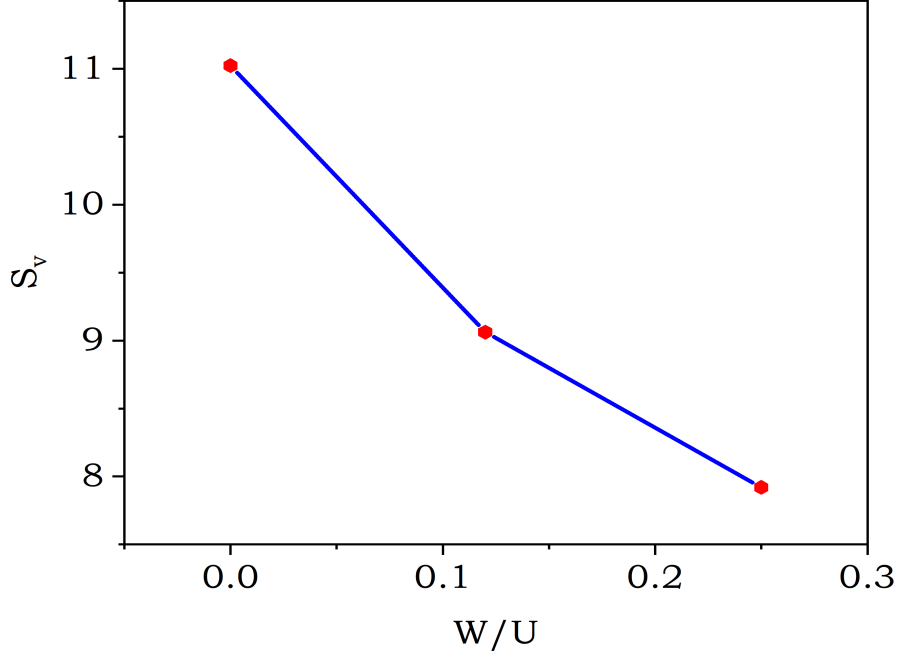
Figure 6.7: Evolution of Von Neumann entanglement entropy for a system with different disorder strength.

In Fig. 6.7, saturated von neumann entropy for three different disorder strength is depicted. With disorder we see a steady decline of saturation entropy. Additionally in Fig. 6.8 and 6.9 shows same behavior of compressibility and superfluid fraction with respect to defect. Compressiblity is defined as,

$$\kappa = \frac{d\langle N \rangle}{d\mu} \tag{6.32}$$

where $\langle N \rangle$ is defined as,

$$\langle N \rangle = \frac{1}{Z} \sum_p \sum_a \frac{(-\beta)^p}{p!} \langle a | \sum_i \hat{n}_i | a \rangle \tag{6.33}$$

with Z is partition function and $|a\rangle$ is eigenstate of the hamiltonian and $\beta = \frac{1}{k_B T}$. We use Handscomb method [171] to express the expectation value of operator.

And Superfluid Fraction is defined using the winding number prescription [172]. In the World line configuration with periodic boundary conditions, whenever a particle crosses a boundary it means a winding has occurred. This is particularly easy to measure in SSE as all that is need is to check for off diagonal terms that connect two sites across the
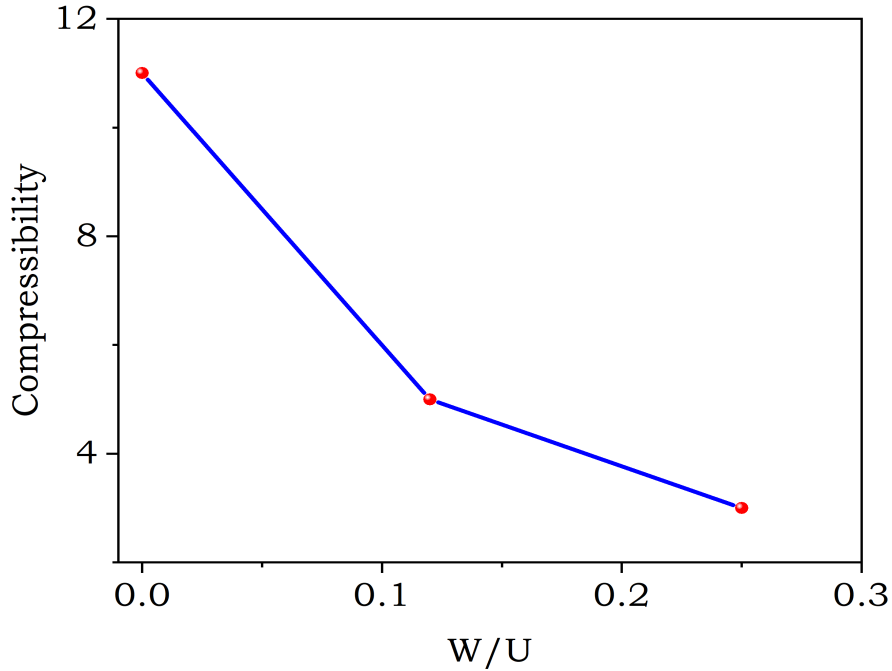
Figure 6.8: Evolution of Compressibility for a system with different disorder strength.

(periodic) boundary. Using winding number fluctuation, superfluid fraction is defined as,

$$\rho_s = \frac{m^* \langle X^2 \rangle L^2}{\hbar^2 \beta N} \tag{6.34}$$

here m^* is effective mass of particle. Such situation is expected. Disorder, as we discussed earlier, causes uncorrelated local condensate or superfluid puddle which effectively impact compressiblity and superfluid fraction in the whole sample. Lack of correlation reduces entropy as expected.

But saying something simply as 'Disorder reduces thermal equilibrium value of observable of a system' is understatement. Effect of disorder is not just simply reducing observable expectation value but something much more exotic. Due to presence of defect or disorder, direct MI-SF transition has transformed to a new type of transformation, BG-SF transition with a new universality class. This sort of of transition is predicted to occur in percolation cluster. BG phase has two different characteristics; one with high compressibility (for incommensurate filling) and another with low compressibility. And there exist a crossover from low κ BG to high κ BG for small change in disorder strength [173]. Disorder can stabilize the SF phase at higher densities, whereas at low densities the disorder stabilizes BG state.
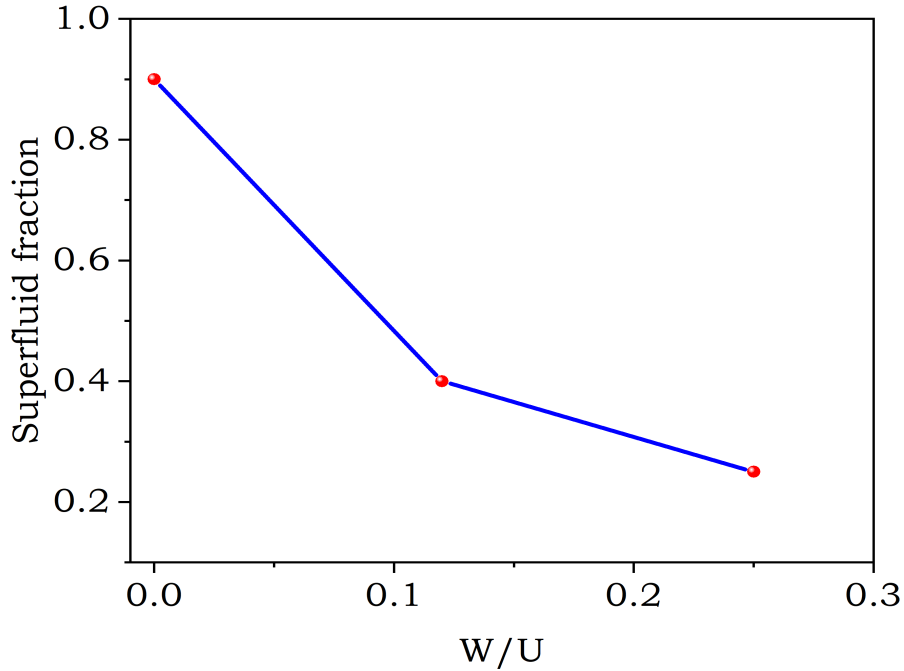
Figure 6.9: Evolution of Superfluid fraction for a system with different disorder strength.

6.3 Summary

In this chapter, we look at the effect of disorder from thermodynamics perspective. Polariton condensate can be considered as isolated quantum system due to lack of coupling with outside environment. Such system tends to follow ETH, system acts as a bath for thermalization of subsystem of its own. Presence of disorder induces localization which invalidate the use of ETH for the system. So, in exact sense, whole system cannot thermalize in the event of dislocation. Here, thermalization occurs on local level with each zone is defined by its own temperature. Disorder form several superfluid puddle across the sample which cannot form a macro condensate by establishing ODLRO. These small local areas with condensate thermalize itself without interacting with other local condensate. This result in the lowering of effective polariton temperature for a defective polariton LASER. In this chapter, we tackle the problem from two different approach and analyze the impact of defect.

Chapter 7

Performance Analysis of Defected Bosonic System

A system is tried to design as perfectly as possible for best performance. But inevitably, some form of non-ideal condition due to limitation of available technology. These sort of ideal condition can alternate expected performance of a system greatly, even can make the whole system obsolete. Presence of different types of defect (point defect, dislocation, vacancy, interstitial defect etc.) is one of the many types of imperfections that can present in a system. Sometimes, presence of such non-ideal cases can give us some different result which is not possible in an ideal system. Imperfection breeds new result and new understanding. But imperfections are complicated to study from theoretical viewpoint. So often, detailed experiment is needed to get an idea of such remarkable result. Then theoretical analysis can be performed based on those result. Such theoretical analysis along with numerical calculations have been done in chapter 05 and 06. In this chapter we will show the impact of defect of some practical applications based on our theoretical analysis done so far. This will shed some light on practical impact of defect.

7.1 Impact of Defect on Small Signal Characteristics of Exciton-Polariton LASER

We have already discussed impact of defect on polariton LASING in chapter 05. In this section we will analyze small signal performance of polariton LASER. Experimental basis of such work can be found in [87]. Here,

7.1.1 Simplified Rate Equation

We will not use detailed equation set 5.19 rather a simplified version introduced by Tassone et.al. [94] and Iorsh [169]. Considering defect equations for electrical pumping scheme are modified as,

$$\frac{dn_{eh}}{dt} = \frac{JS}{q} - \frac{n_{eh}}{\tau_{eh}} - Wn_{eh} \qquad (7.1)$$

$$\frac{dn_x}{dt} = -\frac{n_x}{\tau_x} - \frac{n_x}{\tau_{dx}} + Wn_{eh} - an_x(1+n_p) + ae^{-\frac{\Delta_{sc}}{k_B T}} n_x n_p - bn_x^2(1+n_p) - cn_x n_{eh}(1+n_p) \qquad (7.2)$$

$$\frac{dn_p}{dt} = -\frac{n_p}{\tau_p} - \frac{n_p}{\tau_{dp}} + an_x(1+n_p) - ae^{-\frac{\Delta_{sc}}{k_B T}} n_x n_p + bn_x^2(1+n_p) + cn_x n_{eh}(1+n_p) \qquad (7.3)$$

Here, n_{eh}, n_x, n_p are the concentration of electron hole plasma, exciton and excitons-polaritons respectively, J is current density, S is effective surface area, $\tau_{eh}, \tau_x, \tau_p$ are decay rate of electron-hole plasma, exciton lifetime and exciton-polariton lifetime respectively, W is exciton generation rate, a, b, c are exciton-acoustic phonon scattering rate, exciton-exciton scattering rate and exciton electron-hole plasma scattering rate respectively. The detail regarding equations 7.1-7.3 can be found in Irosh et.al [169]. Our modification here is the introduction of $\frac{n_x}{\tau_{dx}}$ and $\frac{n_p}{\tau_{dp}}$ as same as equation set 5.19. Here τ_{dx} is inverse of exciton capture rate at high momentum excitonic state where τ_{dp} is inverse of exciton capture rate at $k = 0$.

7.1.2 LI Characteristics

Before delving into detail of small signal analysis, we analyze the effect of defect on lasing threshold.

Introduction of defect causes LASING threshold to increase as from Fig. 7.1. This result is consistent with other device especially with normal semiconductor device. In order achieve accepted performance, most of such imperfect device requires more energy. Here is also the same case. From numerical calculation, we find that with no defect ($\tau_{dx} = \tau_{dp} = \infty$), polariton LASER shows a threshold of $200A/cm^2$ but with defect this
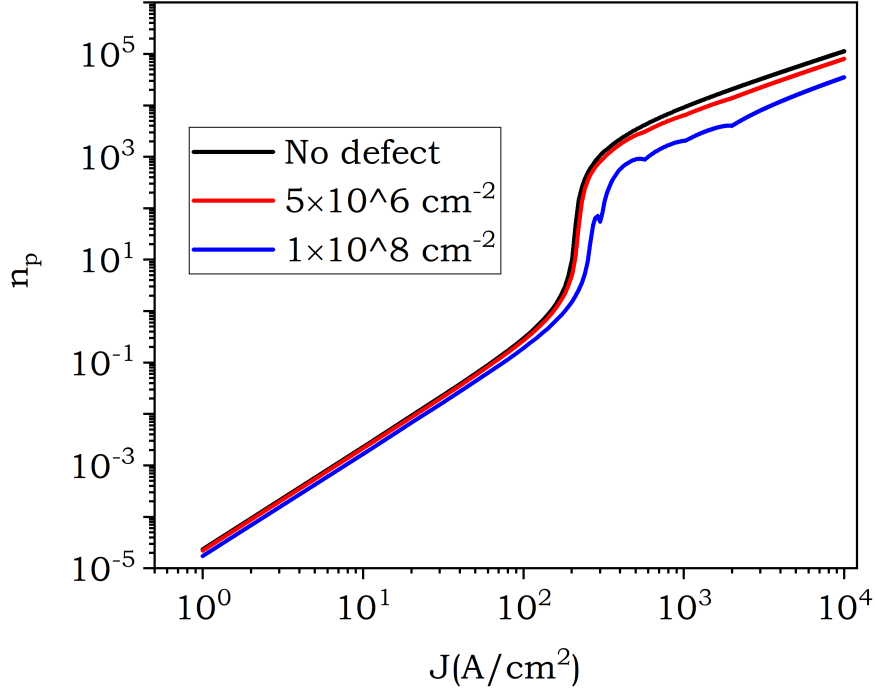
Figure 7.1: LI characteristics of polariton LASER with and without defect.

threshold increases to $250 A/cm^2$ for defect density of $5 \times 10^6 cm^{-2}$ and to $350 A/cm^2$ for defect density of $5 \times 10^6 cm^{-2}$.

7.1.3 Small Signal Analysis of Polariton LASER

Now we will analyze small signal characteristics based on equation 7.1-7.3. One of the main reason to use simplified rate equation (equation 7.1-7.3) rather than equation set 5.19 is that simplified rate equation can be further simplified and approximated to give us some analytical expression of small signal characteristics. For small signal analysis equation 7.2 and 7.3 can be written as [169],

$$\frac{d}{dt}\begin{bmatrix} dn_x \\ dn_p \end{bmatrix} = \begin{bmatrix} P_1 & P_2 \\ P_3 & P_4 \end{bmatrix}\begin{bmatrix} dn_x \\ dn_p \end{bmatrix} + \begin{bmatrix} dn_p(W - cn_{x\infty}n_{p\infty}) \\ dn_p cn_{x\infty}n_{p\infty}) \end{bmatrix} \quad (7.4)$$

where,

$$P_1 = -\frac{1}{\tau_{dx}} - \frac{1}{\tau_x} + an_{p\infty} + 2bn_{x\infty}n_{p\infty} + cn_{eh\infty}n_{p\infty} - an_{p\infty}e^{-\frac{\delta_{esc}}{k_B T}} \quad (7.5)$$

155

$$P_2 = an_{p\infty} + 2bn_{x\infty} + cn_{eh\infty}n_{p\infty} - an_{p\infty}e^{-\frac{\delta_{esc}}{k_BT}} \tag{7.6}$$

$$P_3 = -an_{x\infty} - bn_{x\infty}^2 - cn_{eh\infty}n_{x\infty} + an_{p\infty}e^{-\frac{\delta_{esc}}{k_BT}} \tag{7.7}$$

$$P_4 = -\frac{1}{\tau_{dp}} - \frac{1}{\tau_p} + an_{x\infty} + bn_{x\infty}^2 + cn_{eh\infty}n_{x\infty} - an_{p\infty}e^{-\frac{\delta_{esc}}{k_BT}} \tag{7.8}$$

For calculation of defect free case, a simple consideration of $\tau_{dx} = \tau_{dp} = \infty$ will give us the result. Laplace transform of equation 7.4 gives us the following expression for $n_x(s)$ and $n_p(s)$.

$$n_x(s) = \frac{n_{eh\infty}(cn_{x\infty}n_{p\infty} - W)(-P_4 + W)}{(-P_1 + s)(-P_4 + s) - P_2P_3} \tag{7.9}$$

$$n_p(s) = \frac{n_{eh\infty}(W - cn_{x\infty}n_{p\infty}) + (-P_1 + s)cn_{x\infty}n_{p\infty}}{-P_2P_3 + s^2 - s(P_1 + P_4) + P_1P_4} \tag{7.10}$$

These equation (equation 7.9 and 7.10) along with equations 7.5-7.8 will be used for small signal analysis for both defective and defect free case.

7.1.3.1 Defect Free Polariton LASER

Before going into detail of system with defect, we first analyze the system without defect. Numerical calculation of equation 7.1-7.3 gives us the following results (Fig. 7.2) for four different current densities ($266A/cm^2$, $304A/cm^2$, $570A/cm^2$ and $1026A/cm^2$). With more current densities frequency response shift to higher frequency.

Resonance frequency of such can be determine analytically. Under steady state condition, ($\frac{dn_x}{dt} = \frac{dn_p}{dt} = \frac{d_{eh}}{dt} = 0$), we can safely approximate,

$$\frac{1}{\tau_p} \approx bn_{x\infty}^2 \tag{7.11}$$

which gives us expression of P_2 and P_3 as,

$$P_2 = -bn_{x\infty}^2 \ , \ P_3 = 2bn_{x\infty}n_{p\infty} \tag{7.12}$$

Using these expression, from equation 7.10 we can determine resonance frequency of
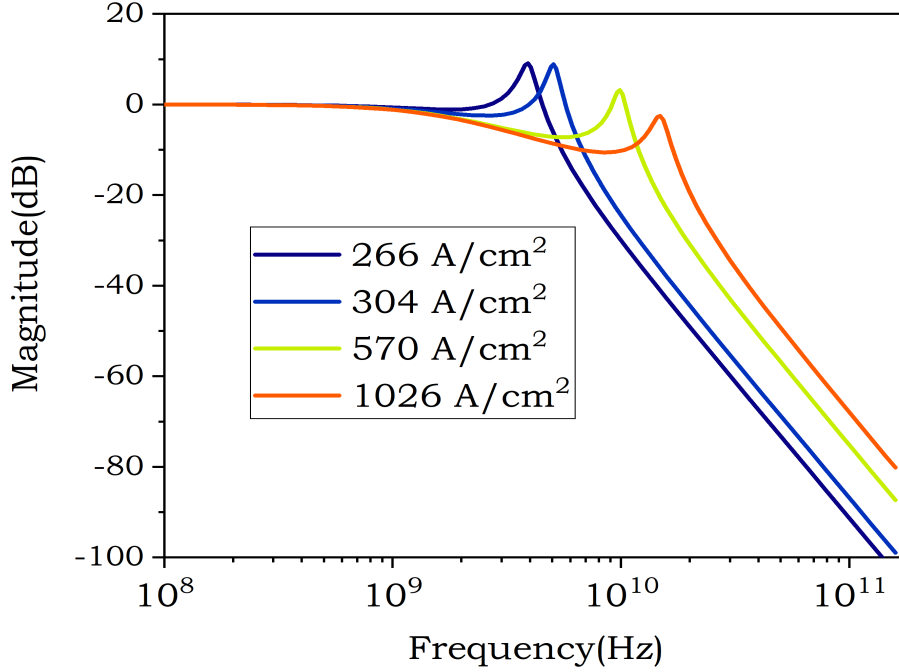
Figure 7.2: Frequency response (magnitude plot) of polariton LASER without any defect for four different current densities, $266A/cm^2$, $304A/cm^2$, $570A/cm^2$ and $1026A/cm^2$.

polariton LASER is,

$$\omega_r = \sqrt{2\frac{bn_{x\infty}n_{p\infty}}{\tau_p}} \tag{7.13}$$

This is the same expression derived by Iorsh et. al [169]. Defect free polariton LASER resonance frequency can be approximated by this equation.

7.1.3.2 Polariton LASER with Defect

Same equation 7.1-7.3 will be used here but with $\tau_{dx} = \tau_{dp} \neq \infty$. Values that has been found for τ_{dx} and τ_{dp} for different current densities are shown in table 7.1. As can be seen with increase in current density, capture rate for both high momentum exciton and low momentum exciton has increased.

In Fig. 7.3, frequency response for polariton LASER with defect is shown for same four different densities as defect free case. One thing is obvious here is the absence of resonant frequency. We can find an analytical answer to this sort of result. Using the same approximation of equation 7.11, we can find an analytical expression for resonant frequency as,

Table 7.1: Effective capture time for high and low momentum exciton.

Current density (A/cm^2)	τ_{dx} (ns)	τ_{dx} (ps)
266	5.5	4.8
304	3	3.5
570	1	0.81
1026	0.33	0.75
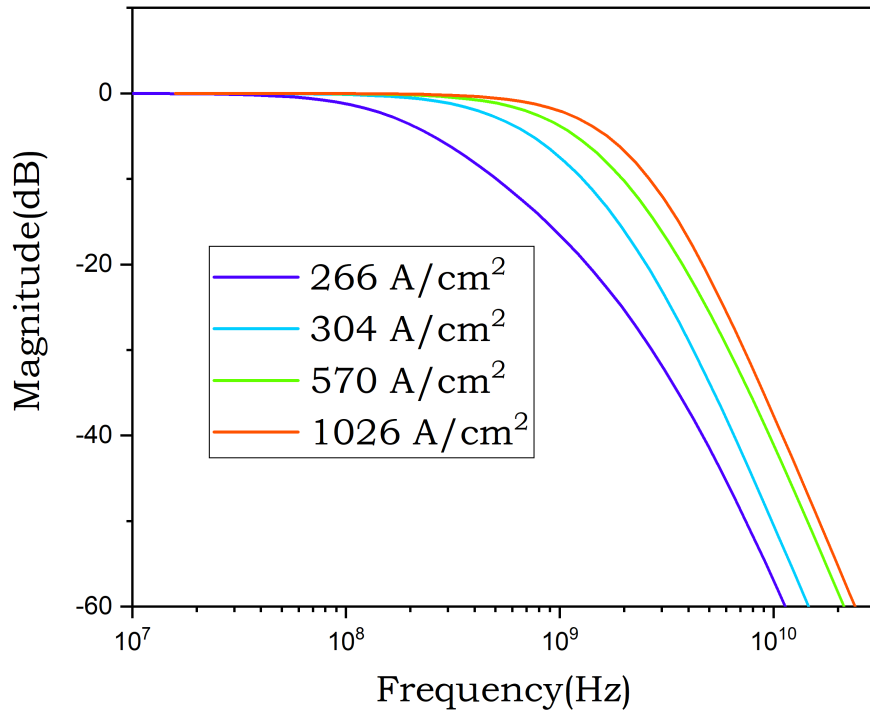
Figure 7.3: Frequency response (magnitude plot) of polariton LASER with defect $(n_d = 1 \times 10^8 cm^{-2})$ for four different current densities, $266 A/cm^2$, $304 A/cm^2$, $570 A/cm^2$ and $1026 A/cm^2$.

$$\omega_r = \sqrt{2\frac{bn_{x\infty}n_{p\infty}}{\tau_p} - \frac{R^2 + 4Rbn_{x\infty}n_{p\infty}}{4}} \qquad (7.14)$$

where $R = \frac{1}{\tau_{dx}} + \frac{1}{\tau_{dp}}$. If $R >> bn_{x\infty}n_{p\infty}$, we can simplify equation 7.14 as,

$$\omega_r = \sqrt{2\frac{bn_{x\infty}n_{p\infty}}{\tau_p} - \frac{R^2}{4}} \qquad (7.15)$$

If $R^2 < 8\frac{bn_{x\infty}n_{p\infty}}{\tau_p}$ system is under-damped and system will show a resonance frequency. But when $R^2 > 8\frac{bn_{x\infty}n_{p\infty}}{\tau_p}$ condition is not fulfilled, system is over-damped (with both of system poles are in left plane and real) and system will not show any resonant frequency.
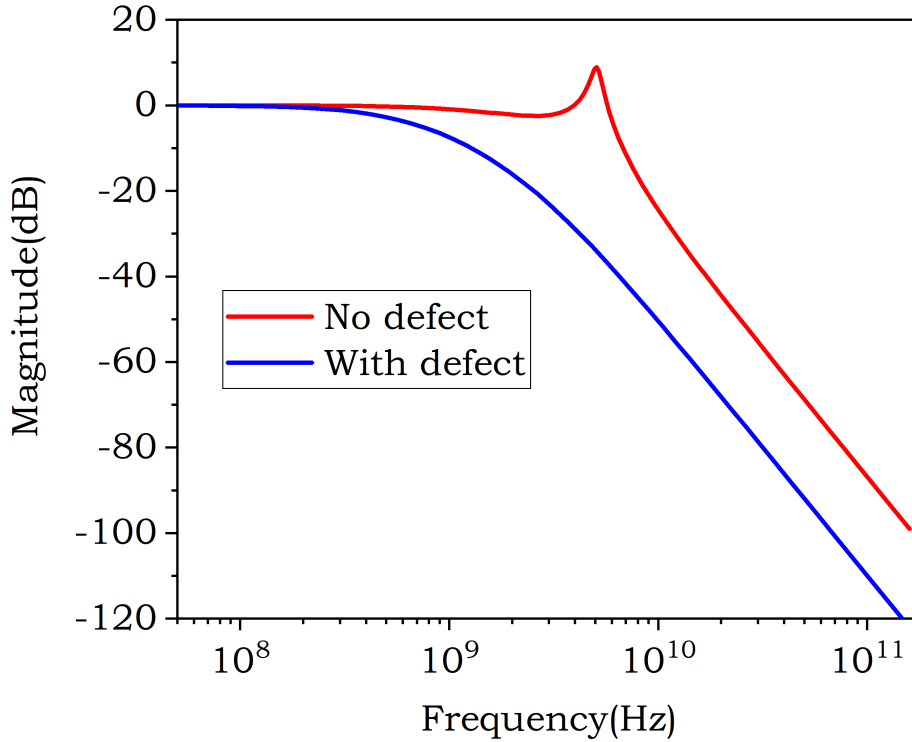
Figure 7.4: Frequency response (magnitude plot) of polariton LASER without and with defect ($n_d = 1 \times 10^8 cm^{-2}$) for current density of $304A/cm^2$.

In Fig. 7.4 and 7.5, we are showing exclusively this effect of under-damped to over-damped transition due to introduction of defect for four different current densities. Presence of defect does not confirm such transformation but condition $R^2 > 8\frac{bn_{x\infty}n_{p\infty}}{\tau_p}$ has to be fulfilled which can be fulfilled using other sort of damping mechanisms. If R is very low, one can find the system in under-damped condition, with a real value of resonant frequency. In our case of defect density of $1 \times 10^8 cm^{-2}$, system has reached over-damped
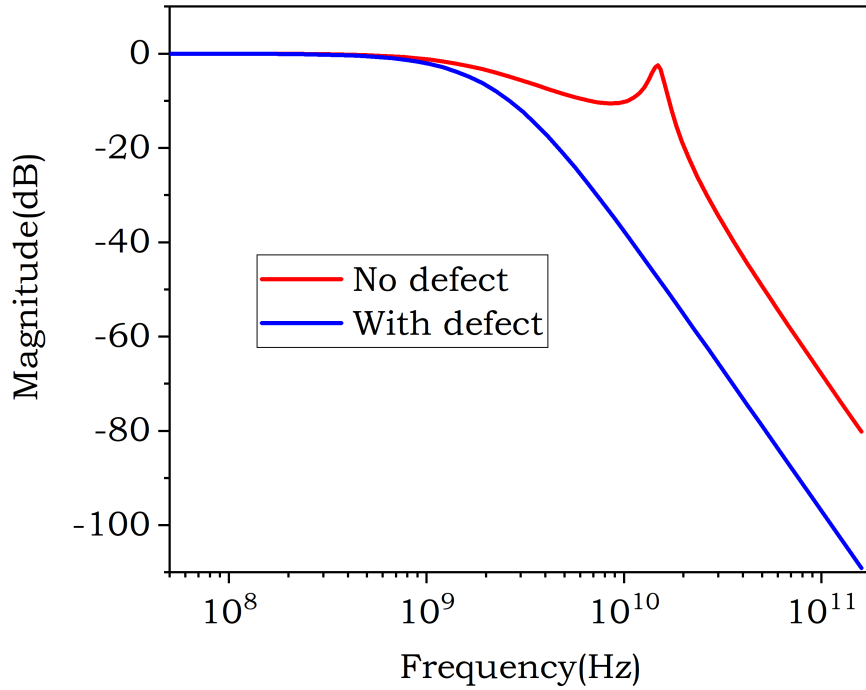
Figure 7.5: Frequency response (magnitude plot) of polariton LASER without and with defect ($n_d = 1 \times 10^8 cm^{-2}$) for current density of $1026 A/cm^2$

region.

From such numerical results, one thing is clear presence of defect effect frequency response by changing the nature of the system (from under damping to over damping) and reduce its -3 dB frequency. A close look at Fig. 7.4, 7.5 reveals that at every current density, we locate such decrement of -3 dB frequency decrement. This can severely hamper the performance of high frequency device such as Laser Diode.

7.1.3.3 Comparison between Numerical and Experimental Result

Frequency response characteristics for such defected case has been done in [87].
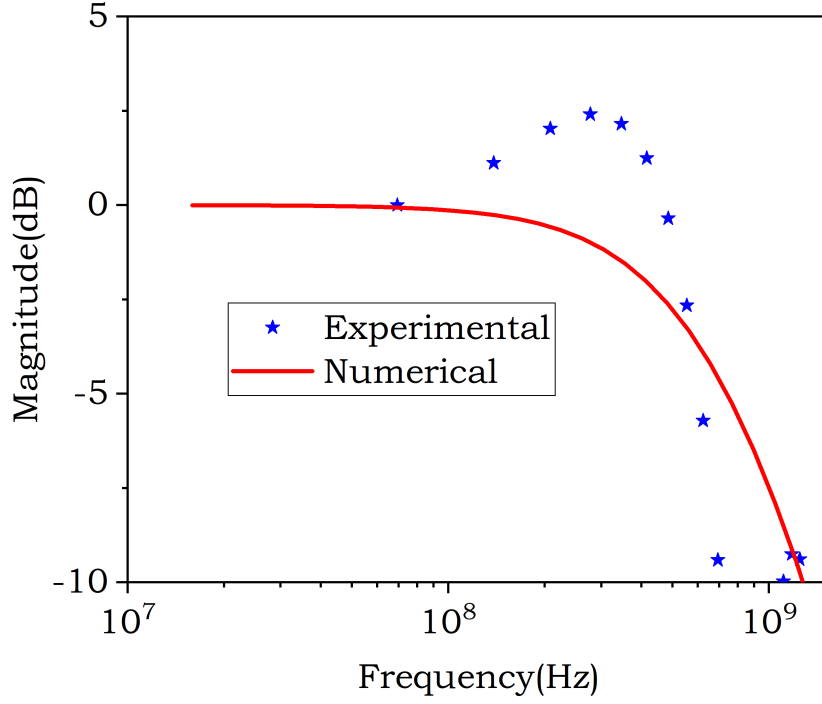
Figure 7.6: Comparison of numerically calculated frequency response (magnitude) of polariton LASER with defect with experimental value [87] for current density $304A/cm^2$

In Fig. 7.6 and 7.7 we are comparing result found by numerical calculation and by direct experiment [87]. Comparison has been done for two different current density $304A/cm^2$ and $1026A/cm^2$. One significant discrepancy between experimental result and numerical result is that the presence of damped resonant frequency in experimental data but numerical result shows nothing such. Our numerical results show that system is completely in over-damped region. But other than that, we can say that other properties like $-3\ dB$ frequency has matched quite well with experimental result especially in higher current densities. Some detail analysis considering influence of defect on scattering rate should be considered to answer the existing mismatch between numerical and experimental results.

One prime reason behind such discrepancy is RC effect that was taken out externally during experiments. During numerical calculations, no such RC is considered which might indicate an inherent damping presence in such system which might be over-estimated during calculating experimental results. Further investigations into with numerical and
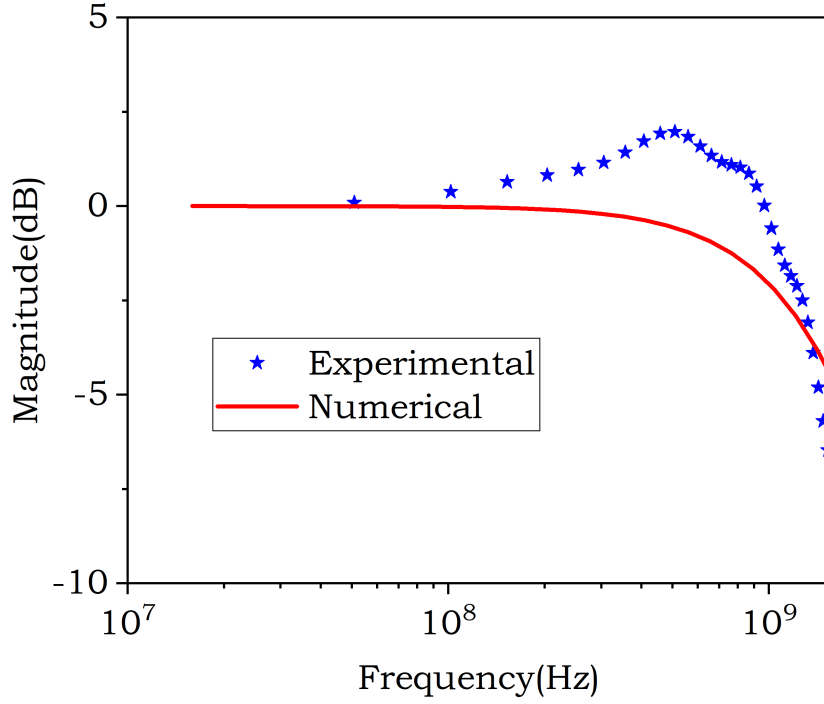
Figure 7.7: Comparison of numerically calculated frequency response (magnitude) of polariton LASER with defect with experimental value [87] for current density$1026A/cm^2$.

experimental calculations might solve such discrepancies.

7.2 Impact of Defect on Quantum Information Processing

We will not present any experimental result on such case and our discussion here is very limited. Nevertheless, theoretical analysis opened the Pandora's box for us to explore for new exotic behavior. In the field of quantum computation, a quantum gate can be realized in many ways [174–176]. One of the realization of sSWAP gate is by utilizing multiple polariton condensate in close vicinity to be coupled effectively with each other [177]. Due to such coupling, such system is best described by Lindblad master equation as,

$$i\hbar\frac{d\hat{\rho}}{dt} = [H(t), \rho(\hat{t})] - i\frac{\gamma}{2}\sum_{i=1,2}\mathcal{L}^{\rangle}(\rho(\hat{\sqcup}))$$ (7.16)

where, $\mathcal{L}\rho(\hat{\sqcup})$ is defined as,

$$\mathcal{L}^{\rangle} = 2c_n\rho(t)c_n^\dagger - \rho(t)c_n^\dagger c_n - c\dagger_n c_n\rho(t) \tag{7.17}$$
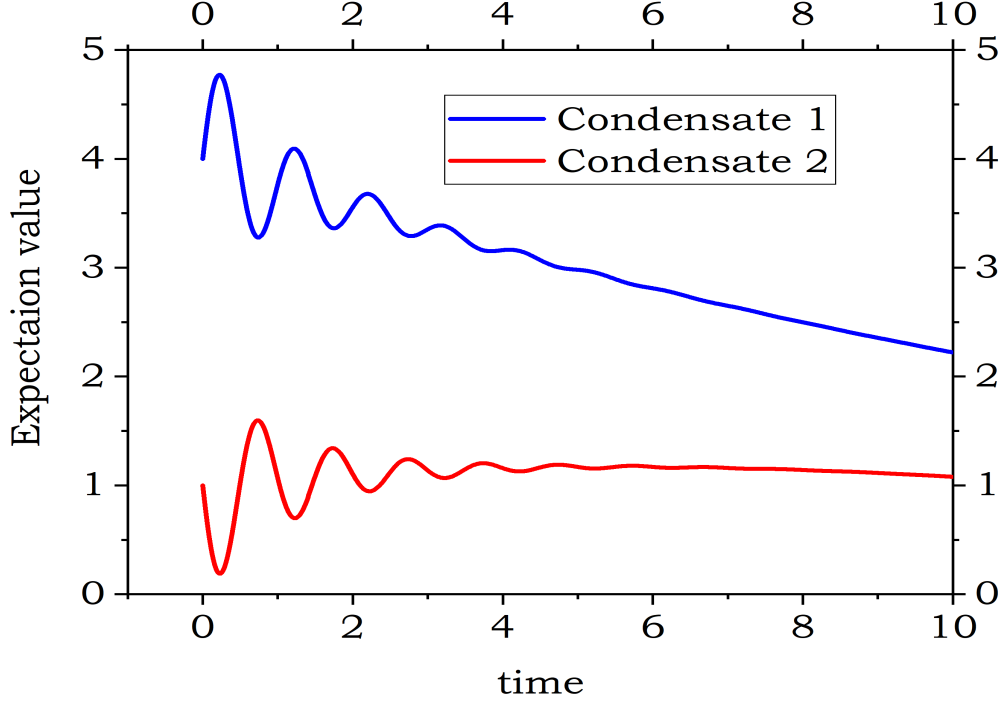
Figure 7.8: Expectation value for number operator for two different coupled condensate with one condensate start with 4 particles and other with 1 particle. Both condensate can exchange particle between them.

$H(t)$ from equation 7.16 is defined as summation of two condensate hamiltonian and of interaction hamiltonian between them,

$$H = H_1 + H_2 + H_{int} \tag{7.18}$$

Expectation value for number operator for two different condensate with different initial condition with coupling between them is shown in Fig. 7.8. Due to exchange of particle and energy between them, condensate 1 population is decreasing at the expense of increased population of condensate 2.

Presence of defect can significantly alter this picture. As we have already discussed in previous chapters of results, defect effectively reduce condensate fraction available to probe. This causes an decrease in condensate population without exchange to another condensate. Additionally, presence of defect can significantly impact interaction hamiltonian, H_{int} between two condensate. This might result in reduced fidelity for such

types of gate. As a result, more pumping might be required for the system to work as expected limit. We are not presenting any results here, rather predict the performance of defective quantum gate based on the analysis so far.

7.3 Summary

Presence of defect can significantly alter the performance of a system, as has been found both theoretically and experimentally. In this chapter, we shed light on practical system based on the theoretical analysis in the previous two chapters and try to explain some experimental behavior of the system along with some prediction. Main focus of this chapter is the explain the high frequency behavior of defective polariton that was reported earlier. Presence of defect change frequency characteristics of polariton LASER diode. Based on simplified rate equation, we explain such change to an acceptable limit. Addition of defect to polariton LASER cause its threshold current to increase which was also explained. Finally, in-short we predict the possible effect of defect on disordered quantum gate.

Chapter 8

Conclusion

Understanding an experimental event using theoretical framework is undoubtedly a daunting task. Despite such trouble, a theoretical understanding of an experiment is extremely important both in field of philosophy and engineering. Sometimes, a theory can say something simple like some old theory but with new perspective. Fermat's theorem of least action and Snell's law both gives us the law of refraction but philosophically Fermat's law is more celebrated than Snell's law as Fermat's law let us understand the behavior of light along with natural event more abstractly by simply stating 'Event will occur in a way which requires least action'. Snell's law may give us some solid usable equation in our practical field but Fermat's law gives us rather a broad picture. This is one of the primary reason, sometimes old theory is needed to be revisited and looked upon with an abstract mind.

Understanding a theory using experiment is straightforward. Theory will be proven on the field of experiment. A theory has to prove its competence with passage of time by various experiment. When an anomaly is detected in experiment, theory need to be revised or modified. Most physical that we had is constructed using simplistic assumption of nature. As already discussed in the introductory part of Chapter 04, despite knowing almost all the properties of constituent particles like electron, proton, neutron we cannot explain behavior of sold using properties of these particles. Introduction of interaction among particle raises complexity which cannot solved easily. As a result of this interaction and other phenomenon, system of interest gets increasingly complex. Analysis of defect is one such complex system. Analysis of system with defect is not possible due inherent nature of defect which is random. Due to progress in probability theory of randomness,

it is somewhat possible to come to some sort of conclusion in this regard.

8.1 Summary of the Work

Presence of defect can affect a system is various way. Main purpose of this dissertation is to analyze the influence of defect on polariton LASING. Experiments show some somewhat peculiar result due to defect for polariton LASER diode. Two main findings were change of frequency response characteristics and lowering of effective polariton temperature. To explain such event, we perform an in depth analysis to understand why defects are causing this?

We started our analysis by solving open dissipative Gross-Pitaevskii equation coupled with external reservoir. Such analysis reveals that presence of defect causes quantized vortices to be pinned close potential extreme. As a result of such pinning, local condensate cannot form a macroscopic condensate. This small regions with local condensate exist individually over their lifetime. Analysis of open dissipative GP equation reveals the temporal and spatial dynamics of condensate under disorder or defect.

Out next stop was to try out numerical analysis of semiclassical Boltzmann equation. These equations are coupled differential rate equation coupled with each other. A complete numerical analysis of such equation set gives us the detail about occupation number in different momentum state. Occupation plot of polariton LASER with and without defect has been calculated numerically. Fitting such occupation plot with Maxwell distribution (as has been done in the experiment) reveals that, defect decreases effective polariton temperature. It is well established polariton do not thermalize with lattice rather thermalize among themselves, create a quasi thermalized situation with an effective polariton temperature. Without defect such effective polariton temperature always tend to be greater than lattice temperature or environment temperature. But with addition of defect such scenario changes, and effective polariton temperature is getting lowered and can even get lower than lattice temperature. Our numerical analysis found effective polariton temperature as low as $180K$ for GaN based polariton LASER diode. One thing to be mentioned here is that all our analysis has been performed on GaN material basis. This numerical result match quite well with experimental findings.

Result of these two analysis seems to be disjointed. One analysis shows that

defect creates local condensate with longer lifetime. Another analysis reveals that defect causes average occupation to decrease for each momentum state which eventually translate to lowering of effective polariton temperature. How come lack of macro condensate lower effective polariton temperature? To answer this question, analysis from thermodynamics point of view has been done. A heuristic approach with the help of Eigenstate Thermalization Hypothesis (ETH) and Many Body Localization (MBL) reveals that local condensate thermalizes among themselves without interacting with other condensate. Each of these local condensates act as isolated quantum system and act as a bath for their own subsystem to thermalize just like the case for macro condensate. Here, lack of long range coherence prevents thermalization to occur across the whole rather inside a local region. Presence of defect or disorder thus create Griffits phase of singularity. Effective local temperature depends on the size of local condensate and total energy contained inside such region by local eigenstate. These eigenstate thermalizes themselves without any interaction with other local eigenstate of other local condensate. Numerical approach by solving disordered Bose Hubbard model also reveals same picture. Presence of disorder potential localizes state which ultimately prevents thermalization. Several thermodynamic property like Compressibility, Superfluid fraction, Momentum distribution, Von Neumann entanglement entropy is analyzed under the influence of defect and shows that presence of defect alters thermodynamic equilibrium point. Even defect can change phase transition or even prevent if Harris criterion is not fulfilled. By analyzing DBHM, it is found that presence of disorder prevent Mott Insulator - Superfluid transition but allows Bose Glass - Superfluid transition.

Finally, we take a look at other experimental findings of defect induced frequency response characteristics. Using simplified rate equation developed from coupled SB rate equations, we analyze the behavior of absence of resonance frequency and frequency characteristics for high frequency response of polariton LASER diode. By deriving analytical expression of resonant frequency for LASER diode with and without defect it is shown that defect increases damping coefficient and can effectively bring an under-damped system to over-damped region with both poles being real and negative. Lower density of defect in a system exhibit some resonating behavior but with larger defect density resonating frequency becomes imaginary. A comparison between numerical result calculated from simplified rate equations and experimental results are provided for

better understanding of the success these theoretical frameworks. Despite having slight dissimilarities between numerical and experimental result, both these shows remarkable resemblance. Addition to this, we use our understanding from our discussion about the influence of defect to predict the behavior of quantum gate in the presence of defect. As defect or disorder can effectively reduce condensate population, quantum gate designed by employing interaction between two separate polariton condensate can be significantly impacted by defect.

8.2   Scopes of Future Work

Understanding the influence of defect on a pure system can benefit us in designing practical system. Defect can act as both hurdles and an opportunity. Presence of defect reveals the new phase of matter 'Glassy Phase'. Other exotic behavior like this can be utilized to design effective system. We just need to incorporate exotic property of defect into our design philosophy. Some future work that can be done to better understand the influence of defect based on our current work,

- Understanding the dynamics of the system in kinetic, spatial and temporal domain with and without defect is essential to have a better grasp on defect. We have done this using open dissipative Gross-Pitaevskii equation and coupled semiclassical Boltzmann rate equations for GaN. Such analysis with different approach for example using Lindblad quantum Master Equation, Jaynes Cummings model etc. and for other different material and at different temperature will be helpful to get a better grasp.

- Thermodynamic approach definitely can be analyzed further to get a better understanding of defect. A more robust approach other than heuristic approach based on ETH and MBL is essential to give such theoretical foundation a solid foothold. Additionally, DBHM model should be solved for larger system with a lot of variation in parameter of t, U, W and even for different types of defect modeling like, speckle disorder, exponential disorder etc. Some such work has already been done. But most of the work takes very low temperature limit. Behavior of DBHM under room temperature requires a detailed investigation.

- Some of the modifications proposed within the existing theoretical framework cannot exactly match experimental data. For example, calculation of defect capture rate considers influence of defect only as an isolated situation of capturing excitons by defect. No consideration is given on defect influencing scattering rate i.e. polariton-phonon scattering rate or polariton-polariton scattering rate. Considering long range and short range potential of defect into calculating scattering rate should give us better result regarding effective polariton temperature and frequency characteristics of polariton LASER diode.

- Recent advancements in quantum information processing is tremendous. Advancement in fabrication technology gives us almost defect free device. Nevertheless, defect will exist in one form or other. Most of existing quantum gates depends on the purity of device for effective operation. Presence of defect at normal temperature can significantly alter behavior of such device. Analysis the influence of defect is essential in this case for robust design of such quantum gates.

Defect is like a Pandora's Box which can either reveal exotic behavior of matter or present itself as a unbreakable barrier. Understanding the impact of defect will be essential for tacking the problem of defect analysis of system in the future.

Bibliography

[1] S. Nonogaki, U. Takumi, and T. Ito, *Microlithography fundamentals in semiconductor devices and fabrication technology*. CRC Press, 2018.

[2] M. K. Mishra, V. Dubey, P. Mishra, and I. Khan, "Mems technology: A review," *J. Eng. Res. Rep*, vol. 4, no. 1, pp. 1–24, 2019.

[3] D. Neumaier, S. Pindl, and M. C. Lemme, "Integrating graphene into semiconductor fabrication lines," *Nature materials*, vol. 18, no. 6, pp. 525–529, 2019.

[4] W. M. Moreau, *Semiconductor lithography: principles, practices, and materials*. Springer Science & Business Media, 2012.

[5] M. H. Anderson, J. R. Ensher, M. R. Matthews, C. E. Wieman, and E. A. Cornell, "Observation of bose-einstein condensation in a dilute atomic vapor," *science*, vol. 269, no. 5221, pp. 198–201, 1995.

[6] A. Görlitz, J. Vogels, A. Leanhardt, C. Raman, T. Gustavson, J. Abo-Shaeer, A. Chikkatur, S. Gupta, S. Inouye, T. Rosenband *et al.*, "Realization of bose-einstein condensates in lower dimensions," *Physical review letters*, vol. 87, no. 13, p. 130402, 2001.

[7] B. DeMarco and D. S. Jin, "Onset of fermi degeneracy in a trapped atomic gas," *science*, vol. 285, no. 5434, pp. 1703–1706, 1999.

[8] B. DeMarco, S. Papp, and D. Jin, "Pauli blocking of collisions in a quantum degenerate atomic fermi gas," *Physical review letters*, vol. 86, no. 24, p. 5409, 2001.

[9] T. Fukuhara, Y. Takasu, M. Kumakura, and Y. Takahashi, "Degenerate fermi gases of ytterbium," *Physical Review Letters*, vol. 98, no. 3, p. 030401, 2007.

[10] M. Greiner, C. A. Regal, and D. S. Jin, "Probing the excitation spectrum of a fermi gas in the bcs-bec crossover regime," *Physical review letters*, vol. 94, no. 7, p. 070403, 2005.

[11] M. Pasienski, D. McKay, M. White, and B. DeMarco, "A disordered insulator in an optical lattice," *Nature Physics*, vol. 6, no. 9, pp. 677–680, 2010.

[12] J. Gleick, *Chaos: Making a new science*. Penguin, 2008.

[13] S. Boccaletti, C. Grebogi, Y.-C. Lai, H. Mancini, and D. Maza, "The control of chaos: theory and applications," *Physics reports*, vol. 329, no. 3, pp. 103–197, 2000.

[14] C. Weisbuch, M. Nishioka, A. Ishikawa, and Y. Arakawa, "Observation of the coupled exciton-photon mode splitting in a semiconductor quantum microcavity," *Physical Review Letters*, vol. 69, no. 23, p. 3314, 1992.

[15] H. Gibbs, G. Khitrova, and S. Koch, "Exciton–polariton light–semiconductor coupling effects," *Nature Photonics*, vol. 5, no. 5, pp. 273–273, 2011.

[16] H. Deng, D. Press, S. Götzinger, G. S. Solomon, R. Hey, K. H. Ploog, and Y. Yamamoto, "Quantum degenerate exciton-polaritons in thermal equilibrium," *Physical review letters*, vol. 97, no. 14, p. 146402, 2006.

[17] J. Baumberg, A. Kavokin, S. Christopoulos, A. Grundy, R. Butté, G. Christmann, D. Solnyshkov, G. Malpuech, G. B. H. von Högersthal, E. Feltin *et al.*, "Spontaneous polarization buildup in a room-temperature polariton laser," *Physical Review Letters*, vol. 101, no. 13, p. 136409, 2008.

[18] A. Amo, J. Lefrère, S. Pigeon, C. Adrados, C. Ciuti, I. Carusotto, R. Houdré, E. Giacobino, and A. Bramati, "Superfluidity of polaritons in semiconductor microcavities," *Nature Physics*, vol. 5, no. 11, pp. 805–810, 2009.

[19] J. Keeling, P. Eastham, M. Szymanska, and P. Littlewood, "Bcs-bec crossover in a system of microcavity polaritons," *Physical Review B*, vol. 72, no. 11, p. 115320, 2005.

[20] Y. G. Rubo, "Half vortices in exciton polariton condensates," *Physical review letters*, vol. 99, no. 10, p. 106401, 2007.

[21] A. Imamog, R. Ram, S. Pau, Y. Yamamoto *et al.*, "Nonequilibrium condensates and lasers without inversion: Exciton-polariton lasers," *Physical Review A*, vol. 53, no. 6, p. 4250, 1996.

[22] A. Kavokin and G. Malpuech, *Cavity polaritons.* Elsevier, 2003.

[23] H. Deng, H. Haug, and Y. Yamamoto, "Exciton-polariton bose-einstein condensation," *Reviews of modern physics*, vol. 82, no. 2, p. 1489, 2010.

[24] R. L. Fork, L. A. Burgess, M. L. Davenport, D. M. Ramey, P. J. Reardon, D. B. Pollock, R. G. Lindquist, and D. M. Fork, "Cohering of multiple polariton lasers for sensing applications," in *Laser Source Technology for Defense and Security IV*, vol. 6952. SPIE, 2008, pp. 131–139.

[25] T. Liew, A. Kavokin, T. Ostatnickỳ, M. Kaliteevski, I. Shelykh, and R. Abram, "Exciton-polariton integrated circuits," *Physical review B*, vol. 82, no. 3, p. 033302, 2010.

[26] A. Amo, T. Liew, C. Adrados, R. Houdré, E. Giacobino, A. Kavokin, and A. Bramati, "Exciton–polariton spin switches," *Nature Photonics*, vol. 4, no. 6, pp. 361–366, 2010.

[27] T. Liew, I. Shelykh, and G. Malpuech, "Polaritonic devices," *Physica E: Low-dimensional Systems and Nanostructures*, vol. 43, no. 9, pp. 1543–1568, 2011.

[28] D. Ballarini, M. De Giorgi, E. Cancellieri, R. Houdré, E. Giacobino, R. Cingolani, A. Bramati, G. Gigli, and D. Sanvitto, "All-optical polariton transistor," *Nature communications*, vol. 4, no. 1, pp. 1–8, 2013.

[29] T. Byrnes, N. Y. Kim, and Y. Yamamoto, "Exciton–polariton condensates," *Nature Physics*, vol. 10, no. 11, pp. 803–813, 2014.

[30] A. Rockett, *The materials science of semiconductors*. Springer Science & Business Media, 2007.

[31] J. Liqiang, Q. Yichun, W. Baiqi, L. Shudan, J. Baojiang, Y. Libin, F. Wei, F. Honggang, and S. Jiazhong, "Review of photoluminescence performance of nano-sized semiconductor materials and its relationships with photocatalytic activity," *Solar Energy Materials and Solar Cells*, vol. 90, no. 12, pp. 1773–1787, 2006.

[32] J. T. Macher and D. C. Mowery, "Measuring dynamic capabilities: practices and performance in semiconductor manufacturing," *British Journal of Management*, vol. 20, pp. S41–S62, 2009.

[33] M. Z. Baten, A. Bhattacharya, T. Frost, I. Iorsh, A. Kavokin, and P. Bhattacharya, "The role of defects in lowering the effective polariton temperature in electric and optically pumped polariton lasers," *Applied Physics Letters*, vol. 108, no. 4, p. 041102, 2016.

[34] S. Chichibu, A. Uedono, A. Tsukazaki, T. Onuma, M. Zamfirescu, A. Ohtomo, A. Kavokin, G. Cantwell, C. Litton, T. Sota *et al.*, "Exciton–polariton spectra and limiting factors for the room-temperature photoluminescence efficiency in zno," *Semiconductor science and technology*, vol. 20, no. 4, p. S67, 2005.

[35] Y. Wang, R. Wang, G. Li, and S. Xu, "Impurity scattering induced excitonic polariton damping and its influence on the reflectance spectra of gan epilayers," *Journal of Applied Physics*, vol. 106, no. 1, p. 013514, 2009.

[36] S. N. Bose, "Wärmegleichgewicht im strahlungsfeld bei anwesenheit von materie," *Zeitschrift für Physik*, vol. 27, no. 1, pp. 384–393, 1924.

[37] E. Schödinger, "Quantisierung als eigenwertproblem.(erste mitteilung)," *Annalen der Physik*, vol. 79, pp. 361–376, 1926.

[38] A. Einstein, "Quantentheorie des einatomigen idealen gases. zweite abhandlung," *Albert Einstein: Akademie-Vorträge: Sitzungsberichte der Preußischen Akademie der Wissenschaften 1914–1932*, pp. 245–257, 2005.

[39] M. W. Zwierlein, C. A. Stan, C. H. Schunck, S. M. Raupach, S. Gupta, Z. Hadzibabic, and W. Ketterle, "Observation of bose-einstein condensation of molecules," *Physical review letters*, vol. 91, no. 25, p. 250401, 2003.

[40] A. L. Fetter, "Rotating trapped bose-einstein condensates," *Reviews of Modern Physics*, vol. 81, no. 2, p. 647, 2009.

[41] O. Morsch and M. Oberthaler, "Dynamics of bose-einstein condensates in optical lattices," *Reviews of modern physics*, vol. 78, no. 1, p. 179, 2006.

[42] J. Kasprzak, M. Richard, S. Kundermann, A. Baas, P. Jeambrun, J. M. J. Keeling, F. Marchetti, M. Szymańska, R. André, J. Staehli *et al.*, "Bose–einstein condensation of exciton polaritons," *Nature*, vol. 443, no. 7110, pp. 409–414, 2006.

[43] J. Frenkel, "On the transformation of light into heat in solids. i," *Physical Review*, vol. 37, no. 1, p. 17, 1931.

[44] G. H. Wannier, "The structure of electronic excitation levels in insulating crystals," *Physical Review*, vol. 52, no. 3, p. 191, 1937.

[45] P. Reineker, *Exciton dynamics in molecular crystals and aggregates*. Springer, 1982, vol. 94.

[46] A. S. Davydov, "The theory of molecular excitons," *Soviet Physics Uspekhi*, vol. 7, no. 2, p. 145, 1964.

[47] K. Song and R. T. Williams, *Self-trapped excitons*. Springer Science & Business Media, 2013.

[48] M. Ueta, H. Kanzaki, K. Kobayashi, Y. Toyozawa, and E. Hanamura, *Excitonic processes in solids*. Springer Science & Business Media, 2012, vol. 60.

[49] D. W. Brown and Z. Ivić, "Unification of polaron and soliton theories of exciton transport," *Physical Review B*, vol. 40, no. 14, p. 9876, 1989.

[50] S. Pekar, "Theory of electromagnetic waves in a crystal in which excitons arise," *Zh. Eksp. Teor. Fiz*, vol. 33, p. 1022, 1957.

[51] J. Hopfield, "Theory of the contribution of excitons to the complex dielectric constant of crystals," *Physical Review*, vol. 112, no. 5, p. 1555, 1958.

[52] D. Fröhlich, E. Mohler, and P. Wiesner, "Observation of exciton polariton dispersion in cucl," *Physical Review Letters*, vol. 26, no. 10, p. 554, 1971.

[53] C. Weisbuch and R. G. Ulbrich, "Resonant polariton fluorescence in gallium arsenide," *Physical Review Letters*, vol. 39, no. 10, p. 654, 1977.

[54] B. Hönerlage, R. Levy, J. B. Grun, C. Klingshirn, and K. Bohnert, "The dispersion of excitons, polaritons and biexcitons in direct-gap semiconductors," *Physics Reports*, vol. 124, no. 3, pp. 161–253, 1985.

[55] R. B. Balili, "Bose-einstein condensation of microcavity polaritons," Ph.D. dissertation, University of Pittsburgh, 2009.

[56] R. Houdré, C. Weisbuch, R. Stanley, U. Oesterle, P. Pellandini, and M. Ilegems, "Measurement of cavity-polariton dispersion curve from angle-resolved photoluminescence experiments," *Physical Review Letters*, vol. 73, no. 15, p. 2043, 1994.

[57] R. Houdré, R. Stanley, U. Oesterle, M. Ilegems, and C. Weisbuch, "Room-temperature cavity polaritons in a semiconductor microcavity," *Physical Review B*, vol. 49, no. 23, p. 16761, 1994.

[58] R. Stanley, R. Houdré, C. Weisbuch, U. Oesterle, and M. Ilegems, "Cavity-polariton photoluminescence in semiconductor microcavities: Experimental evidence," *Physical review B*, vol. 53, no. 16, p. 10995, 1996.

[59] S. Pau, H. Cao, J. Jacobson, G. Björk, Y. Yamamoto, and A. Imamoğlu, "Observation of a laserlike transition in a microcavity exciton polariton system," *Physical Review A*, vol. 54, no. 3, p. R1789, 1996.

[60] L. S. Dang, D. Heger, R. André, F. Boeuf, and R. Romestain, "Stimulation of polariton photoluminescence in semiconductor microcavity," *Physical Review Letters*, vol. 81, no. 18, p. 3920, 1998.

[61] R. Balili, V. Hartwell, D. Snoke, L. Pfeiffer, and K. West, "Bose-einstein condensation of microcavity polaritons in a trap," *Science*, vol. 316, no. 5827, pp. 1007–1010, 2007.

[62] A. Das, P. Bhattacharya, J. Heo, A. Banerjee, and W. Guo, "Polariton bose–einstein condensate at room temperature in an al (ga) n nanowire–dielectric microcavity with a spatial potential trap," *Proceedings of the National Academy of Sciences*, vol. 110, no. 8, pp. 2735–2740, 2013.

[63] R. Huang, Y. Yamamoto, R. André, J. Bleuse, M. Muller, and H. Ulmer-Tuffigo, "Exciton-polariton lasing and amplification based on exciton-exciton scattering in cdte microcavity quantum wells," *Physical Review B*, vol. 65, no. 16, p. 165314, 2002.

[64] H. Deng, G. Weihs, D. Snoke, J. Bloch, and Y. Yamamoto, "Polariton lasing vs. photon lasing in a semiconductor microcavity," *Proceedings of the National Academy of Sciences*, vol. 100, no. 26, pp. 15 318–15 323, 2003.

[65] P. G. Lagoudakis, M. Martin, J. J. Baumberg, G. Malpuech, and A. Kavokin, "Coexistence of low threshold lasing and strong coupling in microcavities," *Journal of Applied Physics*, vol. 95, no. 5, pp. 2487–2489, 2004.

[66] M. Richard, J. Kasprzak, R. Romestain, R. André, and L. S. Dang, "Spontaneous coherent phase transition of polaritons in cdte microcavities," *Physical review letters*, vol. 94, no. 18, p. 187401, 2005.

[67] S. Christopoulos, G. B. H. Von Högersthal, A. Grundy, P. Lagoudakis, A. Kavokin, J. Baumberg, G. Christmann, R. Butté, E. Feltin, J.-F. Carlin *et al.*, "Room-temperature polariton lasing in semiconductor microcavities," *Physical review letters*, vol. 98, no. 12, p. 126405, 2007.

[68] A. Love, D. Krizhanovskii, D. Whittaker, R. Bouchekioua, D. Sanvitto, S. Al Rizeiqi, R. Bradley, M. Skolnick, P. Eastham, R. André *et al.*, "Intrinsic decoherence mechanisms in the microcavity polariton condensate," *Physical Review Letters*, vol. 101, no. 6, p. 067404, 2008.

[69] J. Heo, S. Jahangir, B. Xiao, and P. Bhattacharya, "Room-temperature polariton lasing from gan nanowire array clad by dielectric microcavity," *Nano letters*, vol. 13, no. 6, pp. 2376–2380, 2013.

[70] F. Li, L. Orosz, O. Kamoun, S. Bouchoule, C. Brimont, P. Disseix, T. Guillet, X. Lafosse, M. Leroux, J. Leymarie *et al.*, "Fabrication and characterization of a room-temperature zno polariton laser," *Applied Physics Letters*, vol. 102, no. 19, p. 191118, 2013.

[71] K. Daskalakis, P. Eldridge, G. Christmann, E. Trichas, R. Murray, E. Iliopoulos, E. Monroy, N. Pelekanos, J. Baumberg, and P. Savvidis, "All-dielectric gan microcavity: Strong coupling and lasing at room temperature," *Applied Physics Letters*, vol. 102, no. 10, p. 101113, 2013.

[72] D. Bajoni, P. Senellart, E. Wertz, I. Sagnes, A. Miard, A. Lemaître, and J. Bloch, "Polariton laser using single micropillar gaas- gaalas semiconductor cavities," *Physical review letters*, vol. 100, no. 4, p. 047401, 2008.

[73] B. Zhang, Z. Wang, S. Brodbeck, C. Schneider, M. Kamp, S. Höfling, and H. Deng, "Zero-dimensional polariton laser in a subwavelength grating-based vertical microcavity," *Light: Science & Applications*, vol. 3, no. 1, pp. e135–e135, 2014.

[74] A. Das, J. Heo, M. Jankowski, W. Guo, L. Zhang, H. Deng, and P. Bhattacharya, "Room temperature ultralow threshold gan nanowire polariton laser," *Physical review letters*, vol. 107, no. 6, p. 066405, 2011.

[75] M. Nomura, N. Kumagai, S. Iwamoto, Y. Ota, and Y. Arakawa, "Laser oscillation in a strongly coupled single-quantum-dot–nanocavity system," *Nature Physics*, vol. 6, no. 4, pp. 279–283, 2010.

[76] K. Hennessy, A. Badolato, M. Winger, D. Gerace, M. Atatüre, S. Gulde, S. Fält, E. L. Hu, and A. Imamoğlu, "Quantum nature of a strongly coupled single quantum dot–cavity system," *Nature*, vol. 445, no. 7130, pp. 896–899, 2007.

[77] S. Azzini, D. Gerace, M. Galli, I. Sagnes, R. Braive, A. Lemaître, J. Bloch, and D. Bajoni, "Ultra-low threshold polariton lasing in photonic crystal cavities," *Applied Physics Letters*, vol. 99, no. 11, p. 111106, 2011.

[78] D. Urbonas, T. Stoferle, F. Scafirimuto, U. Scherf, and R. F. Mahrt, "Zero-dimensional organic exciton–polaritons in tunable coupled gaussian defect microcavities at room temperature," *ACS Photonics*, vol. 3, no. 9, pp. 1542–1545, 2016.

[79] S. Satoh and K. Igaki, "Effect of native defect concentration on free-exciton luminescence in zinc selenide," *Japanese Journal of Applied Physics*, vol. 19, no. 10, p. 1953, 1980.

[80] I. Buyanova, J. Bergman, B. Monemar, H. Amano, I. Akasaki, A. Wysmolek, P. Lomiak, J. Baranowski, K. Pakula, R. Stepniewski *et al.*, "Effects of defect scattering on the photoluminescence of exciton-polaritons in n-gan," *Solid state communications*, vol. 105, no. 8, pp. 497–501, 1998.

[81] B. Deveaud, "Exciton-polariton bose-einstein condensates," *Annual Review Of Condensed Matter Physics, Vol 6*, vol. 6, no. BOOK_CHAP, pp. 155–175, 2015.

[82] K. Chen, R. Ghosh, X. Meng, A. Roy, J.-S. Kim, F. He, S. C. Mason, X. Xu, J.-F. Lin, D. Akinwande *et al.*, "Experimental evidence of exciton capture by mid-gap defects in cvd grown monolayer mose2," *npj 2D Materials and Applications*, vol. 1, no. 1, pp. 1–8, 2017.

[83] T. Damen and J. Shah, "Bound exciton resonance in raman cross sections in cds," *Physical Review Letters*, vol. 27, no. 22, p. 1506, 1971.

[84] C. Dietrich, M. Lange, G. Benndorf, J. Lenzner, M. Lorenz, and M. Grundmann, "Competing exciton localization effects due to disorder and shallow defects in semiconductor alloys," *New Journal of Physics*, vol. 12, no. 3, p. 033030, 2010.

[85] A. Reznitsky, A. Klochikhin, S. Permogorov, L. Tenishev, W. Lundin, A. Usikov, M. Schmidt, and C. Klingshirn, "Localization of excitons at small in clusters in diluted ingan solid solutions," *physica status solidi (c)*, no. 1, pp. 280–283, 2003.

[86] L. Sun, H. Dong, W. Xie, J. Lu, Z. Chen, X. Shen, and W. Lu, "Strong bound exciton-photon coupling in zno whispering gallery microcavity," *Optics Express*, vol. 21, no. 25, pp. 30 227–30 232, 2013.

[87] M. Zunaid Baten, T. Frost, I. Iorsh, S. Deshpande, A. Kavokin, and P. Bhattacharya, "Small-signal modulation characteristics of a polariton laser," *Scientific reports*, vol. 5, no. 1, pp. 1–8, 2015.

[88] J. M. Luttgens, F. J. Berger, and J. Zaumseil, "Population of exciton–polaritons via luminescent sp3 defects in single-walled carbon nanotubes," *ACS photonics*, vol. 8, no. 1, pp. 182–193, 2020.

[89] N. Averkiev, G. Savchenko, and R. Seisyan, "Elastic scattering of exciton polaritons," *Physics of the Solid State*, vol. 57, no. 2, pp. 290–295, 2015.

[90] L. I. Deych and A. A. Lisyansky, "Local polariton states in polar crystals with impurities," *Physics Letters A*, vol. 240, no. 6, pp. 329–333, 1998.

[91] W. Ungier and M. Suffczyński, "Exchange interaction in an exciton bound to a neutral donor," *Physical Review B*, vol. 27, no. 6, p. 3656, 1983.

[92] H. Wang, J. H. Strait, C. Zhang, W. Chan, C. Manolatou, S. Tiwari, and F. Rana, "Fast exciton annihilation by capture of electrons or holes by defects via auger scattering in monolayer metal dichalcogenides," *Physical Review B*, vol. 91, no. 16, p. 165411, 2015.

[93] Y. A. Osipyan, V. Timofeev, and E. Shteinman, "Exciton scattering by dislocations in the cdse crystal," *Soviet Physics-JETP*, vol. 35, no. 1, pp. 146–149, 1972.

[94] F. Tassone and Y. Yamamoto, "Exciton-exciton scattering dynamics in a semiconductor microcavity and stimulated scattering into polaritons," *Physical Review B*, vol. 59, no. 16, p. 10830, 1999.

[95] G. Malpuech, A. Di Carlo, A. Kavokin, J. J. Baumberg, M. Zamfirescu, and P. Lugli, "Room-temperature polariton lasers based on gan microcavities," *Applied physics letters*, vol. 81, no. 3, pp. 412–414, 2002.

[96] R. Butté, G. Delalleau, A. Tartakovskii, M. Skolnick, V. Astratov, J. Baumberg, G. Malpuech, A. Di Carlo, A. Kavokin, and J. Roberts, "Transition from strong to weak coupling and the onset of lasing in semiconductor microcavities," *Physical Review B*, vol. 65, no. 20, p. 205310, 2002.

[97] D. Porras, C. Ciuti, J. Baumberg, and C. Tejedor, "Polariton dynamics and bose-einstein condensation in semiconductor microcavities," *Physical Review B*, vol. 66, no. 8, p. 085304, 2002.

[98] L. D'Alessio, Y. Kafri, A. Polkovnikov, and M. Rigol, "From quantum chaos and eigenstate thermalization to statistical mechanics and thermodynamics," *Advances in Physics*, vol. 65, no. 3, pp. 239–362, 2016.

[99] M. Srednicki, "Chaos and quantum thermalization," *Physical review e*, vol. 50, no. 2, p. 888, 1994.

[100] M. Srednicki and F. Stiernelof, "Gaussian fluctuations in chaotic eigenstates," *Journal of Physics A: Mathematical and General*, vol. 29, no. 18, p. 5817, 1996.

[101] R. Mondaini, K. R. Fratus, M. Srednicki, and M. Rigol, "Eigenstate thermalization in the two-dimensional transverse field ising model," *Physical Review E*, vol. 93, no. 3, p. 032104, 2016.

[102] K. Mallayya, M. Rigol, and W. De Roeck, "Prethermalization and thermalization in isolated quantum systems," *Physical Review X*, vol. 9, no. 2, p. 021027, 2019.

[103] J. R. Garrison and T. Grover, "Does a single eigenstate encode the full hamiltonian?" *Physical Review X*, vol. 8, no. 2, p. 021026, 2018.

[104] D. Castelvecchi and A. Witze, "Einstein's gravitational waves found at last," *Nature news*, vol. 11, 2016.

[105] K. Hyatt, J. R. Garrison, A. C. Potter, and B. Bauer, "Many-body localization in the presence of a small bath," *Physical Review B*, vol. 95, no. 3, p. 035132, 2017.

[106] R. Nandkishore and D. A. Huse, "Many-body localization and thermalization in quantum statistical mechanics," *Annu. Rev. Condens. Matter Phys.*, vol. 6, no. 1, pp. 15–38, 2015.

[107] A. V. Kavokin, J. J. Baumberg, G. Malpuech, and F. P. Laussy, *Microcavities*. Oxford university press, 2017, vol. 21.

[108] Y. Yamamoto, F. Tassone, and H. Cao, *Semiconductor cavity quantum electrodynamics*. Springer, 2003, vol. 169.

[109] A. H. Choi, *Handbook of optical microcavities*. CRC Press, 2014.

[110] I. Abram, I. Robert, and R. Kuszelewicz, "Spontaneous emission control in semiconductor microcavities with metallic or bragg mirrors," *IEEE Journal of quantum electronics*, vol. 34, no. 1, pp. 71–76, 1998.

[111] A. Billeb, W. Grieshaber, D. Stocker, E. Schubert, and R. Karlicek Jr, "Microcavity effects in gan epitaxial films and in ag/gan/sapphire structures," *Applied physics letters*, vol. 70, no. 21, pp. 2790–2792, 1997.

[112] M. Pugliese, C. T. Prontera, L. Polimeno, G. Lerario, R. Giannuzzi, M. Esposito, S. Carallo, D. Costa, L. De Marco, M. De Giorgi *et al.*, "Highly reflective periodic nanostructure based on thermal evaporated tungsten oxide and calcium fluoride for advanced photonic applications," *ACS Applied Nano Materials*, vol. 3, no. 11, pp. 10 978–10 985, 2020.

[113] M. Marciniak, T.-S. Chang, T.-C. Lu, F. Hjort, Å. Haglund, Ł. Marona, M. Gramala, P. Modrznyski, R. Kudrawiec, K. Sawicki *et al.*, "Impact of stripe shape on the reflectivity of monolithic high contrast gratings," *ACS Photonics*, vol. 8, no. 11, pp. 3173–3184, 2021.

[114] J. Levrat, "Physics of polariton condensates in gan-based planar microcavities," EPFL, Tech. Rep., 2012.

[115] G. Bastard, E. Mendez, L. Chang, and L. Esaki, "Exciton binding energy in quantum wells," *Physical Review B*, vol. 26, no. 4, p. 1974, 1982.

[116] W. Guo, M. Zhang, A. Banerjee, and P. Bhattacharya, "Catalyst-free ingan/gan nanowire light emitting diodes grown on (001) silicon by molecular beam epitaxy," *Nano letters*, vol. 10, no. 9, pp. 3355–3359, 2010.

[117] M. Combescot, O. Betbeder-Matibet, and R. Combescot, "Exciton-exciton scattering: Composite boson versus elementary boson," *Physical Review B*, vol. 75, no. 17, p. 174305, 2007.

[118] I. A. Shelykh, A. V. Kavokin, and G. Malpuech, "Spin dynamics of exciton polaritons in microcavities," *physica status solidi (b)*, vol. 242, no. 11, pp. 2271–2289, 2005.

[119] V. Savona, F. Tassone, C. Piermarocchi, A. Quattropani, and P. Schwendimann, "Theory of polariton photoluminescence in arbitrary semiconductor microcavity structures," *Physical Review B*, vol. 53, no. 19, p. 13051, 1996.

[120] R. Rapaport, R. Harel, E. Cohen, A. Ron, E. Linder, and L. Pfeiffer, "Negatively charged quantum well polaritons in a gaas/alas microcavity: An analog of atoms in a cavity," *Physical review letters*, vol. 84, no. 7, p. 1607, 2000.

[121] F. Tassone, C. Piermarocchi, V. Savona, A. Quattropani, and P. Schwendimann, "Bottleneck effects in the relaxation and photoluminescence of microcavity polaritons," *Physical Review B*, vol. 56, no. 12, p. 7554, 1997.

[122] A. J. Grundy, "Optically nonlinear spatial and spectral processes in semiconductor microcavities," Ph.D. dissertation, University of Southampton, 2009.

[123] C. Schneider, A. Rahimi-Iman, N. Y. Kim, J. Fischer, I. G. Savenko, M. Amthor, M. Lermer, A. Wolf, L. Worschech, V. D. Kulakovskii *et al.*, "An electrically pumped polariton laser," *Nature*, vol. 497, no. 7449, pp. 348–352, 2013.

[124] H. B. Bebb and E. Williams, "Photoluminescence i: Theory, in semiconductors and semimetals," 1972.

[125] V. Kulakovskiĭ, G. Pikus, and V. B. Timofeev, "Multiexciton complexes in semiconductors," *Soviet Physics Uspekhi*, vol. 24, no. 10, p. 815, 1981.

[126] L. P. Pitaevskii, S. Stringari, and S. Stringari, *Bose-einstein condensation.* Oxford University Press, 2003, no. 116.

[127] N. Bogoliubov, "On the theory of superfluidity," *J. Phys*, vol. 11, no. 1, p. 23, 1947.

[128] R. J. Glauber, "The quantum theory of optical coherence," *Physical Review*, vol. 130, no. 6, p. 2529, 1963.

[129] W. H. Louisell, *Quantum statistical properties of radiation.* John Wiley and Sons, Inc., New York, 1973.

[130] L. Landau, "Em lifshitz statistical physics," *Course of Theoretical Physics*, vol. 5, pp. 396–400, 1980.

[131] O. Penrose, "Cxxxvi. on the quantum mechanics of helium ii," *The London, Edinburgh, and Dublin Philosophical Magazine and Journal of Science*, vol. 42, no. 335, pp. 1373–1377, 1951.

[132] O. Penrose and L. Onsager, "Bose-einstein condensation and liquid helium," *Physical Review*, vol. 104, no. 3, p. 576, 1956.

[133] L. Landau, "Theory of the superfluidity of helium ii," *Physical Review*, vol. 60, no. 4, p. 356, 1941.

[134] L. Tisza, "Transport phenomena in helium ii," *Nature*, vol. 141, no. 3577, pp. 913–913, 1938.

[135] D. J. Griffiths and D. F. Schroeter, *Introduction to quantum mechanics.* Cambridge university press, 2018.

[136] A. S. Bradley and B. P. Anderson, "Energy spectra of vortex distributions in two-dimensional quantum turbulence," *Physical Review X*, vol. 2, no. 4, p. 041001, 2012.

[137] N. D. Mermin and H. Wagner, "Absence of ferromagnetism or antiferromagnetism in one-or two-dimensional isotropic heisenberg models," *Physical Review Letters*, vol. 17, no. 22, p. 1133, 1966.

[138] G. Roumpos, M. D. Fraser, A. Löffler, S. Höfling, A. Forchel, and Y. Yamamoto, "Single vortex–antivortex pair in an exciton-polariton condensate," *Nature Physics*, vol. 7, no. 2, pp. 129–133, 2011.

[139] J. Uffink, "Compendium of the foundations of classical statistical physics," 2006.

[140] J. von Neumann, "Proof of the ergodic theorem and the h-theorem in quantum mechanics," *The European Physical Journal H*, vol. 35, no. 2, pp. 201–237, 2010.

[141] B. Chirikov, "Linear and nonlinear dynamical chaos," *Open Systems & Information Dynamics*, vol. 4, no. 3, pp. 241–280, 1997.

[142] M. V. Berry and M. Tabor, "Level clustering in the regular spectrum," *Proceedings of the Royal Society of London. A. Mathematical and Physical Sciences*, vol. 356, no. 1686, pp. 375–394, 1977.

[143] O. Bohigas, M.-J. Giannoni, and C. Schmit, "Characterization of chaotic quantum spectra and universality of level fluctuation laws," *Physical review letters*, vol. 52, no. 1, p. 1, 1984.

[144] S. W. McDonald and A. N. Kaufman, "Spectrum and eigenfunctions for a hamiltonian with stochastic trajectories," *Physical Review Letters*, vol. 42, no. 18, p. 1189, 1979.

[145] M. V. Berry, "Regular and irregular semiclassical wavefunctions," *Journal of Physics A: Mathematical and General*, vol. 10, no. 12, p. 2083, 1977.

[146] M. Shapiro and G. Goelman, "Onset of chaos in an isolated energy eigenstate," *Physical review letters*, vol. 53, no. 18, p. 1714, 1984.

[147] M. Srednicki, "The approach to thermal equilibrium in quantized chaotic systems," *Journal of Physics A: Mathematical and General*, vol. 32, no. 7, p. 1163, 1999.

[148] T. Mori, T. N. Ikeda, E. Kaminishi, and M. Ueda, "Thermalization and prethermalization in isolated quantum systems: a theoretical overview," *Journal of Physics B: Atomic, Molecular and Optical Physics*, vol. 51, no. 11, p. 112001, 2018.

[149] N. Linden, S. Popescu, A. J. Short, and A. Winter, "Quantum mechanical evolution towards thermal equilibrium," *Physical Review E*, vol. 79, no. 6, p. 061103, 2009.

[150] P. W. Anderson, "More is different: broken symmetry and the nature of the hierarchical structure of science." *Science*, vol. 177, no. 4047, pp. 393–396, 1972.

[151] G. Feher, "Electron spin resonance experiments on donors in silicon. i. electronic structure of donors by the electron nuclear double resonance technique," *Physical Review*, vol. 114, no. 5, p. 1219, 1959.

[152] P. W. Anderson, "Absence of diffusion in certain random lattices," *Physical review*, vol. 109, no. 5, p. 1492, 1958.

[153] A. B. Harris, "Effect of random defects on the critical behaviour of ising models," *Journal of Physics C: Solid State Physics*, vol. 7, no. 9, p. 1671, 1974.

[154] R. B. Griffiths, "Nonanalytic behavior above the critical point in a random ising ferromagnet," *Physical Review Letters*, vol. 23, no. 1, p. 17, 1969.

[155] T. Vojta, "Quantum griffiths effects and smeared phase transitions in metals: Theory and experiment," *Journal of Low Temperature Physics*, vol. 161, no. 1, pp. 299–323, 2010.

[156] I. V. Gornyi, A. D. Mirlin, and D. G. Polyakov, "Interacting electrons in disordered wires: Anderson localization and low-t transport," *Physical review letters*, vol. 95, no. 20, p. 206603, 2005.

[157] D. M. Basko, I. L. Aleiner, and B. L. Altshuler, "Metal–insulator transition in a weakly interacting many-electron system with localized single-particle states," *Annals of physics*, vol. 321, no. 5, pp. 1126–1205, 2006.

[158] L. Fallani, C. Fort, and M. Inguscio, "Bose–einstein condensates in disordered potentials," *Advances in atomic, molecular, and optical physics*, vol. 56, pp. 119–160, 2008.

[159] G. Roati, C. D'Errico, L. Fallani, M. Fattori, C. Fort, M. Zaccanti, G. Modugno, M. Modugno, and M. Inguscio, "Anderson localization of a non-interacting bose–einstein condensate," *Nature*, vol. 453, no. 7197, pp. 895–898, 2008.

[160] C. D'Errico, "Anderson localization of a weakly interacting bose-einstein condensate," Ph.D. dissertation, PhD Thesis, University of Florence, 2008.

[161] L. Pollet, N. Prokof'ev, B. Svistunov, and M. Troyer, "Absence of a direct superfluid to mott insulator transition in disordered bose systems," *Physical review letters*, vol. 103, no. 14, p. 140402, 2009.

[162] W. Krauth, N. Trivedi, and D. Ceperley, "Superfluid-insulator transition in disordered boson systems," *Physical review letters*, vol. 67, no. 17, p. 2307, 1991.

[163] K. G. Lagoudakis, F. Manni, B. Pietka, M. Wouters, T. C. H. Liew, V. Savona, A. V. Kavokin, R. André, and B. Deveaud-Plédran, "Probing the dynamics of spontaneous quantum vortices in polariton superfluids," *Physical review letters*, vol. 106, no. 11, p. 115301, 2011.

[164] G. Uhlenbeck and L. Gropper, "The equation of state of a non-ideal einstein-bose or fermi-dirac gas," *Physical Review*, vol. 41, no. 1, p. 79, 1932.

[165] S. Pau, G. Björk, J. Jacobson, H. Cao, and Y. Yamamoto, "Stimulated emission of a microcavity dressed exciton and suppression of phonon scattering," *Physical Review B*, vol. 51, no. 11, p. 7090, 1995.

[166] W. Zhao, P. Stenius, and A. Imamoḡlu, "Kinetics of condensation in trapped exciton gases," *Physical Review B*, vol. 56, no. 9, p. 5306, 1997.

[167] T. Goudon, V. Miljanović, and C. Schmeiser, "On the shockley–read–hall model: generation-recombination in semiconductors," *SIAM Journal on Applied Mathematics*, vol. 67, no. 4, pp. 1183–1201, 2007.

[168] D. Wickramaratne, J.-X. Shen, C. E. Dreyer, M. Engel, M. Marsman, G. Kresse, S. Marcinkevičius, A. Alkauskas, and C. G. Van de Walle, "Iron as a source of efficient shockley-read-hall recombination in gan," *Applied Physics Letters*, vol. 109, no. 16, p. 162107, 2016.

[169] I. Iorsh, M. Glauser, G. Rossbach, J. Levrat, M. Cobet, R. Butté, N. Grandjean, M. A. Kaliteevski, R. A. Abram, and A. V. Kavokin, "Generic picture of the emission properties of iii-nitride polariton laser diodes: Steady state and current modulation response," *Physical Review B*, vol. 86, no. 12, p. 125308, 2012.

[170] M. Rigol, V. Dunjko, and M. Olshanii, "Thermalization and its mechanism for generic isolated quantum systems," *Nature*, vol. 452, no. 7189, pp. 854–858, 2008.

[171] D. Handscomb, "The monte carlo method in quantum statistical mechanics," in *Mathematical Proceedings of the Cambridge Philosophical Society*, vol. 58, no. 4. Cambridge University Press, 1962, pp. 594–598.

[172] E. L. Pollock and D. M. Ceperley, "Path-integral computation of superfluid densities," *Physical Review B*, vol. 36, no. 16, p. 8343, 1987.

[173] U. Ray, *Properties of dirty bosons in disordered optical lattices*. University of Illinois at Urbana-Champaign, 2015.

[174] D. Greenbaum, "Introduction to quantum gate set tomography," *arXiv preprint arXiv:1509.02921*, 2015.

[175] F. Schmidt-Kaler, H. Häffner, M. Riebe, S. Gulde, G. Lancaster, T. Deuschle, C. Becher, C. F. Roos, J. Eschner, and R. Blatt, "Realization of the cirac–zoller controlled-not quantum gate," *Nature*, vol. 422, no. 6930, pp. 408–411, 2003.

[176] X. Li, Y. Wu, D. Steel, D. Gammon, T. Stievater, D. Katzer, D. Park, C. Piermarocchi, and L. Sham, "An all-optical quantum gate in a semiconductor quantum dot," *Science*, vol. 301, no. 5634, pp. 809–811, 2003.

[177] S. Ghosh and T. C. Liew, "Quantum computing with exciton-polariton condensates," *npj Quantum Information*, vol. 6, no. 1, pp. 1–6, 2020.